

---

# Nanocapsules for self-healing materials

Dissertation

zur Erlangung des akademischen Grades

„Doktor der Naturwissenschaften“

eingereicht am

Fachbereich Chemie, Pharmazie und Geowissenschaften

der Johannes Gutenberg-Universität Mainz

**Johannes Fickert**

geboren in Günzburg

Mainz, im April 2013



Max-Planck-Institut für Polymerforschung Mainz





Die vorliegende Arbeit wurde im Zeitraum von März 2010 bis März 2013 am Max-Planck-Institut für Polymerforschung in Mainz im Arbeitskreis Physikalische Chemie der Polymere von \_\_\_\_\_ angefertigt.

Dekan:

Erster Gutachter:

Zweiter Gutachter:

Tag der mündlichen Prüfung: 03.05.2013



***Für meine Nina***



---

1	<i>Introduction</i> .....	11
2	<i>Theoretical section</i> .....	16
2.1	Heterophase systems .....	16
2.1.1	Emulsions and their stability .....	16
2.1.2	Miniemulsion .....	17
2.2	Formation of nanocapsules .....	19
2.2.1	Colloidal morphologies .....	19
2.2.2	Thermodynamic considerations .....	20
2.2.3	Formation of nanocapsules .....	22
2.2.4	Synthesis of functionalized nanocapsules .....	28
2.3	Self-healing .....	33
2.3.1	Intrinsic self-healing .....	34
2.3.2	Extrinsic self-healing: vascular .....	37
2.3.3	Extrinsic self-healing: micro-/nanocapsules .....	39
2.3.4	Chemistry of self-healing .....	43
2.3.5	Conventional and self-healing coatings for corrosion prevention.....	47
3	<i>Methods</i> .....	49
3.1	Dynamic light scattering .....	49
3.2	Transmission electron microscopy .....	50
3.3	Scanning electron microscopy .....	51
4	<i>Efficient encapsulation of self-healing agents in polymer nanocontainers functionalized by orthogonal reactions</i> .....	54
4.1	Miniemulsion polymerization in the presence of a nonsolvent in the droplets .....	54
4.2	Synthesis of functional nanocontainers .....	55
4.3	Variation of the solvent quality .....	61
4.4	Role of the surfactant in the formation of the nanocapsules .....	63
4.5	Thickness of the polymer shell .....	66
4.6	Stability of the nanocapsules.....	67
4.7	Self-healing reaction .....	71
4.8	Conclusions.....	72

5	<i>Design and characterization of functionalized silica nanocontainers for self-healing materials</i> .....	74
5.1	Encapsulation of the monomer in non-functionalized nanocapsules.....	75
5.2	Encapsulation of the monomer in functionalized nanocapsules .....	79
5.3	Encapsulation of the Grubbs' catalyst and its stability .....	84
5.4	Self-healing reaction .....	87
5.5	Conclusions .....	89
6	<i>Polymer nanocapsules via the emulsion-solvent evaporation process</i> .....	92
6.1	Encapsulation of self-healing agents in polymer nanocapsules.....	93
6.1.1	Strategy.....	93
6.1.2	Encapsulation of HD.....	93
6.1.3	Encapsulation of healents for solvent- or plasticizer-assisted self-healing .....	99
6.1.4	Encapsulation of polymerizable self-healing agents.....	100
6.2	Copolymer structures tailored for the preparation of nanocapsules .....	104
6.2.1	Formation of the capsules .....	104
6.2.2	Encapsulation of ROMP monomers .....	113
6.2.3	Encapsulation of ROMP catalysts.....	115
6.2.4	Self-healing reaction .....	116
6.3	Conclusions .....	118
7	<i>Self-stabilized pH-responsive nanocapsules</i> .....	120
7.1	Formation of surfactant-free nanocapsules and nanoparticles.....	121
7.2	pH-responsive stability .....	124
7.3	Concentration .....	127
7.4	Encapsulation of ROMP monomer and catalyst.....	129
7.5	pH-responsive release .....	130
7.6	Conclusions .....	132
8	<i>Incorporation of the nanocapsules into a zinc matrix by electrodeposition</i> .....	133
8.1	Introduction .....	133
8.2	Electrodeposition .....	134



---

9	<i>Experimental details</i> .....	139
9.1	Chemicals .....	139
9.2	General characterization of the samples .....	141
9.2.1	DLS .....	141
9.2.2	TEM and SEM .....	141
9.3	Efficient encapsulation of self-healing agents in polymer nanocontainers functionalized by orthogonal reactions .....	141
9.4	Design and characterization of functionalized silica nanocontainers for self-healing materials .....	144
9.5	Encapsulation of self-healing agents in polymer nanocapsules .....	147
9.6	Copolymer structures tailored for the preparation of nanocapsules .....	148
9.7	Self-stabilized pH-responsive nanocapsules .....	152
9.8	Incorporation of nanocapsules into a zinc matrix by electrodeposition .....	155
10	<i>Conclusions</i> .....	157
11	<i>Zusammenfassung</i> .....	161
	<i>Abbreviations and characters</i> .....	165
	<i>References</i> .....	169
	<i>Acknowledgements</i> .....	177
	<i>Appendix</i> .....	179



# 1 Introduction

The invention of new materials has shaped the development of human history decisively. The significance of materials for the mankind is shown by the fact that time periods of human early history, such as the Stone Age, Bronze Age or Iron Age, are named after the predominant material.

In retrospect, almost all strategies for improving the reliability and strength of materials developed over the ages were ultimately based on the consideration of damage prevention. Materials were planned and prepared in a way that the formation of damage as a function of strain and stress is delayed as much as possible. The extent of damage at best remains constant but will not be reduced by itself for such materials. Since damage during usage can never be ruled out, defective materials have to be repaired or replaced resulting in costs and consumption of resources. In a time of shortages of energy and resources, technologies that are able to increase the lifetime of engineered products are of huge interest.

A particularly interesting concept for this application is the concept of self-healing. Self-healing materials are materials which are able to heal or repair themselves automatically and autonomously without any external intervention.<sup>1</sup> The self-healing approach is inspired by biological systems where healing occurs either at level of molecules (*e.g.* repair of DNA) or at macroscopic level (*e.g.* mending of wounds or merging of broken bones). Materials with the ability to heal could help to save energy and material by regenerating the damaged materials instead of disposing them. As indicated by the increasing amount of publications and patents in the field of self-healing chemistry, this innovative material class has gained much interest over the past decade. Actually, the self-healing approach is not something very new in materials science. Perhaps the first example for self-healing behavior is the mortar that was used by the Romans over two thousand years ago.<sup>2</sup> The mortar holding the stones together did not possess very good mechanical properties compared to current standards but showed an excellent durability. Although originally not intended, the particular stability was achieved by the autonomous healing of defects inside the constructions by a controlled dissolution and phase separation of the mortar, which was induced by the reaction between the mortar and moisture in the air.<sup>3</sup> The first patent for a polymer possessing intentional self-healing character was published in 1969 but the

potential of this approach was probably not fully appreciated and therefore not followed up.<sup>4</sup> The research in the field of self-healing was continued not until the year 1994 by Dry et al.,<sup>5-6</sup> but only received huge interest in 2001 when White et al. published their pioneer work about the recovery of the mechanical properties of a self-healing composite.<sup>7</sup> Microcapsules filled with monomer were incorporated into a matrix containing the catalyst. In case of mechanical damage, the monomer was released from the ruptured capsules, filled the crack, and reacted with the catalyst resulting in healing of the defect.

One type of damage that the self-healing approach can help to prevent is corrosion. The degradation of materials and their properties due to environmental influences is a large burden on the economies around the world. Corrosion can cause expensive and dangerous damage to various man-made materials such as bridges, buildings or vehicles. The worldwide costs of corrosion are estimated at about 3% of the gross domestic product (GDP) of industrialized nations, which are over 1.4 trillion euros per year.<sup>8</sup> In order to prevent corrosion, steel is usually covered by a protective zinc layer followed by a chromate conversion coating (CCC) on top for the passivation of the surface of the coating. Chromate itself provides an unmatched ability of “self-healing” due to the migration of soluble Cr(VI) species incorporated into the CCC.<sup>9</sup> Because hexavalent chromium is highly toxic and carcinogen, chromating with Cr(VI) has to be replaced by alternative and environment-friendly processes. In the European Union, the use of chromium(VI) is already highly restricted by directives on end-of-life vehicles and on the restriction of the use of hazardous substances.<sup>10-11</sup>

The combination of self-healing materials and corrosion protection layers represents a promising strategy for replacing chromates. The concept is based on the separate encapsulation of the components of a two-part self-healing system in order to provide long-term stability of the healing agents. These filled nanocontainers should be incorporated into anticorrosive coatings. In case of corrosion or cracks, the healing agents should be released resulting in healing at room temperature by creating a protection layer at the defect.

The objective of this thesis is the exploration of new approaches to encapsulate self-healing agents in nanocapsules. The two main challenges for designing useful capsule-based self-healing materials are a good dispersion of the capsules in the matrix and an efficient encapsulation of the healing agents. The first point is a common issue in composites and hybrid materials and is usually solved by incorporating functional groups at the surface of

the fillers.<sup>12-14</sup> Thus, an ideal container for self-healing materials shall be a capsule with functional groups on the shell. The miniemulsion technique is a suitable method for producing materials matching the requirements of functionality and encapsulation. Various processes including phase separation, interfacial polymerization, and solvent evaporation can be employed to form nanocapsules in order to encapsulate liquid healing agents very efficiently.

The focus of the current thesis was on the formation of functional nanocapsules in miniemulsion for the encapsulation of self-healing agents. Three different routes for the synthesis of core-shell particles have been carried out. Firstly, an orthogonal polymerization reaction between two liquid monomers partitioned in the two liquid phases of a miniemulsion yielded nanocapsules with various functional groups. The formation of the nanocapsules could be realized in the presence of a self-healing agent in the liquid core. Secondly, silica nanocontainers functionalized with thiol or amine groups were prepared using the interface of direct miniemulsion droplets for the hydrolysis and condensation of alkoxy silanes. It was shown, that healing agents such as monomers and catalysts could be successfully encapsulated in the silica core-shell particles. In the third chapter, the emulsion-solvent evaporation process is described as a simple and mild method to encapsulate healing agents such as plasticizers, monomers and catalysts in core-shell nanoparticles using various pre-synthesized polymers. In addition, a new concept for the synthesis of pH-responsive nanocapsules without use of surfactant was presented. Finally, several synthesized nanocapsules were applied to electrodeposition for the incorporation into a zinc matrix in order to provide possible self-healing activity for corrosion protection.





Chapter 2

Theoretical section

## 2 Theoretical section

### 2.1 Heterophase systems

A heterophase system is described as a system of at least two immiscible components, for which one (dispersed phase) is distributed in the other (continuous phase). Normally, surfactants are used to stabilize heterophase systems. Heterophase mixtures that have a dispersed phase in the submicron range are designated as colloidal systems. Depending on the physical state (gaseous, liquid or solid) of the involved phases different systems are defined. Most of these systems are very common in daily life. There is the case of aerosols (solids or liquids dispersed in a gaseous continuous phase, *e.g.* fog or smoke) or emulsions (liquid dispersed in another liquid, *e.g.* milk or mayonnaise). The general term of all these systems is the dispersion.<sup>15</sup>

#### 2.1.1 Emulsions and their stability

Emulsions are metastable colloidal dispersions consisting of two immiscible liquids. The internal (dispersed) phase is thereby distributed in the form of small droplets in the external (continuous) phase, *i.e.* they form a heterogeneous mixture of finely dispersed droplets. For the formation of these droplets shear forces are necessary, which are usually applied by shaking, stirring or sonication. The addition of surfactant prevents coalescence between the droplets and improves therefore the stability of emulsions. The most common emulsions have an aqueous phase. When the dispersed phase is consisting of an oil and the continuous phase of water, the dispersion are called direct or oil-in-water emulsions (o/w-emulsions). In an inverse or water-in-oil emulsion (w/o), the water droplets are dispersed in a continuous phase of oil. Emulsions can be classified into macro-, micro- and miniemulsions based on the stability and the droplet size.

Macroemulsions - conventional emulsions – are not formed spontaneously but require energy input, usually in the form of low shear forces like shaking or stirring. Dispersions with a broad size distribution of droplet diameters in the range of 100 nm to several microns are obtained. The newly formed interface can be covered by surfactants, which stabilize the



system kinetically, but not thermodynamically. Therefore, the macroemulsion is unstable and phase separation occurs after some time.<sup>16</sup>

Thermodynamically stable microemulsions on the other hand are formed spontaneously. Compared to macroemulsions, considerably higher amounts of surfactants (> 10 wt% related to the dispersed phase) are used. In addition, a cosurfactant (in most cases an alcohol of medium chain length) is used to further reduce the interfacial tension and ensure the stability of the microemulsion. The resulting droplets and the swollen micelles have a diameter in the range of 5 to 50 nm. Due to their small droplet size, light can penetrate through the microemulsions without being scattered and therefore such emulsions are usually translucent.<sup>17</sup>

The characteristics of miniemulsions are discussed separately in the following chapter because of its significant relevance for this thesis.

### 2.1.2 Miniemulsion

First reports about miniemulsions were published in 1973 by *Ugelstad et al.*<sup>18-19</sup> The miniemulsion is a special class of emulsion that consists of narrowly distributed droplets with a size ranging from 50 to 500 nm in another liquid phase.<sup>20</sup> The use of high energy homogenization such as ultrasound or high-pressure homogenization usually results in the small size distribution of the droplets.

Miniemulsions are stabilized against the two main destabilization processes that can lead to breaking of emulsions: coalescence ([Figure 2.1 top](#)) and *Ostwald* ripening ([Figure 2.1 bottom](#)).<sup>21</sup>

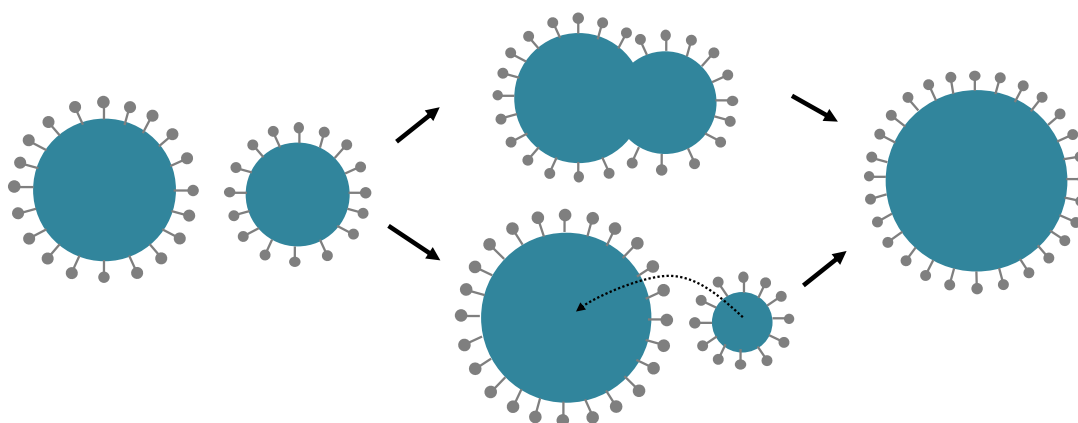


**Figure 2.1** Scheme of coalescence (top) and Ostwald ripening (bottom).

Coalescence is defined as the fusion of two or more droplets due to collisions. In miniemulsion, the coalescence is suppressed by the use of surfactants, which provide steric and/or electrostatic stabilization to the droplets.

The *Ostwald* ripening is hindered by the addition of an osmotic reagent to the dispersed phase. *Ostwald* ripening is described as the growth of the larger droplets in size at the expense of the smaller droplets. This is a diffusion process which occurs due to a certain solubility of the dispersed phase in the continuous phase. The driving force of this aging process is the higher *Laplace* pressure in smaller droplets:

$$P_L = \frac{2 \cdot \gamma_{LL}}{r} \quad \text{Equation 1}$$

where  $P_L$  is the *Laplace* pressure,  $\gamma_{LL}$  the interfacial tension between two liquids, and  $r$  the radius of the droplet.

The role of the osmotic reagent is to build up an osmotic pressure counterbalancing the *Laplace* pressure in order to prevent the diffusion of the dispersed phase from smaller to larger droplets (Figure 2.2). As a consequence, the osmotic agents should have a very low solubility in the continuous phase to be efficient. *Hydrophobes* such as long-chain alkanes (e.g. hexadecane) and *lipophobes* such as inorganic salts (e.g. sodium chloride) are commonly used as osmotic reagents in direct and inverse miniemulsions, respectively.<sup>21-22</sup>

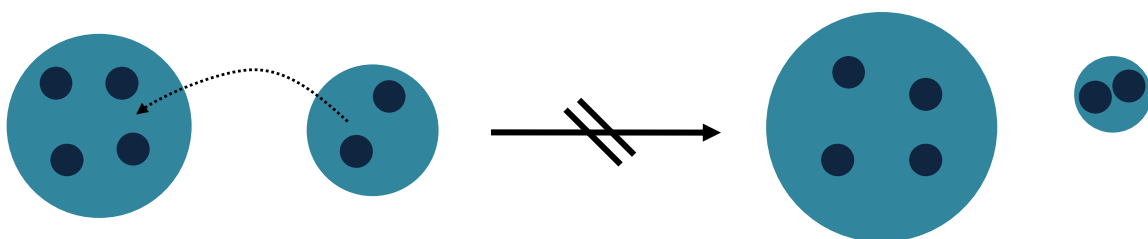


**Figure 2.2** Schematic illustration of the hindrance of Ostwald ripening by the presence of an osmotic agent (shown as dark spots). The dotted arrow symbolizes the diffusion of the dispersed phase through the continuous phase.

## 2.2 Formation of nanocapsules

Core-shell particles with a liquid core – also called nanocapsules - have attracted increasing interest in various fields of applications such as adhesives, coatings, paints, cosmetics, or pharmaceuticals. Such particles consist of two materials with different chemical composition, in which one material forms the shell and the other the core. The core is composed of a liquid and the shell of a solid, which can be prepared with various materials in regard to the applications.

The following sections give an overview of possible morphologies, thermodynamical considerations, and the synthetic approaches concerning core-shell particles.

### 2.2.1 Colloidal morphologies

In general, composite particles with two phases can have various colloidal morphologies, such as core-shell, inverted core-shell, hemisphere, Janus, microdomains, or “confetti”-like structures (Figure 2.3).

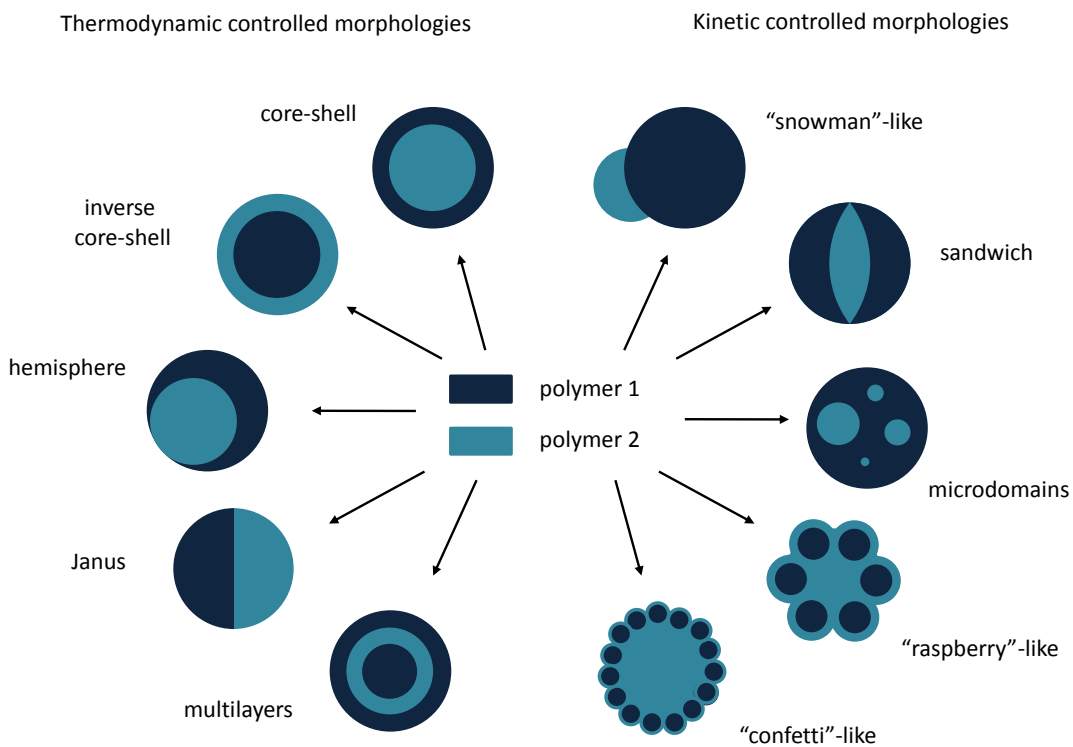


**Figure 2.3** Scheme of thermodynamically and kinetically controlled morphologies of two-phase particles (based on Musyanovych et al.<sup>23</sup>).

For the synthesis of a certain well-defined structure, it is fundamental to control the phase morphology during the preparation of the particle. The arrangement of the phases within the latex particles is mainly determined by thermodynamic and kinetic factors. The equilibrium morphology of the resulting composite particle is controlled by thermodynamic factors, while kinetic factors are linked to the easiness with which the thermodynamically stable configuration can be reached.<sup>23</sup>

### 2.2.2 Thermodynamic considerations

The first fundamental considerations of the theoretical prediction of three-phase interactions in shear and electrical fields were published over 40 years ago by Torza and Mason.<sup>24</sup> In this work, the interfacial behavior of systems containing two immiscible organic liquids, named as phase 1 and phase 3, immersed in a third immiscible liquid (phase 2) was investigated. They proposed that the resulting equilibrium state is dependent on the different interfacial tensions  $\gamma_{ij}$  and spreading coefficient  $S_i$ , which is described as:

$$S_i = \gamma_{jk} - (\gamma_{ij} + \gamma_{ik}) \quad \text{Equation 2}$$

where  $S_i$  is the spreading coefficient of liquid  $i$  and  $\gamma$  is the interfacial tension between two liquids  $i, j$  or  $k$ .

With the assumption that the interfacial tension between phase 1 and phase 2 is larger than the one between phase 2 and phase 3 ( $\gamma_{12} > \gamma_{23}$ ), three different types of equilibrium configurations are possible (see [Figure 2.4](#)): complete engulfing (core-shell) takes place when  $S_1 < 0$ ,  $S_2 < 0$  and  $S_3 > 0$ ; partial engulfing (acorn) occurs only if  $S_1, S_2, S_3 < 0$ ; and  $S_1 < 0$ ,  $S_2 > 0$  and  $S_3 < 0$  leads to non-engulfing (separate particles).

The generality of this approach was demonstrated for various three-phase liquid systems by comparing experimental results with theoretical predictions calculated from the interfacial tension measurements.<sup>24</sup>

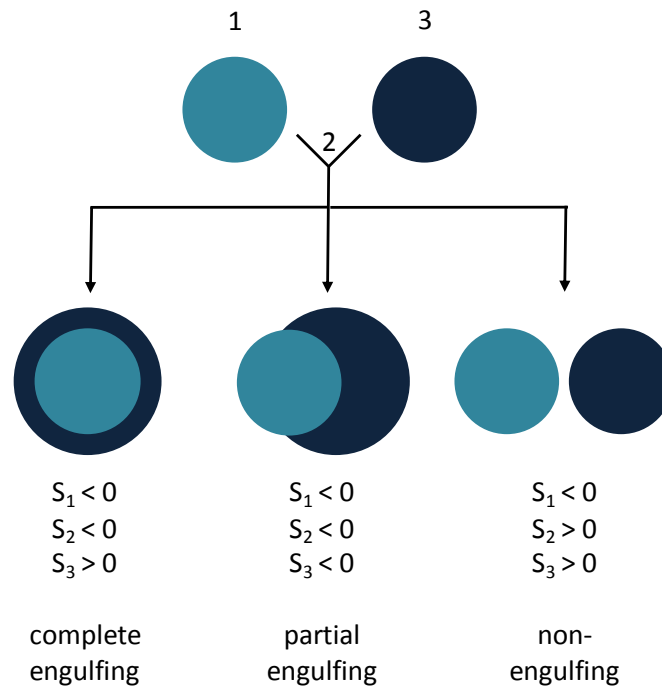


**Figure 2.4** Encapsulation of a liquid: Schematic representation of different equilibrium morphologies corresponding to the spreading coefficients for two immiscible phases 1 and 3 dispersed in a continuous phase 2.

The considerations published by Torza and Mason relied on liquid phases with low viscosities, which are able to achieve the equilibrium state - normally the configuration with the lowest interfacial energy - by rapid diffusion. On the other hand, the mobility of the polymer chains of high molecular polymers is limited and therefore the most thermodynamic stable configuration may not always be accomplished. In these systems, the Gibbs free energy change during the formation process is predominant for the final particle morphology.<sup>23</sup> Sundberg et al. proposed in their thermodynamic analysis of a two-stage particle formation that the thermodynamically favored configuration of a three-phase system, *e.g.* polymer 1, polymer 2 and water, would be the one with the minimum free surface energy  $G$ ,<sup>25-26</sup> which is defined as:

$$G = \sum \gamma_{ij} A_{ij} \quad \text{Equation 3}$$

where  $G$  is the Gibbs' free energy of the system,  $\gamma_{ij}$  the interfacial tension between phases  $i$  and  $j$  and  $A_{ij}$  their interfacial area.

Further, Sundberg et al. found that the surfactant and the nature of two immiscible polymers have a high influence on the interfacial tensions.<sup>27</sup> They demonstrated the change of the particle morphology from core-shell to hemispherical by varying the nature of surfactant.

However, even when thermodynamic stable structures are favorable, thermodynamically the formation of unfavorable morphologies is possible in some cases. This can be the case, when there is a difference between the surface and bulk properties of a polymer or when kinetic factors during the preparation process become predominant.

In general, the formation of polymer particles in aqueous dispersion consisting of two phases can be influenced by several parameters, such as different hydrophilicities of the monomers and the polymers as well as differences in solubility of the monomers and polymers in the continuous phase,<sup>28-29</sup> mobility of the polymer chains,<sup>30</sup> type and amount of surfactant and initiator,<sup>27,31-32</sup> or the temperature during preparation.<sup>33-34</sup>

### 2.2.3 Formation of nanocapsules

Nanocapsules can be produced from a large variety of natural or synthetic monomers and polymers using different methods to fulfill requirements for various applications.<sup>35</sup> This chapter gives an overview of the different methods for synthesizing nanocapsules.

#### 2.2.3.1 Layer-by-layer technique

The formation of core-shell nanocapsules with a shell out of polyelectrolytes can be performed by the layer-by-layer (LbL) technique.<sup>36-39</sup> The approach is based on the self-assembly of opposite charged polyelectrolytes resulting into multilayers of consecutive adsorbed polyanions and polycations. Subsequent decomposition of the core can be carried out to form capsules (Figure 2.5). For example, polystyrene,<sup>40</sup> silica (SiO<sub>2</sub>),<sup>41</sup> or melamine formaldehyde<sup>42</sup> were used as sacrificial cores. Cationic poly(diallyldimethylammonium chloride) (PDADMAC) or poly(allylamine hydrochloride) and poly(acrylic acid) sodium salt or poly(styrene sulfonate) sodium salt as anionic counterpart as well as biodegradable electrolytes such as alginate or chitosan can be used as polyelectrolytes.<sup>43-44</sup>

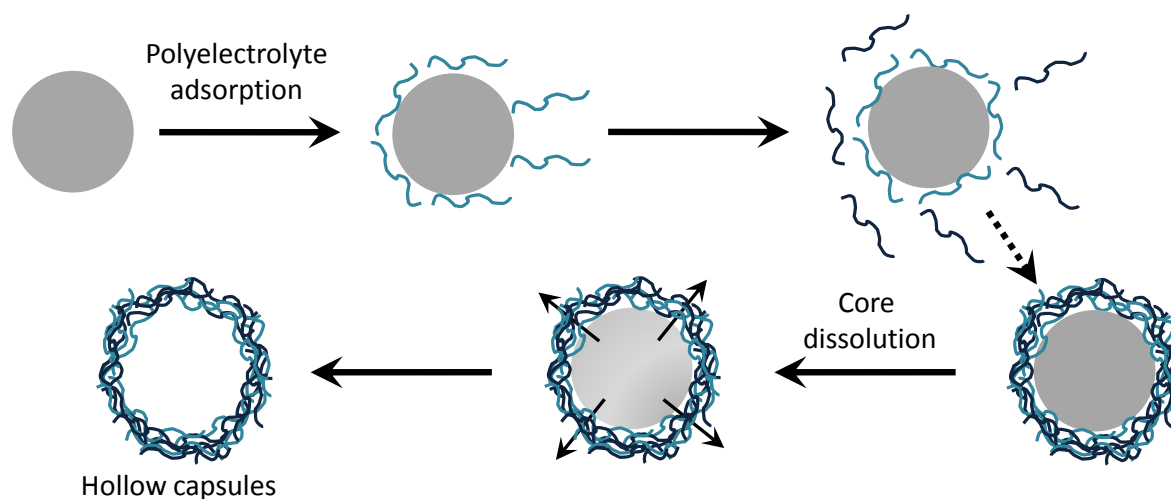


**Figure 2.5** Scheme of the polyelectrolyte adsorption process and subsequent dissolution of the core.

### 2.2.3.2 Phase separation during polymerization

Nanocapsules can be obtained by polymerization in a one-step miniemulsion process (Figure 2.6). In this case, the formation process is based on the phase separation between the polymer and the liquid core polymerization. Before polymerization, the hydrophobic non-polymerizable oil (hexadecane) and the monomer form a homogeneous solution in the miniemulsion droplets. During the polymerization, the polymer becomes immiscible with the oil and precipitates at the droplet interface, resulting in core-shell particles consisting of a liquid core and a polymer shell surrounding the oil. The driving force for the formation of nanocapsules is based on the difference in hydrophilicity of the oil and the synthesized polymer. The different interfacial tensions of the interfaces polymer/water, polymer/oil, and oil/water have to be tuned in a way that the core-shell morphology is the thermodynamically favored one according to the considerations of Torza and Mason (see chapter 2.2.2).<sup>45</sup>

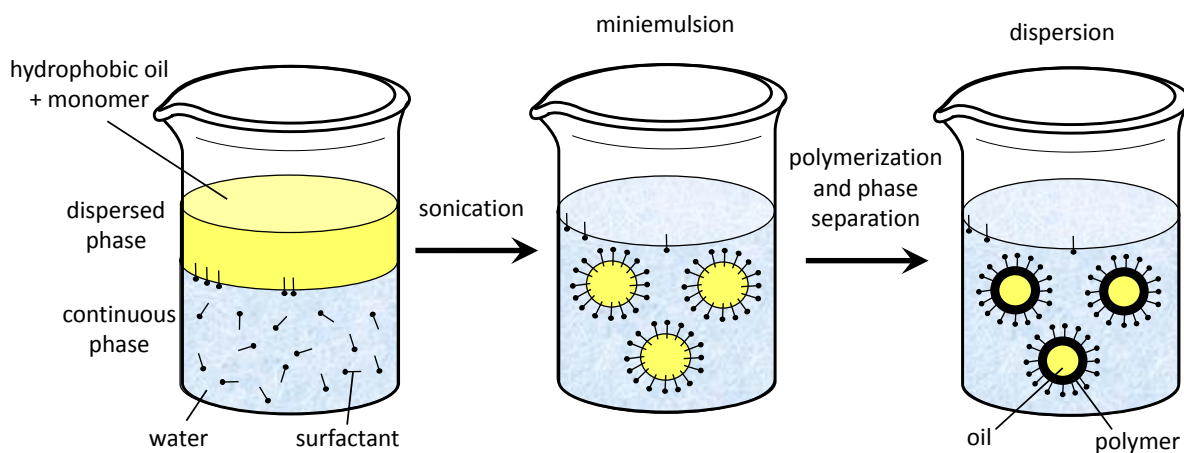


**Figure 2.6** Schematic illustration of the formation of nanocapsules due to phase separation during polymerization

As an example, nanocapsules could be formed directly by the polymerization of methyl methacrylate (MMA) in presence of hexadecane. In contrast, the difference in hydrophilicity of pure polystyrene (PS) and hexadecane was not sufficient to obtain core-shell morphologies. The hydrophilicity of PS had to be increased by the addition of either a hydrophilic comonomer or an appropriate initiator in order to obtain nanocapsule structures.<sup>46</sup> The addition of functional hydrophilic comonomers allows further the incorporation of functional groups on the surface of the capsules, which is discussed more in detail in [chapter 2.2.4](#). The influence of different monomers and monomer mixtures, of the amount and kind of surfactant, and of the hydrophobic oil hexadecane on morphology of the obtained composite colloids has been summarized by Tiarks et al.<sup>46</sup>

### 2.2.3.3 Interfacial polymerization

Another well-established method in the preparation of nanocapsules is the interfacial polymerization. Various types of polymerization could be conducted for the formation of hollow nanoparticles.

Core-shell particles were obtained by interfacial radical alternating copolymerization of hydrophilic vinyl ethers with hydrophobic maleates in direct as well as in inverse miniemulsion.<sup>47-48</sup> Since homopolymerization of the monomers is not possible, the reaction is forced to happen at the droplets interface where both monomers can get in contact.



Furthermore, anionic polymerization was carried out to prepare nanocapsules. The monomer *n*-butyl cyanoacrylate (BCA) was slowly added to the continuous phase of an inverse miniemulsion and polymerized at the interface of the aqueous droplets leading to the formation of a PBCA shell. Hydroxide ions present in the dispersed phase and hydroxyl groups of the surfactant acted thereby as nucleophiles for the initiation of the anionic polymerization.<sup>49</sup>

Polyadditions reactions were also performed at the interface of the droplets. Polyurea, polythiourea and polyurethane shells could be obtained in inverse miniemulsion by using water soluble diamine or diol components located in the droplets. The hydrophobic diisocyanate or dithioisocyanate monomers were added after formation of the miniemulsion; leading to a polymerization at the interface.<sup>50</sup> Polyurethane nanocapsules were also prepared in direct miniemulsion. This was performed by the reaction between the low reactive isophorone diisocyanate (IPDI) present in the oil droplets and a diol or a polyol dissolved in water and added to the aqueous continuous phase after miniemulsification of the diisocyanate.<sup>51-52</sup>

Apart from radical, anionic, and polyaddition reactions at the interface, polycondensations are possible as well. Inorganic nanocapsules can be synthesized by hydrolysis and polycondensations of silica precursors in direct miniemulsion.<sup>53-54</sup> The reaction equations of the sol-gel processes are shown in Figure 2.7. Firstly, a hydroxysilane (Si(OH)<sub>4</sub>) is generated by partial or full hydrolysis of the alkoxy silane (Si(OR)<sub>4</sub>) (sol process). The condensation reaction between two silanol groups among elimination of water occurs in the following gel process.

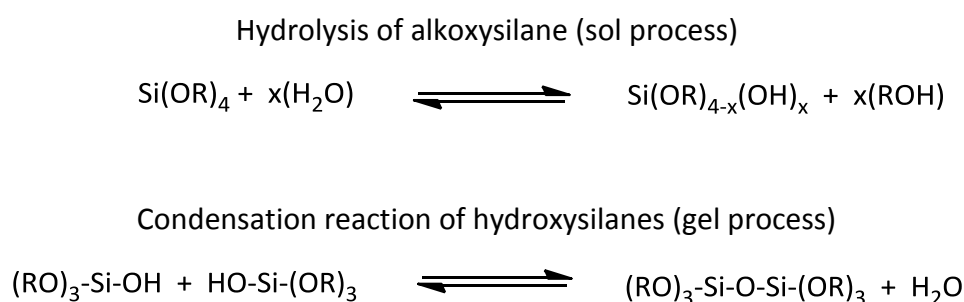


**Figure 2.7** Reaction equations of the sol-gel process.

The silica precursor, commonly a tetraalkoxysilane such as tetraethoxysilane (TEOS), is dissolved in the dispersed phase together with the hydrophobe liquid to be encapsulated. The continuous phase consists of water and the stabilizing surfactant which also acts as a catalyst in the sol-gel process.

Both reactions of the sol-gel process take place at the interface of the droplets leading to a  $\text{SiO}_2$  network encapsulating the hydrophobic liquid. The formation of the inorganic shell around the hydrophobic liquid by the sol-gel process is illustrated in [Figure 2.8](#).

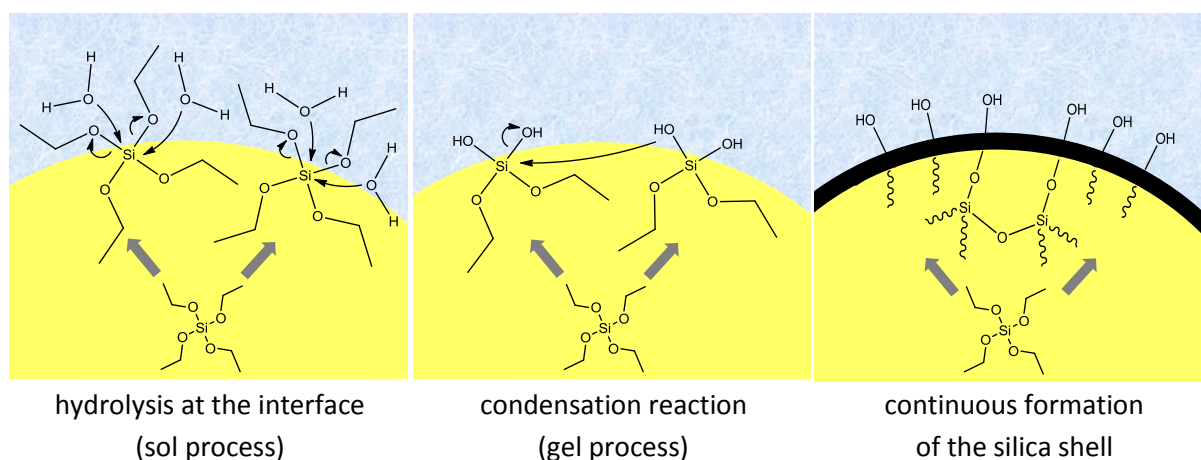


**Figure 2.8** Schematic illustration of the sol-gel process at the droplet interface leading to inorganic silica nanocapsules. TEOS is present in the droplet and diffuses to the interface where the sol-gel process is initiated by contacting with water.

Droplets in inverse miniemulsions were also used as templates for the formation of silica capsules. TEOS present in the continuous phase diffused to the droplet interface, where the hydrolysis and condensation reactions took place resulting in the creating of a silica shell around the water droplets.<sup>55</sup>

### 2.2.3.4 Phase separation induced by solvent evaporation

The formation of nanocapsules could be induced by the evaporation of a solvent combined with the miniemulsion process. Nanoprecipitation of pre-synthesized polymers onto miniemulsion droplets was used to efficiently encapsulate an aqueous core surrounded of a polymeric shell. The polymer was dissolved in the continuous oil phase consisting of a

mixture of solvent (*e.g.* dichloromethane) and non-solvent (*e.g.* cyclohexane). After miniemulsification, the solvent was slowly evaporated leading to the precipitation of the polymer at the interface of hydrophilic droplet and oil forming a surrounding shell. Poly(D,L-lactide)- and poly(methyl methacrylate)-based nanocapsules could be successfully synthesized by this method.<sup>56-57</sup>

Nanocontainers with a hydrophobic core could be further prepared by the (mini)emulsion solvent evaporation technique in direct miniemulsions. The general preparation procedure for the formation of core-shell nanocontainers is shown in [Figure 2.9](#). The pre-synthesized polymer was also dissolved in a mixture of a good solvent (with a relative low boiling point, *e.g.* chloroform or dichloromethane) for the polymer and a poor solvent for the polymer (typically a non-volatile hydrophobic oil such as hexadecane). After preparation of the miniemulsion, the evaporation of the volatile solvent led to phase separation and precipitation of the polymer inside the droplets forming the capsular morphology.

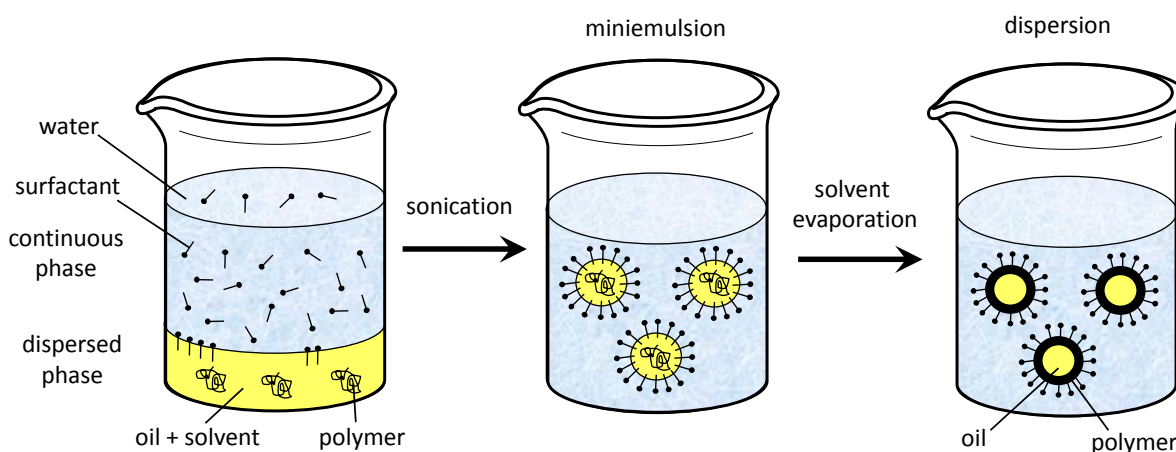


**Figure 2.9** Schematic view of the formation of nanocapsules by the miniemulsion solvent evaporation technique.

The phase separation process can be described more precisely as shown in [Figure 2.10](#). Due to the evaporation of the good solvent, a change in the droplet composition takes place resulting in the phase separation of the polymer as small droplets within the emulsion droplets. These polymer-rich droplets move then to the interface of the oil droplet where they coalesce and the formation of the shell occurs.<sup>58</sup>

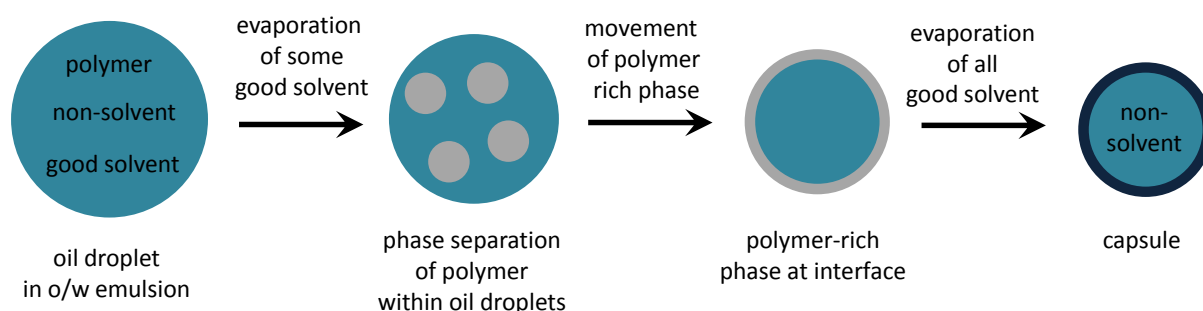


**Figure 2.10** Schematic illustration of the mechanism of shell formation.<sup>59</sup>

Furthermore, the emulsion-solvent evaporation technique was applied for the preparation of microcapsules encapsulating an aqueous core. In an inverse emulsion, the polymer was dissolved in the aqueous phase containing a good solvent for the polymer (*e.g.* acetone). After emulsification and subsequent evaporation of the volatile co-solvent, microcapsules were obtained.<sup>60</sup>

### 2.2.4 Synthesis of functionalized nanocapsules

Generally, functionalized polymers in miniemulsion can be synthesized either by the (co)polymerization of one or several monomers, or by the (post)modification of polymers existing in the dispersed phase of the miniemulsion. Functionalized nanoparticles and their applications have been widely discussed in literature. The synthesis of nanoparticles bearing functional groups could be performed in direct or inverse miniemulsion by various types of polymerizations.<sup>61</sup> However, functionalized nanocapsules are less common due to their more challenging synthesis. The following part gives an overview of the prepared functional nanocapsules reported in the literature. The mentioned approaches are listed in [Table 2.1a,b](#). The surface functionalization of a capsule shell can be achieved by radical copolymerization of a hydrophobic monomer with a hydrophilic functional comonomer in direct miniemulsion according to [chapter 2.2.3.2](#). Acrylic acid or methacrylic acid were copolymerized with styrene resulting in the introduction of carboxylic groups on the surface of the capsule shell.<sup>46,62</sup> This approach was extended to sulfonate, hydroxyl and amine functionalization by copolymerization of styrene sulfonate, 2-hydroxyl methacrylate (HEMA), and *tert*-butylaminoethyl methacrylate (TMAEMA) as hydrophilic comonomers,

respectively.<sup>63-64</sup> Nanocapsules with poly(ethylene oxide)/poly(propylene oxide) surface functionalized with phosphate groups were obtained by copolymerization of styrene and/or divinylbenzene in the presence of a polymerizable surfactant carrying the introduced functional groups.<sup>65</sup> Hydroxyl functionalized organic-inorganic hybrid core-shell particles were prepared by copolymerization of styrene with 3-(trimethoxysilyl)propyl methacrylate and *n*-isopropyl acrylamide (NIPAM).<sup>66</sup> The interfacial alternating radical polymerization of the hydrophobic monomer dibutyl maleate with the functional hydrophilic comonomer vinyl gluconamide was performed in inverse miniemulsion resulting into hydroxyl functionalized submicron nanocontainers.<sup>48</sup>

Interfacial polyaddition in inverse miniemulsion allows the formation of capsules with a hydrophilic core and provides several functionalities in the shell (see [chapter 2.2.3.3](#)). Nanocontainers with different types of shell polymers such as polyurethane, polyurea, polythiourea, crosslinked starch, dextran or polyethylene imine were obtained.<sup>50,67</sup> The functional groups were directly incorporated in the capsules by the use of excess of one or more monomers, or by adding functionalized monomers or copolymers with additional functionality which do not react in the polyaddition. Therefore, amino, hydroxyl, isocyanate, thiocyanate, or thiol groups were incorporated in the shell.<sup>50</sup> Hydroxyl and amine groups could further be introduced by the partial hydrolysis of the polyurethane shell.<sup>68</sup> The hydroxyl and amine functionalized surface could be subsequently changed into carboxyl functionalization by a carboxymethylation reaction.<sup>68</sup>

Alkyne functionalization was provided by the preparation of poly(*n*-butyl cyanoacrylate-*co*-propargyl cyanoacrylate) P(BCA-*co*-PCA) nanocapsules via interfacial anionic polymerization. Polyurethane capsules carrying azide groups could be synthesized via interfacial polyaddition. The alkyne and azide functionalized capsules further offered the possibility to become post-functionalized using click-chemistry (*e.g.* carboxyl functionalized by reaction with propionic acid).<sup>69</sup> Azide functionalized nanocapsules were also synthesized by atom transfer radical polymerization (ATRP) of *n*-butyl methacrylate in presence of various crosslinkers and a surfmer bearing the azide functionality. The azide functionality of the latter nanocapsules was used to attach small molecules (*e.g.* dyes) and to convert to ATRP initiators for the preparation of a second polymer shell.<sup>70</sup>

The synthesis of hollow silica nanoparticles was performed by using the template based *Stöber* method with subsequent decomposition of the Fe<sub>3</sub>O<sub>4</sub> sacrificial core. The surface was

further functionalized with amine groups by addition of (3-aminopropyl)trimethoxysilane (APTMS).<sup>71</sup> Silica-titania nanocapsules prepared in the analogous manner were surface modified with amine, carboxyl and vinyl groups using (3-aminopropyl)triethoxysilane (APTES), carboxylethylsilanetriol sodium salt, and 3-(trimethoxysilyl)propyl methacrylate (MPS), respectively.<sup>72</sup>

Nanocapsules carrying hydroxyl groups were obtained by absorbing chitosan on the surface of polystyrene particles followed by a crosslinking reaction with glutaraldehyde and subsequent dissolution of the sacrificial core.<sup>73</sup>

Functionalized nanocapsules were also obtained by the layer-by-layer (LbL) technique (chapter 2.2.3.1). Nanocapsules bearing sulfonate or carboxylic functionalization in presence of amine groups were prepared by the one after another adsorption of several polyelectrolytes (e.g. poly(sodium 4-styrenesulfonate) (PSS) or poly(methacrylic acid) (PMAA) alternately with poly(allylamine hydrochloride) or poly(diallyldimethylammonium chloride) (PDADMAC) on sacrificial cores followed by subsequent core decomposition.<sup>74-76</sup> Further, the deposition of polyelectrolytes directly on oil droplets provided the preparation of sulfonate and amine functionalized nanocontainers without decomposition step.<sup>77</sup>

The seed precipitation polymerization of *n*-isopropylacrylamide (NIPAM) with aminoethyl methacrylate (AEMA) on poly(divinylbenzene) (PDVB) covered iron oxide particles followed by subsequent removal of the magnetic core yielded amine functionalized nanocapsules.<sup>78</sup>

The use of pre-synthesized poly(methyl methacrylate-*co*-methacrylic acid) [P(MMA-*co*-MAA)] in a two-step process composed of a combination of the solvent diffusion and solvent evaporation method yielded into pH-responsive carboxyl functionalized submicron capsules.<sup>79</sup> By crosslinking the shell with cystamine, extra supplementary disulfide bonds were introduced in the shell providing supplementary redox sensitivity.<sup>79-80</sup> The carboxyl functionalized nanocontainers were also coupled with 2-aminoethyl methacrylate resulting in additional vinyl-functionalization.<sup>81</sup>

**Table 2.1a** Summary of nanocapsule formation with functional groups on the surface.

Functionality on the surface	functional (co)monomer	shell material	formation process	ref.
carboxyl	acrylic acid (AA) methacrylic acid (MAA)	polystyrene based	free radical copolymerization in direct miniemulsion	46,62
sulfonate	sodium <i>p</i> -styrene sulfonate (SS)	polystyrene based	free radical copolymerization in direct miniemulsion	63
hydroxyl	2-hydroxyethyl methacrylate (HEMA)	polystyrene based	free radical copolymerization in direct miniemulsion	64
amine	<i>tert</i> -butylaminoethyl methacrylate (TMAEMA)	polystyrene based	free radical copolymerization in direct miniemulsion	64
phosphate	Tego XP-1008	polystyrene based	free radical copolymerization in direct miniemulsion	65
hydroxyl	3-(trimethoxysilyl)propyl methacrylate (MPS)	organic-inorganic hybrid, polystyrene based	free radical copolymerisation in direct miniemulsion	66
hydroxyl	vinyl gluconamide	poly(dibutyl maleate- <i>alt</i> -vinyl gluconamide)	interfacial alternating radical copolymerization in inverse miniemulsion	48
amine	diethylenetriamine (DET) 1,6-hexanediamine (HMDA) 1,4-diaminobutane (DAB) poly(ethylene imine) (PEI)	polyurea, polythiourea, crosslinked poly(ethylene imine) (PEI)	interfacial polyaddition in inverse miniemulsion	50,68
thiol/amine	cysteamine/ diethylenetriamine	polyurea, polythiourea	interfacial polyaddition in inverse miniemulsion	50
hydroxyl	1,6-hexanediol starch dextrane <i>L</i> -arginine	polyurethane, crosslinked starch, crosslinked dextran, polyurea	interfacial polyaddition in inverse miniemulsion	50,67
isocyanate	tolylene 2,4-diisocyanate (TDI)	polyurethane/polyurea	interfacial polyaddition in inverse miniemulsion	50
thiocyanate	tolylene 2,4-diisothiocyanate (TDIT)	polythiourea	interfacial polyaddition in inverse miniemulsion	50
hydroxyl/ amine	tolylene 2,4-diisocyanate (TDI)	polyurethane/polyurea	1) interfacial polyaddition in inverse miniemulsion 2) hydrolysis	68
carboxyl/ amine	tolylene 2,4-diisocyanate (TDI)/ monochloroacetic acid	polyurethane/polyurea	1) interfacial polyaddition in inverse miniemulsion 2) hydrolysis 3) carboxymethylation	68
alkyne	propargyl cyanoacrylate	poly( <i>n</i> -butyl cyanoacrylate- <i>co</i> - propargyl cyanoacrylate (P(BCA- <i>co</i> -PCA)))	interfacial anionic polymerization in inverse miniemulsion	69
azide	2,2-bis(azidomethyl)-1,3- propanediol (BAP)	polyurethane	interfacial polyaddition in inverse miniemulsion	69
carboxyl	propionic acid	polyurethane	1) interfacial polyaddition in inverse miniemulsion 2) „click reaction“	69
azide	azide functionalized reactive surfactant	poly( <i>n</i> -butyl methacrylate) based	ATRP in direct miniemulsion	70
amine	(3-aminopropyl)trimethoxysilane (APTMS) (3-aminopropyl)triethoxysilane (APTES)	SiO <sub>2</sub>	1) sacrificial template <i>Stöber</i> method 2) surface functionalization	71-72

**Table 2.1b** Summary of nanocapsule formation with functional groups on the surface.

Functionality on the surface	functional (co)monomer	shell material	formation process	ref.
carboxyl	carboxylethylsilanetriol sodium salt	SiO <sub>2</sub>	1) sacrificial template <i>Stöber</i> method 2) surface functionalization	72
vinyl	3-(trimethoxysilyl)propyl methacrylate (MPS)	SiO <sub>2</sub>	1) sacrificial template <i>Stöber</i> method 2) surface functionalization	72
hydroxyl	chitosan	crosslinked chitosan	sacrificial polymer template method	73
sulfonate/ amine	4-styrolsulfonate/ allylamine	poly(sodium 4-styrenesulfonate) (PSS) poly(allylamine hydrochloride)	1) LbL technique 2) core dissolution	74-76
sulfonate/ amine	4-styrolsulfonate/ diallyldimethylammonium chloride	poly(sodium 4-styrenesulfonate) (PSS) poly(diallyldimethylammonium chloride) (PDADMAC)	1) LbL technique 2) core dissolution	75-76
carboxylic/ amine	methacrylic acid/ allylamine	poly(methacrylic acid) polyallylamine hydrochloride)	1) LbL technique 2) core dissolution	75-76
sulfonate/ amine	4-styrolsulfonate/ diallyldimethylammonium chloride	poly(sodium 4-styrenesulfonate) (PSS) poly(diallyldimethylammonium chlorid) (PDADMAC)	LbL technique on liquid core	77
amine	2-aminoethyl methacrylate (AEMA)	poly(divinylbenzene) poly( <i>n</i> -isopropylacrylamide- <i>co</i> -2-aminoethyl methacrylate)	1) free radical polymerization 2) core decomposition	78
carboxylic	methacrylic acid	poly(methyl methacrylate- <i>co</i> -methacrylic acid)	solvent diffusion/ solvent evaporation	79
carboxylic/ disulfide	methacrylic acid/ cystamine	crosslinked poly(methyl methacrylate- <i>co</i> -methacrylic acid)	1) solvent diffusion/ solvent evaporation 2) crosslinking	79-80
carboxylic/ vinyl	methacrylic acid/ 2-aminoethyl methacrylate (AEMA)	poly(methyl methacrylate- <i>co</i> -methacrylic acid)	1) solvent diffusion/ solvent evaporation 2) esterification	81

The various reactions for the post-functionalization of the nanocapsule shells are listed separately in [Table 2.2](#).



**Table 2.2** Different examples for post-functionalization of functional nanocapsules.

Functionality	functional (co)monomer	shell material	post-functionalization	ref.
hydroxyl/amine	tolylene 2,4-diisocyanate (TDI)	polyurethane/polyurea	hydrolysis	68
carboxyl/amine	monochloroacetic acid/ tolylene 2,4-diisocyanate (TDI)	polyurethane/polyurea	hydrolysis followed by carboxymethylation	68
carboxyl	propionic acid	polyurethane	„click reaction“	69
amine	3-aminopropyl trimethoxy silane (APTMS)	SiO <sub>2</sub>	addition of functional comonomer	71-
	3-aminopropyl triethoxy silane (APTES)			72
carboxyl	carboxylethylsilanetriol sodium salt	SiO <sub>2</sub>	addition of functional comonomer	72
vinyl	3-(trimethoxysilyl)propyl methacrylate (MPS)	SiO <sub>2</sub>	addition of functional comonomer	72
carboxylic/disulfide	methacrylic acid/ cystamine	crosslinked poly(methyl methacrylate-co-methacrylic acid)	crosslinking by addition of functional monomer	79-80
carboxylic/vinyl	methacrylic acid/ 2-aminoethyl methacrylate (AEMA)	poly(methyl methacrylate-co-methacrylic acid)	esterification	81

## 2.3 Self-healing

Self-healing can be defined as the ability to heal autonomously after being damaged. Self-healing materials are capable to partially or completely heal from caused damage or fatigue and refurbish lost or degraded properties by the use of resources, which are inherently available to the system.<sup>82</sup> Such materials can be metals, ceramics, polymers, and their composites that can repair themselves after thermal, mechanical, ballistic or other damages. This concept is inspired by biological systems, in which self-healing is commonplace, e.g. repairing of DNA or merging of broken bones.

Self-healing materials can be classified broadly into two main groups, which are intrinsic and extrinsic. The latter can further be divided into materials based on vascular or capsular systems (Figure 2.11).

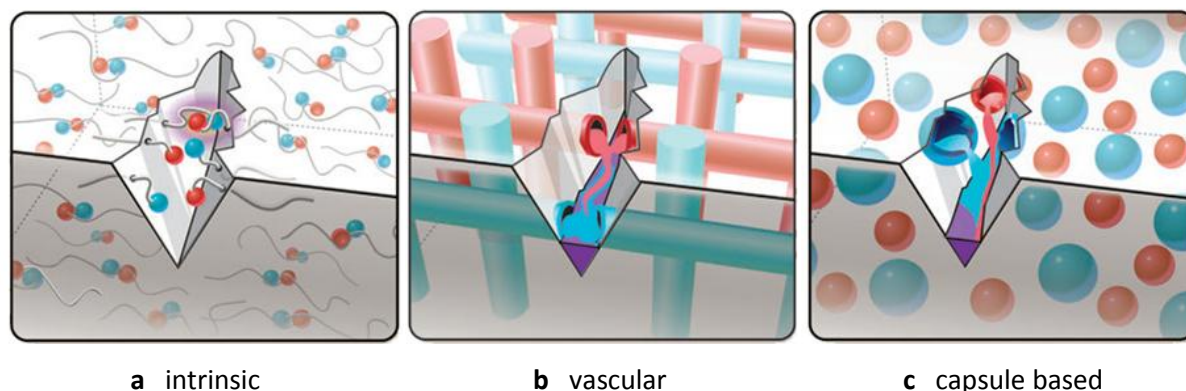


**Figure 2.11** Schematic illustration of the reported approaches to self-healing, which are (a) intrinsic, (b) vascular, and (c) capsule based materials. Adapted from Blaiszik et al.<sup>82</sup>

Each approach differs in the way the self-healing system is integrated into the bulk materials (matrix). Intrinsic materials build up the matrix and contain a concealed functionality that initiates healing, *e.g.* by thermally reversible reactions or hydrogen bonding. In vascular materials, fibers or hollow channels filled with self-healing agents permeate the matrix. The release occurs after rupturing the vasculature by external damage. In capsules-based self-healing materials, the healing agents are encapsulated in capsules which are incorporated in the matrix. Release occurs upon opening by damage or trigger.<sup>82</sup>

### 2.3.1 Intrinsic self-healing

Healing in intrinsic self-healing materials takes place by inbuilt reversibility of bonding in the matrix polymer. The self-healing process can be conducted by thermally reversible reactions, hydrogen bonding, ionic coupling, dispersed meltable thermoplastic phases, or molecular diffusion. Because reversible reactions are used, normally multiple healing of intrinsic materials is possible. In literature, intrinsic self-healing materials have been reported using three main routes, which are reversible covalent bonding, chain re-entanglement, and non-covalent healing (Figure 2.12).<sup>82</sup>

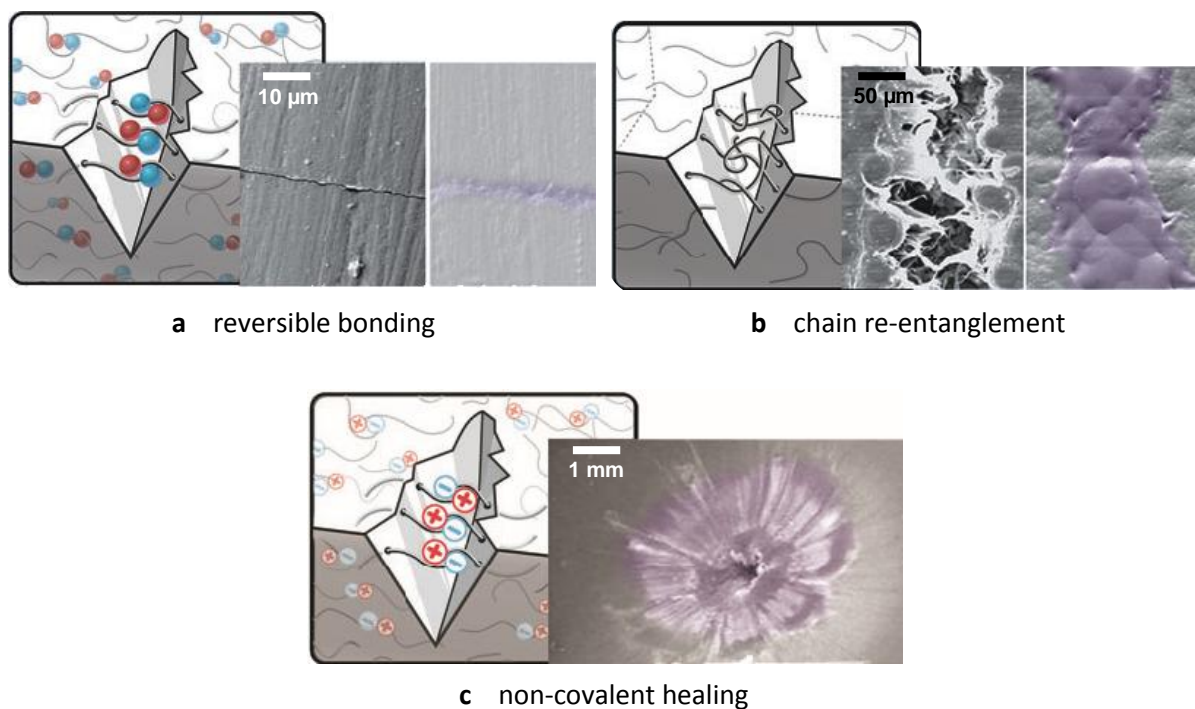


**Figure 2.12** Main schemes for intrinsic self-healing adapted from Blaiszik et al.<sup>82</sup> (a) Reversible bonding scheme using Diels-Alder-retro-Diels-Alder as healing reaction adapted from Murphy et al.<sup>83</sup> (b) Phase-separated poly(caprolacton) in an epoxy resin as an example for self-healing with chain re-entanglement adapted from Luo et al.<sup>84</sup> (c) Poly(ethylene-co-methacrylic acid) as self-healing ionomer for noncovalent healing adapted from Varley et al.<sup>85</sup>

Self-healing based on reversible bonding makes use of the reversibility of chemical reactions (Figure 2.12a). The most popular used approaches for intrinsic self-healing is based on the Diels-Alder (DA) and retro-Diels-Alder (rDA) reactions (Figure 2.13). By using external heat, the rDA reaction takes place and the crosslinked polymeric state is transformed into monomeric state. Consecutively, the DA reaction occurs and is accompanied by a healing through rearrangement of the polymer chains.

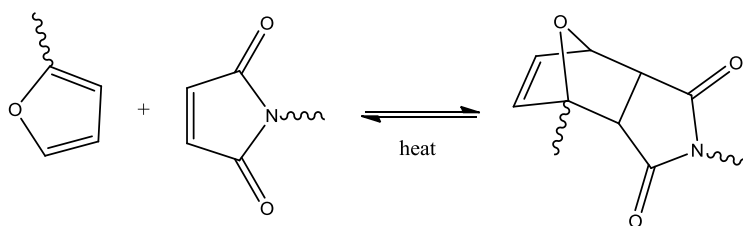


**Figure 2.13** Mechanism of polymerization and repair of Diels-Alder crosslinked polymers.

A thermally triggered self-healing system of furan-maleimide polymers based on DA reactions was firstly published by Chen et al.<sup>86-87</sup> Park et al. used the DA reaction for the introduction of healing properties in a polymer derived from cyclopentadiene and examined the self-healing performance in a bulk matrix<sup>88</sup> as well as in a carbon fiber composite.<sup>89</sup> Another cyclopentadiene derivative for a thermally healable polymer network was shown by Murphy et al.<sup>83</sup> Peterson et al. used a furan-maleimide reversible crosslinked gel dispersed in an epoxy-amine matrix as self-healing system, which could be activated thermally.

Self-healing in thermoset materials could also be performed by incorporating a meltable thermoplastic material. Healing was carried out by melting and following redispersion of the thermoplastic polymer resulting in filling the damage and connecting the surrounding matrix material. Hayes et al. demonstrated the incorporation of linear thermoplastics poly(bisphenol-A-co-epichlorohydrin) into an epoxy matrix for possible multiple healing.<sup>90-91</sup> A thermally remendable thermoset epoxy resin with dispersed phase-separated poly(caprolactone), which melted and went through a volumetric expansion in order to fill the crack, has been reported by Luo et al. and is shown in [Figure 2.12b](#).<sup>84</sup>

Ionomers are copolymers carrying both electrically neutral repeating units and ionized units, that can form clusters acting as reversible crosslinkers, which can be stimulated by external stimuli such as temperature or ultraviolet irradiation ([Figure 2.12c](#)). Studies of poly(ethylene-co-methacrylic acid) copolymers as ionomers for self-healing were done by Kalista et al.<sup>92-93</sup> and further investigated by Varley et al.<sup>85,94</sup>

Supramolecular polymers, in which the monomers are connected by non-covalent bonding, can be also used for self-healing. Cordier et al. reported the synthesis of a thermoreversible rubber from supramolecular assembly for application as a self-healing material. A cut between two pieces could be healed simply by bringing them in contact.<sup>95</sup> Burnworth et al. demonstrated a supramolecular polymer which can be healed optically by the use of ultraviolet light.<sup>96</sup> This approach is composed of low-molecular polymers with ligand-end groups which are linked non-covalently through metal-ligand interactions excitable by light.

An older approach is self-healing via molecular diffusion. Studies about the healing mechanism in styrene-isoprene-styrene block copolymers and polystyrene were carried out by O'Connor et al. and McGarel et al.<sup>97-99</sup> Healing via molecular diffusion and entanglement of dangling chains could further be performed in a polyurethane gel by Yamaguchi et al.<sup>100-101</sup>

### 2.3.2 Extrinsic self-healing: vascular

In vascular self-healing systems capillaries or hollow channels/fibers, which are incorporated into a matrix, are filled with the healing agents. Depending of the grade of interconnection networks are designated as one- (1D), two- (2D), or three- (3D) dimensional as shown in Figure 2.14.

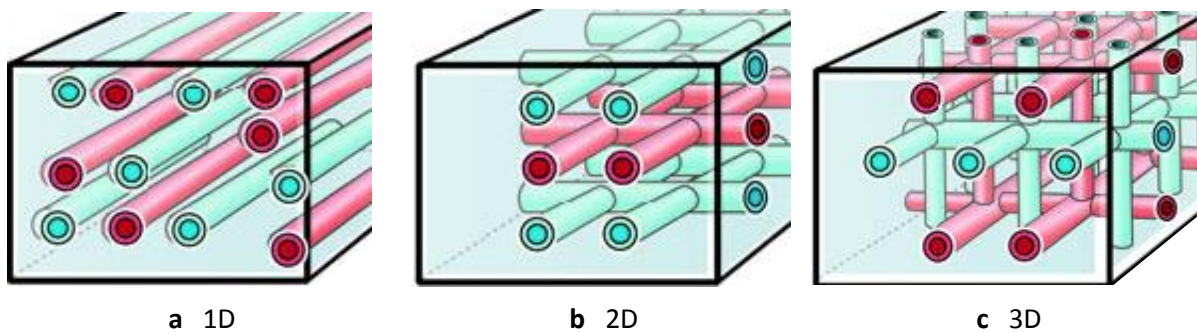


**Figure 2.14** Vascular healing materials classified according to the connectivity of the vascular network. (a) one-dimensional (1D), (b) two-dimensional (2D), and (c) three-dimensional (3D). Schemes are adapted from Blaiszik et al.<sup>82</sup>

In general, there are two main techniques for the preparation of network structures depending on the type of connectivity. On the one hand, hollow glass fibers (HGFs) as channels with a diameter of  $\sim 60 \mu\text{m}$  loaded with self-healing agents can be incorporated in the matrix. HGFs can be produced easily using the well-known glass hollow fiber drawing techniques. These vasculars show a high compatibility with many polymer matrices, and an inert behavior towards a lot of self-healing agents, such as two-part epoxy resin systems or cyanoacrylates. These fibers are often used for self-healing systems and involve advantages in workability, but networks are limited to 1D (Figure 2.14a).

2D or 3D networks are more challenging in preparation. The technique that is mainly used for the manufacture is the direct-ink writing of a fugitive ink framework followed by penetration with an uncured polymeric precursor. After solidification, the framework is taken out resulting in a hollow channel network embedded in the polymer matrix. It is possible to control both network form and the number of connections by this method, but the nature of the matrix material around the fugitive framework is limited.

A system with additional connection points between the vasculars has some advantages compared to 1D. There is a higher reliability in healing concerning possible blocking in the channels as well as a larger reservoir available for the healing at the local point. Furthermore, refilling of the agents after consumption can be performed more easily.

In contrast to the capsule-based system ([chapter 2.3.3](#)), the healing agents are brought in the channels after the network has been incorporated into the matrix. Therefore, the healing agents must have a certain surface wettability, chemical reactivity, and viscosity. A low surface wettability and a high viscosity of the healing agent can lead to an inefficient loading of the network, while chemical incompatibility between healing agent and network is fundamental for a long-term functioning system. These properties have also an influence on the design of the arterial network and especially on the diameter of the channels due to the effect of viscosity and wettability on the transport and release of the healing agents.

The network's wall stiffness, the adhesion between matrix and network, the network's volume fraction, as well as the channel distribution and uniformity have an influence on the mechanical properties of the matrix with an incorporated vascular network. In comparison to capsules-based system, the vascular system can access a larger reservoir and the network can be reloaded providing multiple healing.<sup>82</sup>

The first investigation of self-healing 1D systems were performed by Dry et al.<sup>6,102</sup> They investigated the healing performance of hollow fibers with a diameter of millimeters filled with a cyanoacrylate or a separated two-part epoxy system both dispersed in a matrix. Bleay et al.<sup>103</sup> arranged commercially available HGFs with a diameter of 15  $\mu\text{m}$  filled with various agents in unidirectional layers for laminated materials. Further, larger 60- $\mu\text{m}$ -diameter HGFs were produced by Pang et al.<sup>104-105</sup> in order to load the vascular system more effectively. Polyvinyl chloride tubes in a 2D network containing a separated two-part epoxy system were fabricated by Williams et al. within composite sandwich structures ([Figure 2.14b](#)).<sup>106-107</sup> Toohey et al.<sup>108-109</sup> produced a 3D interconnected vascular self-healing epoxy using direct-ink writing ([Figure 2.14c](#)). They created a 3D network of dicyclopentadiene (DCPD) monomer filled microchannels ( $\sim 200 \mu\text{m}$  in diameter) dispersed in an epoxy matrix, into which the Grubbs' catalyst was incorporated. Furthermore, hollow fibers filled with a two-part epoxy self-healing system were prepared in the way that one part is isolated from the other in order to hold them stable.<sup>110</sup>

### 2.3.3 Extrinsic self-healing: micro-/nanocapsules

In capsule-based self-healing materials the healing agents are encapsulated in the core of separate capsules. The capsules can be ruptured by damage or opened by trigger in order to release the healing agents and heal the crack. In contrast to intrinsic and vascular systems described in previous chapters, multiple healing is not possible because the healing agents are introduced in the capsules before the capsules have been integrated into the matrix. At the place where healing has occurred, the healing agents have reacted and therefore no further healing is possible. Basically, there are four different kinds of capsule-based self-healing systems, which are illustrated in Figure 2.15.<sup>82</sup>

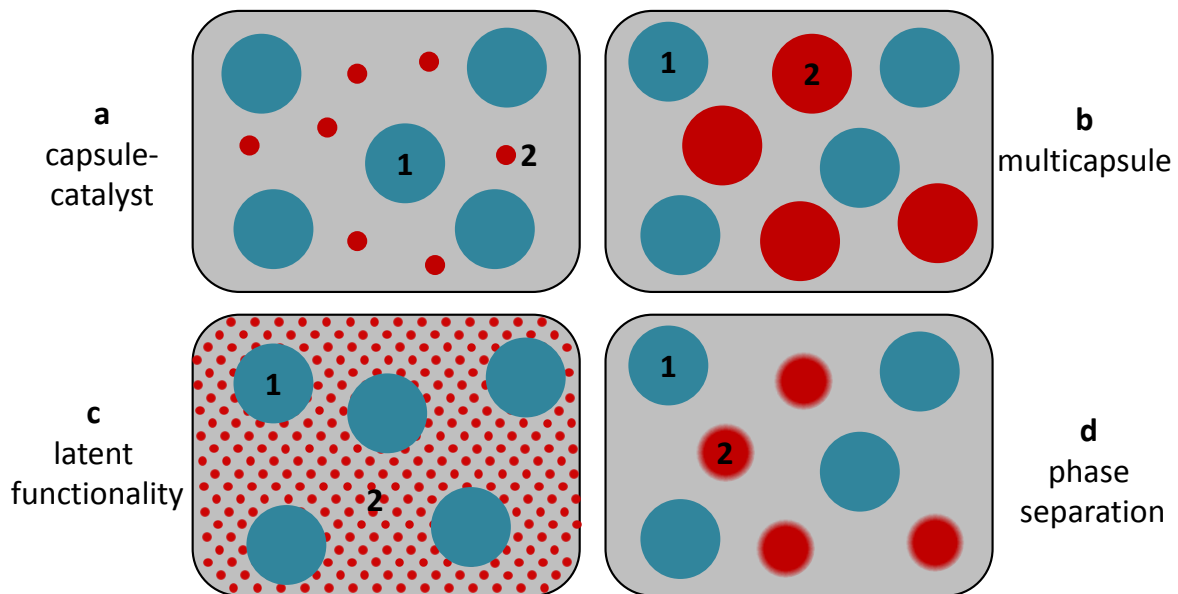


**Figure 2.15** Capsule-based self-healing materials consisting of two components labeled as 1 and 2. (a) capsules-catalyst: the healing agent is encapsulated and the catalyst is dispersed in the matrix, (b) multicapsule: both healing components are encapsulated, (c) latent functionality: healing reaction between one encapsulated healing agent and reactive groups available in the matrix, (d) phase separation: one component is encapsulated and the other one is present as phase-separated droplets within the matrix phase. This scheme is based on Blaiszik et al.<sup>82</sup>

In a *capsule-catalyst system*, the healing agent is encapsulated in the capsules and the appropriate catalyst is dispersed without further encapsulation (Figure 2.15a). This approach was firstly demonstrated by White et al using DCPD as liquid healing monomer encapsulated in urea-formaldehyde (UF) microcapsules in combination with Grubbs' first-generation

catalyst distributed in a epoxy matrix.<sup>7</sup> The autonomic healing concept is illustrated in Figure 2.16.

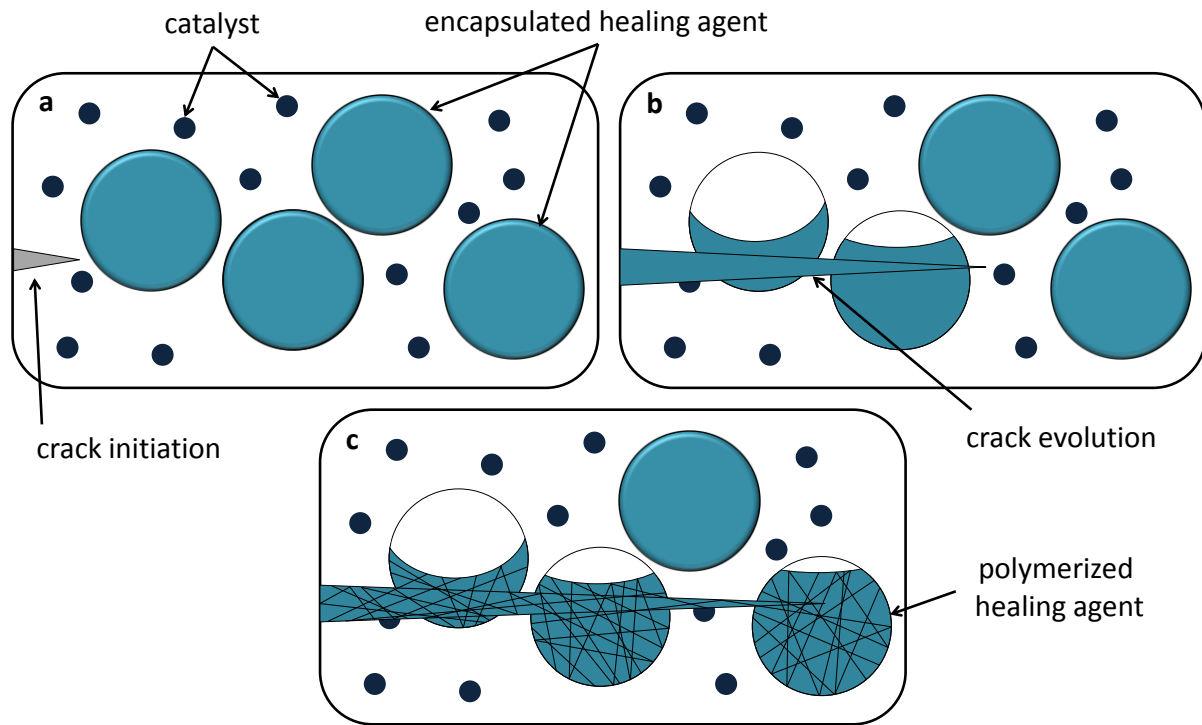


**Figure 2.16** Autonomic healing concept consisting of healing agent encapsulated in UF microcapsules and catalyst both incorporated into an epoxy matrix. (a) Crack formation due to damage event. (b) Crack increases and ruptures the capsules releasing the healing agent into the crack volume. (c) The healing agent polymerizes upon contact with catalyst healing the crack (based on White et al.<sup>7</sup>).

Brown et al. demonstrated significant healing efficiency in a row of publications concerning autonomic self-healing by in UF-microcapsules encapsulating DCPD and Grubbs' catalyst in the matrix.<sup>111-114</sup> The DCPD-Grubbs' system has been further incorporated into various bulk matrices such as epoxy,<sup>7,111-119</sup> fiber-reinforced epoxy composites,<sup>120-124</sup> epoxy vinyl ester,<sup>125</sup> and thermoplastic block copolymers.<sup>126</sup> Several ROMP catalysts were studied by Wilson et al.,<sup>127-128</sup> Kamphaus et al.,<sup>129</sup> and Li et al.<sup>130</sup> in terms of effectiveness. Rule et al. embedded Grubbs' catalyst in wax microspheres to conserve its activity and to increase the dispersability in the epoxy matrix.<sup>131</sup> Various diene monomer derivatives, e.g. 5-ethylidene-2-norbornene, were tested by Liu et al. and Lee et al.<sup>132-133</sup> Moll et al. incorporated microcapsules filled with DCPD and Grubbs' catalyst in a glass fiber-reinforced epoxy composites for re-establishment of barrier properties.<sup>120</sup> A two-part self-healing system



consisting of epoxy and imidazole was reported by Rong et al. and Yin et al.<sup>134-137</sup> Both parts were encapsulated separately in UF-microcapsules, which were embedded into epoxy matrix.

The second described capsule-based system is called *multicapsule*. In this approach, both self-healing agents are encapsulated separately (Figure 2.15b). Keller et al. showed a system consisting of discretely microencapsulated poly(dimethyl siloxane) (PDMS) and the appropriate crosslinker.<sup>138-139</sup> Further, Cho et al.<sup>140</sup> used PDMS filled capsules in combination with encapsulated dimethyldiiododecanoate tin (DMDNT) catalyst for anticorrosion applications, and Beiermann et al.<sup>141</sup> varied the catalyst part to encapsulated di-*n*-butyltin dilaurate (DBTL). Yuan et al. demonstrated an alternative self-healing approach using encapsulated epoxide and mercaptan for healing an epoxy matrix.<sup>142</sup> Jin et al. used a similar two part system consisting of an aliphatic polyamine and a monomeric epoxide encapsulated in discrete capsules.<sup>143</sup> Billiet et al. reported the use of maleimide chemistry for self-healing applications, in which they used the Michael addition reaction between bismaleimides and amines or thiols.<sup>144</sup> A multicapsule system consisting of capsules filled with epoxy-resin on the one and boron trifluoride diethyl etherate  $[(C_2H_5)_2O \cdot BF_3]$  on the other hand for a cationic chain polymerization as self-healing reaction was presented by Xiao et al.<sup>145-146</sup> Further, the click reaction between azide and alkyne as a self-healing system was shown by Gragert et al.<sup>147</sup> They verified the healing reaction by incorporating microcapsules filled with polymeric azides and alkyne monomers into a polymer matrix containing a  $Cu^I$ -catalyst.

In the self-healing system characterized as *latent functionality*, one part of the healing agent is encapsulated or dispersed as particles, and the other part is composed of remaining reactive functional groups in the matrix or an environmental stimulus (Figure 2.15c). Caruso et al. demonstrated solvent-promoted and resin-solvent self-healing based on the polymerization between the matrix carrying amine groups and a healing agent encapsulated in UF-microcapsules.<sup>148-149</sup> The incorporation of thermosetting, meltable, epoxy particles in a coldsetting epoxy composite matrix as another latent approach was reported by Zako et al.<sup>150</sup> Suryanarayana et al. described a remendable system based on microcapsules containing linseed oil, which was found to prevent corrosion after release and oxidation due to environmental exposure.<sup>151</sup> In addition, the encapsulation of various healing agents in PU,

acrylic and other paints showed reduced incidence of corrosion in steel.<sup>152</sup> Sauvant-Moynot et al. reported a self-healing coating based on encapsulated self-curing epoxy-amine adducts.<sup>153</sup> The corrosion inhibitor benzotriazol was entrapped into mesoporous silica particles, which were embedded in a sol-gel coating by Grigoriev et al.<sup>154</sup> PU-microcapsules containing low reactive isophorone diisocyanate (IPDI) as core material, which is able to serve as a one-part self-healing system in an aqueous environment, were fabricated by Yang et al.<sup>155</sup> Huang et al. extended this approach by encapsulating the more reactive hexamethylene diisocyanate (HDI) for self-healing in anticorrosion layers.<sup>156</sup> Another one-part self-healing approach is based on glycidyl methacrylate (GMA)-loaded microcapsules which act as a healant in epoxy matrices by solvent effects and chemical reactions.<sup>157</sup> Such GMA microcapsules were further dispersed in a matrix composed of living poly(methyl methacrylate) (PMMA) synthesized by ATRP.<sup>158</sup> In addition, the results of the embedment of GMA capsules in a matrix of living polystyrene (PS) synthesized by reversible addition-fragmentation chain transfer polymerization (RAFT) were published by Yao et al.<sup>159</sup>

In the fourth capsules-based healing system, designated as *phase separation*, one healing agent is encapsulated and the other one is present as phase-separated droplets in the matrix material (Figure 2.15d). Cho et al. reported an example for the approach based on hydroxyl end-functionalized polydimethylsiloxane (HOPDMS) and polydiethoxysiloxane (PDES) phase-separated in an epoxy matrix. UF-microcapsules filled with tin catalysts (DBTL or DMDNT) were also dispersed in the matrix for the catalysis of polycondensation healing reaction between HOPDMS and PDES in the event of rupture and release.<sup>140,160</sup>

In the self-healing approaches mentioned in this chapter, the capsules and healing agents ranged from 5 to 100  $\mu\text{m}$  in diameter. This size range is best for healing large damage events, but not for healing cracks in micron or nanometer size. For healing very small damage event, submicron healing materials are beneficial. In addition, to incorporate capsules in thin layers of several microns, a capsule diameter in submicron range is essential. Due to the significance of nanocapsules for this thesis, the reported publications in relation with nanocontainers in self-healing approaches are presented separately from the various capsule-based approaches. Blaiszik et al. reported firstly the fabrication of submicron capsules containing DCPD as healing agent. The encapsulation method was adapted from White et al.<sup>7</sup> for UF-microcapsules, adding a sonication step and hexadecane for the droplet

stability in order to reduce the size of the capsules.<sup>161</sup> These UF-nanocapsules were further coated with a silica layer to functionalize and protect the capsules, and to provide less aggregation when they are dispersed in the epoxy matrix.<sup>162</sup> The encapsulation of a self-healing agent suitable for metathesis polymerization in nanocapsules via free-radical polymerization of styrene in miniemulsion was demonstrated by van den Dungen et al.<sup>163</sup> Ouyang et al. reported the encapsulation of triethylene glycol dimethacrylate (TEGDMA), a suitable monomer for self-healing reactions based on radical polymerization, in polyurethane submicron nanocontainers by interfacial polycondensation in miniemulsion.<sup>164</sup> The fabrication of silica nanocontainer containing 2-mercaptobenzothiazole for corrosion protection, which also showed self-healing properties after a manually inflicted damage in the anticorrosion coating, was demonstrated by Maia et al.<sup>165</sup>

#### 2.3.4 Chemistry of self-healing

This chapter should deal with the chemistry of self-healing more in detail. Various types of self-healing reactions and therefore agents have been reported in the literature and discussed in [chapter 2.3.3](#), which are listed in order of reaction in [Table 2.3](#). All these self-healing approaches have in common that the reactions proceed at room temperature without trigger.

## 2 Theoretical section

**Table 2.3** Literature summary of chemicals and reactions used for capsule-based self-healing approaches.

Self-healing reaction	self-healing agent 1	self-healing agent 2	catalyst	ref.
ring-opening metathesis polymerization (ROMP)	dicyclopentadiene (DCPD) 5-ethyliden-2-norbornene (ENB)		Grubbs' catalysts tungsten(VI) chloride (WCl <sub>6</sub> )	7,111- 114,116- 133,162,166- 167
anionic polymerization	epoxy		CuBr <sub>2</sub> (2-methylimidazole) <sub>4</sub>	134-137
cationic polymerization	epoxy		boron trifluoride diethyl etherate (C <sub>2</sub> H <sub>5</sub> ) <sub>2</sub> O·BF <sub>3</sub>	145-146
polyaddition	epoxy	mercaptan	amine	142
polyaddition	epoxy	amine		143,153,157, 168-169
polyaddition	isophorone diisocyanate (IPDI) hexamethylenediamine (HDI)	H <sub>2</sub> O		155,156
<i>Michael</i> polyaddition	bismaleimide	amine thiol		144
polycycloaddition ("click"-reaction)	polymeric azide	alkyne	bromo-tris(triphenylphosphin)-copper <sup>I</sup> -catalyst Cu <sup>I</sup> Br(PPh <sub>3</sub> ) <sub>3</sub>	147
polycondensation	silanol-terminated PDMS (HOPDMS)	poly(diethoxysilane) (PDES)	di- <i>n</i> -butyltin dilaurate (DBTL) dimethyldineodecanoate tin (DMDNT)	140,141,160
hydrosilylation	hydrosiloxane copolymer	vinyl-terminated PDMS	Pt catalyst	138-139
living free-radical polymerization	glycidyl methacrylate (GMA)	living PMMA (ATRP) living PS (RAFT)		158,159

The synthetic schemes for the different types of healing reactions are described hereinafter (Figure 2.17a,b).

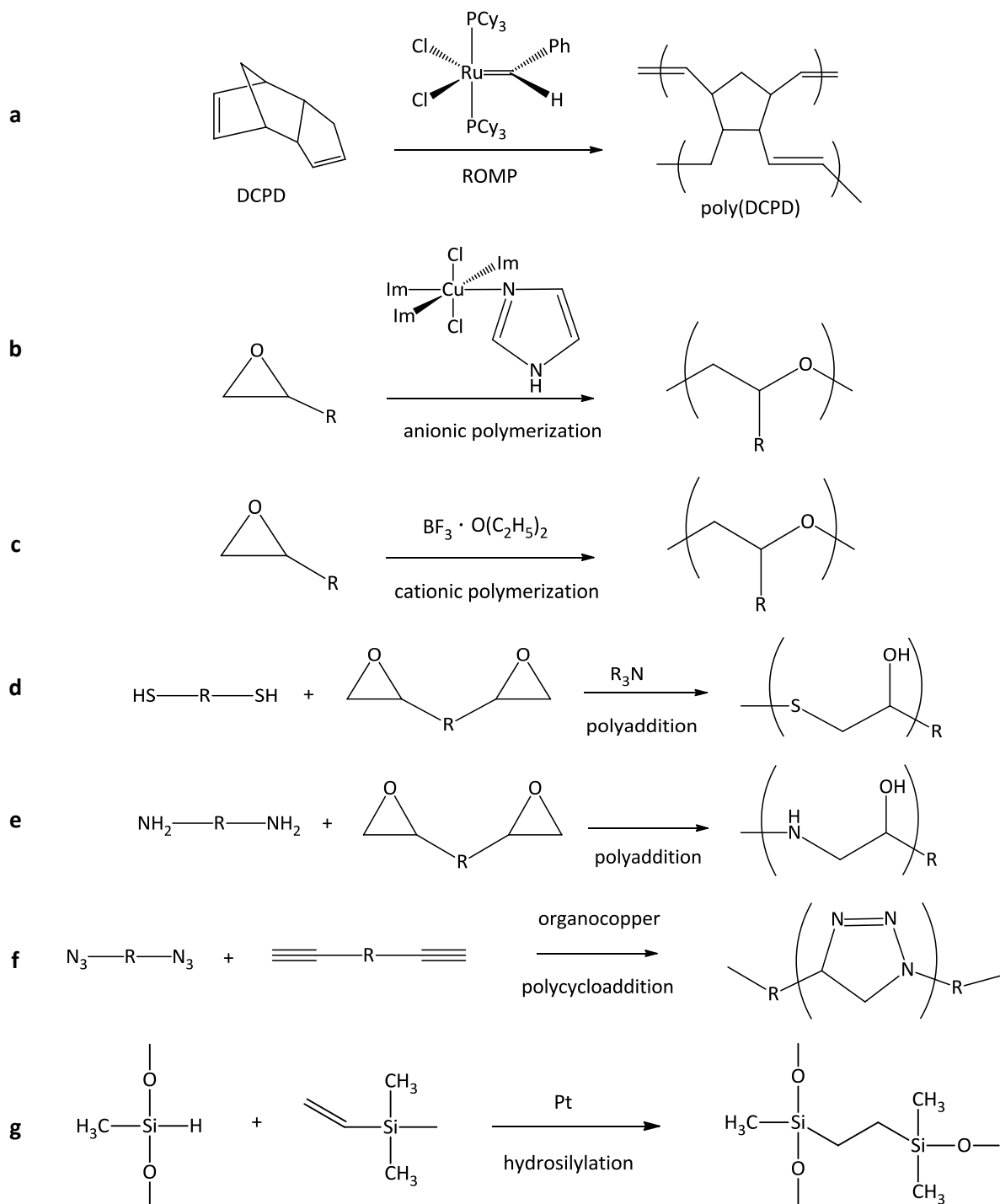


**Figure 2.17a** Reaction schemes for the discussed self-healing reactions. **(a)** ring-opening metathesis polymerization (ROMP) performed with norbornene-derivatives and ROMP catalysts; **(b), (c)** encapsulated epoxy was polymerized anionically or cationically in presence of respective catalyst; **(d)** polyaddition reaction between epoxy and mercaptan catalyzed by tertiary amines; **(e)** polyaddition between epoxy and amine; **(f)** cycloaddition of polymeric azide and alkyne (“click”-reaction) catalyzed by copper catalyst; **(g)** hydrosilylation of hydrosiloxane polymer and vinyl-terminated PDMS.

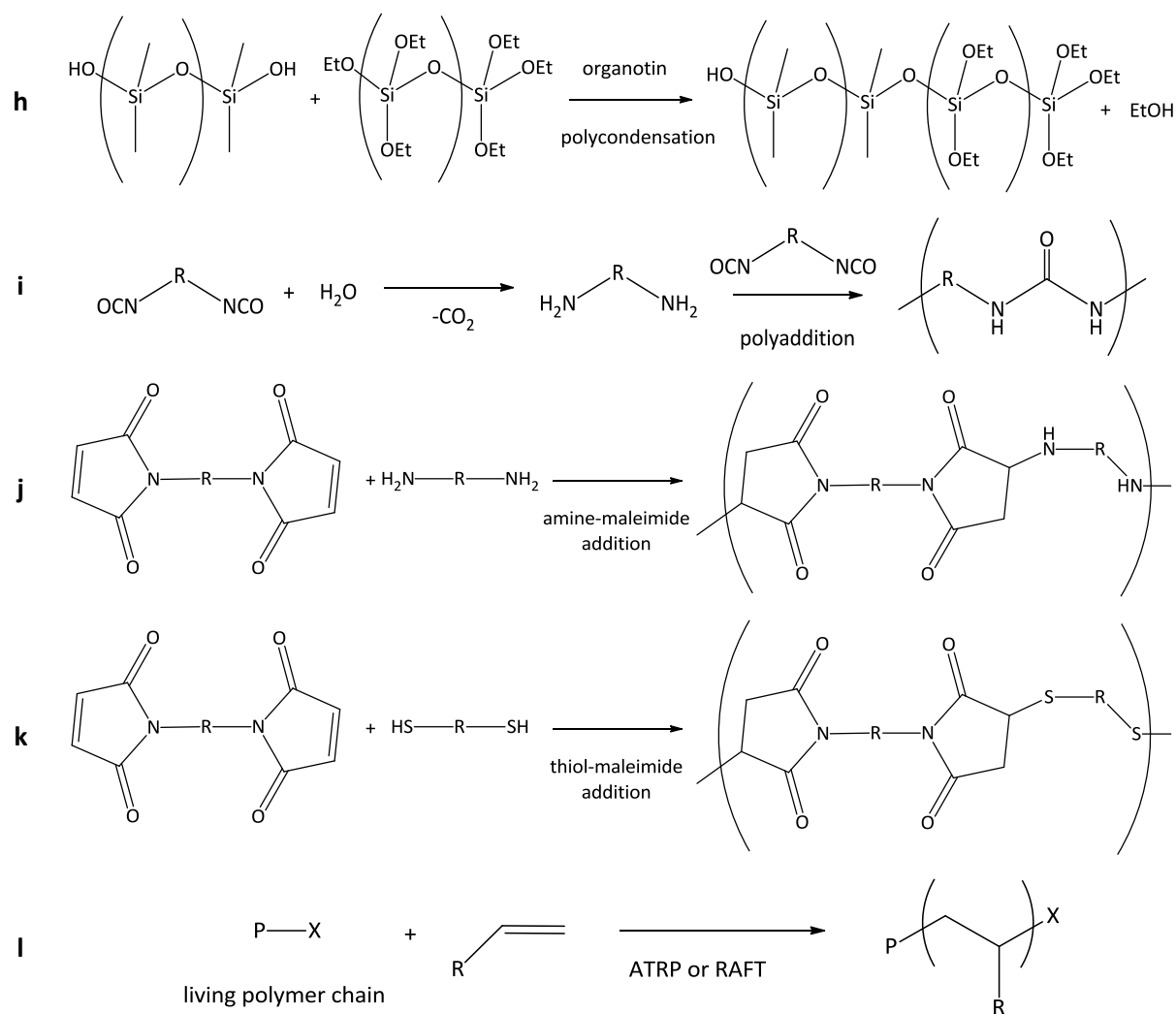


**Figure 2.17b** Reaction schemes for the discussed self-healing reactions. **(h)** polycondensation between silanol-terminated PDMS (HOPDMS) and poly(diethoxysilane) (PDES) in presence of various tin catalysts; **(i)** polyaddition reaction with diisocyanates as healing agents: parts of the encapsulated diisocyanates react with environmental water to amines, which further polymerize with the residual diisocyanates; **(j)**, **(k)** maleimide chemistry based self-healing reaction with multifunctional amines or thiols, respectively; **(l)** living PMMA synthesized by ATRP and living PS synthesized by RAFT, which were used as matrix materials for the healing reaction with the encapsulated vinyl monomers.

### 2.3.5 Conventional and self-healing coatings for corrosion prevention

As mentioned in the introduction, there is a need for an alternative corrosion protection due to regulatory restrictions for the use of chromium(VI) in anticorrosive layers. The concept of self-healing combined with conventional anticorrosive layers is a promising strategy for replacing chromates. The new aspects of the capsule-based self-healing approach and a schematic illustration of the arrangement of the former conventional corrosion prevention are given in [Figure 2.18 left](#).

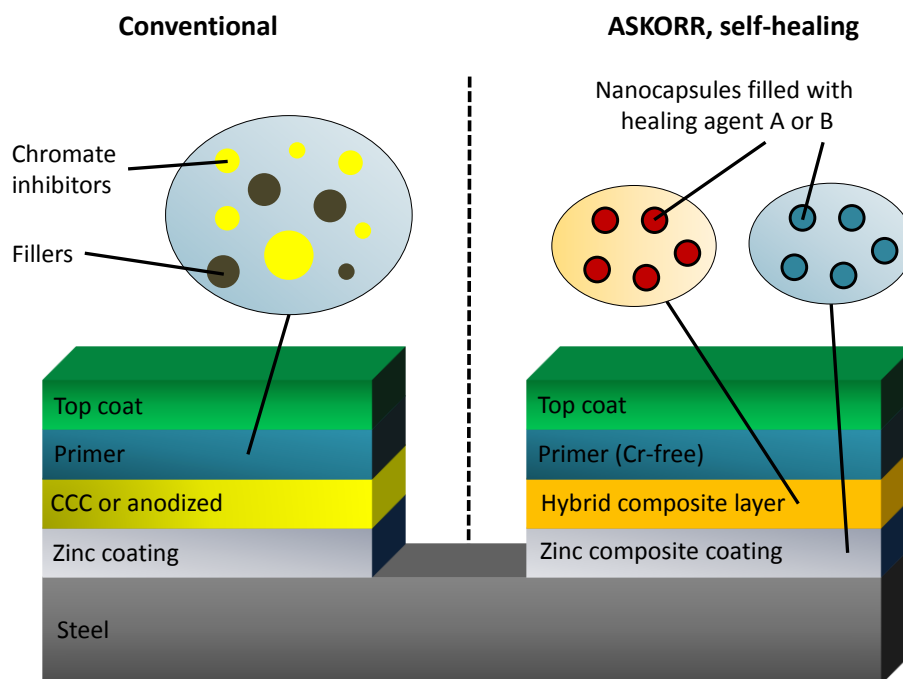


**Figure 2.18** Schematic illustration of a conventional (left) and the proposed ASKORR self-healing coating (right) for corrosion protection of steel (based on Hughes et al.<sup>170</sup>).

In a classical anticorrosion system, steel is covered by a protective zinc layer having a thickness of few microns. This is followed by the deposition of a 100 – 200 nm thick chromate conversion coating (CCC) or an anodized coating produced from a chromic acid bath with a thickness up to several microns. On this base, a 20 – 25  $\mu\text{m}$  thick primer layer (normally an epoxy resin) is deposited, which contains fillers and chromate inhibitors (e.g. strontium chromate) in a quantity up to 30 wt%. The end step in these processes results

in the formation of the top coat, which acts as a barrier for water and electrolytes and consists usually of a polyurethane-based layer containing pigments and fillers.<sup>170</sup>

The idea of the ASKORR – an acronym of “*Aktive Schichten für den Korrosionsschutz*” – concept is based on the replacement of chromates by incorporating self-healing materials into the protection layers (Figure 2.18 right). Therefore, the components of a two-part self-healing system are encapsulated in different capsules. One type of capsules is incorporated into the zinc coating, while the other type is embedded in a hybrid composite layer, which is deposited instead of the Cr-containing CCC or anodized coating on top of the zinc.



## 3 Methods

### 3.1 Dynamic light scattering

By means of dynamic light scattering (DLS), it is possible to determine the hydrodynamic particle size of dispersed colloids and their size distribution. This method facilitates the measurement of particles with particle sizes from below 5 nm to several microns.

The setup of a typical dynamic light scattering device is shown in [Figure 3.1](#). In this technique, a transparent cuvette filled with the diluted dispersion is irradiated by a laser beam. The light is scattered in all directions by scattering centers, which can be dissolved macromolecules, droplets of emulsions or dispersed particles. Due to the Brownian motion of the scattering centers, their position changes continuously, and therefore there is a steady variation in the interference pattern of the scattering. As a consequence, the detected signal intensity varies over the time. Frequency and magnitude of the particle movement depends on the viscosity of the solvent, the temperature, and the size of the moving colloids. Small particles show fast movement, which is expressed in rapidly changing signals. Large colloids, in contrast, move slower which leads to a slower change of the intensity at the photomultiplier detector (PMT). In dependence of the particle size the intensity measurements are performed in the range of micro- or milliseconds. By means of the autocorrelation function, the translation diffusion coefficient  $D_T$  of the particles can be calculated, which is according to the Stokes-Einstein equation ([Equation 4](#)) indirect proportional to the hydrodynamic radius of the particles:<sup>171-172</sup>

$$R_H = \frac{k_B \cdot T}{6 \cdot \pi \cdot \eta \cdot D_T} \quad \text{Equation 4}$$

where  $R_H$  is the hydrodynamic diameter,  $k_B$  the Boltzmann constant,  $T$  the temperature,  $\eta$  the dynamic viscosity, and  $D_T$  the translational diffusion coefficient.

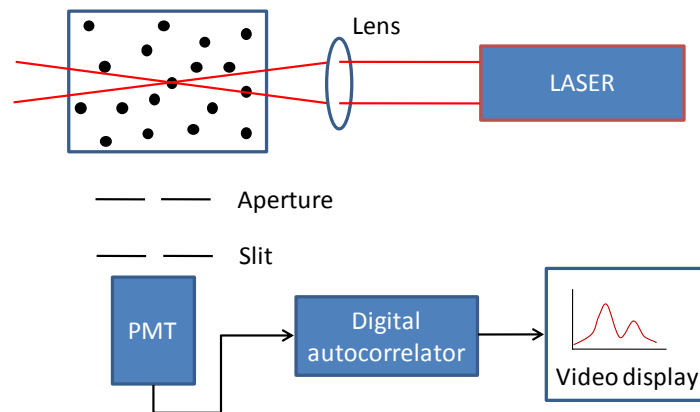


**Figure 3.1** Schematic configuration of a dynamic light scattering device. Illustration is based on a figure taken from Nicomp 380 User Manual.<sup>171</sup>

### 3.2 Transmission electron microscopy

The limit of resolution in conventional light microscopy is restricted by *Abbe's Equation* (Equation 5). The resolution (minimum resolvable distance)  $r$  is therein described by the wavelength  $\lambda$  of the irradiated light, the refractive index  $n$  of the medium, and the aperture angle  $\alpha$ :

$$r = \frac{\lambda}{2 \cdot n \cdot \sin \alpha} \quad \text{Equation 5}$$

The resolution in conventional optical microscopy is therefore limited to around 200 nm. Electron microscopy, however, makes use of the wave character of the electron instead of the wavelength of the visual light resulting in a significant increase of resolution up to nanometer scale. The transmission electron microscope (TEM) is similar to the configuration of a conventional light microscope (Figure 3.2).

In the electron gun, electrons are created by thermal emission of an incandescent cathode and accelerated by high voltage (50 – 200 kV). High vacuum is applied to the equipment in order to avoid deflection by scattering of electrons with molecules in the gas phase.

The electron beam is bundled by electromagnetic condenser lenses and further passes through the specimen. There, various interactions of the electrons with the atoms of the sample take place including absorption, diffraction, elastic and inelastic scattering. The two latter types of scattering are predominant for the image formation. After passing through the specimen, the electrons are focused by objective lenses and the intermediate image is

expanded to the fluorescent screen or other imaging devices by the projector lenses. The thickness of the sample should be below 100 nm to ensure transmissibility of the electrons through the sample. The contrast of the sample depends on the electron density: the higher the density, the darker the sample.<sup>173</sup>

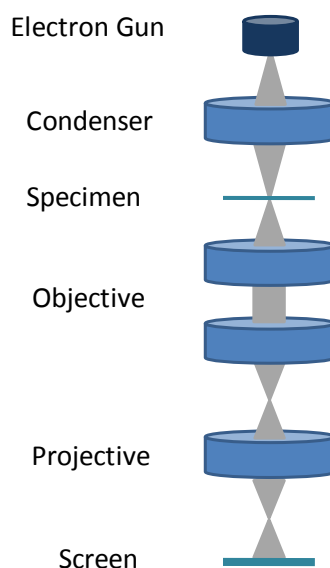


**Figure 3.2** Schematic configuration of a transmission electron microscope (TEM).

In this thesis, the TEM was mainly used to check which colloidal morphology – particle or core-shell structure - was obtained after synthesis.

### 3.3 Scanning electron microscopy

While the TEM is comparable with a transmitted-light microscope, the scanning electron microscope (SEM) is similar to a reflected light microscope. An electron beam, which has typically an energy ranging from 0.1 to 50 keV, is thermionically emitted from an electron gun and focused by condenser lenses to a small spot (1 – 10 nm in diameter) on the surface of the specimen. The beam does not pass through the sample but scans the surface piece by piece. SEM has the advantage in comparison to TEM that thicker samples can be measured and a certain depth of field is presentable. When the electron beam hits onto the sample surface, various interactions between the electrons and the atomic nuclei take place within the interaction volume (Figure 3.3).

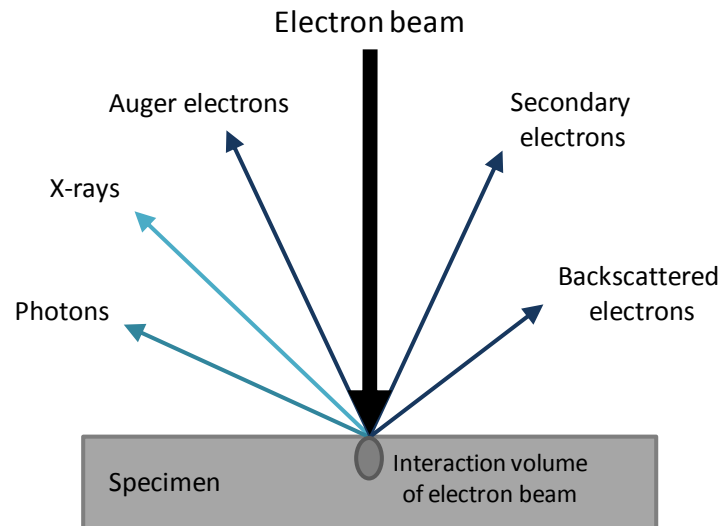


**Figure 3.3** Schematic illustration of the interaction of the electron beam with the sample.

The tear-drop shaped interaction volume of the electron beam (Figure 3.3) increases when the acceleration voltage is raised. Moreover, a lower average atomic number of the sample induces a larger interaction volume. Inelastic interactions lead to the emission of secondary electrons, Auger electrons, X-rays, and photons whereas backscattered electrons are created by elastic interactions. The typical image recorded by scanning electron microscopy is made from detection of secondary electrons. Due to their relative low kinetic energy, they are often directly absorbed by the sample, and therefore only secondary electrons from the sample surface can be detected. Steep surfaces or edges appear brighter than flat surfaces because more electrons can escape from elevations. This provides the possibility to obtain information about the surface topography.<sup>174</sup>

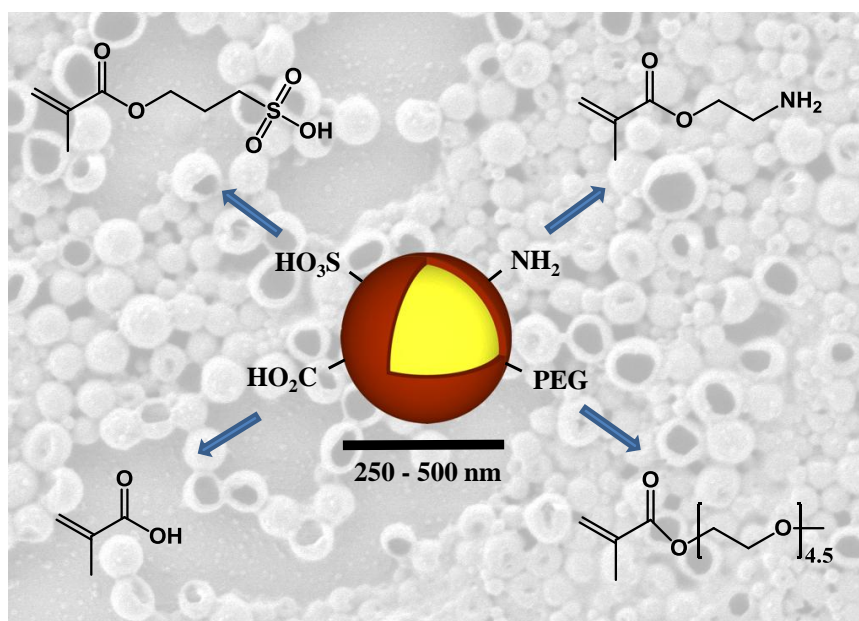
The SEM was mainly used to verify the colloidal morphology observed by TEM measurements.

## Chapter 4

# Efficient encapsulation of self-healing agents in polymer nanocontainers functionalized by orthogonal reactions

based on

*Macromolecules* **2012**, 45, 6324-6332.



#### 4 Efficient encapsulation of self-healing agents in polymer nanocontainers functionalized by orthogonal reactions

The two main challenges for designing useful capsule-based self-healing materials are a good dispersion of the capsules in the matrix and an efficient encapsulation of the healing agents. The first point is a common issue in composites and hybrid materials and is usually solved by incorporating functional groups at the surface of the fillers.<sup>12-14</sup> Thus, an ideal container for self-healing materials should be a capsule with functional groups on the surface of the shell. Miniemulsion polymerization can be used for producing materials matching the requirements mentioned above that are 1) functionality and 2) encapsulation. A fulfillment of the second requirement was presented by Van den Dungen and Klumpermann.<sup>163</sup> The authors polymerized miniemulsion droplets of styrene in the presence of a norbornene derivative. However, no hollow capsules could be observed under TEM and no functionality was included into the shell. As already mentioned in [chapter 2.2.3.2](#), a straightforward approach to yield polymer nanocapsules with functional groups at their surfaces dispersed in water is the copolymerization of a hydrophobic monomer in the presence of a small amount of hydrophilic functional monomer dissolved in the aqueous continuous phase. Although functional groups were introduced as comonomers in nanoparticles and nanocapsules, there is no report about the functionalization of core-shell colloids produced in miniemulsion with a liquid healing agent in the core. In this chapter, the synthesis of nanocapsules via an orthogonal reaction, their characterization, and investigations on their stability is presented. The structures of the hollow nanocapsules were clearly identified by transmission electron microscopy.

##### 4.1 Miniemulsion polymerization in the presence of a nonsolvent in the droplets

Monomers for metathesis polymerization were selected for the encapsulation because this reaction can be processed at room temperature, hence, allowing a healing reaction without additional heating or irradiation (for reaction scheme see [Figure 2.17a](#)). Other monomers are then used in order to synthesize a polymer shell around the monomer to be encapsulated by free-radical polymerization. To clearly distinguish between the monomers

for metathesis and for free-radical polymerization, the annotation monomer-[m] and monomer-[r] is used, respectively.

The formation of a polymer shell around an originally homogeneous droplet composed of liquid monomer-[r] and nonsolvent, is triggered by the polymerization of the monomer-[r] and the subsequent phase separation between the polymer formed and the nonsolvent.<sup>65</sup> In this case, the scenario is different since the original droplet is composed of a homogeneous mixture of the hydrophobic monomer-[r] styrene, a nonsolvent, and additionally the dicyclopentadiene (DCPD) which is a solvent for the polymer produced from monomer-[r] (Figure 4.1).

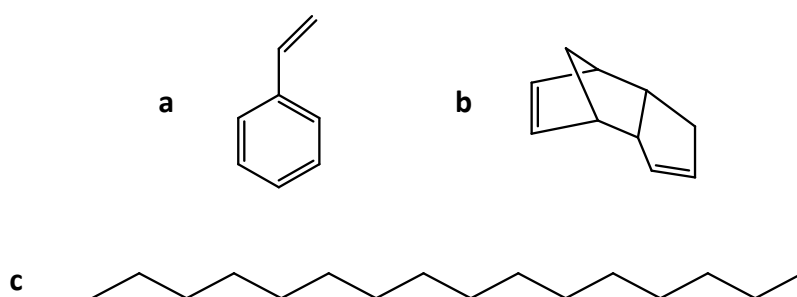


**Figure 4.1** Chemical structures of (a) monomer-[r] styrene, (b) monomer-[m] dicyclopentadiene (DCPD), and (c) the nonsolvent hexadecane (HD).

The liquid present at the end of the polymerization is therefore composed of the DCPD, the nonsolvent, and possibly some non-polymerized styrene. Therefore, the successful formation of nanocapsules is directly dependent on the solvent quality of the liquid core given by its *Hildebrandt* solubility parameter  $\delta$ . Solvents with low  $\delta$  such as alkanes<sup>65,175</sup> were already chosen as liquid core in direct miniemulsions for synthesizing nanocapsules. The thermodynamical considerations for the successful formation of core-shell structures from a three-component mixture are described by Torza and Mason (chapter 2.2.2).

## 4.2 Synthesis of functional nanocontainers

The introduction of a hydrophilic monomer in the aqueous phase of a direct miniemulsion of hydrophobic monomer is a straightforward method to produce functional nanoparticles (see chapter 2.2.3.2). Here, different (meth)acrylate monomers with amino, sulfonate, carboxylic acid, and PEG functionality were used (Figure 4.2).

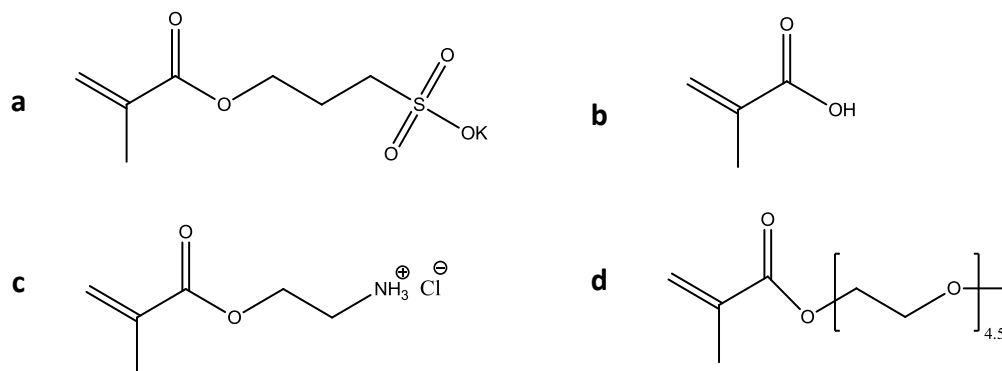


**Figure 4.2** Chemical structures of (a) sulfopropyl methacrylate (SMA), (b) methacrylic acid (MAA), (c) 2-aminoethyl methacrylate hydrochloride (AEMA), (d) poly(ethylene glycol) methacrylate (PEGMA).

Since one of the objective of this work was to encapsulate DCPD, it was verified that DCPD did not participate in the polymerization reaction yielding the capsules shell. Therefore, the dispersion JF166-1 (Table 4.1) synthesized in D<sub>2</sub>O was dissolved in THF-*d*<sub>8</sub> and measured by <sup>1</sup>H NMR spectroscopy (Figure 4.3). The spectrum was compared with the spectra of the monomer DCPD and the polymer PDCPD.<sup>176</sup> As expected, DCPD was not polymerized due to the absence of resonance stabilization and steric hindrance in the DCPD radical. The fact that the peaks at about 5.4 and 5.9 ppm are still well separated after encapsulation shows that DCPD is sufficiently inert towards radical polymerization because the presence of PDCPD would lead to a significant broadening of these signals. Van den Dungen et al. observed the same behavior for the free-radical polymerization of styrene in the presence of a dinorbornene.<sup>163</sup>

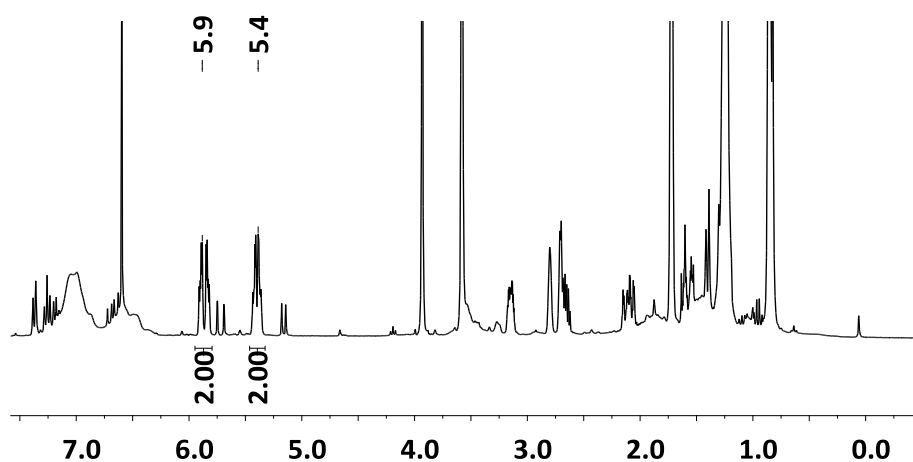


**Figure 4.3** <sup>1</sup>H NMR spectrum of sample JF166-1 synthesized with D<sub>2</sub>O and further dissolved in THF-*d*<sub>8</sub>.



The synthesized latexes were found to be stable after polymerization and hydrodynamic diameters were measured to be between 200 and 500 nm depending on the nature and quantity of the comonomers and surfactants (Table 4.1).

**Table 4.1** Characteristics including number of charges/nm<sup>2</sup> and  $\zeta$  potential for the dialyzed dispersions of functional nanocapsules (DCPD:HD = 50:50 [wt:wt] and core:shell = 2:1 [wt:wt]).

Entry	comonomer		functional groups		$\xi$ [mV]	$D_h$ [nm]	conversion [%]	
	nature	amount [wt%]	nature	[nm <sup>-2</sup> ]			styrene	comonomer
JF145-3	-	-	-	-	-	290 ± 100	65	-
JF125-2 <sup>a</sup>	-	-	-	-	-	340 ± 90	-	-
JF166-1	SMA	9	SO <sub>3</sub> <sup>-</sup>	3.8	-57 ± 9	310 ± 90	74	64
JF86-3 <sup>a</sup>	SMA	9	SO <sub>3</sub> <sup>-</sup>	-	-	320 ± 60	-	-
JF166-2	MAA	9	COO <sup>-</sup>	0.4	-59 ± 9	260 ± 80	86	35
JF166-3	AEMA	9	NH <sub>3</sub> <sup>+</sup>	2.9	+58 ± 8	440 ± 170	76	65
JF166-4	SMA	8.5	SO <sub>3</sub> <sup>-</sup>	3.1	-57 ± 10	240 ± 30	56	-
	PEGMA	5.7						
JF118-3 <sup>a</sup>	SMA	8.5	SO <sub>3</sub> <sup>-</sup>	-	-	210 ± 50	-	-
	PEGMA	5.7						
JF86-1 <sup>b</sup>	SMA	8.5	SO <sub>3</sub> <sup>-</sup>	-	-	300 ± 60	-	-
	PEGMA	5.7						
JF166-5	MAA	8.5	COO <sup>-</sup>	0.7	-63 ± 7	270 ± 80	54	-
	PEGMA	5.7						
JF166-6	AEMA	8.5	NH <sub>3</sub> <sup>+</sup>	4.5	+62 ± 9	490 ± 170	73	76
	PEGMA	5.7						
JF64-1	PEGMA	5.7	-	-	-	280 ± 80	-	-

<sup>a</sup> DVB instead of styrene for crosslinking;

<sup>b</sup> mixture of DVB and styrene (DVB:S = 50.5:49.5 [wt:wt]).

Firstly, the structure of the nanocapsules synthesized with and without a hydrophilic monomer was compared. Since the organic liquids are not present in the high vacuum chambers of the microscope, it is expected that a core-shell particle morphology in dispersion yields a hollow capsular structure under TEM observations. The micrographs revealed that the homopolymerization of styrene yielded a mixture of monolithic particles and capsules with an average hydrodynamic diameter of 290 nm (Table 4.1, Figure 4.4a, Entry JF145-3).

On the contrary, the polymerization of DVB yielded only nanocapsules (Figure 4.4b, Entry JF125–2). This is explained by the higher hydrophilicity of the vinyl bonds present in PDVB compared to the saturated bonds in PS.

Nanocapsules were obtained when styrene was copolymerized with a hydrophilic functional monomer, regardless of its chemical nature. (Figure 4.4). The hydrophilic monomer is then used as functional component introduced via an orthogonal reaction and simultaneously as structure-directing agent for yielding a clear phase separation between the polymer and the liquid core. The latter allows the formation of a polymer shell at the interface of the miniemulsion droplets. SEM microscopy was performed to verify that the colloids were spherical since the observations by TEM could theoretically indicate the presence of hollow capsules but also of rings or hollow cylinders. As expected, spherical colloids were observed as shown in Figure 4.4l,m. It should be noted that SEM images show burst or collapsed capsules due to the applied vacuum during measurement. Indeed, the fact that the holes are not randomly oriented but systematically pointing opposite to the substrate is an indication that the holes are created by the vacuum.

The distribution of the charged functional groups on the surface of the dialyzed nanocapsules could be determined (Table 4.1) with several assumptions as described in detail in the experimental part (chapter 9.3). The amount of charges per nm<sup>2</sup> on the nanocapsule surface is higher than the typical values obtained for monolithic nanoparticles synthesized in similar conditions. This is explained by the fact that in a polymerization of a homogeneous droplet of monomer, the functional monomers can be also buried in the particle, which is unlikely to happen here because the liquid core is a bad solvent. This is confirmed by the net negative or positive values of the  $\zeta$  potential measured for the dialyzed dispersions of nanocapsules (Table 4.1).

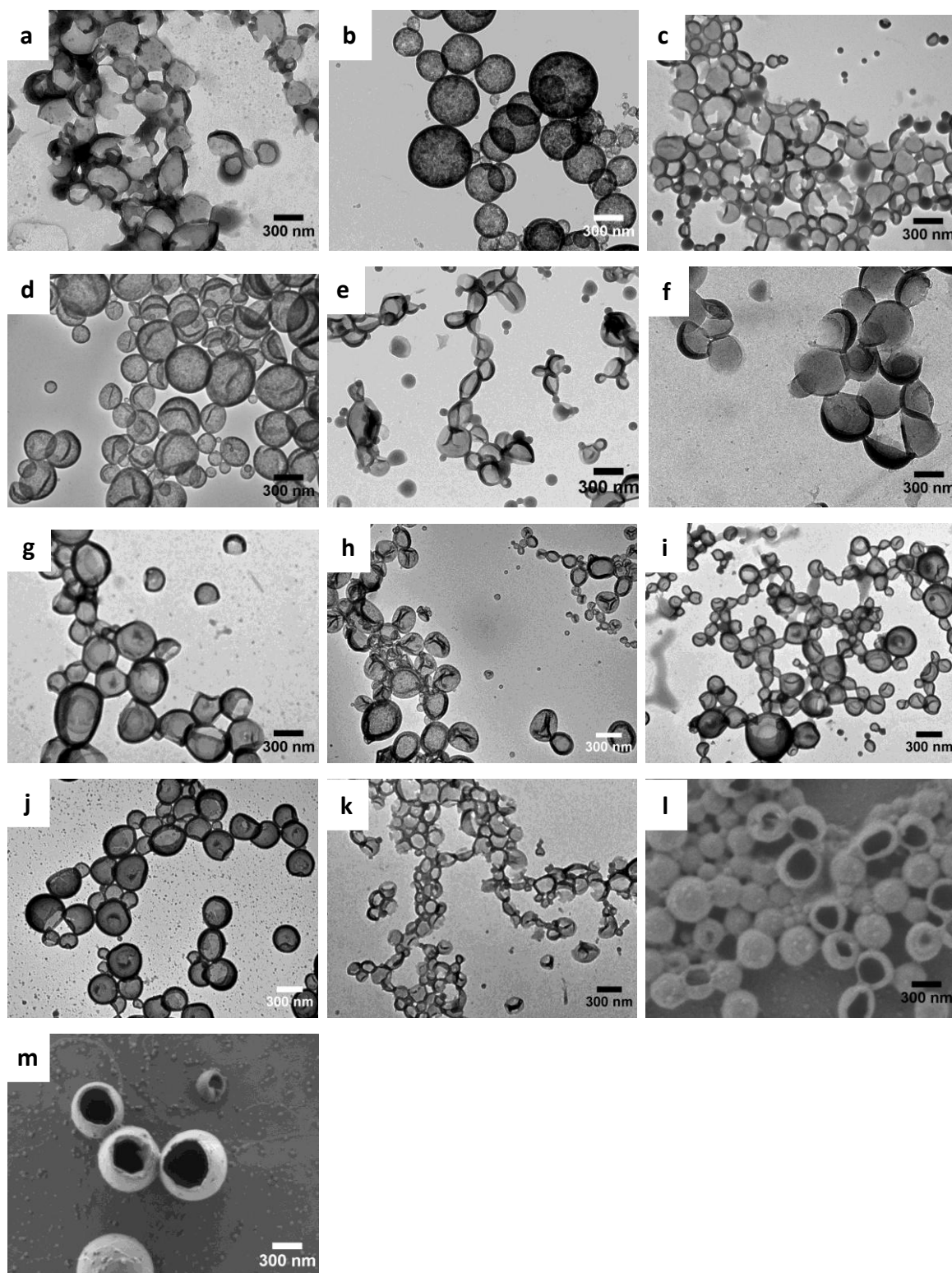


**Figure 4.4** TEM micrographs of dried colloids obtained from the samples (a) JF145-3 (PS), (b) JF125-2 (PDVB), (c) JF166-1 P(S-co-SMA), (d) JF86-3 P(DVB-co-SMA), (e) JF166-2 P(S-co-MAA), (f) JF166-3 P(S-co-AEMA), (g) JF166-4 P(S-co-SMA-co-PEGMA), (h) JF86-1 P(S-co-DVB-co-SMA-co-PEGMA), (i) JF166-5 P(S-co-MAA-co-PEGMA), (j) JF166-6 P(S-co-AEMA-co-PEGMA), (k) JF64-1 P(S-co-PEGMA).

SEM micrographs of the nanocapsules from (l) JF166-4 P(S-co-SMA-co-PEGMA), (m) JF166-6 P(S-co-AEMA-co-PEGMA).

The composition of the liquid core of all samples was DCPD:HD = 50:50 [wt:wt].

The conversion of the copolymerization was estimated by gravimetry measurements after dialysis of the capsules. The values were found to be mainly ~60–70% (Table 4.1), which is notably less than for the free-radical homopolymerization of styrene in miniemulsion without nonsolvent, for which conversion close to 100% can be usually achieved. It is attributed to the fact that the monomer is diluted in a mixture of nonsolvent and DCPD and therefore the polymerization kinetics is slower. Furthermore, although the use of a hydrophobic initiator prevents the formation of a significant amount of homopolymer of the hydrophilic monomer, it has the drawback that not all of the hydrophilic monomer is polymerized. Indeed, it was found previously that 33% styrenesulfonate remained unreacted in a typical copolymerization reaction between styrene and styrenesulfonate in miniemulsion by  $^1\text{H}$  NMR spectroscopy (0.9 wt% compared to the initial amount of monomers).<sup>177</sup> Crosslinked polymer shells could be also functionalized by adding a functional group to DVB (JF86-3, Table 4.1, Figure 4.4d) or a mixture of styrene and DVB (JF86-1, Table 4.1, Figure 4.4h). This encapsulation process is not limited to DCPD and it was shown that 5-norbornen-2-yl acetate (NA) and 5-ethylidene-2-norbornene (EN) could be encapsulated as well (Table 4.2, Figure 4.5).

**Table 4.2** Characteristics of the dispersions with 5-ethylidene-2-norbornene (EN) and 5-norbornen-2-yl acetate (NA).

Entry	comonomer		functional group	liquid core		$D_h$ [nm]
	nature	amount [wt%]		nature	[wt%]	
JF98-1	SMA	8.5	$\text{SO}_3^-$	EN	50	$340 \pm 150$
	PEGMA	5.7		HD	50	
JF98-2	SMA	8.5	$\text{SO}_3^-$	NA	50	$350 \pm 140$
	PEGMA	5.7		HD	50	

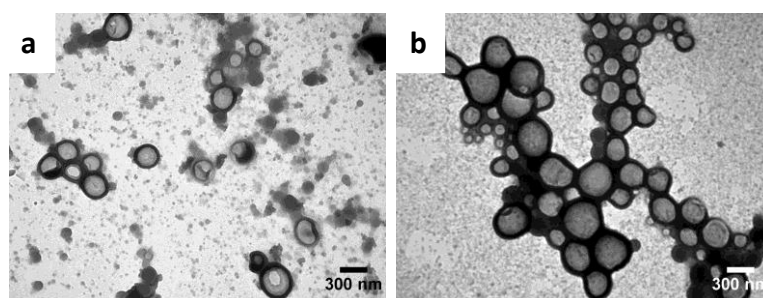


**Figure 4.5** TEM micrographs of  $P(S\text{-co-SMA-co-PEGMA})$  nanocapsules with liquid cores containing (a) EN (JF98-1), (b) NA (JF98-2).

### 4.3 Variation of the solvent quality

An ideal nanocapsule for self-healing materials would require the participation of all the components building the nanocapsule to the self-healing reaction. Although, solvents can participate to the self-healing of a matrix,<sup>148</sup> in our case, it is preferable to have a high DCPD/HD ratio as liquid core. Therefore, the influence of the DCPD/HD ratio on the formation of the nanocapsules was investigated. The DCPD amount was increased to 70% and 94% and for both cases, the dried P(S-co-SMA) colloids did not show a clear capsule structure but rather monolithic structures (Figure 4.6). The variation of the composition of the core did not influence the size of the colloids. Indeed latexes functionalized with SMA and synthesized with DCPD:HD ratios of 50:50, 75:25, 94:6 displayed hydrodynamic diameters of  $260 \pm 60$  (JF166-1),  $230 \pm 100$  (JF144-1),  $230 \pm 70$  nm (JF144-4) (see Table 4.3), respectively.

**Table 4.3** Characteristics of the dispersions with various DCPD:HD ratios.

Entry	polymer	hydrophobic comonomer		hydrophilic comonomer		liquid core		$D_h$ [nm]
		nature	[wt%]	nature	[wt%]	nature	[wt%]	
JF166-1	P(S-co-SMA)	S	91.0	SMA	9.0	DCPD HD	50 50	$310 \pm 90$
JF144-1	P(S-co-SMA)	S	91.0	SMA	9.0	DCPD HD	75 25	$230 \pm 100$
JF144-4	P(S-co-SMA)	S	91.0	SMA	9.0	DCPD HD	94 6	$230 \pm 70$
JF64-2	P(S-co-PEGMA)	S	94.3	PEGMA	5.7	DCPD HD	94 6	$270 \pm 110$
JF21-1	P(S-co-MAA)	S	91.0	MAA	9.0	DCPD HD	94 6	$220 \pm 60$
JF64-4	P(S-co-MAA-co-PEGMA)	S	85.8	MAA PEGMA	8.5 5.7	DCPD HD	94 6	$300 \pm 90$
JF86-4	P(DVB-co-SMA)	DVB	91.0	SMA	9.0	DCPD HD	94 6	$300 \pm 100$
JF86-2	P(S-co-DVB-co-SMA-co-PEGMA)	S DVB	43.3 42.5	SMA PEGMA	8.5 5.7	DCPD HD	94 6	$250 \pm 80$

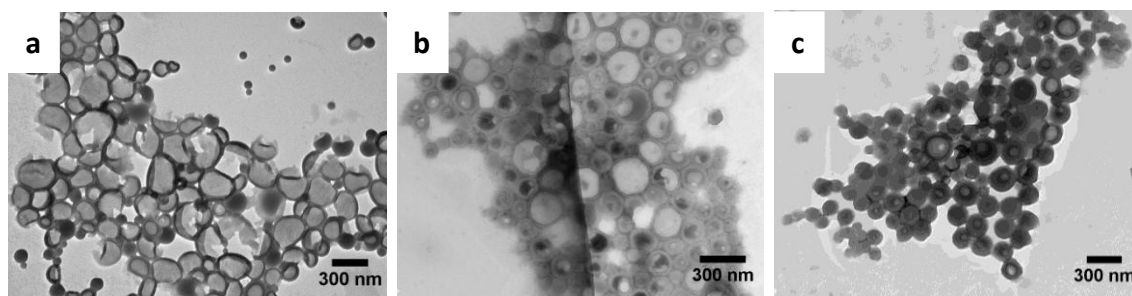


**Figure 4.6** TEM micrographs of *P(S-co-SMA)* nanocapsules with different DCPD:HD ratios [wt:wt] (a) 50:50 (JF166-1), (b) 75:25 (JF144-1), (c) 94:6 (JF144-4).

Note that the absence of hexadecane (100% DCPD as dispersed phase) yielded latexes with particles that were not stable and precipitated. This confirmed the role of hexadecane as nonsolvent and hydrophobe for preventing Ostwald ripening. The use of other functional monomers such as PEGMA, MAA, or SMA and PEGMA did not help for obtaining nanocapsules (Figure 4.7a-c). Hollow structures were not observed even for the dried crosslinked colloids (Figure 4.7d-e).

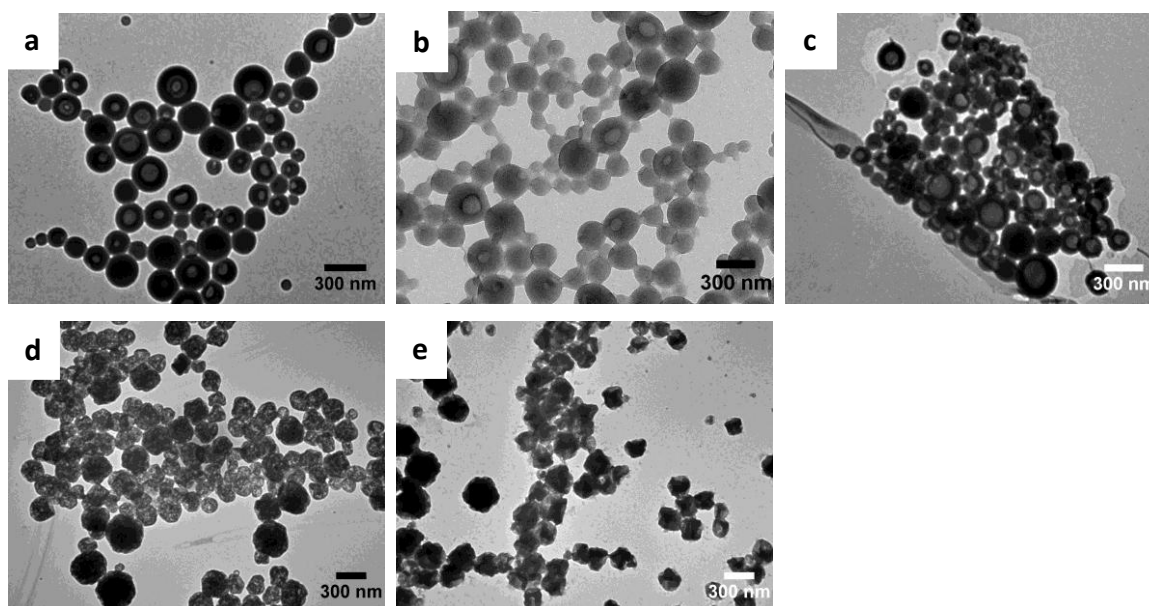


**Figure 4.7** TEM micrographs of (a) JF64-2 *P(S-co-PEGMA)*, (b) JF21-1 *P(S-co-MAA)*, (c) JF64-4 *P(S-co-SMA-co-PEGMA)*, (d) JF86-4 *P(DVB-co-SMA)*, (e) JF86-2 *P(S-co-DVB-co-SMA)*. The composition of the liquid core was DCPD:HD = 94:6 [wt:wt].

#### 4.4 Role of the surfactant in the formation of the nanocapsules

The colloids synthesized by copolymerizing styrene and the various hydrophilic monomers displayed similar hydrodynamic diameters after polymerization (Table 4.1).

As mentioned, the repartition of obtained colloid morphologies (acorn, monolithic particles and droplets, or core-shell) is depending on the spreading coefficient of the different possible interfaces (chapter 2.2.2). In our case, these spreading coefficients are essentially controlled by the nature of the organic phases and by the concentration of surfactant and hydrophilic comonomer. As expected, the average size of the colloids decreased for increased surfactant concentration (Figure 4.8, Table 4.4).

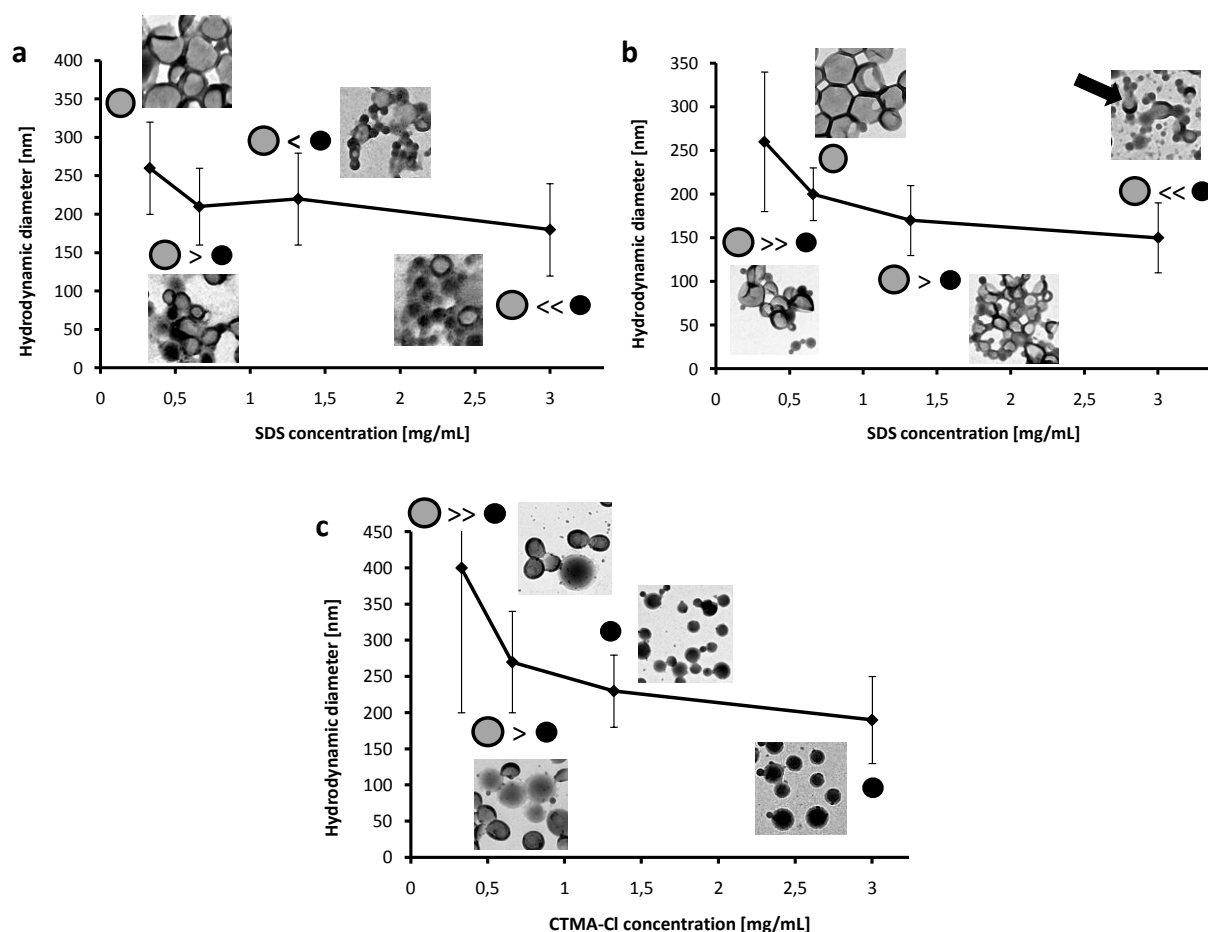


**Figure 4.8** Plots of the hydrodynamic diameter vs. the concentration of surfactant for different polymer dispersions (a) *P(S-co-SMA)*, (b) *P(S-co-MAA)*, (c) *P(S-co-AEMA)*. Representative TEM micrographs are shown as insets. The arrow indicates the presence of non-closed capsules.

#### 4 Polymer nanocontainers functionalized by orthogonal reactions

**Table 4.4** Characteristics of the dispersions with various amount of surfactant SDS or CTMA-Cl. DCPD:HD = 50:50 [wt:wt]; S:hydrophilic comonomer = 91:9 [wt:wt].

Entry	polymer	hydrophilic comonomer	surfactant		$D_h$ [nm]
			nature	[mg·mL <sup>-1</sup> ]	
JF166-1	P(S-co-SMA)	SMA	SDS	0.33	310 ± 90
JF147-1	P(S-co-SMA)	SMA	SDS	0.66	210 ± 50
JF147-2	P(S-co-SMA)	SMA	SDS	1.32	220 ± 60
JF147-3	P(S-co-SMA)	SMA	SDS	3.00	180 ± 60
JF166-2	P(S-co-MAA)	MAA	SDS	0.33	260 ± 80
JF148-2	P(S-co-MAA)	MAA	SDS	0.66	200 ± 30
JF148-3	P(S-co-MAA)	MAA	SDS	1.32	170 ± 40
JF148-4	P(S-co-MAA)	MAA	SDS	3.00	150 ± 40
JF166-3	P(S-co-AEMA)	AEMA	CTMA-Cl	0.33	440 ± 170
JF170-3	P(S-co-AEMA)	AEMA	CTMA-Cl	0.66	300 ± 60
JF170-2	P(S-co-AEMA)	AEMA	CTMA-Cl	1.32	260 ± 70
JF170-4	P(S-co-AEMA)	AEMA	CTMA-Cl	3.00	400 ± 200

Nanocapsules could be obtained only with low concentration of surfactants ( $\leq 0.66 \text{ mg}\cdot\text{mL}^{-1}$ ) as shown in Figure 4.8 for different combinations comonomer/surfactant. The spreading coefficient for the interface DCPD/continuous phase and HD/continuous phase increased with increasing surfactant concentration and therefore acorn particles were formed. The corresponding TEM micrographs are shown in Figure 4.9. This demonstrates an important drawback of the method, in the sense that the diameter cannot be decreased by increasing the surfactant concentration above a certain threshold; otherwise nanocapsules are not formed anymore.



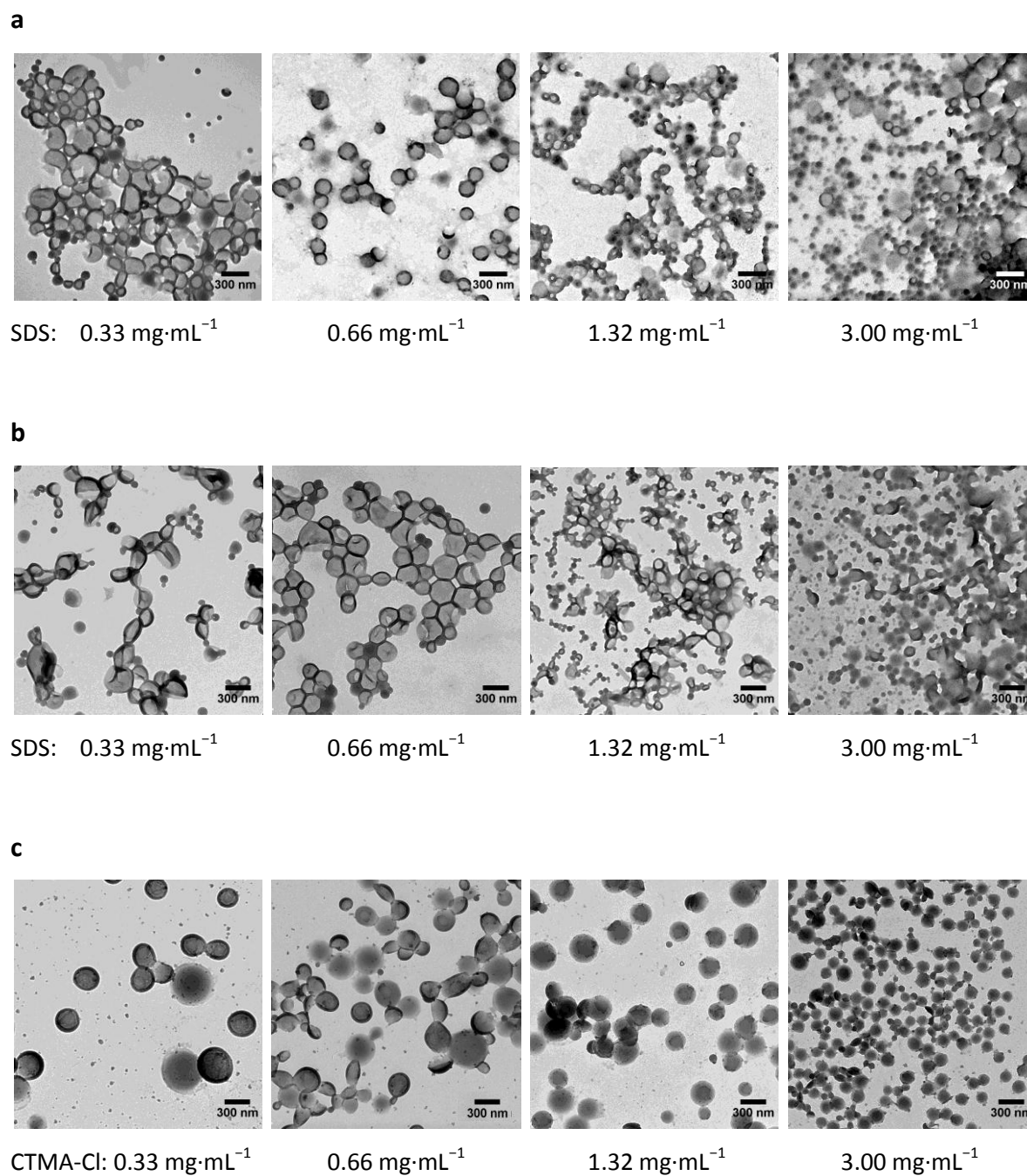


**Figure 4.9** Plots showing the morphology of the nanocapsule and their hydrodynamic diameters in dependence on the concentration of surfactant used for the miniemulsions for (a) P(S-co-SMA), (b) P(S-co-MAA), (c) P(S-co-AEMA).

#### 4.5 Thickness of the polymer shell

If not broken by mechanical damage, the release profile of a substance situated in the core migrating in a hypothetical hydrophobic matrix across the capsules shell shall be dependent on the thickness of the shell. As expected, the thickness of the polymer shell can be controlled to a certain extent by the amount of monomers used in the miniemulsions. For P(S-co-SMA-co-PEGMA) nanocapsules (Figure 4.10a-c), the thickness increased from 39 (JF166-4) to 49 nm (JF146-4) when the comonomer ratio was increased from 33 to 50 wt% (Table 4.5). Using less comonomer (20 wt%) yielded in *a priori* contradictory result (Table 4.5) since the thickness of the shell was estimated to be 64 nm by TEM. However, the capsules are not fully closed and therefore the amount of 20 wt% comonomer is too low for yielding a shell covering the entire surface of the colloids. The same trend was observed with P(S-co-SMA) nanocapsules (Table 4.5, Figure 4.10d-f).

**Table 4.5** Characteristics and capsules thickness for different functionalized nanocapsules depending on the amount of monomers-[r] used in the miniemulsions (DCPD:HD = 50:50, S:SMA:PEGMA = 86:8:6, S:SMA = 91:9). The fraction of dispersed phase  $\varphi_d$  was kept constant at 20 wt%.

Entry	polymer	fraction of monomer in dispersed phase [wt%]	$D_h$ [nm]	thickness of the shell <sup>a</sup> [nm]
JF146-3	P(S-co-SMA-co-PEGMA)	20	320±80	64 ± 15 <sup>b</sup>
JF166-4	P(S-co-SMA-co-PEGMA)	33	260±60	39 ± 5
JF146-4	P(S-co-SMA-co-PEGMA)	50	280±100	49 ± 13
JF145-1	P(S-co-SMA)	20	320±80	56 ± 11 <sup>b</sup>
JF166-1	P(S-co-SMA)	33	310±90	33 ± 6
JF145-2	P(S-co-SMA)	50	240±60	42 ± 6

<sup>a</sup> measured by TEM;

<sup>b</sup> non-closed shell.

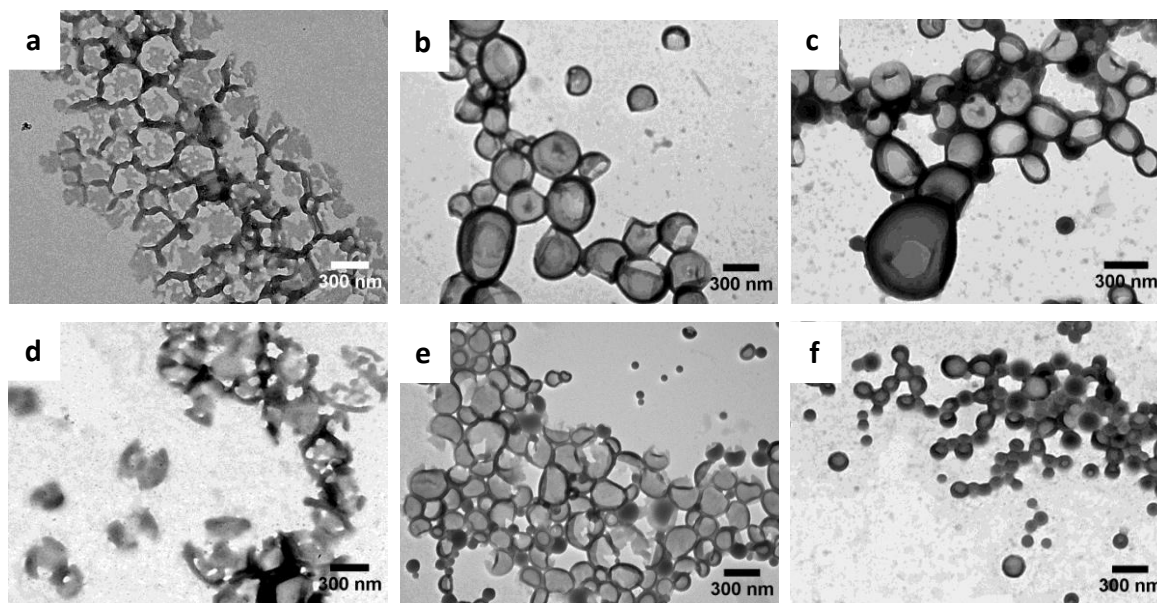


**Figure 4.10** TEM micrographs of *P(S-co-SMA-co-PEGMA)* nanocapsules with different monomer amounts (**a**) JF146-3 (20 wt%), (**b**) JF166-4 (33 wt%), (**c**) JF146-4 (50 wt%) and of *P(S-co-SMA)* nanocapsules with different monomer amount (**d**) JF145-1 (20 wt%), (**e**) JF166-1 (33 wt%), (**f**) JF145-2 (50 wt%).

#### 4.6 Stability of the nanocapsules

One recurring issue for nanocapsules is their stability after removal of the continuous phase (water in this case). Indeed, the electron micrographs of true core-shell colloids with a volatile core display a morphology showing one or several holes that are most probably produced by the evaporation of the liquid core in the high vacuum.<sup>65</sup> However a legitimate issue for this study is to know if the holes are present in nanocapsules that are dried at room temperature.

To answer this, we performed AFM measurements on nanocapsules containing DCPD and HD deposited on cleaned silicon wafers and dried at room temperature. Topography images show that the nanocapsules are cracked or buckled after drying either with non-crosslinked (JF166-4, Figure 4.11a) or crosslinked shells (JF118-3, Figure 4.11b). Similar structures were detected when the nanocapsules were filled with HD only (JF132-1 and JF132-2, Figure 4.11c,d). AFM measurements were then performed in water to check if the nanocapsules structure remained intact in the dispersion. The same non-crosslinked nanocapsules showed a smooth spherical surface (Figure 4.12a) whereas the crosslinked

nanocapsules still displayed a buckled surface but without holes (Figure 4.12b). This is probably due to the stress generating in the highly crosslinked shell.

**Table 4.6** Characteristics of the dispersions used for stability investigations. (S:SMA:PEGMA = 86:8:6, DVB:SMA:PEGMA = 86:8:6). The liquid core was kept constant at 67 wt% of dispersed phase.

Entry	polymer	liquid core		$D_h$ [nm]
		nature	[wt%]	
JF166-4	P(S-co-SMA-co-PEGMA)	DCPD	50	260 ± 60
		HD	50	
JF118-3	P(DVB-co-SMA-co-PEGMA)	DCPD	50	210 ± 50
		HD	50	
JF132-1	P(S-co-SMA-co-PEGMA)	HD	100	340 ± 120
JF132-2	P(DVB-co-SMA-co-PEGMA)	HD	100	350 ± 80

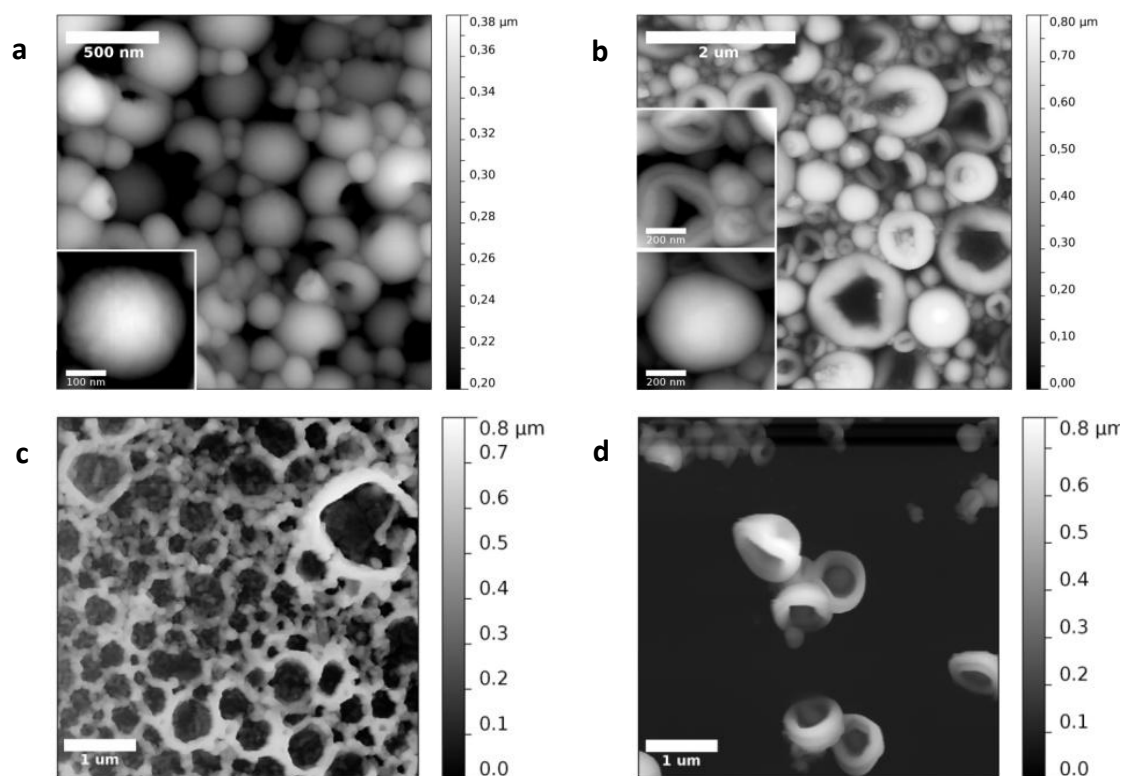


**Figure 4.11** Tapping mode height images in air of (a) JF166-4 P(S-co-SMA-co-PEGMA), (b) JF118-3 P(DVB-co-SMA-co-PEGMA), (c) JF132-1 P(S-co-SMA-co-PEGMA) and (d) JF132-2 P(DVB-co-SMA-co-PEGMA). Samples (a), (b) contain HD/DCPD and (c), (d) contained pure HD as liquid core.

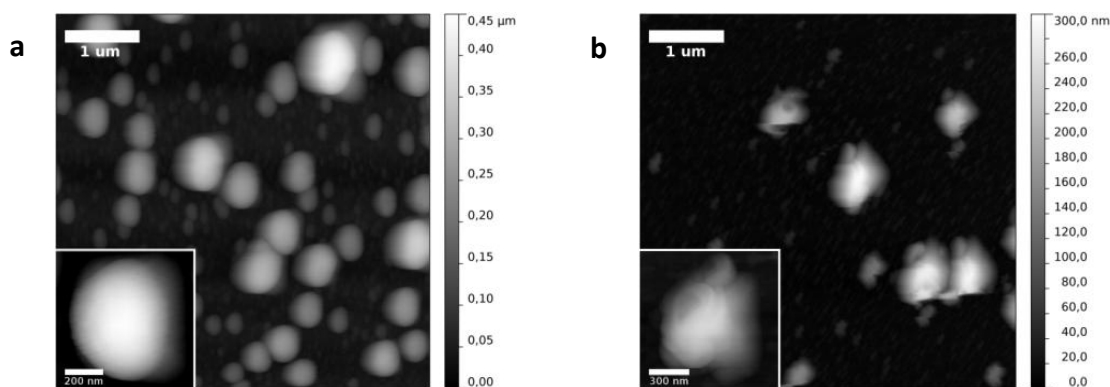


**Figure 4.12** Liquid tapping mode height images of (a) JF166-4 P(S-co-SMA-co-PEGMA) and (b) JF118-3 P(DVB-co-SMA-co-PEGMA) nanocapsules.

Furthermore, it is also important to know in which state (*e.g.* as powder or dispersion) the nanocapsules can be used as fillers for self-healing materials. Therefore, we compared the structure and redispersibility of the nanocapsules after drying them at room temperature, by the freeze-drying process, or separating them from the aqueous phase by centrifugation. It was observed that the non-crosslinked nanocapsules from P(S-co-SMA-co-PEGMA) (JF166-4) were not stable after freeze-drying or centrifugation (Figure 4.13). The agglomerates could not be redispersed in water.

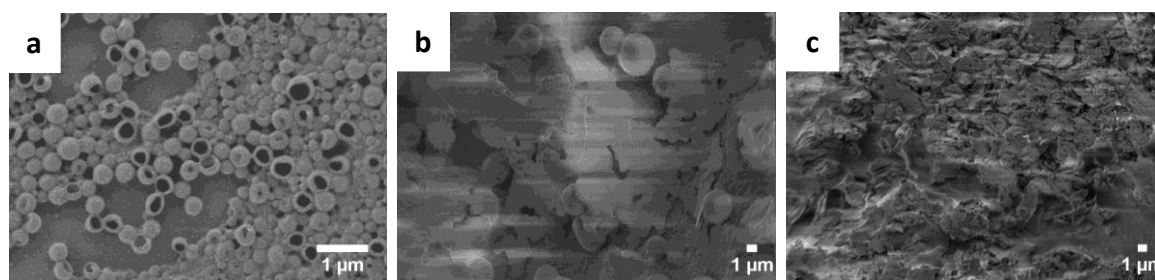


**Figure 4.13** SEM micrographs of the P(S-co-SMA-co-PEGMA) (JF166-4) (a) after drying at room temperature, (b) after centrifugation, (c) after freeze-drying.

The structure of the nanocapsules could be stabilized by crosslinking the polymer with DVB. Indeed the initial morphology of the P(DVB-co-SMA-co-PEGMA) (JF118-3) nanocapsules was conserved after freeze-drying or centrifugation (Figure 4.14a-c). It was possible to redisperse the nanocapsules after freeze-drying (Figure 4.14d). These observations indicate that for self-healing applications, the nanocapsules with non-crosslinked polymer shell shall be used as dispersion when mixed with a matrix. Nanocapsules with crosslinked polymer shell can be

further used after centrifugation, or after freeze-drying if the liquid core is not evaporated or sublimated during the process.

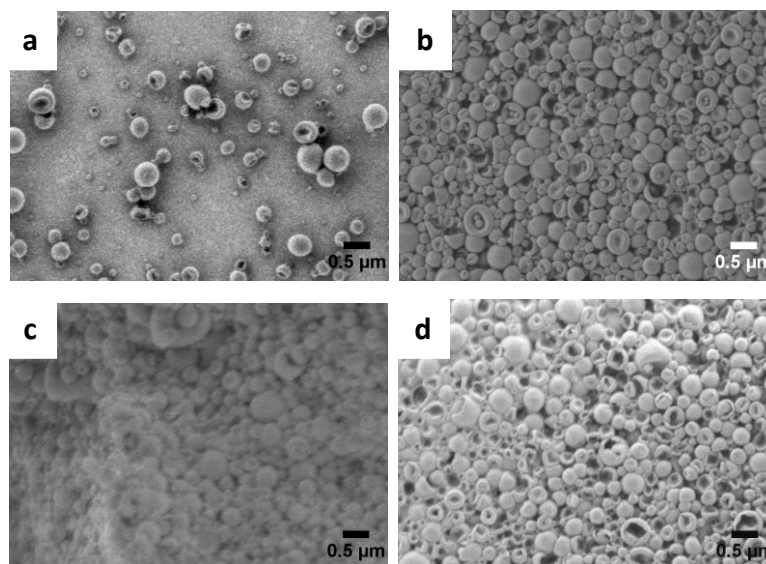


**Figure 4.14** SEM micrographs of the *P(DVB-co-SMA-co-PEGMA)* (JF118-3) (a) after drying at room temperature, (b) after centrifugation, (c) after freeze-drying, (d) after redispersion.

The stability of the nanocapsules against the salting out effect was also investigated with solutions containing different concentrations of KCl. The stability was correlated with the amount of functional groups reported in Table 4.1. Indeed, the stability followed the order SMA > AEMA > MAA > PEGMA (Figure 4.15).

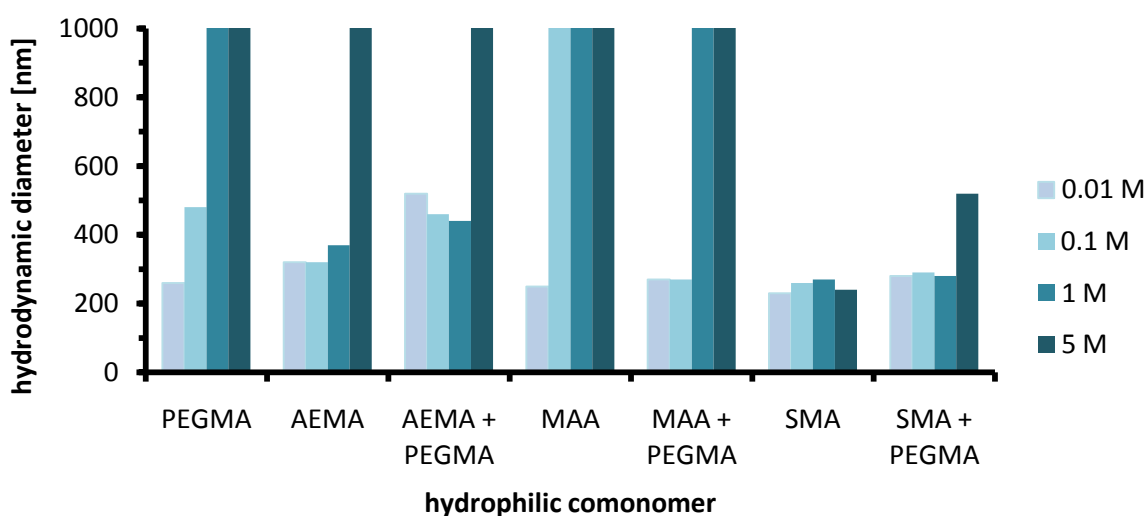


**Figure 4.15** Hydrodynamic diameter  $D_h$  of the nanocapsules in solutions of KCl with different concentrations with shells presenting different functionalities.  $D_h > 1 \mu\text{m}$  were counted as  $1 \mu\text{m}$ .

The nanocapsules with P(S-co-SMA) were found to be particularly robust toward salting out, which make them ideal candidate to be embedded in an inorganic matrix prepared from ionic precursors.

#### 4.7 Self-healing reaction

The nanocapsules were mixed with dissolved or dispersed Grubbs' catalyst to check for the polymerization of encapsulated DCPD. All self-healing experiments were performed under air conditions. Sample SHP1 (Table 4.7) was prepared by dissolving the nanocapsules and Grubbs' catalyst in THF. The conversion to PDCPD was found to be 56%. Possible reasons for this rather low conversion are the facts that: the beginning of the polymerization is performed in solution thus with a slow kinetics; there is precipitation of crosslinked PDCPD, and/or a premature degradation of catalyst in solution due to the presence of oxygen. The nanocapsules were mixed with Grubbs' catalyst dissolved in small amounts of THF so that the shell of the polymeric nanocapsules was not dissolved, but only swollen (SHP2, Table 4.7). High yields of polymerization (91%) were found thanks to the higher local concentration of reagents. In SHP3, the nanocapsules were mixed with in chapter 5.3 described silica nanocapsules containing Grubbs' catalyst (sample JF136-4, Table 5.7) and a yield of 74% was obtained. The lower yield compared to previous yield can be attributed to the absence of THF in this case, which is a good solvent for the Grubbs' catalyst. Therefore, the efficiency of the self-healing reaction is enhanced when the polymerization happen locally, which also means that the DCPD nanocapsules would be suitable to heal damages at the local scale.

**Table 4.7** Composition and yield of the resulting mixed dispersions for self-healing tests.

Entry	JF166-1 (with DCPD) [g]	Grubbs' catalyst		THF [g]	yield for the self- healing reaction [%]
		type	amount [mg]		
SHP1	2.0	solution	1.25	10.0	56
SHP2	4.0	solution	2.5	0.5	91
SHP3	4.0	dispersion	2.5	0	74

## 4.8 Conclusions

In this chapter, the synthesis of core-shell particles encapsulating ROMP monomers by free-radical polymerization was described. The nanocapsules were formed and functionalized with various functional groups including sulfonate, carboxylate, ammonium, and poly(ethylene glycol) (PEG) by an orthogonal reaction. Detailed investigations on the distribution of the charged functional groups on the nanocapsule surface were performed. The orthogonal reaction, the concentration of surfactant, and the ratio of core to shell were found to have an influence on the structure of the colloids. The thickness of the polymer shell could be controlled to a certain extent by the monomer amount used in the miniemulsions. Furthermore, the colloidal and mechanical stability of the functionalized nanocontainers was investigated. It was found that nanocapsules functionalized with sulfonate groups were most stable against salting out with KCl because of the presence and availability of the groups at the surface of shells. AFM investigations demonstrated that non-crosslinked nanocapsules did not remain intact upon drying of the dispersion, which indicates that they shall be used exclusively as dispersion. On the contrary, crosslinked capsules can be used even after centrifugation. Self-healing experiments were carried out successfully verifying that the self-healing agent remained active after encapsulation.

The encapsulation of healants by free-radical polymerization is a simple and cost-effective method. Furthermore, the range of functional groups as pendant groups offered in vinyl monomers is very large and allows the compatibilization of the capsules as fillers and a matrix to be repaired. However, the encapsulation of ROMP catalysts is not possible due to their high reactivity towards vinyl monomers. Finally, this approach is not limited to ROMP as self-healing reaction but can be derived to other reactions such as polyaddition or polycondensations reactions.

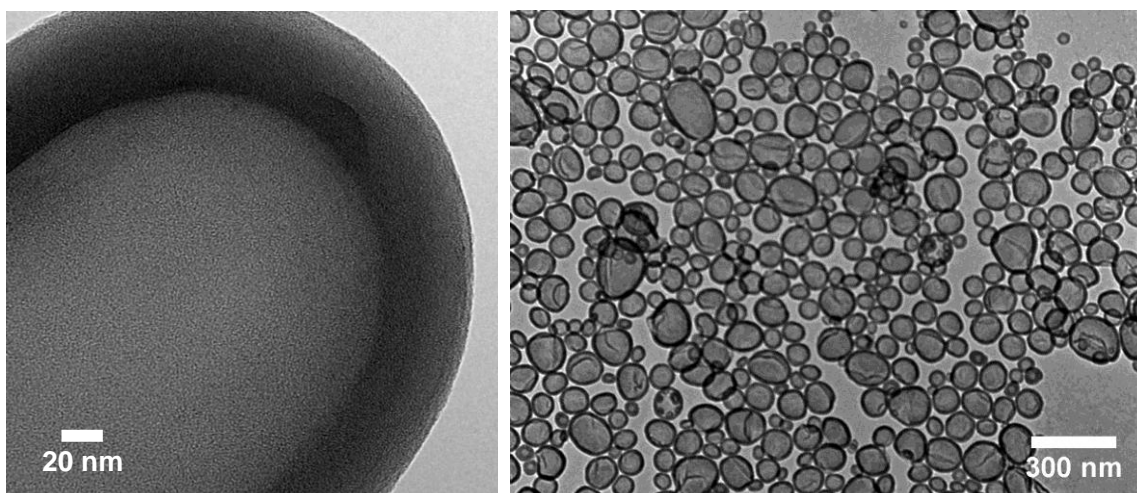


## Chapter 5

# Design and characterization of functionalized silica nanocontainers for self-healing materials

based on

*J. Mater. Chem.* **2012**, *22*, 2286-2291.



### 5 Design and characterization of functionalized silica nanocontainers for self-healing materials

In the previous chapter, the formation of functionalized nanocapsules for encapsulation of self-healing agents using internal phase separation induced by orthogonal free-radical polymerization in miniemulsion droplets was presented. This approach is however limited to the encapsulation of ROMP monomers and cannot be used for ROMP catalysts since they react with the vinyl monomers.

In the original article of White et al., dicyclopentadiene (DCPD) was encapsulated in urea/formaldehyde nanocapsules ([chapter 2.3.3](#)).<sup>7</sup> However, the same nanocapsule synthesis could not be applied for the encapsulation of Grubbs' catalyst due to the chemical sensitivity of the catalyst. Therefore an emulsion-solvent evaporation was proposed to perform the encapsulation.<sup>162</sup> Both types of nanocontainers could be coated with a silica shell for better dispersion in the matrix,<sup>162</sup> needing two steps for the completion of the encapsulation. The polymer nanocapsules were synthesized either by polyaddition or emulsion evaporation techniques and served as template for the hydrolysis and condensation of the non-functionalized alkoxy silane. The first approach in particular is limited by the fact that urea formaldehyde resins are known to release the human carcinogen formaldehyde with time. The second approach has the limitation to encapsulate the catalyst in a solid matrix, thus limiting its mobility for self-healing reactions.

In general, silica nanocontainers have the advantage over polymer nanocontainers to be mechanically and thermally more stable. Further, they may offer a better compatibility and dispersion in inorganic matrices compared to capsules with polymer shells.

Therefore, novel inorganic silica nanocapsules synthesized by the use of miniemulsion droplets as templates for the interfacial hydrolysis of non-functionalized and functionalized alkoxy silanes are introduced in this chapter. Both reagents ROMP monomer and catalyst are encapsulated in liquid form to provide enough mobility for a possible self-healing reaction.

## 5.1 Encapsulation of the monomer in non-functionalized nanocapsules

HD/DCPD mixtures could be successfully used for the formation of stable aqueous miniemulsions using cetyltrimethylammonium chloride (CTMA-Cl) as surfactant. The preparation of the non-functionalized silica nanocapsules was performed by interfacial hydrolysis and subsequent polycondensation of tetraethoxysilane (TEOS) as described in chapter 2.2.3.3. The structures of the used chemicals are shown in Figure 5.1.

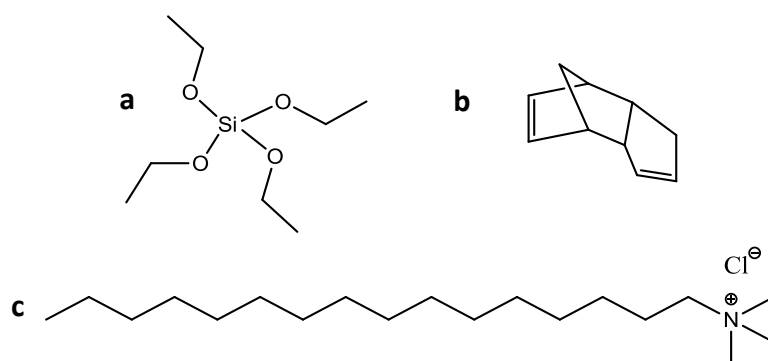


**Figure 5.1** Chemical structures of (a) tetraethoxysilane (TEOS), (b) dicyclopentadiene (DCPD), and (c) cetyltrimethylammoniumchloride (CTMA-Cl).

First experiments with only DCPD as droplet template instead of a mixture HD/DCPD led to very large and broadly distributed colloids with an average hydrodynamic diameter of  $D_h = 810 \pm 190$  nm (JF41-3, Table 5.1). Mixtures of very large capsules and smaller nanoparticles were detected by TEM (Figure 5.2a).

**Table 5.1** Composition of the dispersions prepared with increasing amount of dispersed phase. The ratio (TEOS:HD:DCPD) of 6:1:1 (wt) being kept constant.

Entry	HD [g]	DCPD [g]	TEOS [g]	dispersed phase [wt%]	$D_h$ [nm]
JF41-3	0	0.66	2.0	8.1	$810 \pm 160$
JF41-2	0.33	0.33	2.0	8.1	$140 \pm 70$
JF70-1	0.50	0.50	3.0	11.8	$170 \pm 40$
JF70-2	0.66	0.66	4.0	15.1	$230 \pm 70$
JF70-3	1.00	1.00	6.0	21.0	$250 \pm 90$

Upon addition of hexadecane in the dispersed phase, the colloids formed were much smaller (JF41-2,  $D_h = 140$  nm), indicating that the miniemulsions were efficiently stabilized against *Ostwald* ripening as observed for other systems.<sup>178</sup> The colloids observed with TEM displayed a capsular structure (Figure 5.2b), indicating the success of the condensation of the alkoxy silane around the miniemulsion droplets.

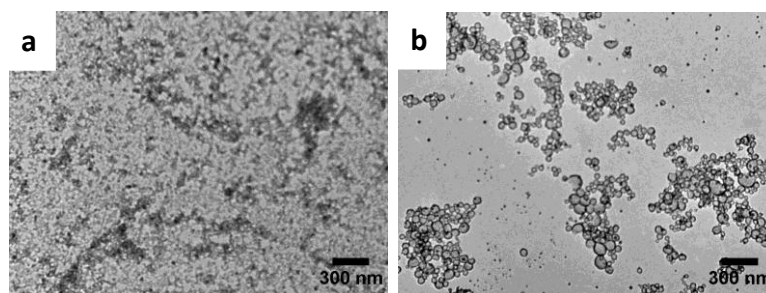


**Figure 5.2** TEM micrographs of the samples prepared with a liquid core out of (a) only DCPD (JF41-3) and (b) 50 wt% DCPD in HD (JF41-2).

<sup>29</sup>Si MAS-NMR spectroscopy confirmed the formation of silica network ( $Q_4 = 70\%$ ) and the absence of free ( $Q_0$ ) or mono-reacted alkoxy silane ( $Q_1$ ) as shown in Figure 5.3. Some resonances corresponding to  $Q_2 = 8\%$  and  $Q_3 = 21\%$  are observed indicating that the condensation was not fully achieved.

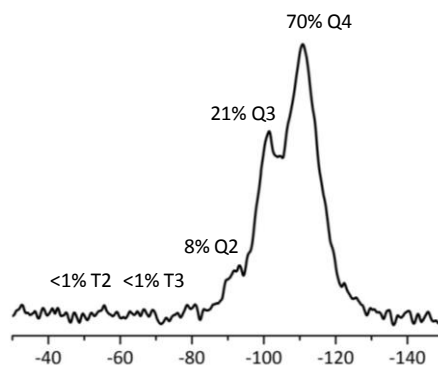


**Figure 5.3** <sup>29</sup>Si MAS NMR spectrum of sample JF41-2.

The nanocontainers could also be prepared in higher quantity by increasing the dispersed phase from 8.1 wt% (JF41-2) to 21.0 wt% (JF70-3, Table 5.1). Nanocapsules could still be formed (Figure 5.4) although the average diameter of the capsules increased from 140 nm (JF41-2) to 250 nm (JF70-3) with a steady increase of diameter for the intermediate dispersed phase.

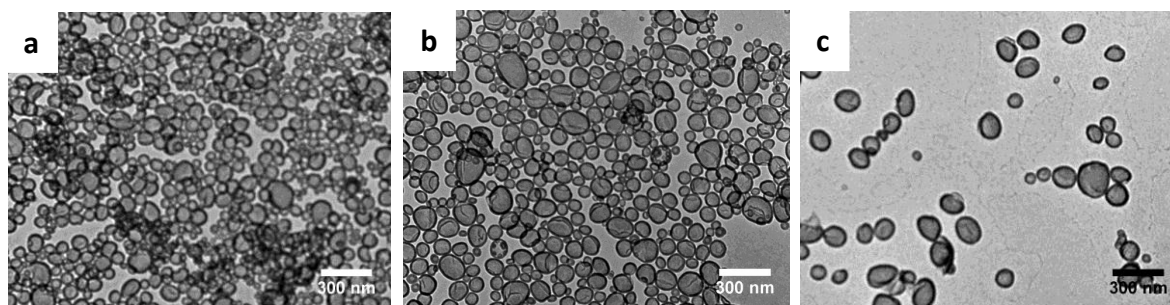


**Figure 5.4** TEM micrographs of the samples prepared with different amounts of the dispersed phase. (a) 11.8 wt% (JF70-1), (b) 15.1 wt% (JF70-2), (c) 21.0 wt% (JF70-3).

Indeed coalescence and therefore an increase of the colloid size is favored by increasing the volume of the dispersed phase. As expected,<sup>178</sup> it was also possible to control the size of the nanocontainers by varying the amount of surfactant in the miniemulsion. Stable nanocapsules with hydrodynamic diameters up to 410 nm (JF91-3, Table 5.2, Figure 5.5) could be synthesized.

**Table 5.2** Composition of the nanocapsules prepared with two different amounts of the dispersed phase. The amount of surfactant in the miniemulsions was varied to obtain different sizes for the nanocapsules.

Entry	HD [g]	DCPD [g]	TEOS [g]	H <sub>2</sub> O [g]	CTMA-Cl [mg·mL <sup>-1</sup> ]	$D_h$ [nm]
<b>fraction of dispersed phase <math>\varphi_d = 8.1</math> wt%</b>						
JF41-2	0.33	0.33	2.0	30	0.77	140 ± 70
JF69-1	0.33	0.33	2.0	30	0.50	160 ± 80
JF69-2	0.33	0.33	2.0	30	0.33	200 ± 100
<b>fraction of dispersed phase <math>\varphi_d = 21.1</math> wt%</b>						
JF91-1	0.5	0.5	3.0	15	0.67	280 ± 110
JF91-2	0.5	0.5	3.0	15	0.53	340 ± 140
JF91-3	0.5	0.5	3.0	15	0.40	410 ± 80

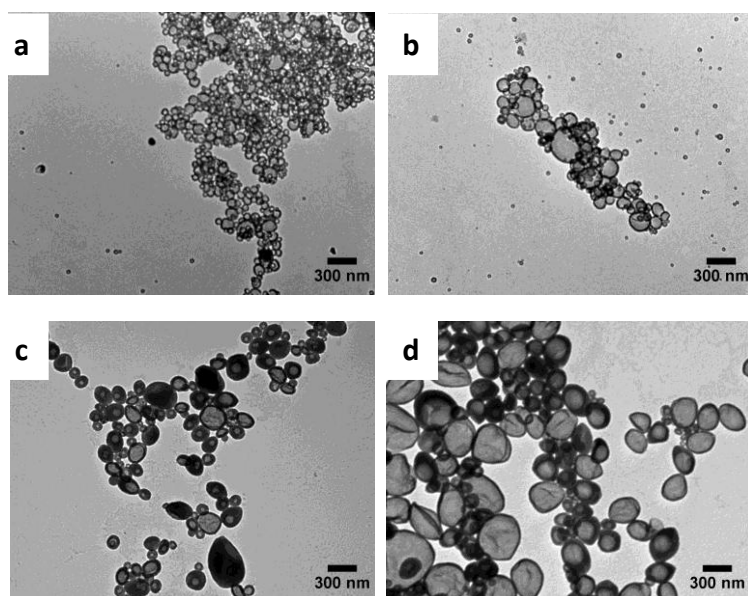


**Figure 5.5** TEM micrographs of the samples prepared with different amount of surfactant (a) JF69-1, (b) JF69-2, (c) JF91-2, (d) JF91-3.

The quantity of liquid core in the dispersed phase was increased compared to the amount of TEOS to vary the thickness of the shell. Closed nanocapsules could be obtained with a ratio of TEOS:HD:DCPD = 1:0.25:0.25 (JF68-1, Table 5.3, Figure 5.6a). Above this amount of hexadecane (Figure 5.2), some capsules were found to be non-closed by TEM measurements (Figure 5.6b-d). The amount of non-closed capsules increased with the amount of the liquid core.

**Table 5.3** Composition of the nanocapsules prepared with different amount of liquid cores.  $\varphi_c$  represents the proportion of the core of the dispersed phase.

Entry	HD [g]	DCPD [g]	$\varphi_c$ [wt%]	$D_h$ [nm]
JF41-2	0.33	0.33	25	140 ± 70
JF68-1	0.5	0.5	33	160 ± 80
JF68-2	0.75	0.75	43	170 ± 70
JF68-3	1.0	1.0	50	190 ± 80
JF68-4	2.0	2.0	67	240 ± 100

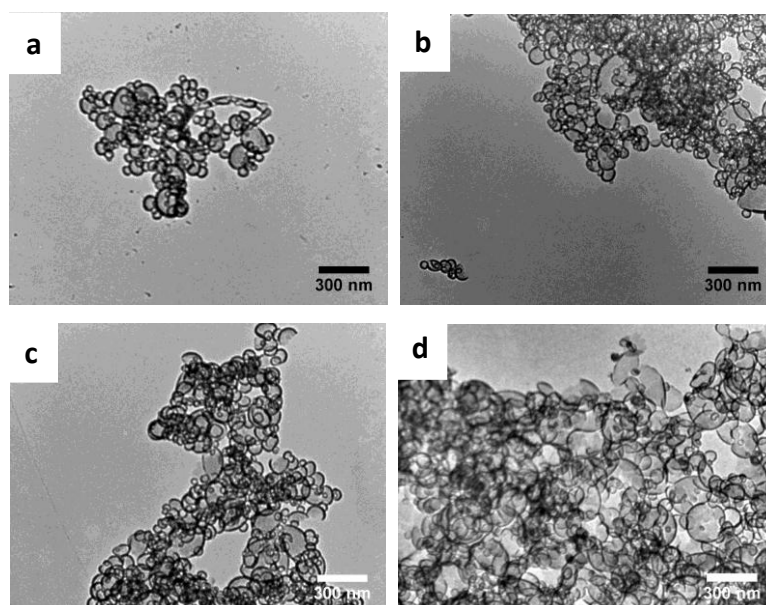


**Figure 5.6** TEM micrographs of the samples prepared with different amounts of liquid core (50 wt% DCPD in HD) (**a**) 33 wt% (JF68-1), (**b**) 43 wt% (JF68-2), (**c**) 50 wt% (JF68-3), and (**d**) 67 wt% (JF68-4).

## 5.2 Encapsulation of the monomer in functionalized nanocapsules

It is known that silica particles are favorably integrated in zinc layers when they are functionalized with thiol and amine groups. Therefore mixtures of TEOS and functionalized precursors (MPTMS for  $-\text{SH}$ , APTES for  $-\text{NH}_2$ ) were used for building the nanocapsules similarly to the copolymerization procedures for fabricating functionalized polymer nanoparticles in miniemulsion.<sup>61</sup>



**Figure 5.7** Chemical structures of (**a**) 3-mercaptopropyltrimethoxysilane (MPTMS) and (**b**) 3-aminopropyltriethoxysilane (APTES).

First experiments were performed according to the experimental part but using MPTMS as sole alkoxy silane with either a 50 wt% solution of DCPD in HD (JF56-2,  $D_h = 120 \pm 50$  nm), or only HD (JF56-3,  $D_h = 200 \pm 80$  nm) as liquid core. In both cases, only nanoparticles were obtained as demonstrated in [Figure 5.8](#).

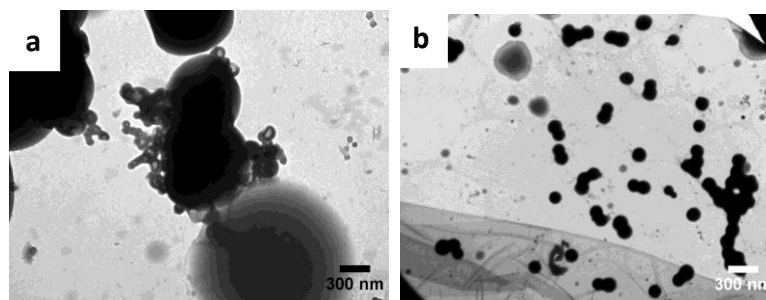


**Figure 5.8** TEM micrographs of the samples prepared with MPTMS as sole alkoxysilane (a) JF56-2 with HD and DCPD, and (b) JF56-3 with HD as liquid core.

This is probably due to the much higher reactivity of MPTMS than TEOS that does not allow a shell to be formed. Indeed, methoxysilanes are hydrolyzed 6-10 times faster than ethoxysilanes.<sup>179</sup> Moreover, the organic substitution in MPTMS increases also the hydrolysis rate.<sup>179</sup> The use of mixtures of MPTMS and TEOS with different ratios (Table 5.4) yielded nanocapsules as evidenced by TEM and SEM measurements (Figure 5.9). Up to 50 wt% MPTMS could be used in the miniemulsion without a significant influence on the hydrodynamic diameter of the nanocapsules.

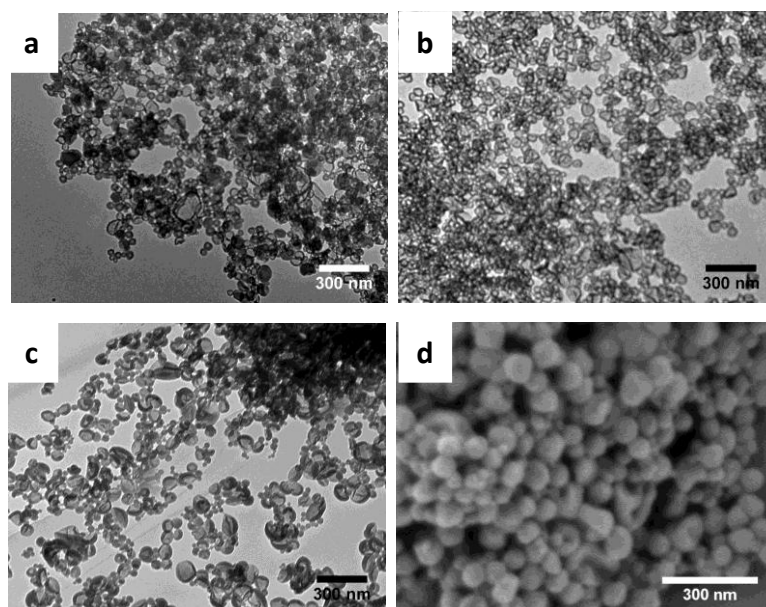


**Figure 5.9** TEM micrographs of samples prepared with the various TEOS:MPTMS ratios [wt:wt]: (a) 90:10, (b) 80:20, (c) 50:50. (d) SEM image of sample with 80:20 ratio.



**Table 5.4** Composition of miniemulsions containing DCPD and hydrodynamic diameters of the functionalized nanocapsules after the reaction.

Entry	precursors		$D_h$ [nm]
	nature	ratio [wt:wt]	
JF69-4	TEOS : MPTMS	0.9 : 0.1	120 ± 60
JF69-3	TEOS : MPTMS	0.8 : 0.2	110 ± 60
JF92-2	TEOS : MPTMS	0.5 : 0.5	130 ± 50
JF107-5	TEOS : APTES	0.95 : 0.05	120 ± 60

$^{29}\text{Si}$  MAS NMR spectra of the dried nanocapsules are shown in Figure 5.10. An overview of the content of  $Q^{(n)}$  and  $T^{(n)}$  groups in the different samples is given in Table 5.5. MPTMS had no influence on the condensation of TEOS that reacted since the relative amount of  $Q_4$  compared to the amount of TEOS used in the MTPMS:TEOS mixture was not significantly different (see Figure 5.3 for comparison). Larger amounts of MPTMS yielded less dense networks since  $T_3/T_2 = 2.3$  when 50 wt% MPTMS was used (JF92-2) compared to  $T_3/T_2 = 4.5$  for 20 wt% MPTMS. The comparison between freeze-dried nanocapsules (JF69-3nt, Figure 5.10b) and the same capsules subsequently treated in the vacuum oven showed no significant differences in the intensities of the resonances (JF69-3, Figure 5.10a).

**Table 5.5** Content of  $Q^{(n)}$  and  $T^{(n)}$  groups in the different samples obtained from  $^{29}\text{Si}$  MAS NMR spectroscopy by deconvolution of the spectra.

Entry	$Q_2$	$Q_3$	$Q_4$	$T_1$	$T_2$	$T_3$
JF69-3nt <sup>a</sup>	3	28	46	0	3	20
JF69-3 <sup>b</sup>	2	32	44	0	4	18
JF92-2 <sup>b</sup>	0	16	19	2	19	44
JF41-2 <sup>b</sup>	8	21	70	0	< 1	< 1
JF107-5 <sup>b</sup>	< 1	27	69	0	< 1	3

<sup>a</sup> freeze-dried prior to the measurement;

<sup>b</sup> freeze-dried and treated in a vacuum oven (80 °C, 16 h) prior to the measurements.

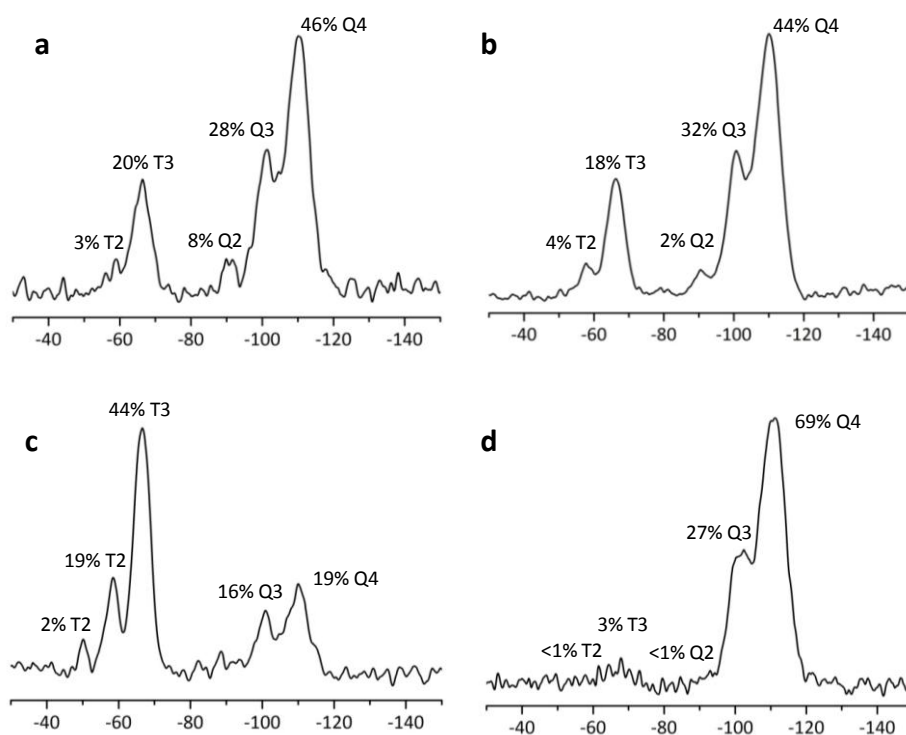


**Figure 5.10**  $^{29}\text{Si}$  MAS spectra of (a) JF69-3, (b) JF69-3nt, (c) JF92-2, and (d) JF107-5. The content of  $Q^{(n)}$  and  $T^{(n)}$  sites in the different samples were obtained by deconvolution of the spectra. All samples were freeze-dried and treated in a vacuum oven ( $80^\circ\text{C}$ , 16h) prior to the measurements except sample JF69-3nt, which was only freeze-dried.

Nanocapsules with a high amount of APTES (>5 wt%) yielded either gels or unstable colloids that sedimentated rapidly even in the presence of double amount of surfactant. APTES is a base and therefore catalyzed the condensation reaction,<sup>179</sup> leading to uncontrolled gelation of the system. Gelation, large aggregates, small particles, and non-closed capsules were observed when the APTES was added before sonication, or 1 min, 1 h, and 2.5 h after the sonication, respectively (Figure 5.11).

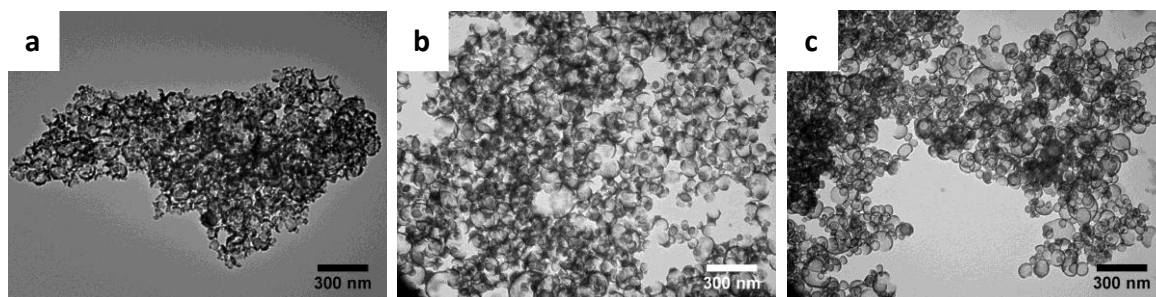


**Figure 5.11** TEM micrographs of selected samples prepared with 5 wt% APTES added (a) directly after sonication, (b) 2.5 h after (c) 17.5 h (JF107-5) after sonication.

The same amount was added to the dispersion but 17.5 h after sonication and stable nanocapsules could be obtained (Figure 5.11). The investigation of the capsule structure by TEM under similar conditions in function of the time revealed that the structure was not changing significantly after 12 h.<sup>180</sup> Since APTES was found in the silica colloids by <sup>29</sup>Si-NMR spectroscopy (Figure 5.10d, JF107-5) and that no secondary nanoparticles of APTES were detected by electron microscopy or DLS, it can be assumed that the APTES reacted on and with the nanocapsules produced by the condensation of TEOS. The catalytic effect of APTES on the condensation is confirmed by the higher value of  $Q_4/(Q_2+Q_3)$  observed with APTES than with the other samples.

XPS measurements were performed to localize the functional groups of the silica nanocapsules. Due to a depth of penetration of ~3 nm, the outer part of the shell (~20 nm in thickness) could be investigated by XPS, whereas informations about the average composition of shell was given by NMR spectroscopy. The amount of sulfur measured by XPS was always lower than the amount measured by NMR spectroscopy (JF69-3, JF92-2, Table 5.6). The functionalization was therefore less efficient than expected. As discussed above, MPTMS has a higher reactivity than TEOS and therefore it may have reacted first at the interface oil/water, yielding a silica shell with a gradient of composition. On the contrary, the shell is enriched (compared to the bulk composition of the shell) with functional groups when APTES is used in the reaction (JF107-5, Table 5.6). This is due to the fact that APTES was added after the TEOS to the miniemulsion.

**Table 5.6** Experimental ratios of sulfur or nitrogen (from the functional precursor) over silicon atom determined by solid-state NMR spectroscopy and XPS measurements, and concentration of functional groups on the particle surface as determined by titration experiments.

Entry	precursor	ratio <sup>29</sup> Si NMR [mol%]	ratio XPS [mol%]	groups/dispersed phase [mmol·g <sup>-1</sup> ]
JF69-3nt	MPTMS	22 <sup>a</sup>	8 <sup>a</sup>	-
JF69-3	MPTMS	23 <sup>b</sup>	9 <sup>b</sup>	0.3
JF92-2	MPTMS	65 <sup>b</sup>	25 <sup>b</sup>	0.6
JF107-5	APTES	3 <sup>b</sup>	6 <sup>b,c</sup>	0.1

<sup>a</sup> Freeze-dried prior to the measurement;

<sup>b</sup> Freeze-dried and treated in a vacuum oven (80 °C, 16 h) prior to the measurements;

<sup>c</sup> The amount of nitrogen from the surfactant and from the APTES could be differentiated in the XPS measurements by their different binding energies.

Furthermore, the thiol and amine groups that are accessible in dispersion were determined by titrating the silica nanocapsules with the Ellman's reagent and fluorescamine, respectively (Table 5.6, Figure 5.12). It is noteworthy that the silica nanocapsules with amine functionality are fluorescent after titration.

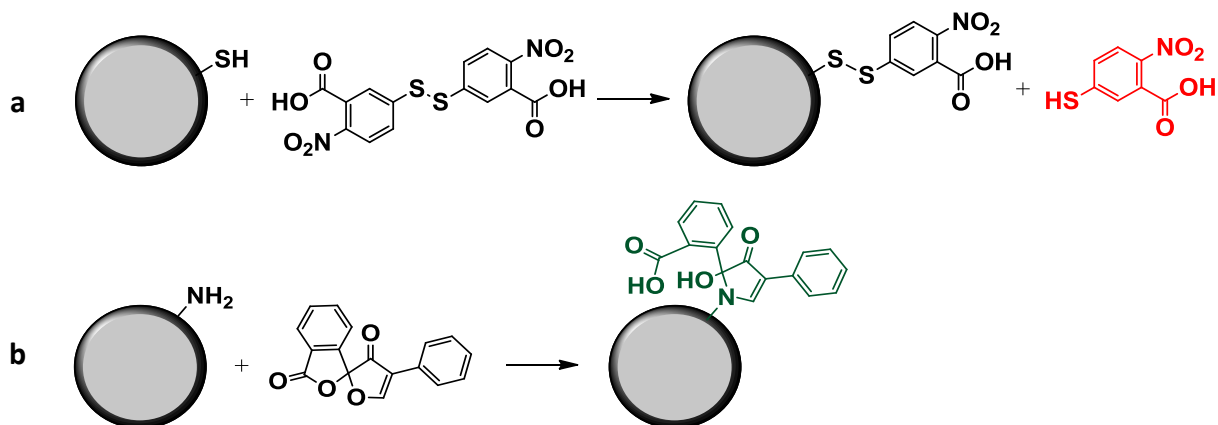


**Figure 5.12** Scheme for the reactions between the functionalized silica nanocapsules (core in grey, silica shell in black) with (a) the Ellman's reagent for the titration of thiol groups; (b) fluorescamine for the titration of primary amine groups.

### 5.3 Encapsulation of the Grubbs' catalyst and its stability

The stability of the Grubbs' catalyst is still an issue in the field of self-healing materials since suitable systems shall remain active for long time. Encapsulation was performed in a glovebox since previous experiments have shown that the catalyst was degraded. The degradation of Grubbs' catalyst is unmistakably accompanied by a change of color from violet (Grubbs' 1<sup>st</sup> generation) or green (Hoveyda-Grubbs' 2<sup>nd</sup> generation) to grey. The chemical structures are presented in Figure 5.13.

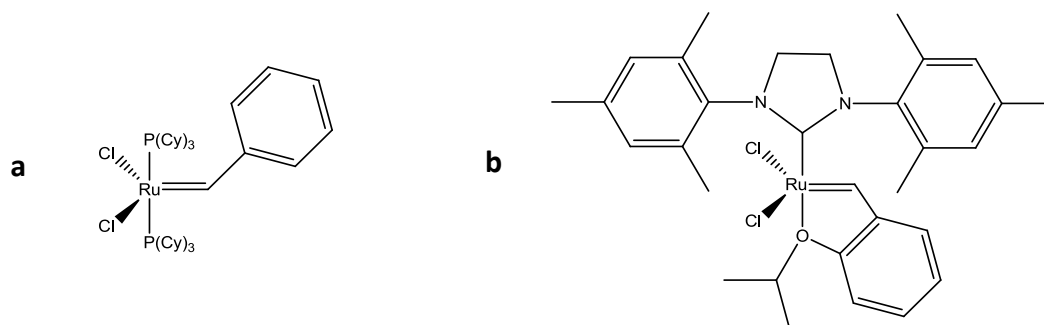


**Figure 5.13** Chemical structure of (a) Grubbs' catalyst 1<sup>st</sup> generation, and (b) Hoveyda-Grubbs' catalyst 2<sup>nd</sup> generation.

**Table 5.7** Composition of the dispersed phase for the preparation of the miniemulsions containing Grubbs' catalyst and hydrodynamic diameters of the obtained nanocapsules after reaction.

Entry	TEOS [g]	solvent		HD [mg]	catalyst		$D_h$ [nm]
		nature	amount [g]		nature	amount [mg]	
JF90-3	1.0	XYL	0.5	125.0	Grubbs' 1 <sup>st</sup>	6.5	320 ± 130
JF109-1	2.0	CHCl <sub>3</sub>	1.0	125.0	Grubbs' 1 <sup>st</sup>	10	210 ± 80
JF110-1	2.0	CH <sub>2</sub> Cl <sub>2</sub>	1.0	125.0	Grubbs' 1 <sup>st</sup>	10	170 ± 70
JF110-2	2.0	TOL	1.0	125.0	Grubbs' 1 <sup>st</sup>	10	410 ± 240
JF115-1	1.0	TOL	0.5	62.5	Grubbs' 1 <sup>st</sup>	10	180 ± 90
JF115-2	1.0	TOL	0.5	62.5	Hoveyda-Grubbs' 2 <sup>nd</sup>	10	190 ± 100
JF131-1 <sup>a</sup>	2.0	CHCl <sub>3</sub>	1.0	125.0	Hoveyda-Grubbs' 2 <sup>nd</sup>	15	170 ± 90
JF136-4	2.0	XYL	1.0	125.0	Hoveyda-Grubbs' 2 <sup>nd</sup>	15	300 ± 150

<sup>a</sup> D<sub>2</sub>O instead of water; 1-phenylheptadecane (PHD) instead of HD.

The successful encapsulation of Grubbs' catalysts could be performed in presence of hexadecane to prevent *Ostwald* ripening and different solvents such as chloroform, dichloromethane, toluene, and xylene without degradation of the catalyst (Table 5.7, Figure 5.14).

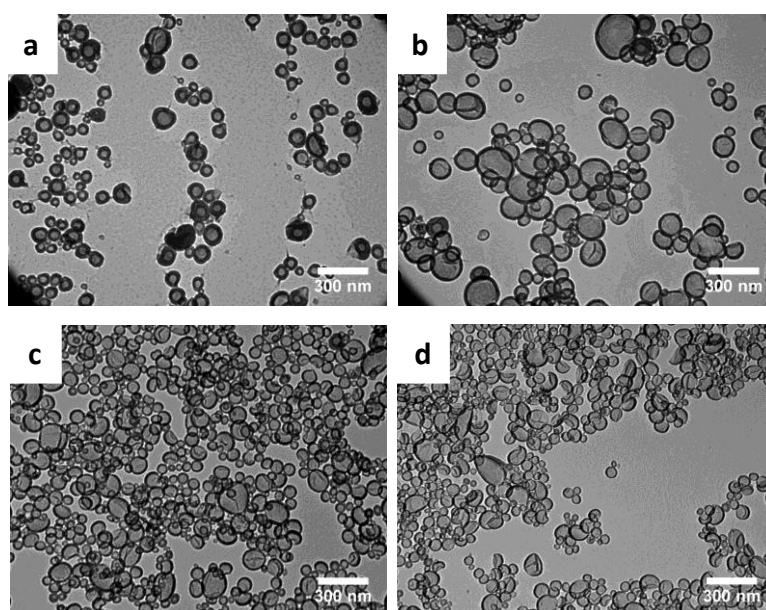


**Figure 5.14** TEM micrographs of the samples prepared with different liquid cores (a) dichloromethane (JF110-1,  $D_h = 170$  nm), (b) toluene with larger capsules (JF110-2,  $D_h = 410$  nm); (c) toluene with smaller capsules (JF115-2,  $D_h = 190$  nm), (d) xylene (JF90-3,  $D_h = 140$  nm).

This is to the best of our knowledge the first time that such catalysts are encapsulated as a solution. Encapsulations are usually performed either in polymer particles,<sup>161</sup> or paraffin matrixes.<sup>181</sup> Therefore it represents a considerable advance compared to previous systems since it should allow higher mobility of the catalyst in self-healing events. The color of the dispersions remained green even after 38 days (JF131-1), and only one peak at 16.6 ppm for the ruthenium carbene<sup>182</sup> was detected by <sup>1</sup>H NMR spectroscopy for dispersions synthesized with D<sub>2</sub>O instead of H<sub>2</sub>O (Figure 5.15).

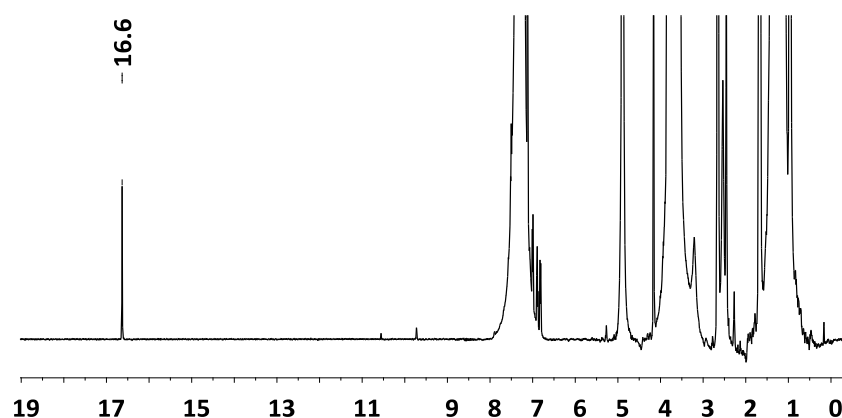


**Figure 5.15** <sup>1</sup>H NMR spectrum of sample JF131-1 with encapsulated Hoveyda-Grubbs' catalyst 2<sup>nd</sup> generation.

Ruthenium could be detected qualitatively on dried dispersion (JF115-2) as shown by EDX measurements (Figure 5.16). No functionalization of the silica shell with Grubbs' catalyst was attempted owing to its sensitivity.

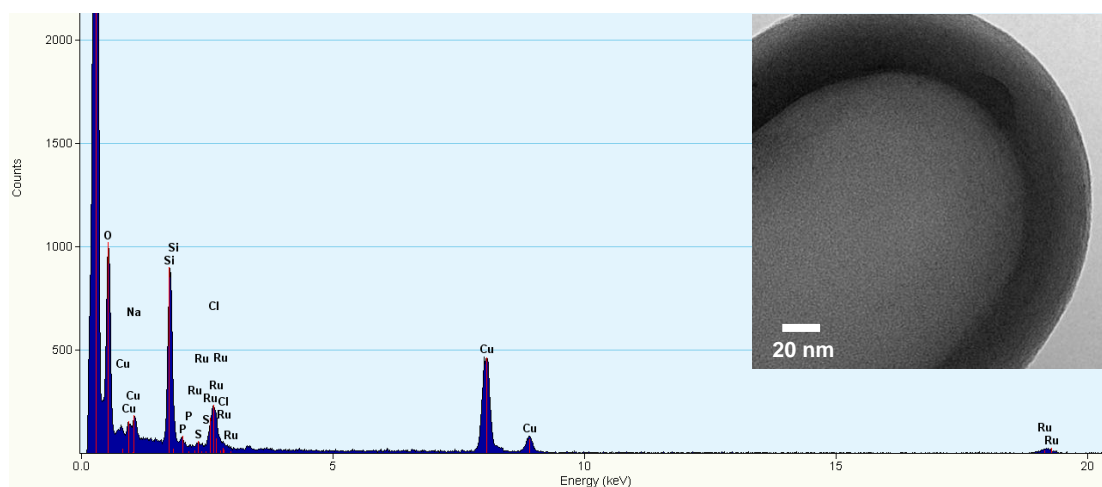


**Figure 5.16** EDX spectrum of the silica nanocapsule encapsulating the Grubbs' catalyst (sample JF115-2). Ruthenium could be detected.

## 5.4 Self-healing reaction

The nanocapsules containing Grubbs' catalyst and DCPD were mixed and opened by a treatment with ultrasound in argon or air to verify that both chemicals were still active.

**Table 5.8** Composition of the resulting mixed dispersions for self-healing tests.

Entry	dispersion containing		argon atmosphere	sonication
	DCPD	Grubbs' catalyst		
SH2	JF139-5	JF136-4	No	Yes
SH3	JF139-5	JF136-4	Yes	Yes

The polymer PDCPD was found to be formed during the self-healing reaction in both cases as shown by  $^{13}\text{C}$  CP-MAS NMR measurements (Figure 5.17).

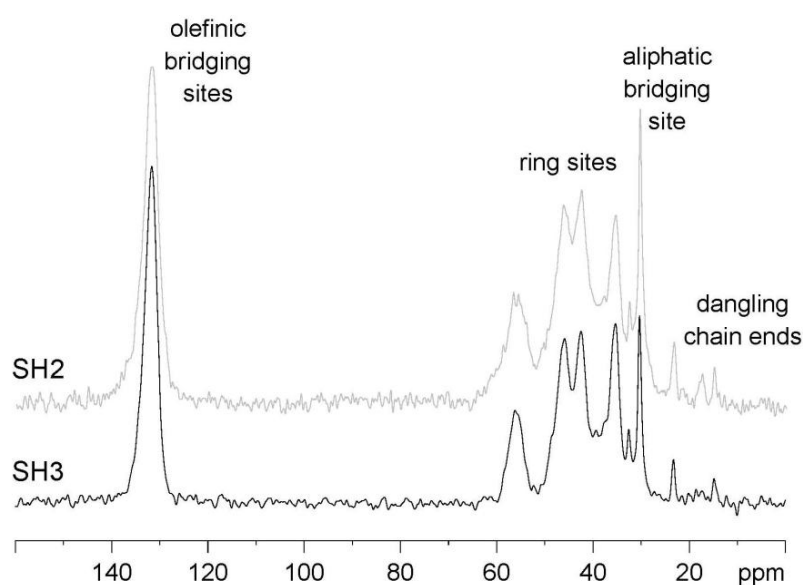


**Figure 5.17**  $^{13}\text{C}$  CP-MAS NMR spectra of dried sample SH2 and SH3.

The self-healing reaction was also quantitatively monitored by TGA measurements (Figure 5.18).

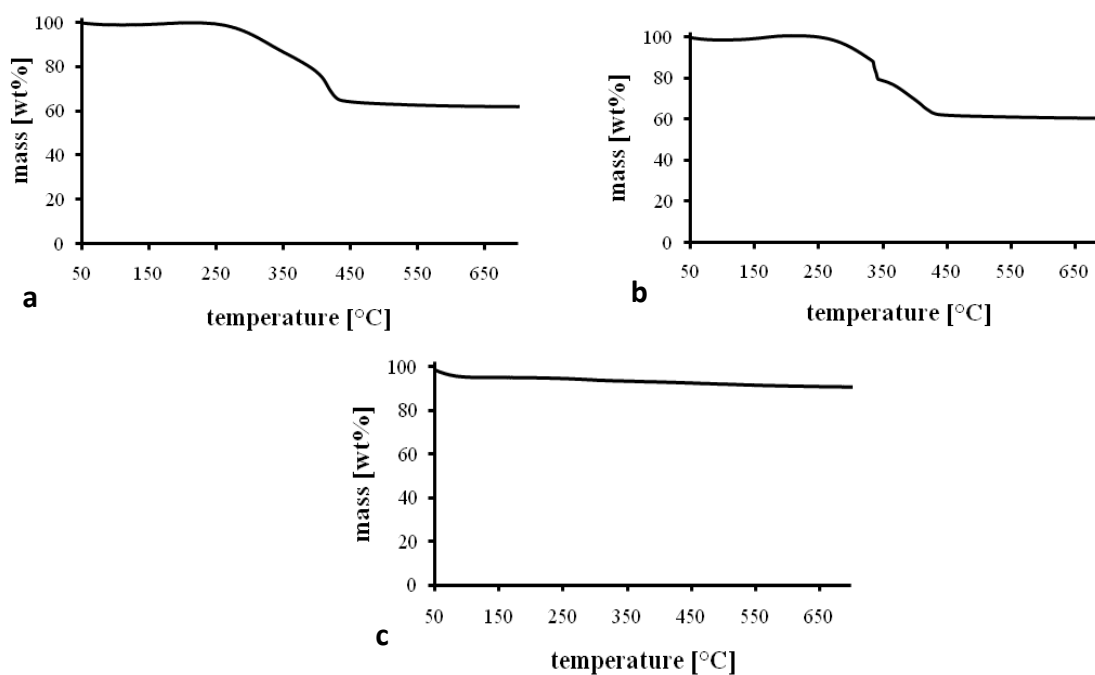


**Figure 5.18** TGA thermograms of freeze-dried samples (a) SH2, (b) SH3, (c) JF139-5 (DCPD capsules).

The dispersions of encapsulated catalyst and monomer were mixed, sonicated, and let further reacted. After drying the mixed dispersion at 80 °C under vacuum, there was only the silica shell and possible PDCPD left in the sample. The weight loss (~38 wt%, [Figure 5.18a](#)) was explained by the amount of the self-healing polymer in the dried sample in addition to the decrease due to the post-condensation of silica (~6 wt%) that occurred during the measurement. The latter value was calculated from TGA measurement of silica capsules that did not experience polymerization ([Figure 5.18c](#)). The theoretical amount of DCPD in the sample SH2 is 31 wt% and therefore the polymerization yield was found to be ~100%, meaning that the catalyst and monomer remained active after encapsulation. No significant differences in weight loss were observed when the sonication was performed under air or argon atmosphere ([Figure 5.18b](#)).



## 5.5 Conclusions

In this second part of the results and discussion chapter, the synthesis of silica nanocontainers for self-healing materials by hydrolysis and polycondensation of alkoxysilanes using the interface of miniemulsion droplets as templates was reported. The size of the nanocapsules, the thickness of their shell, and the solid content of the dispersions could be varied in a wide range. This approach allows the efficient encapsulation of metathesis monomer and catalyst in a one-step process. The catalyst was encapsulated in solution to allow better mobility when released for a self-healing reaction. Further, the silica shell was functionalized by amine and thiol groups. The functional groups were quantified by  $^{29}\text{Si}$  MAS-NMR spectroscopy, XPS, and chemical titration. Therefore a precise picture for the gradient of concentration of functional groups inside the shell could be given. The composition of the shell was enriched in amine functionality compared to the composition in the feed whereas the contrary was observed when a thiol-functionalized trimethoxysilane was reacted. The self-healing agents were found to remain active after encapsulation as proved by successful self-healing reactions monitored qualitatively by  $^{13}\text{C}$  solid-state NMR spectroscopy and quantitatively by TGA measurements.



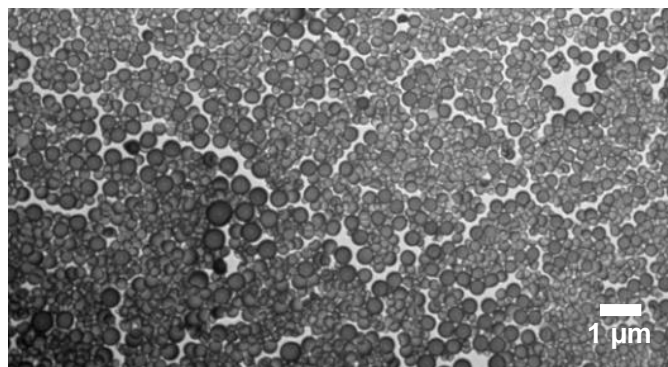
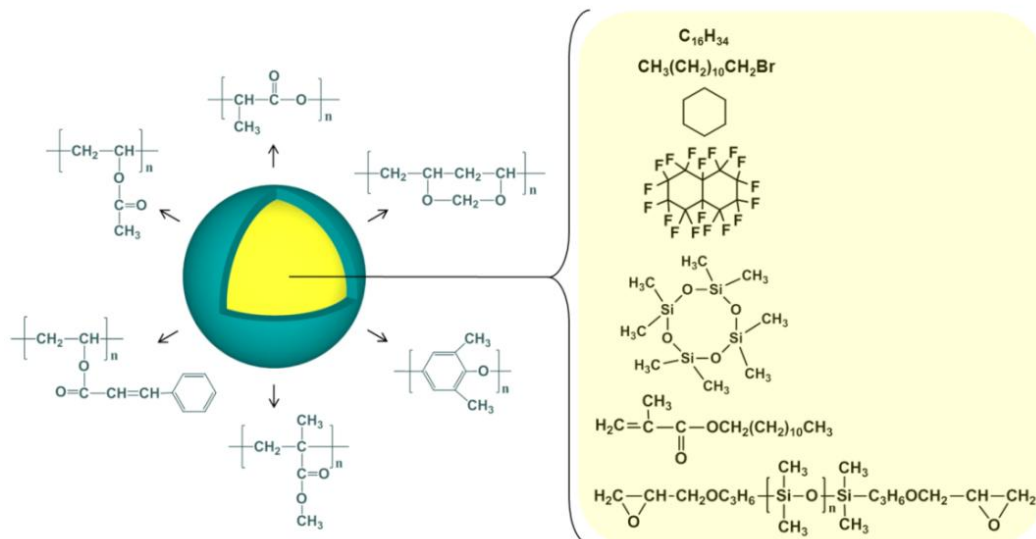
# Chapter 6

## Polymer nanocapsules via the emulsion-solvent evaporation process

based on

*Small* **2012**, 8, 2954-2958;

*Macromolecules* **2013**, 46, 573-579.



## 6 Polymer nanocapsules via the emulsion-solvent evaporation process

In [chapter 4](#), the results about the formation of functionalized nanocapsules synthesized by miniemulsion polymerization were presented. As mentioned, such nanocontainers could be used for the encapsulation of ROMP monomers, but ROMP catalysts were not possible to be encapsulated due to metathesis reaction with vinyl monomers. In order to overcome this problem, silica nanocontainers can be used to encapsulate sensitive self-healing agents such as Grubbs' catalyst, which was demonstrated in [chapter 5](#). Since fillers in composite materials are advantageously fractured when their mechanical properties are lower than the matrix's one, nanocapsules with silica shells may not be appropriate for repairing a polymer matrix. For such applications, polymer nanocontainers are more suitable. Jackson et al. have tackled the problem by preparing nanoparticles embedding Grubbs' catalysts by the emulsion-solvent evaporation procedure, which is a very mild synthetic pathway.<sup>162</sup> However, the catalyst was embedded in the hard polymer particles, limiting the mobility of the reactive species and the amount of encapsulated substance.

In this section, the encapsulation of self-healing agents in polymer core-shell nanoparticles using different pre-synthesized polymers as shells by the miniemulsion-solvent evaporation method is presented. The work is divided into two parts. The first part "*Encapsulation of self-healing agents in polymer nanocapsules*" is focused on the encapsulation of high boiling point solvents, plasticizers, and monomers for self-healing reactions in a large variety of polymer nanocapsules. Only commercially available polymers were used in order to highlight the universality of this strategy. The second part "*Copolymers structures tailored for the preparation of nanocapsules*" deals with the role of the hydrophilicity of the polymer on the successful formation of the capsules. Therefore, copolymers of styrene and hydrophilic comonomers are introduced where the hydrophilicity can be controlled by the nature and content of comonomer units in the copolymer. The nanocapsules were applied for the first encapsulation of ROMP catalysts in the liquid core of polymer nanocontainers.

## 6.1 Encapsulation of self-healing agents in polymer nanocapsules

### 6.1.1 Strategy

The strategy is achieved by the combination of the “solvent evaporation” and the miniemulsion technique, as shown in [chapter 2.2.3.4](#). The nanocapsules filled with healants were formed by an internal phase separation between polymer and the healant that occurs when the good solvent evaporates from the miniemulsion droplets. To the best of our knowledge, this is the very first study for the encapsulation of self-healing agents in different polymer nanocapsules by combination the “solvent evaporation” and miniemulsion techniques. Some of these nanocapsules are reported for the first time using polymers that were in some cases not yet been used in colloidal systems. The pre-synthesized polymer and healants were dissolved in a large quantity of a good solvent for the polymer (with low boiling point) to obtain a homogeneous hydrophobic phase. After adding the aqueous surfactant solution, the mixture is stirred at high shearing speed and then treated by ultrasonication to obtain small and homogeneously distributed miniemulsion droplets. The healant was then encapsulated in polymer nanocapsule through internal phase separation when the good solvent evaporates from the system.

### 6.1.2 Encapsulation of HD

Commercially available polymers with very different properties were applied in this study, including poly(L-lactide) (PLLA), poly(methyl methacrylate) (PMMA), poly(vinyl formal) (PVF), poly(vinyl acetate) (PVAc), poly(2,6-dimethyl-1,4-phenylene oxide) (PPO), and poly(vinyl cinnamate) (PVCi). The chemical structures of the used polymers are shown in [Figure 6.1](#).

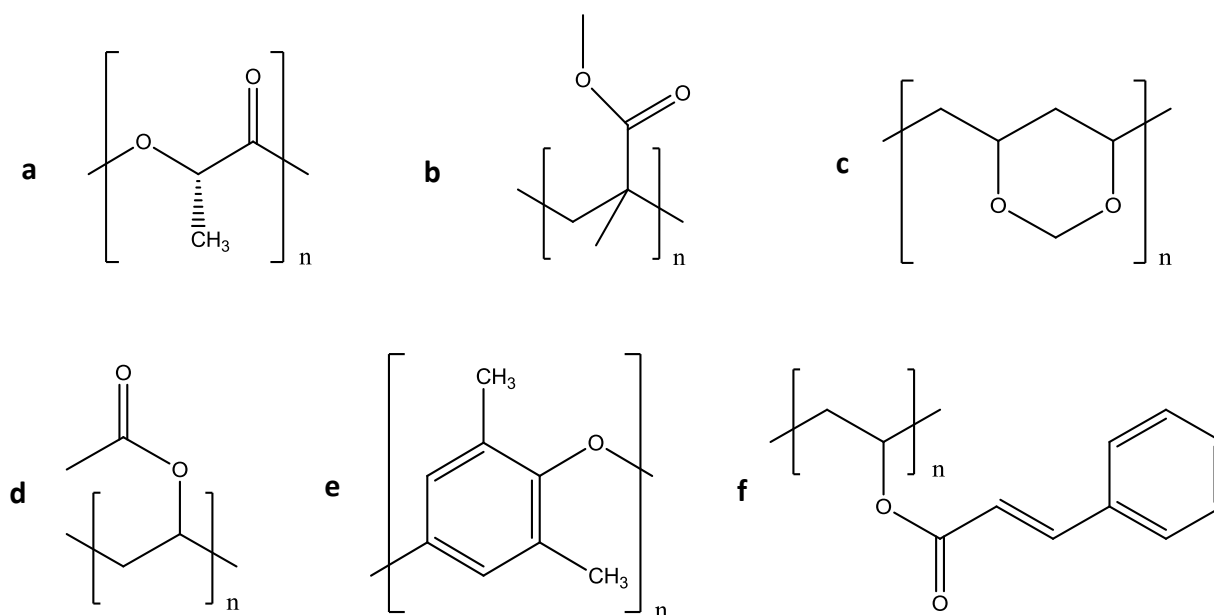


**Figure 6.1** Chemical structures of the used commercial polymers: (a) poly(L-lactide) (PLLA), (b) poly(methyl methacrylate) (PMMA), (c) poly(vinyl formal) (PVF), (d) poly(vinyl acetate) (PVAc), (e) poly(2,6-dimethyl-1,4-phenylene oxide) (PPO), and (f) poly(vinyl cinnamate) (PVCi).

The successful preparation of polymer nanocapsules is a crucial step to fulfill the encapsulation of self-healing agents. Taking this into account, hexadecane (HD) was firstly applied as model compound for the substance to be encapsulated since it is widely used in preparation of miniemulsions. HD is chemically inert but can be used as plasticizer-assisted self-healing.<sup>183</sup> When phase separation occurred in droplets upon evaporation of the good solvent and under suitable wetting conditions, the polymer is forming a shell as predicted by the model of Mason and Torza (see [chapter 2.2.2](#)). Sodium dodecyl sulfate (SDS) was used to stabilize the oil droplets. Chloroform was chosen as the good solvent for all polymers because of its high vapor pressure and limited solubility in water. Unless otherwise stated, the system feed ratio was designed as follow: 250 mg polymer, 250 mg HD, 5 mL chloroform, 10 mL of a  $1.0 \text{ mg}\cdot\text{mL}^{-1}$  aqueous solution of SDS. A summary of the composition and the DLS measurements of all synthesized capsules is shown in [Table 6.1](#).

**Table 6.1** Summary of compositions and DLS results for all capsules.

Entry	polymer	non-solvent/healing agents	$D_h$ [nm]
1	PLLA	hexadecane	320 ± 140
2	PMMA	hexadecane	340 ± 80
3	PVAc	hexadecane	250 ± 90
4	PVF	hexadecane	250 ± 55
5	PPO	hexadecane	320 ± 110
6	PVCi	hexadecane	240 ± 70
7	PLLA	1-bromododecane	360 ± 200
8 <sup>a</sup>	PLLA	cyclohexane	240 ± 60
9	PLLA	perfluorodecaline	320 ± 180
10	PVF	octamethylcyclotetrasiloxane	240 ± 120
11	PVF	lauryl methacrylate	260 ± 120
12	PVF	PDMS-DE	230 ± 70

<sup>a</sup> Dichloromethane was used as solvent and evaporation was performed at room temperature.

The weight ratio of polymer and HD was intentionally designed as 1:1 to obtain a clear phase separation between polymer and HD and clear morphologies. Representative SEM micrographs are shown in [Figure 6.2](#). The wall thickness can be in principle tuned simply by adjusting the feed ratio of the dispersed phase. The aim of this work was to demonstrate the generality and versatility of the proposed method, not going into details for any composition.

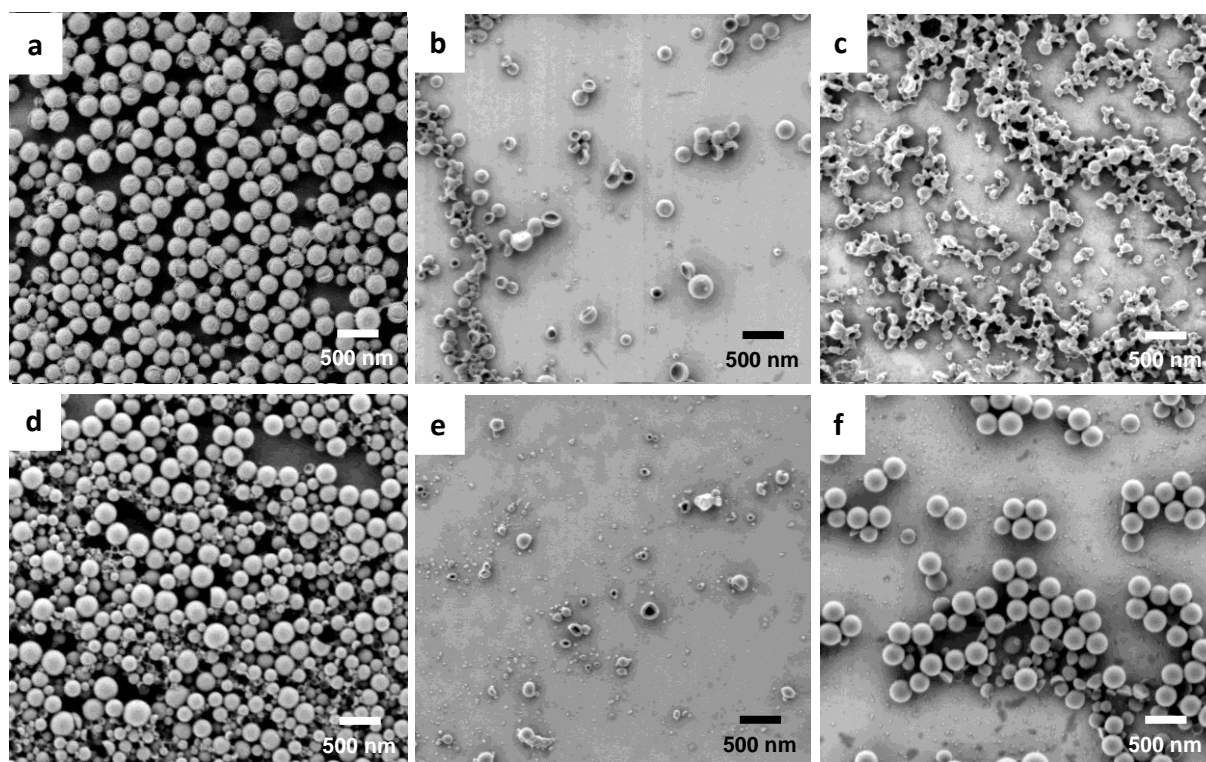


**Figure 6.2** SEM micrographs of the nanocapsules obtained with (listed in Table 6.1): (a) PLLA, Entry 1), (b) PMMA (Entry 2), (c) PVAc (Entry 3), (d) PVF (Entry 4), (e) PPO (Entry 5), (f) PVCi (Entry 6).

The initial failure of organic coatings usually comes from microcracks that are hard to detect. Sometimes, these cracks are too small to rupture the capsule shells and release the healant. Although external stimuli could be used to release the compounds,<sup>184-188</sup> the fabrication of biodegradable capsules to load healants is an interesting alternative. Since the PLLA polymer is known to degrade in the presence of water,<sup>189</sup> once microcracks are formed and the PLLA capsules are in contact with moisture, they will degrade gradually and release the healants continuously.<sup>189</sup> Therefore, PLLA was chosen as a typical example to prepare biodegradable nanocapsules for loading healants. The transmission electron micrograph of PLLA nanocapsules is shown in Figure 6.3a.



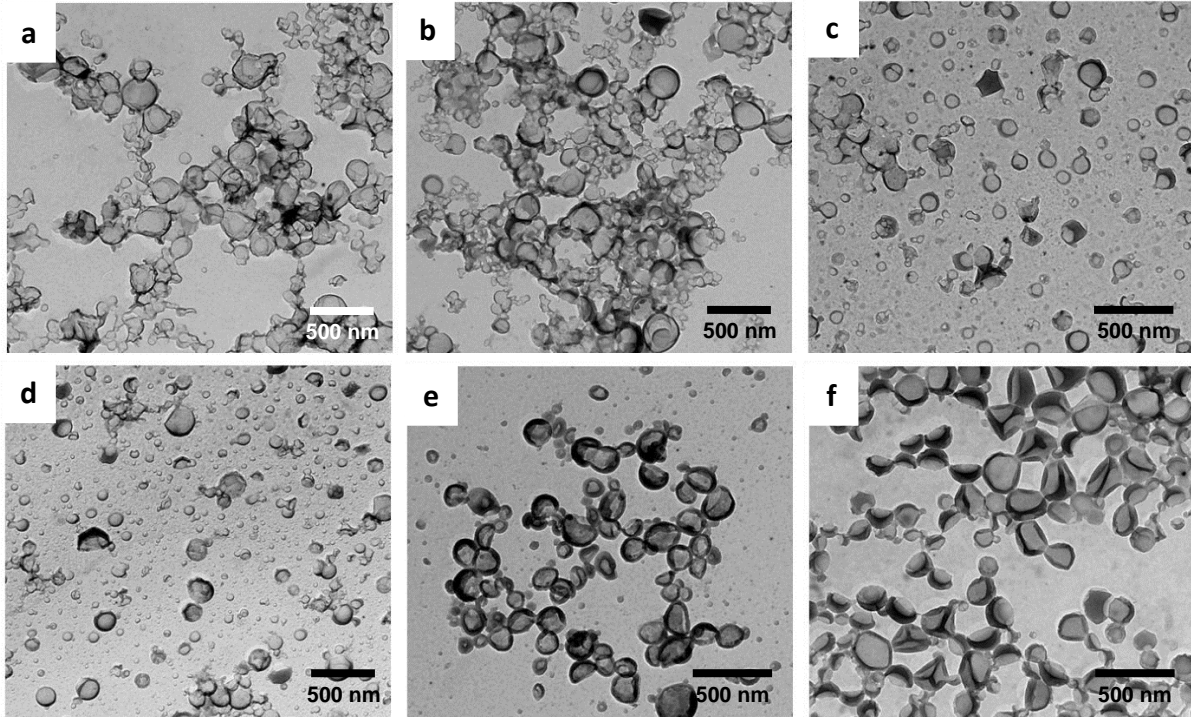


**Figure 6.3** TEM images of nanocapsules obtained with different polymers (listed in Table 6.1): (a) PLLA (Entry 1), (b) PMMA (Entry 2), (c) PVAc (Entry 3); (d) PVF (Entry 4); (e) PPO (Entry 5), (f) PVCi (Entry 6).

The hollow structure due to the evaporation of the core of the core-shell nanoparticles was clearly identifiable. The obtained nanocapsules displayed thin wall thickness  $d$ , around 15 nm (measured from TEM) which is consistent with the theoretical calculation that gives  $\sim 23$  nm with Equation 6:

$$d = r \cdot \left( 1 - \sqrt[3]{\frac{1}{1 + \left( \frac{m_p \cdot \rho_{core}}{m_{core} \cdot \rho_p} \right)}} \right) \quad \text{Equation 6}$$

where  $r$ ,  $m_p$ ,  $\rho_{core}$ ,  $m_{core}$ ,  $\rho_p$  being the radius of the capsule, mass of polymer, density of the core, mass of core, and density of polymer, respectively.

A closer look at the micrographs indicates the existence of irregular nanostructures caused by the random collapse of nanocapsules under the high vacuum required for both the chambers of the sputtering machine (for the carbon layer) and the chamber of the transmission electron microscope. The stable, non-collapsed structures in the scanning

electron micrographs in Figure 6.2a confirmed that the collapse of the capsules occurred only in the high-vacuum chamber. PLLA is applied as one representative example, and other biodegradable polymer nanocapsules could also be used to encapsulate healant by a similar route, in which the selection of solvent and healant plays as important role. Other non-biodegradable polymers were also applied to identify the formation of polymer nanocapsules. Figure 6.3b shows the TEM image of the obtained PMMA nanocapsules. The bowl structures appeared in Figure 6.2b are possibly caused by the collapse of the shell when HD evaporates.

The use of the method was further extended to homopolymers that were never used as capsule shell or even as colloids, such as polyvinylformal (PVF), poly(phenylene oxide) (PPO), and poly(vinyl cinnamate) (PVCi). It is known that the release of agents present in core-shell colloids can be monitored by heating the capsules above the glass transition  $T_g$  of the polymers. Figure 6.3c-e show polymer nanocapsules obtained with PVAc, PVF, and PPO as shell which have  $T_g$  at  $\sim 28$ , 108, and 215 °C respectively. The PPO can be additionally used for high temperature applications. It is also possible to create nanocapsules directly with a functional polymer as shown in Figure 6.3f. Indeed PVCi is a functional polymer that can be crosslinked via a [2+2] photo-cycloaddition and therefore PVCi could be photo-crosslinked to obtain structure-locked capsules. PVCi nanocapsules are then suitable for fabrication of self-healing materials when other polymer nanocapsules are unstable. It is worth to mention that two different collapsing forms can be detected by TEM: a) collapse from one-side to obtain “bowl-like” or spherical cap structures (Figure 6.3f, Figure 6.4a), or b) collapse from several directions (Figure 6.4b).

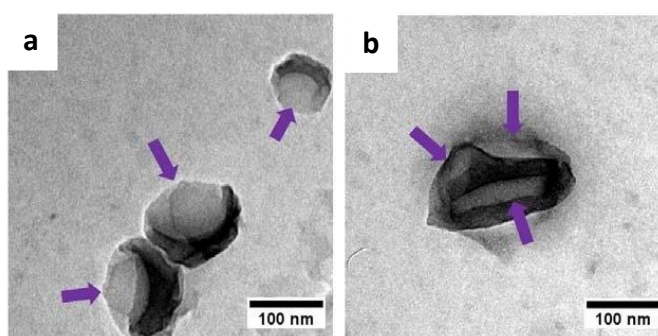


**Figure 6.4** TEM micrographs show two typical collapsed structures under high vacuum. The arrow show the collapsed direction: (a) collapsed from a single direction (PVCi capsule, Entry 6) (b) collapsed from triple or multiple directions (PLLA capsule, Entry 8).

### 6.1.3 Encapsulation of healants for solvent- or plasticizer-assisted self-healing

As aforementioned, HD was applied above as a model compound to demonstrate the generality of the method. The model substances were extended to 1-bromododecane, cyclohexane and perfluorodecaline, which represent healants for solvent- or plasticizer-assisted self-healing with other polarities.

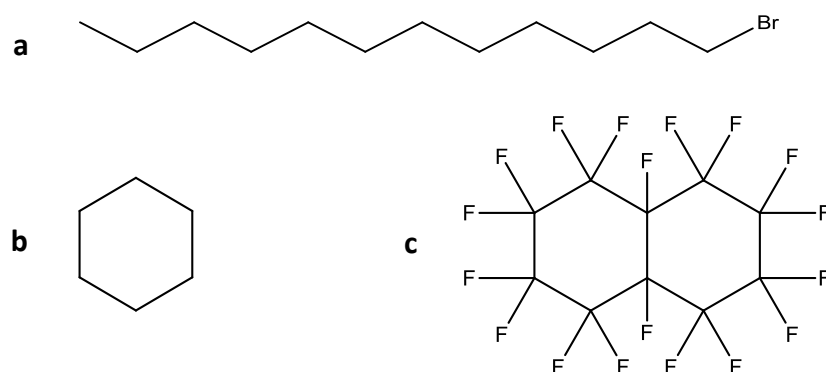


**Figure 6.5** Chemical structure of the healants for solvent- or plasticizer assisted self-healing: (a) 1-bromododecane, (b) cyclohexane, and (c) perfluorodecaline.

In all cases, PLLA was used to fabricate the shell. The transmission electron micrographs of PLLA polymer nanocapsules are shown in Figure 6.6.

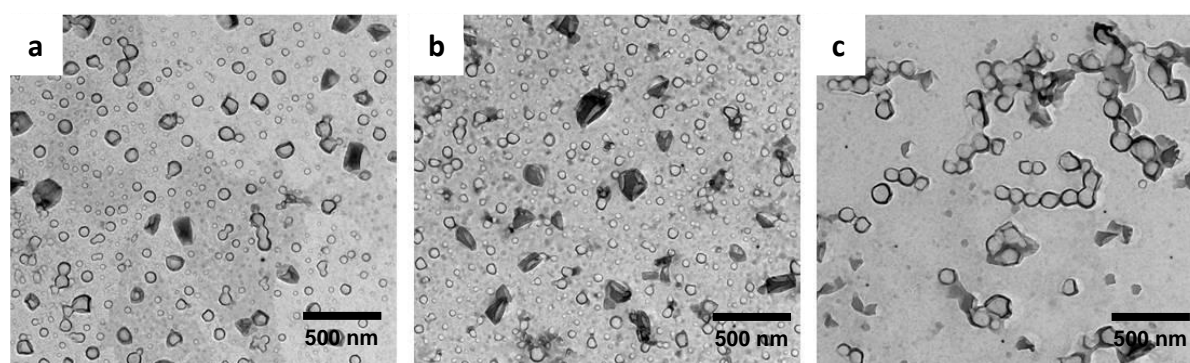


**Figure 6.6** Transmission electron micrographs of PLLA capsules obtained with different non-solvents as liquid core (listed in Table 6.1): (a) 1-bromododecane (Entry 7), (b) cyclohexane (Entry 8), (c) perfluorodecaline (Entry 9).

It is clearly seen that the micrographs of all samples have core-shell nanostructures since the scanning electron micrographs of Figure 6.7 indicated the formation of spherical colloids (no

ring-structures were created). Some holes could be easily detected on the surfaces of nanocapsules (see [Figure 6.7c](#)) which are caused by the evaporation of perfluorodecaline or by the external beam. It is worth mentioning that the dark stripes appearing in [Figure 6.7a,b](#) are polymer nanocapsules that collapsed from different directions during drying in high vacuum (see [Figure 6.4b](#)). The chosen model systems hence indicate that the encapsulation of self-healing agents such as alkanes, cycloalkanes, halogenoalkanes, and perfluoroalkanes are possible with this method.

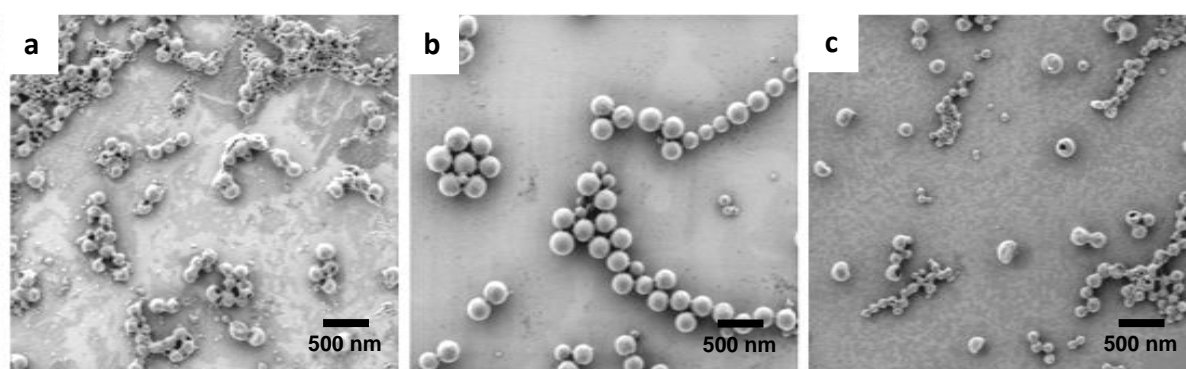


**Figure 6.7** SEM micrographs of PLLA capsules obtained with different non-solvents (listed in [Table 6.1](#)): (a) 1-bromododecane (Entry 7), (b) cyclohexane (Entry 8); (c) perfluorodecaline (Entry 9).

### 6.1.4 Encapsulation of polymerizable self-healing agents

The method was further used to encapsulate chemicals that can be used for self-healing reactions based on polymerizations, following the ideas of the previous chapters. As shown in [Figure 6.9a](#), octamethylcyclotetrasiloxane, which is a monomer that can be polymerized by cationic or anionic ring-opening polymerization, could be successfully encapsulated by PVF nanocapsules. Lauryl methacrylate and poly(dimethylsiloxane) diglycidyl ether terminated (PDMS-DE) were also encapsulated in PVF nanocapsules as shown in [Figure 6.9b,c](#) and [Figure 6.10](#) by SEM. The chemical structures of the mentioned compounds are given in [Figure 6.8](#).

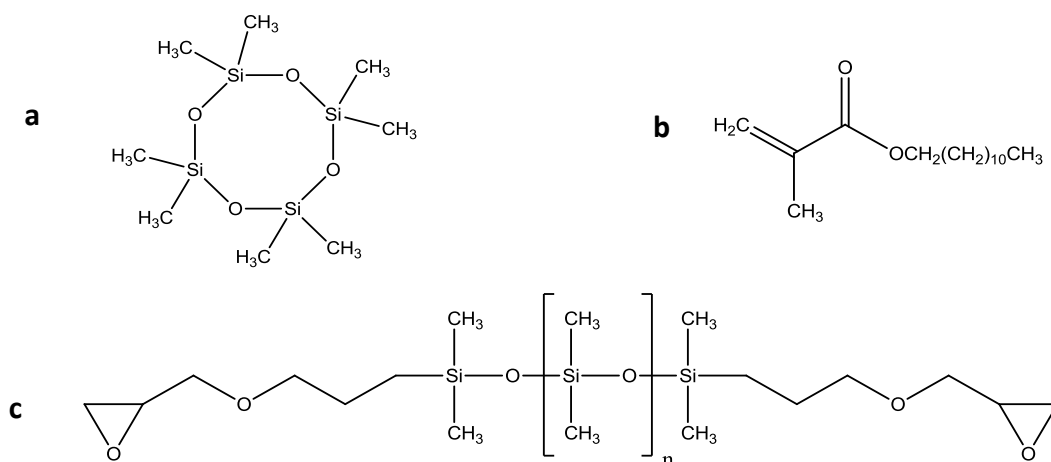


**Figure 6.8** Chemical structures of the encapsulated polymerizable self-healing agents: (a) octamethylcyclotetrasiloxane, (b) lauryl methacrylate, (c) poly(dimethylsiloxane) diglycidyl ether terminated (PDMS-DE,  $M_w \sim 800 \text{ g}\cdot\text{mol}^{-1}$ ).

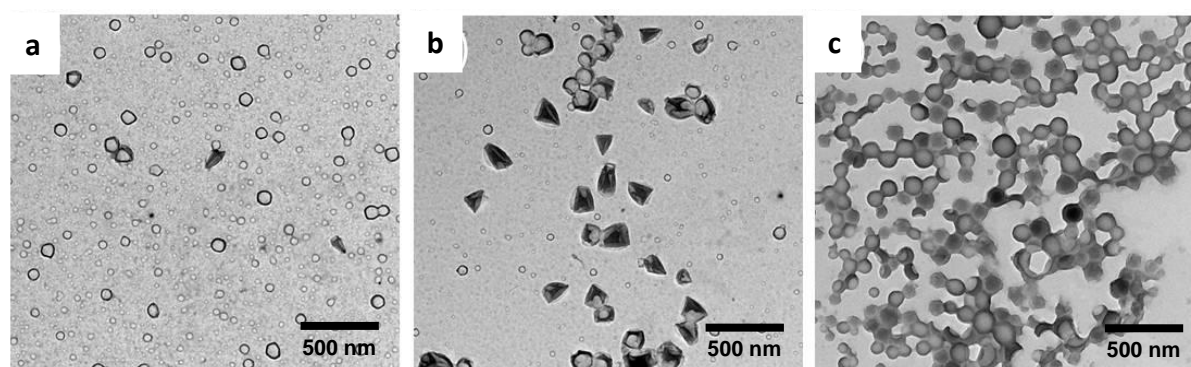


**Figure 6.9** TEM micrographs of PVF nanocapsules with core of (listed in Table 6.1): (a) octamethylcyclotetrasiloxane (Entry 10), (b) lauryl methacrylate (Entry 11), (c) poly(dimethylsiloxane) diglycidyl ether terminated (Entry 12).

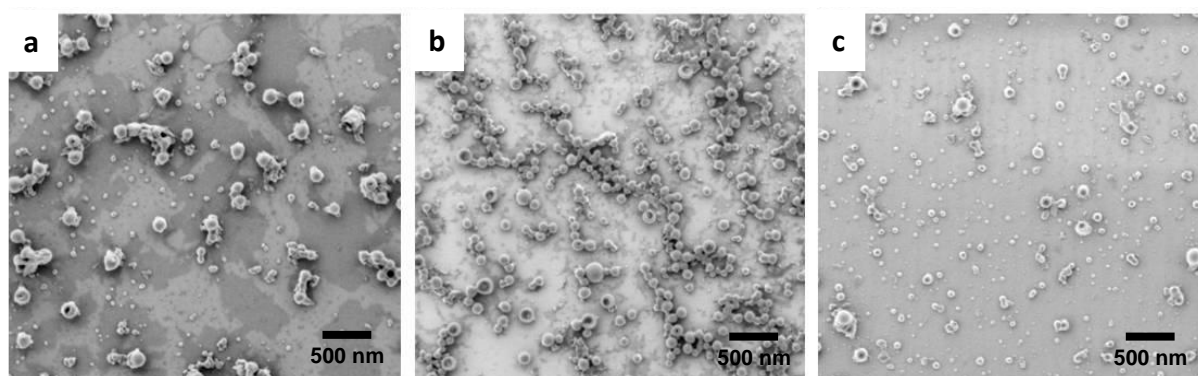


**Figure 6.10** SEM micrographs of PVF nanocapsules (listed in Table 6.1): (a) loaded with octamethylcyclotetrasiloxane (Entry 10), (b) loaded with lauryl methacrylate (Entry 11), (c) loaded with poly(dimethylsiloxane) with diglycidyl ether terminated (Entry 12).

Despite the carbon coating of the capsules before TEM measurements, there is less contrast for the sample with PDMS-DE between the core and the shell compared to other samples. This is due to the fact that the PDMS-DE oligomer ( $M_w \sim 800 \text{ g}\cdot\text{mol}^{-1}$ ) is not evaporated from the capsules. The purified PDMS-DE loaded nanocapsules were analyzed by  $^1\text{H}$  NMR in deuterated chloroform as shown in Figure 6.11.

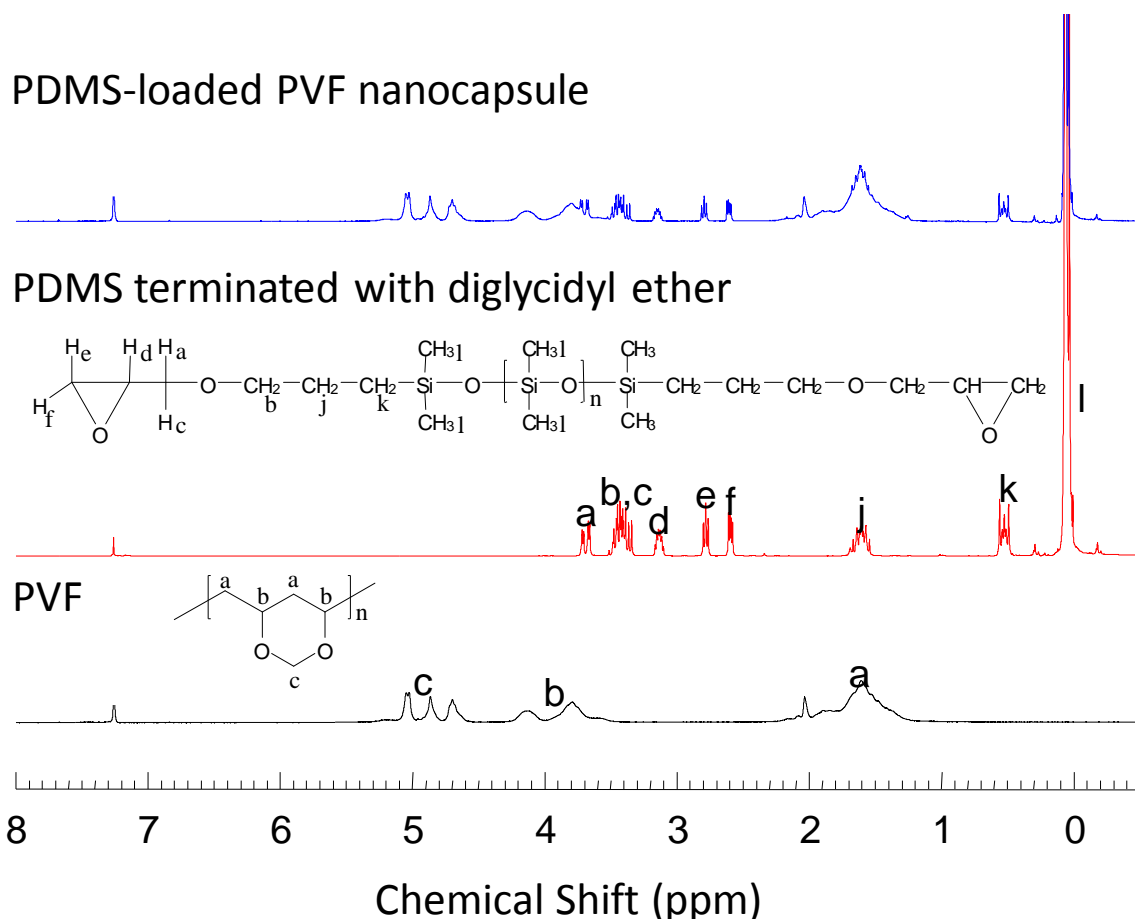


**Figure 6.11**  $^1\text{H}$  NMR spectra of PVF, PDMS-DE and PDMS-DE loaded capsule (Entry 12 in Table 6.1) shows the successful loading of PDMS in PVF nanocapsules.

The result shows that the peaks for both products appeared which means the PDMS-DE has been successfully encapsulated inside the core. The encapsulation efficiency was found to be  $\sim 94\%$  by comparing the integral of the signal at 0 ppm ( $\text{CH}_3$  to Si in PDMS-DE) to the one between 4.5 and 5.2 ppm ( $\text{OCH}_2\text{O}$  in PVF) before and after purification. Although octamethylcyclotetrasiloxane<sup>190-191</sup> and PDMS-DE<sup>192</sup> can be hydrolyzed under acidic or basic conditions, both compounds are expected to remain stable under our mild preparative conditions (pH = 7, 40 °C,  $\sim 10$  h). Using the integral at 0 ppm ( $\text{CH}_3$  to Si in PDMS-DE) as

reference, the integrals of the signals at 2.73 ppm ( $\text{CH}_2$  in epoxy group of PDMS-DE) before and after preparation were used to calculate the extent of hydrolysis. It was found that only ~7% epoxy groups were hydrolyzed after the preparation of the nanocapsules. Thus, nanocapsules with monomers for ionic (octamethylcyclotetrasiloxane), condensation (PDMS-DE), and radical (lauryl methacrylate) self-healing polymerization reactions could be prepared.

## 6.2 Copolymer structures tailored for the preparation of nanocapsules

### 6.2.1 Formation of the capsules

Various copolymers consisting of styrene and different hydrophilic comonomers were investigated as shells to encapsulate hydrophobic liquids via phase separation in miniemulsion droplets triggered by the evaporation of a solvent present in the dispersed phase. Previous experiments have shown that the PMMA block is in contact with water when lamellar structured shells are produced from P(S-*b*-MMA) synthesized by anionic polymerization.<sup>175</sup> Moreover, nanocapsules can be formed easily from PMMA whereas core-shell structures could not be evidenced when PS was employed (JF126-2, [Figure 6.12](#), [Table 6.3](#)).

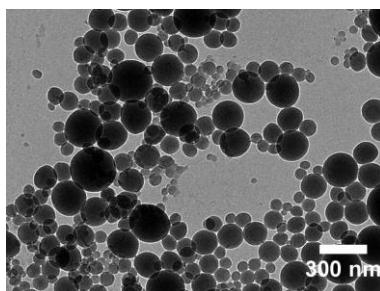


**Figure 6.12** TEM micrograph of the PS colloids (sample JF126-2).

The use of random copolymers synthesized by the inexpensive free-radical polymerization was investigated as substitute for the block copolymer, for which the synthesis is more demanding. The role of the comonomer in the formation of the nanocapsules was explored as well.

For phase separation processes in miniemulsion droplets triggered by a copolymerization, it is known that the polar monomer units of the copolymer act as structure-driving agent during the formation of the nanocapsules (see [chapter 2.2.3.2](#)). Therefore, it is expected that the presence of a comonomer more polar than styrene in the copolymer facilitates the phase separation with the liquid core induced by the evaporation of the solvent initially present in the droplets. Acrylamide (AAm), methyl methacrylate (MMA), and methacrylic acid (MAA) were chosen because the reported values of copolymerization parameters



indicate almost random copolymer structures at low conversion. The chemical structures of the synthesized copolymers are shown in Figure 6.13.

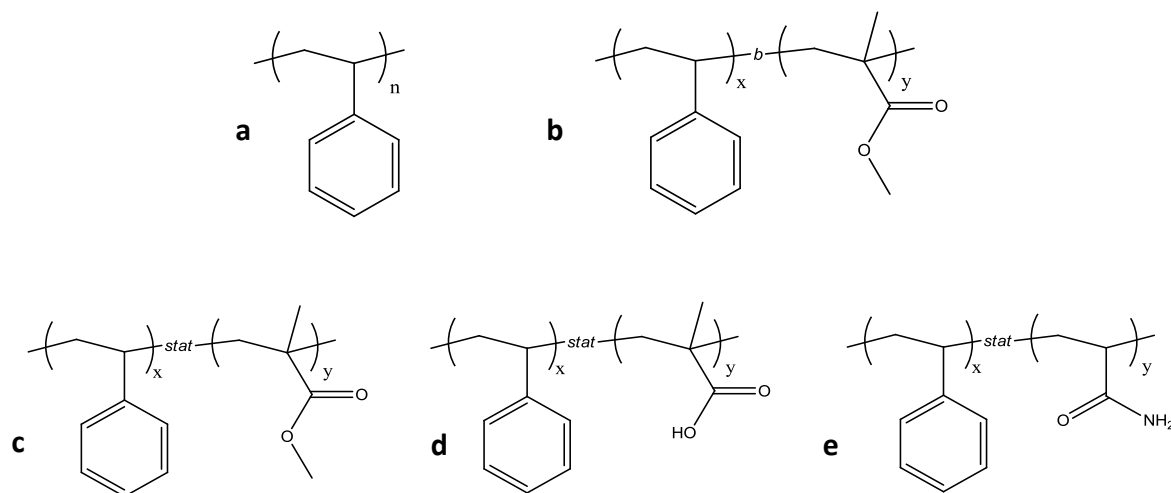


**Figure 6.13** Chemical structure of the synthesized polymers: (a) polystyrene [PS], (b) poly(styrene-*b*-methyl methacrylate) [P(S-*b*-MMA)], (c) poly(styrene-*stat*-methyl methacrylate) [P(S-*stat*-MMA)], (d) poly(styrene-*stat*-methacrylic acid) [P(S-*stat*-MAA)], (e) poly(styrene-*stat*-acrylamide) [P(S-*stat*-AAm)].

Indeed, the copolymerization parameters  $r_1/r_2$  were 1.4/1.3,<sup>193</sup> 0.4/0.6,<sup>194</sup> and 0.5/0.5,<sup>195</sup> for AAm/S, MAA/S, and MMA/S, respectively; these values are reported for copolymerizations in dioxane, a solvent chemically close to the solvent used in this study (THF). Other copolymers were prepared by polymer analogue reactions, starting from P(S-*stat*-MAA) to yield P(S-*stat*-AAm) and P(S-*stat*-MMA). The reaction schemes are presented in Figure 6.14.

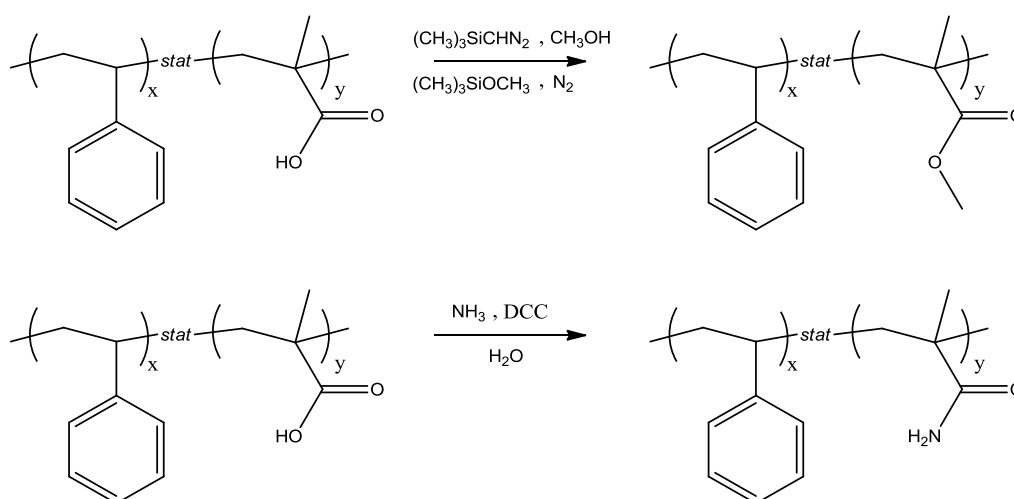


**Figure 6.14** Scheme of the reactions for obtaining methyl ester (top) and methacrylamide (bottom) derivatives of the copolymer with methacrylic acid units.

The characteristics of the synthesized copolymers are shown in Table 6.2. The compositions and the molecular weights of the synthesized copolymers were determined by  $^1\text{H}$  NMR spectroscopy and gel permeation chromatography (GPC), respectively.

**Table 6.2** Compositions and molecular weights of the used copolymers.

Entry	polymer	$M_w$ [g·mol $^{-1}$ ]	$M_n$ [g·mol $^{-1}$ ]	PDI
RS125	P(S $_{0.48}$ - <i>b</i> -MMA $_{0.52}$ )	37,250	35,400	1.1
SC10	P(S $_{0.91}$ - <i>stat</i> -MAA $_{0.09}$ )	54,000	29,000	1.0
SC5	P(S $_{0.86}$ - <i>stat</i> -MAA $_{0.14}$ )	30,150	11,600	2.6
SC13	P(S $_{0.88}$ - <i>stat</i> -MMA $_{0.12}$ )	51,900	33,100	1.6
SC39	P(S $_{0.69}$ - <i>stat</i> -MMA $_{0.31}$ )	44,000	16,100	2.7
SC41	P(S $_{0.67}$ - <i>stat</i> -MMA $_{0.33}$ )	52,950	31,900	1.7
SC6	P(S $_{0.53}$ - <i>stat</i> -MMA $_{0.47}$ )	71,000	43,450	1.6
SC15	P(S $_{0.50}$ - <i>stat</i> -MMA $_{0.50}$ )	42,550	25,300	1.7
SC14	P(S $_{0.49}$ - <i>stat</i> -MMA $_{0.51}$ )	56,000	37,000	1.5
SC26 <sup>a</sup>	P(S $_{0.47}$ - <i>stat</i> -MMA $_{0.53}$ )	76,200	50,700	1.5
SC31	P(S $_{0.73}$ - <i>stat</i> -AAm $_{0.27}$ )	54,500	34,650	1.6
SC44	P(S $_{0.67}$ - <i>stat</i> -AAm $_{0.33}$ )	56,800	33,050	1.7
SC36 <sup>a</sup>	P(S $_{0.72}$ - <i>stat</i> -AAm $_{0.24}$ - <i>stat</i> -MAA $_{0.04}$ )	48,150	27,250	1.8

<sup>a</sup> synthesized by polymer-analogue reactions.

The major constraint for fabricating core-shell nanoparticles with hexadecane core is that the copolymers need to be soluble in the mixture chloroform/hexadecane. It was the case for all synthesized copolymers except for P(S $_{0.67}$ -*stat*-MAA $_{0.33}$ ), P(S $_{0.47}$ -*stat*-MAA $_{0.53}$ ), and P(S $_{0.50}$ -*stat*-AAm $_{0.50}$ ), and therefore these copolymers were not further used. The quality of the nanocapsules obtained was estimated by qualitative analysis of TEM micrographs of the dried copolymer dispersions. The presence of 14% MAA (SC9-1, Table 6.3) in the copolymer was sufficient to yield well-defined nanocapsules (Figure 6.15a,e). A higher concentration of SDS in the miniemulsion (SC9-2, Table 6.3) led to a decrease of the amount of nanocapsules in the system (Figure 6.15b). Indeed, the higher SDS concentration lowers the interfacial tension between hexadecane and the aqueous solution from 14.9 mN·m $^{-1}$  ([SDS] = 1 g·L $^{-1}$ ) to 8.1 mN·m $^{-1}$  ([SDS] = 2 g·L $^{-1}$ ). The surfactant hence stabilized both the polymer/ and the hexadecane/aqueous phases interfaces; the formation of well-defined core-shell colloids was not possible.

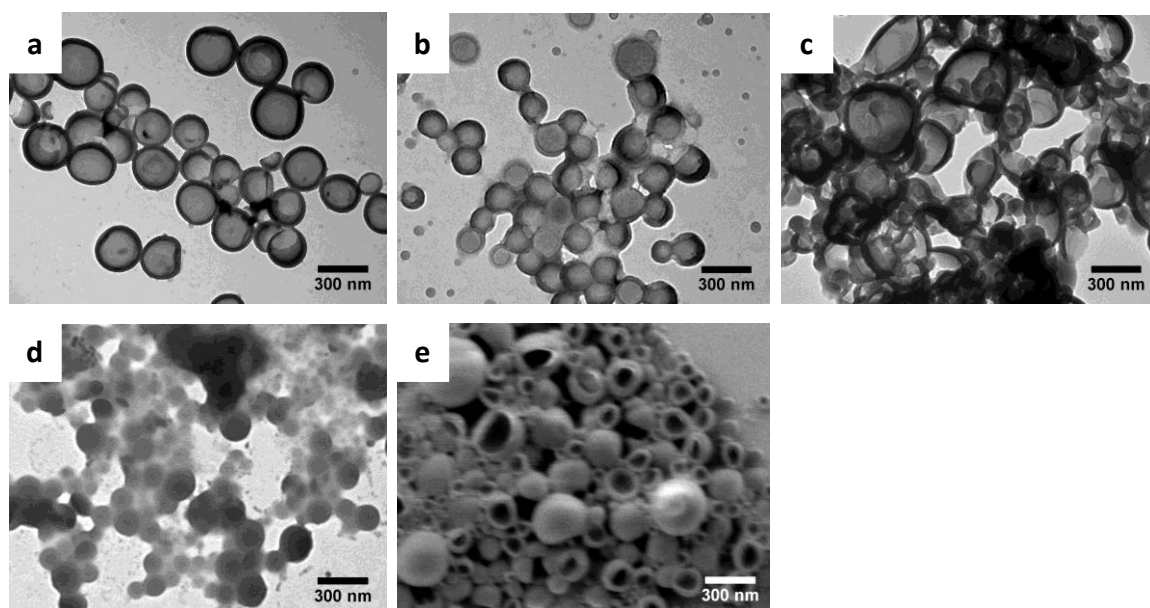


**Figure 6.15** TEM micrographs prepared with copolymer  $P(S_{0.86}\text{-stat-MAA}_{0.14})$  (a) SC9-1 (10 mg SDS), (b) SC9-2 (20 mg SDS), (c) SC16-1 (10 mg CTMA-Cl), (d) SC16-2 (15 mg CTMA-Cl). (e) SEM micrograph of sample SC9-1 [ $P(S_{0.86}\text{-stat-MAA}_{0.14})$ , 10 mg SDS].

Compared to the copolymer with MAA units, a similar amount of MMA units in the copolymer (12%) did not yield nanocapsules, independently on the SDS amount (SC40-12, Figure 6.16a; SC40-2, Figure 6.16b). Increasing the amount of MMA to 31% (SC40-3, Figure 6.16c; SC40-4, Figure 6.16d) and 33% (SC40-13, Figure 6.16e) yielded similar results. Only when the amount of MMA units reached 47% in the copolymer and for the lower concentration of surfactant (SC9-3), the colloids were found to be predominantly capsules as shown in Figure 6.16f. Similarly to the case of MAA, a higher concentration of SDS with  $P(S_{0.53}\text{-stat-MMA}_{0.47})$  was not suitable for the formation of a capsular morphology (SC9-4, Figure 6.16g).

**Table 6.3** Initial composition of the polymeric emulsions and properties of the colloids prepared with the copolymers.

Entry	polymer	CHCl <sub>3</sub> [g]	SDS [mg]	CTMA-Cl [mg]	D <sub>h</sub> [nm]	capsules <sup>c</sup>
<b>colloids from pure polystyrene</b>						
JF126-2	polystyrene	5	10	0	330 ± 110	-
<b>colloids from copolymers with MAA units</b>						
SC9-1	P(S <sub>0.86</sub> -stat-MAA <sub>0.14</sub> )	2.5	10	0	250 ± 80	++
SC9-2			20	0	220 ± 50	+
SC16-1 <sup>a</sup>			0	10	210 ± 40	+
SC16-2 <sup>a</sup>			0	15	240 ± 20	-
<b>colloids from copolymers with MMA units</b>						
SC40-12	P(S <sub>0.88</sub> -stat-MMA <sub>0.12</sub> )	2.5	10	0	260 ± 100	o
SC40-2			20	0	260 ± 100	o
SC40-3	P(S <sub>0.69</sub> -stat-MMA <sub>0.31</sub> )	2.5	10	0	240 ± 70	o
SC40-4			20	0	190 ± 60	o
SC40-13	P(S <sub>0.67</sub> -stat-MMA <sub>0.33</sub> )	2.5	10	0	220 ± 70	o
SC9-3	P(S <sub>0.53</sub> -stat-MMA <sub>0.47</sub> )	2.5	10	0	310 ± 140	+
SC9-4			20	0	230 ± 70	o
SC40-6	P(S <sub>0.50</sub> -stat-MMA <sub>0.50</sub> )	2.5	0	10	230 ± 60	-
SC30-4 <sup>b</sup>	P(S <sub>0.47</sub> -stat-MMA <sub>0.53</sub> )	5	10	0	250 ± 70	++
<b>colloids from copolymers with AAm units</b>						
SC33-1	P(S <sub>0.73</sub> -stat-AAm <sub>0.27</sub> )	2.5	10	0	250 ± 80	++
SC33-2			20	0	220 ± 50	++
SC40-7			0	10	260 ± 100	++
SC47-2			P(S <sub>0.67</sub> -stat-AAm <sub>0.33</sub> )	2.5	10	0
<b>colloids from copolymers with mainly MAAm units</b>						
SC37 <sup>b</sup>	P(S <sub>0.72</sub> -stat-MAAm <sub>0.24</sub> -stat-MAA <sub>0.04</sub> )	5	10	0	330 ± 150	++

<sup>a</sup> conditions: 180 mg polymer, 420 mg hexadecane as dispersed phase;

<sup>b</sup> synthesized by polymer-analogue reactions;

<sup>c</sup> key: (++) only capsules, (+) predominantly capsules (>80%), (o) predominantly open capsules/particles, (-) no capsules.

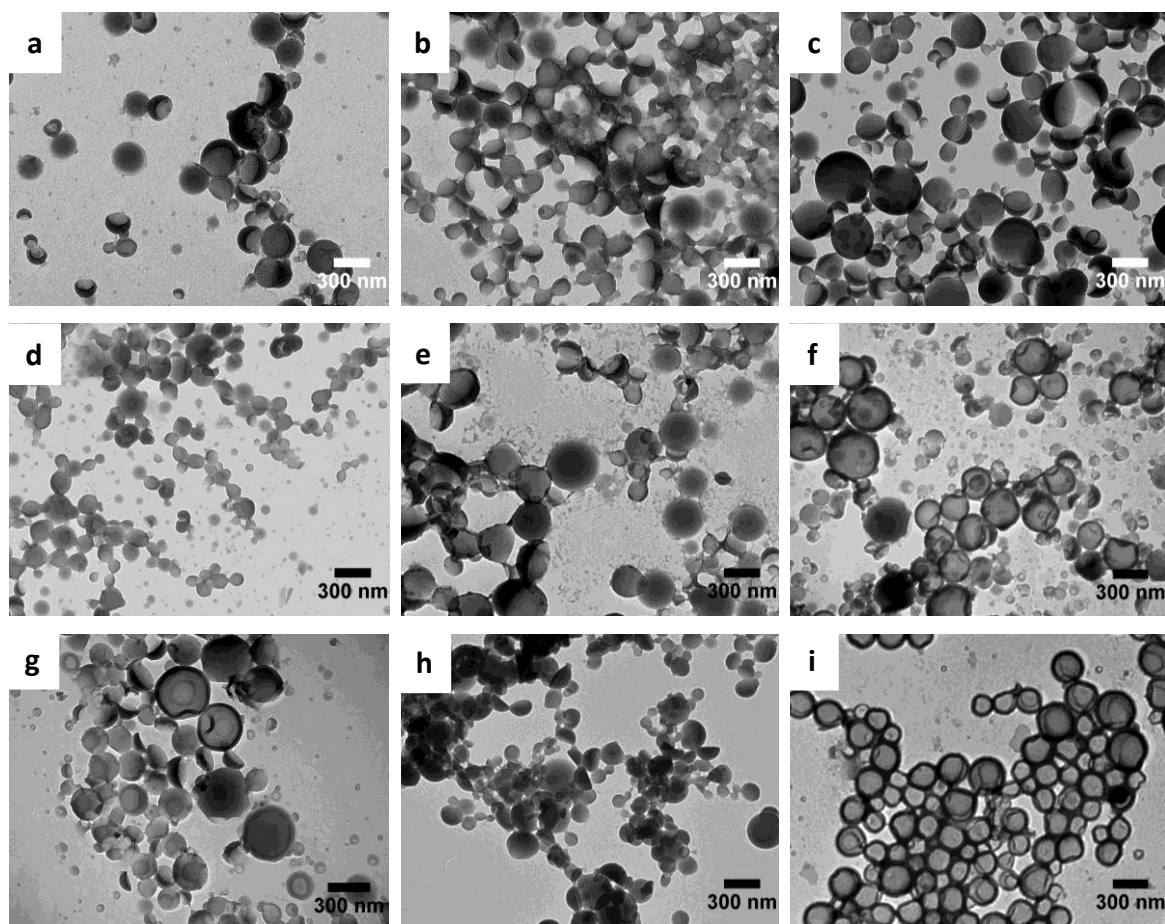


**Figure 6.16** TEM micrographs prepared with:  $P(S_{0.88}\text{-stat-MMA}_{0.12})$  copolymer (a) SC40-12 (10 mg SDS), (b) SC40-2 (20 mg SDS);  $P(S_{0.69}\text{-stat-MMA}_{0.31})$  copolymer (c) SC40-3 (10 mg SDS), (d) SC40-4 (20 mg SDS);  $P(S_{0.67}\text{-stat-MMA}_{0.33})$  copolymer (e) SC40-13 (10 mg SDS);  $P(S_{0.53}\text{-stat-MMA}_{0.47})$  copolymer (f) SC9-3 (10 mg SDS), (g) SC9-4 (20 mg SDS);  $P(S_{0.50}\text{-stat-MMA}_{0.50})$  copolymer (h) SC40-6 (10 mg CTMA-Cl);  $P(S_{0.47}\text{-stat-MMA}_{0.53})$  copolymer (i) SC30-4 (10 mg SDS).

As shown in Figure 6.16i, well-defined nanocapsules were obtained with the introduction of an even higher amount of MMA (53%, SC30-4). This means that a sufficient amount of MMA units in the copolymer allows the formation of nanocapsules. Although PMMA is not very polar, the interfacial tension against water is significantly lower than for polystyrene, *i.e.* 16 against  $32 \text{ mN}\cdot\text{m}^{-1}$ .<sup>196</sup> This is also the reason why the block copolymer  $P(S\text{-}b\text{-MMA})$  yielded core-shell structures. Indeed, previous XPS experiments have shown that  $\sim 75\%$  of the surface was composed of PMMA due to the patchy structure of the nanocapsules.<sup>175</sup>

The copolymers with 24% (SC37), 27% (SC33-1, SC33-2), and 33% (SC47-2) of (meth)acrylamide synthesized by polymer-analogue reaction, and free-radical polymerization yielded always well-defined nanocapsules independently on the amount of SDS used in the miniemulsions, as shown in Figure 6.17a,b,c,e.

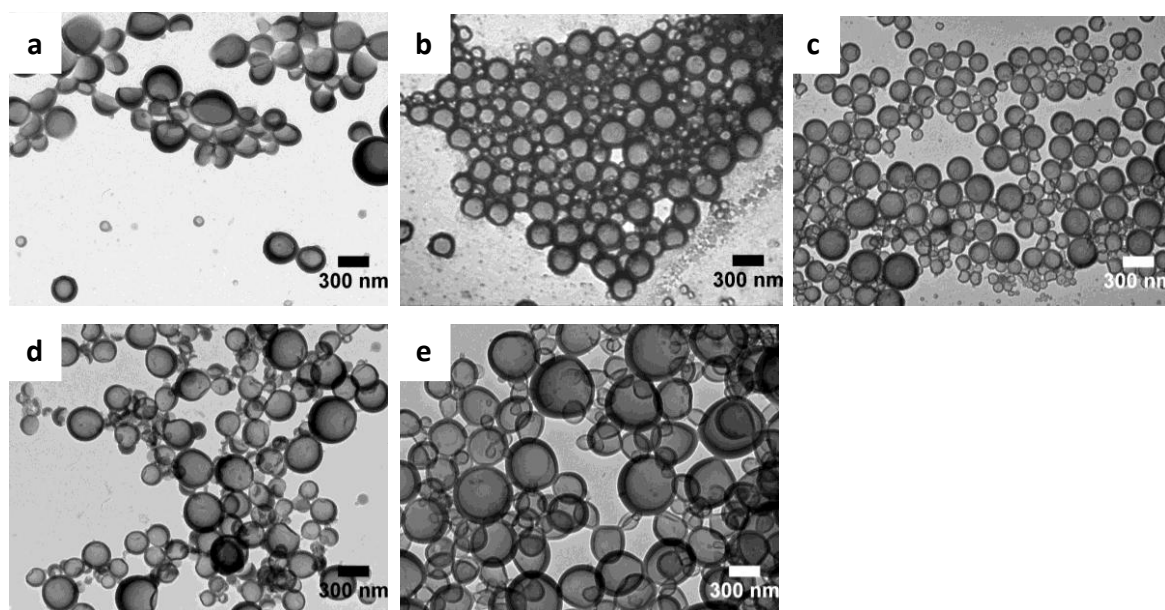


**Figure 6.17** TEM micrographs prepared with different copolymers of (meth)acrylamide **(a)** SC37 [ $P(S_{0.72}\text{-stat-MAAm}_{0.24}\text{-stat-MAA}_{0.04})$ , 10 mg SDS], **(b)** SC33-1 [ $P(S_{0.73}\text{-stat-AAm}_{0.27})$ , 10 mg SDS], **(c)** SC33-2 [ $P(S_{0.73}\text{-stat-AAm}_{0.27})$ , 20 mg SDS], **(d)** SC40-7 [ $P(S_{0.73}\text{-stat-AAm}_{0.27})$ , 10 mg CTMA-Cl], **(e)** SC47-2 [ $P(S_{0.67}\text{-stat-AAm}_{0.33})$ , 10 mg SDS].

Remarkably, nanocapsules could also be obtained with CTMA-Cl as surfactant when MAA and AAm were used as monomers (SC16-1, [Figure 6.15c](#); SC40-7, [Figure 6.17d](#)). As for SDS, a higher concentration of CTMA-Cl hindered the formation of capsules (SC16-2, [Figure 6.15d](#)). The 50:50 copolymer of styrene and MMA (SC40-6) did not allow the formation of capsular morphologies with CTMA-Cl ([Figure 6.16h](#)). This is probably due to the difference of surface tension between solutions of SDS and CTMA-Cl, *i.e.* 37 and 41  $\text{mN}\cdot\text{m}^{-1}$  at 1  $\text{g}\cdot\text{L}^{-1}$  respectively. In this case, the CTMA-Cl is not able to stabilize efficiently the polymer/aqueous solution surface. The fact that high amounts of surfactant hinders the formation of core-shell nanoparticles is important because it implies that nanocapsules with smaller sizes cannot be produced by this technique, hence limiting the method to capsule size of  $\sim 200$  nm and more for the aforementioned experimental conditions.

Hereinafter, a tentative prediction of the colloidal morphologies from thermodynamic parameter is given. In order to estimate the spreading coefficients as defined by Torza and Mason ([chapter 2.2.2](#)), the surface tensions of the polymers  $\gamma_{pV}$  were estimated by calculating the molar parachor for the different copolymers (given in [Equation 7](#)),<sup>197</sup>

according to the values assigned by Quayle,<sup>198</sup> and by calculating the molar volume of monomer units:<sup>197</sup>

$$\gamma_{PV} = \left( x \cdot \frac{P_{PS}}{V_{PS}} + y \cdot \frac{P_2}{V_2} \right)^4 \quad \text{Equation 7}$$

with *PS* as abbreviation of polystyrene and 2 representing the homopolymer of the other comonomer (acrylamide, methacrylic acid, or methyl methacrylate). The contributions of styrene, methyl methacrylate, methacrylic acid and acrylamide were calculated by subtracting the contribution of two hydrogens to the tabulated values of ethylbenzene, methyl isobutyrate, isoturic acid, and propionamide, which were determined by Quayle.<sup>198</sup>

The interfacial tensions (co)polymers/hexadecane and (co)polymers/aqueous surfactant solution  $\gamma_{PL}$  (L = O or W) were calculated following Young's equation (Equation 8):

$$\gamma_{PL} = \gamma_{PV} - \gamma_{LV} \cdot \cos \theta \quad \text{Equation 8}$$

where  $\theta$  is the contact angle of the oil or water droplet on the polymer surface, respectively.

The end groups were neglected in the calculation. Tanaka et al. showed that some end-groups such as sulfate groups originating from the decomposition of the initiator have a significant influence on the morphology of the particles obtained by the solvent evaporation method.<sup>199</sup> In our case, the end-groups are not polar because the hydrophobic AIBN was used as initiator for the polymerization and therefore the morphology of the particles was not significantly influenced.

The three spreading coefficients were then calculated according to Equation 2 (chapter 2.2.2):

$$\begin{aligned} S_O &= \gamma_{PW} - (\gamma_{OP} + \gamma_{OW}) \\ S_W &= \gamma_{OP} - (\gamma_{OW} + \gamma_{PW}) \\ S_P &= \gamma_{OW} - (\gamma_{OP} + \gamma_{PW}) \end{aligned} \quad \text{Equation 9a,b,c}$$

The values are reported in Table 6.4 as well as the predicted morphologies of the colloids (Figure 6.18).

**Table 6.4** Thermodynamic parameters for the prediction of the colloidal morphologies.

Polymer	SDS [g·L <sup>-1</sup> ]	$\gamma$ [mN·m <sup>-1</sup> ]			$S_O$	$S_W$	$S_P$	predicted morphology
		$\gamma_{ow}$	$\gamma_{op}$	$\gamma_{pw}$				
P(S <sub>0.88</sub> -stat-MMA <sub>0.12</sub> )	0	52	15	34	< 0	< 0	> 0	core-shell
	1	15	15	23	< 0	< 0	< 0	doublet
	2	8	15	31	> 0	< 0	< 0	inverse core-shell
P(S <sub>0.49</sub> -stat-MMA <sub>0.51</sub> )	0	52	15	44	< 0	< 0	< 0	doublet
	1	15	15	30	< 0	< 0	< 0	doublet
	2	8	15	31	> 0	< 0	< 0	inverse core-shell
P(S <sub>0.90</sub> -stat-MAA <sub>0.10</sub> )	0	52	15	43	< 0	< 0	< 0	doublet
	1	15	15	37	> 0	< 0	< 0	inverse core-shell
	2	8	15	30	> 0	< 0	< 0	inverse core-shell
P(S <sub>0.73</sub> -stat-AAm <sub>0.27</sub> )	0	52	15	50	< 0	< 0	< 0	doublet
	1	15	15	31	> 0	< 0	< 0	inverse core-shell
	2	8	15	30	> 0	< 0	< 0	inverse core-shell

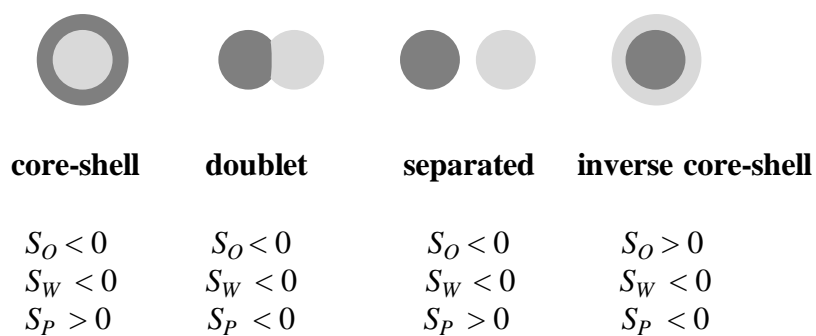


**Figure 6.18** Predicted morphology of the colloids according to the sign of the spreading coefficients.

It is difficult to discuss the morphologies obtained with the model proposed by Torza and Mason. Indeed, the calculated interfacial tensions between the aqueous solution of SDS and the polymers are too high to yield a positive spreading coefficient (Table 6.4). This is due to the relatively high values of contact angle (typically more than 60°) of the droplets of aqueous solutions on the polymer films. The polar groups are probably oriented preferably toward the substrate to minimize the surface tension of the film, thus yielding an interface film/air enriched in hydrophobic groups that conducts to higher contact angle for the



droplets of aqueous solutions. The interfacial tension between the copolymer and water is lower in the case of MAA than for AAm containing copolymers. Indeed, the MAA units are partially ionized in the aqueous solution whereas the acrylamide units remain electroneutral. Therefore, for the latter case, more surfactant can be added.

## 6.2.2 Encapsulation of ROMP monomers

DCPD was used as a suitable and common monomer for ring-opening metathesis polymerization (Table 6.5). Since the copolymers are soluble in DCPD, it was necessary to mix them with HD to create a precipitating solution for the copolymer after evaporation of the chloroform. All the copolymers  $P(S_{0.49}\text{-stat-MMA}_{0.51})$ ,  $P(S_{0.91}\text{-stat-MAA}_{0.09})$ , and  $P(S_{0.73}\text{-stat-AAm}_{0.27})$  yielded an encapsulation of the mixture DCPD/HD and core-shell structures (Figure 6.19).

**Table 6.5** Compositions for the preparation of the nanocapsules with encapsulated DCPD monomer and Hoveyda-Grubbs' catalyst 2<sup>nd</sup> generation for ring-opening metathesis polymerization.

Entry	polymer	CHCl <sub>3</sub> [g]	HD [mg]	DCPD [mg]	catalyst [mg]	M <sub>w</sub> [g/mol]	M <sub>n</sub> [g/mol]	PDI	D <sub>n</sub> [nm]
SC50-1	$P(S_{0.49}\text{-stat-MMA}_{0.51})$	2.5	150	150	0	42,550	25,300	1.7	200 ± 50
SC50-2	$P(S_{0.91}\text{-stat-MAA}_{0.09})$	5	150	150	0	53,750	29,400	1.8	240 ± 20
SC50-3	$P(S_{0.73}\text{-stat-AAm}_{0.27})$	2.5	150	150	0	54,500	34,650	1.6	210 ± 60
SC51-1	$P(S_{0.49}\text{-stat-MMA}_{0.51})$	2.5	300	0	15	42,550	25,300	1.7	290 ± 130
SC51-2	$P(S_{0.91}\text{-stat-MAA}_{0.09})$	5	300	0	15	53,750	29,400	1.8	310 ± 60
SC51-3	$P(S_{0.73}\text{-stat-AAm}_{0.27})$	2.5	300	0	15	54,500	34,650	1.6	300 ± 130

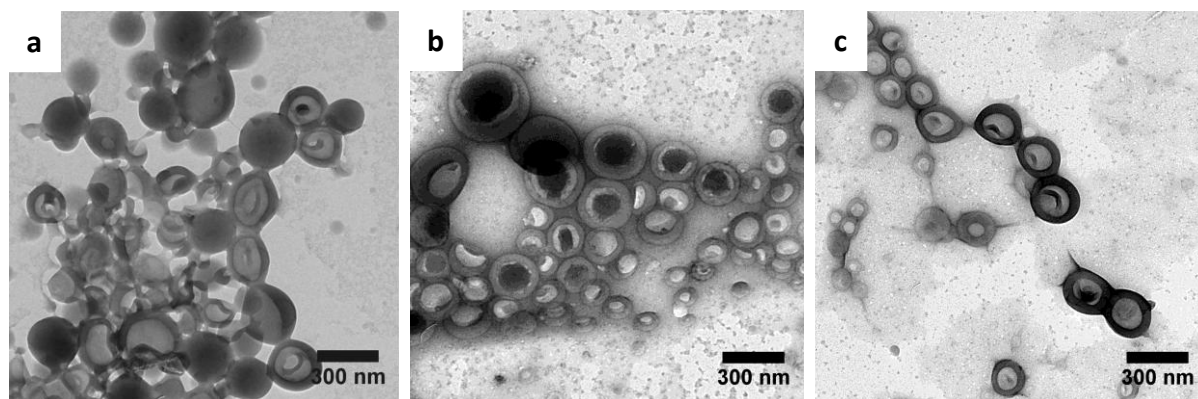


**Figure 6.19** Nanocapsules with liquid core composed of DCPD:HD (50:50) with different polymer shells (a)  $P(S_{0.49}\text{-stat-MMA}_{0.51})$ , (b)  $P(S_{0.91}\text{-stat-MAA}_{0.09})$ , (c)  $P(S_{0.73}\text{-stat-AAm}_{0.27})$ .

The amount of DCPD after evaporation of the chloroform was quantified by measuring the dispersion of nanocapsules in  $D_2O$  with  $^1H$  NMR spectroscopy using an internal standard 4,4-dimethyl-4-silapentane-1-sulfonic acid (DSS). The chemical structure of DSS is given in Figure 6.20.

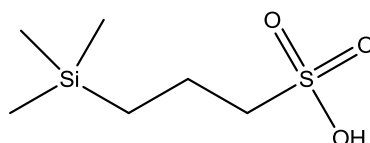


**Figure 6.20** Chemical structure of the internal NMR standard 4,4-dimethyl-4-silapentane-1-sulfonic acid (DSS).

In the three cases,  $\sim 100\%$  of the monomer was found in the dispersions, which means that no significant amount of DCPD has been evaporated during the procedure (Figure 6.21).

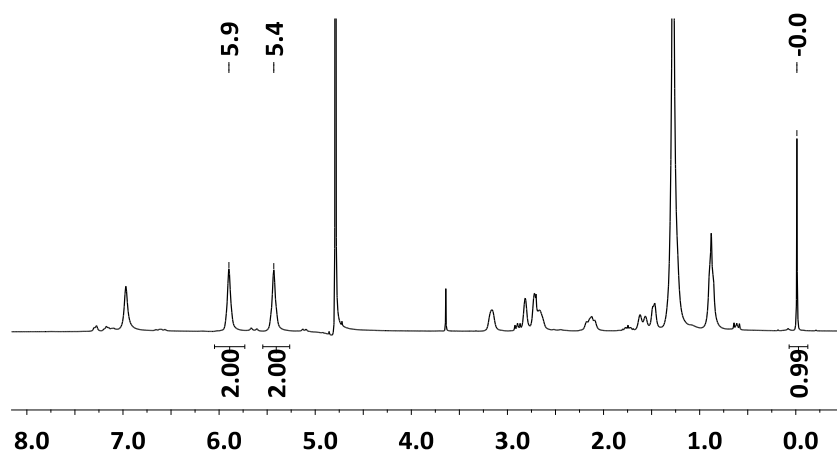


**Figure 6.21** Representative  $^1\text{H}$  NMR spectrum of the nanocapsules with encapsulated DCPD. The polymer shell is composed of  $P(S_{0.91}\text{-stat-MAA}_{0.09})$  and the signals detected at 5.9 and 5.4 ppm are originating from DCPD. The signal at  $\sim 0$  ppm is corresponding to DSS.

### 6.2.3 Encapsulation of ROMP catalysts

As, mentioned, the encapsulation methods based on internal phase separation in miniemulsion droplets triggered by a radical polymerization cannot be used for ROMP catalysts (see [chapter 4](#)). However, the use of pre-synthesized copolymers in the miniemulsion-solvent evaporation process is a very mild method for the encapsulation of sensitive chemicals. An interesting application for such system is the encapsulation of ROMP catalysts for self-healing reactions. The Hoveyda-Grubbs' catalysts 2<sup>nd</sup> generation could be encapsulated using the three different copolymers as shown in [Figure 6.22](#). The corresponding compositions for the preparation of the catalyst loaded nanocapsules are given in [Table 6.5](#).

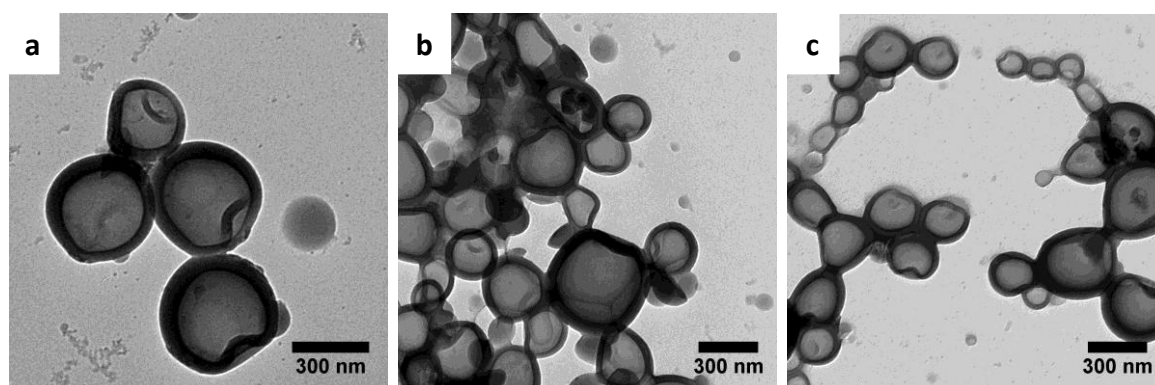


**Figure 6.22** Nanocapsules with encapsulated Hoveyda-Grubbs' catalyst 2<sup>nd</sup> generation with different polymer shells (a)  $P(S_{0.49}\text{-stat-MMA}_{0.51})$ , (b)  $P(S_{0.91}\text{-stat-MAA}_{0.09})$ , (c)  $P(S_{0.73}\text{-stat-AAm}_{0.27})$ .

The color of the dispersions remained unchanged after the encapsulation and the proton of the ruthenium carbene was detected by  $^1\text{H}$  NMR spectroscopy as shown in Figure 6.23. This verifies that the catalyst was still stable and active after the encapsulation process.

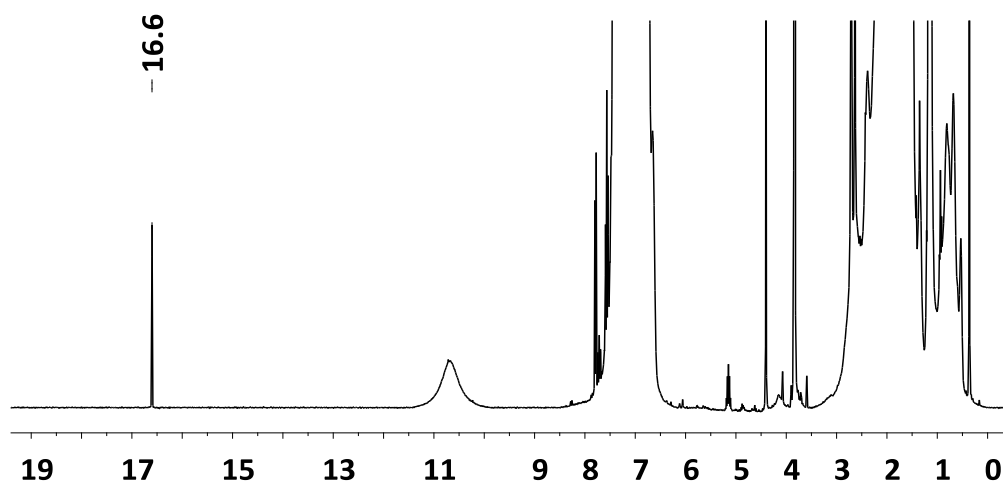


**Figure 6.23** Representative  $^1\text{H}$  NMR spectrum of the nanocapsules with the Hoveyda-Grubbs' catalyst 2<sup>nd</sup> generation (freeze-dried and dissolved in THF). Here the polymer shell is composed of  $P(S_{0.91}\text{-stat-MAA}_{0.09})$ . The signal at 16.6 ppm is corresponding to the proton of the ruthenium carbene.

#### 6.2.4 Self-healing reaction

The dispersions of nanocapsules containing DCPD and Grubbs' catalyst were mixed and opened by treatment with ultrasound under air conditions to prove that both self-healing agents were still active. The self-healing reaction was monitored quantitatively by gravimetric measurements and qualitatively by FT-IR spectroscopy (Figure 6.24). The conversion was found to be between 84 and 93% in comparison to the theoretical amount of encapsulated DCPD in each sample (Table 6.6). The polymerization of the healing agent could be verified by infrared spectroscopy on dried samples showing an absorption at  $975\text{ cm}^{-1}$ , which is characteristic for the trans double bond of ring-opened PDCPD (Figure 6.24a).<sup>7</sup> The FT-IR spectra of sample SH2 containing MAA and SH3 containing AAm units in the shell clearly display also these characteristic peaks (Figure 6.24c,d). In sample SH1, this peak is covered by the shell polymer containing PMMA, however a broadening of the peak can be observed (Figure 6.24b). Since PMMA is inert toward the self-healing reaction, it can be concluded that both DCPD and Grubbs' catalyst remained active and

available after encapsulation in the three types of polymer shells. No significant difference in the self-healing reaction could be observed.

**Table 6.6** Composition of the resulting mixed dispersions for self-healing experiments including the gravimetrically determined conversion.

Entry	dispersion containing		shell material	conversion of self-healing reaction [%]
	DCPD	Grubbs' catalyst		
SH1	SC50-1	SC51-1	P(S <sub>0.49</sub> -stat-MMA <sub>0.51</sub> )	93
SH2	SC50-2	SC51-2	P(S <sub>0.91</sub> -stat-MAA <sub>0.09</sub> )	87
SH3	SC50-3	SC51-3	P(S <sub>0.73</sub> -stat-AAm <sub>0.27</sub> )	84

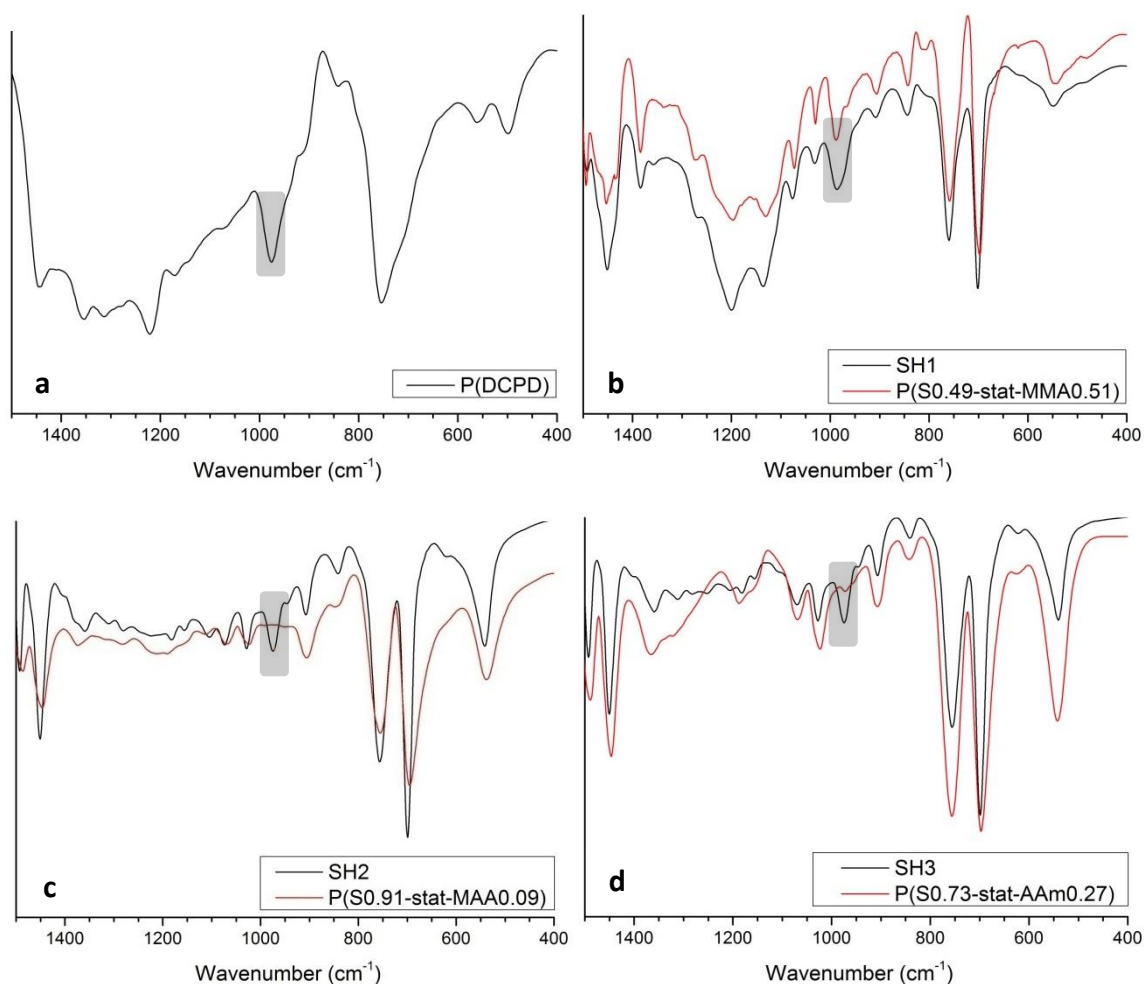


**Figure 6.24** IR spectra referred to (a) PDCPD prepared with Grubbs' catalyst and DCPD monomer (reference), (b) sample SH1 with corresponding shell polymer P(S<sub>0.49</sub>-stat-MMA<sub>0.51</sub>), (c) SH2 with corresponding shell polymer P(S<sub>0.91</sub>-stat-MAA<sub>0.09</sub>), and (d) sample SH3 with corresponding shell polymer P(S<sub>0.73</sub>-stat-AAm<sub>0.27</sub>). The highlighted area at 975 cm<sup>-1</sup> shows the characteristic peak of trans double bonds of PDCPD.

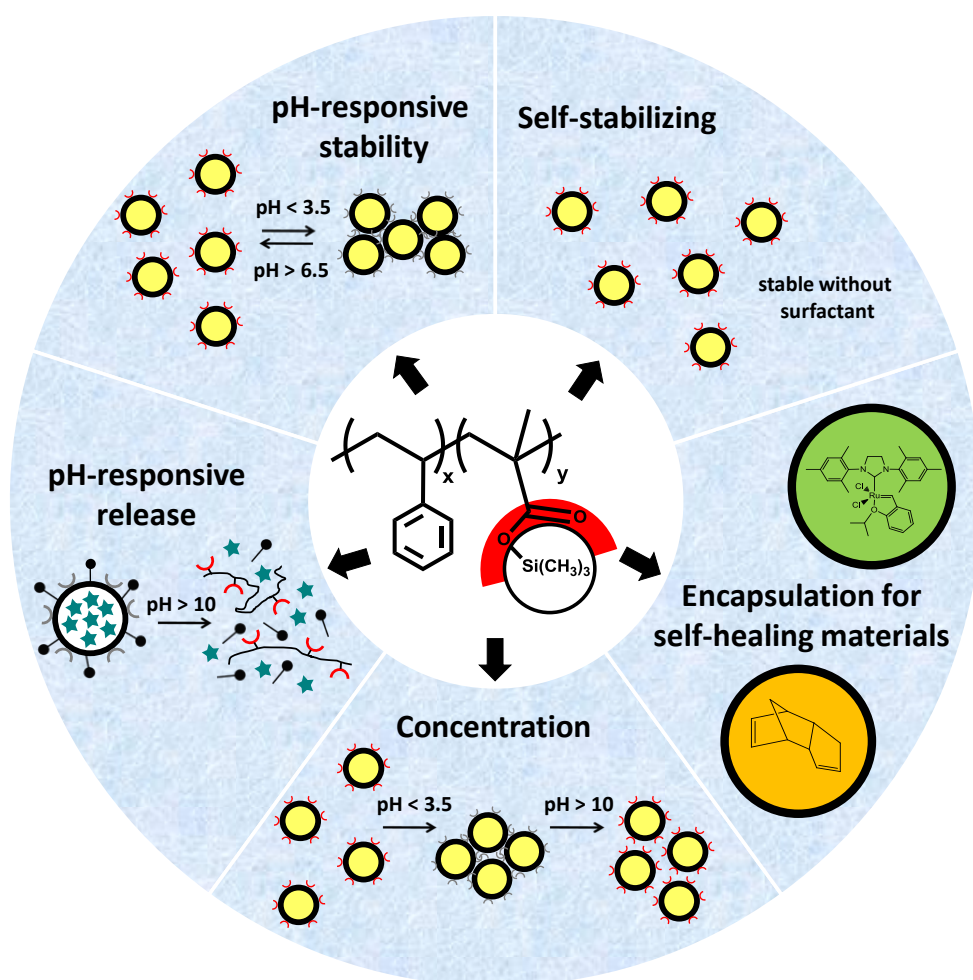
### 6.3 Conclusions

The presented third concept dealt with the preparation of polymer nanocapsules by the emulsion-solvent evaporation process. In the first part, a general and facile method to load self-healing agents such as plasticizers, solvents, and monomers, into polymer nanocapsules using various commercial polymers as shell materials was described. Polymers with very different properties were applied, including poly(L-lactide) (PLLA), poly(methyl methacrylate) (PMMA), poly(vinyl formal) (PVF), poly(vinyl acetate) (PVAc), poly(2,6-dimethyl-1,4-phenylene oxide) (PPO), and poly(vinyl cinnamate) (PVCi). Nanocapsules with encapsulated alkanes, halogenalkanes, cycloalkanes, and perfluoroalkanes used for solvent- or plasticizer-assisted self-healing could be obtained. Furthermore, the encapsulation of monomers for ionic, condensation, and radical self-healing polymerization reactions was demonstrated. The encapsulation efficiency and stability of the encapsulated diglycidyl ether terminated poly(dimethylsiloxane) (PDMS-DE) after encapsulation was proved by  $^1\text{H}$  NMR spectroscopy.

In the second part of this section, copolymers of styrene and various hydrophilic monomers were synthesized by free-radical polymerization and polymer-analogue reactions. It was shown that these statistical copolymers can be as suitable as block copolymers for the preparation of well-defined core-shell nanoparticles with an emulsion-solvent evaporation process. Acrylamide, acrylic acid, and methyl methacrylate units are playing the role of the structure-directing agent during the phase separation between the liquid core and the polymer inside the droplets. However, at least 50% of methyl methacrylate units shall be present in the copolymer to yield well-defined nanocapsules whereas less comonomer is necessary in case of acrylamide or methacrylic acid units. Core-shell morphologies could be obtained with both CTMA-Cl and SDS as surfactants. Unfortunately, it was difficult to discuss the obtained morphology with the model proposed by Torza and Mason due to non-conclusive results from contact angle measurements. Monomers and catalysts for ring-opening metathesis polymerization could be successfully encapsulated inside nanocontainers formed by statistical copolymers. Finally, the self-healing agents were found to be active after encapsulation which was proved a successful self-healing reaction.

## Chapter 7

# Self-stabilized pH-responsive nanocapsules



## 7 Self-stabilized pH-responsive nanocapsules

In the previous [chapter 6](#), the miniemulsion-solvent evaporation technique was used in combination with various pre-synthesized polymers and allowed the encapsulation of organic solvents as well as self-healing agents. This work was focused on the formation of capsules and on efficient encapsulation of reagents. In order to develop an intelligent capsule-based self-healing system, it is also beneficial that the encapsulated reagents can be released by a trigger when healing is necessary. Among the large family of available stimuli, the change of pH is particularly interesting in our case due to the fact that it does not require *per se* an additional source of energy. The strategies that were used for yielding pH-responsive colloids are based on the utilization of pH-responsive units in a polymer,<sup>79,200</sup> nanoparticles,<sup>201</sup> and low molecular weight or macromolecular pH-responsive stabilizers.<sup>202,203</sup>

Furthermore, the miniemulsion-solvent evaporation method suffers from important drawbacks, which are the presence of surfactant in the final dispersion and the very low concentration of nanocapsules produced, *i.e.* typically <5 wt%. Because of their small sizes, nanocapsules cannot be easily filtrated and centrifugation was shown to be detrimental to their structural integrity because of the inherent poor mechanical properties of nanocapsules with thin shells (see [chapter 4.6](#)).

Herein, the aforementioned major issues are simultaneously tackled by proposing a concept for the synthesis of smart nanocapsules via the solvent evaporation process without surfactant that allows facile and repeatable separation of the nanocapsules from the aqueous continuous phase. The key point of this strategy is the design of a polymer with encoded processability that possess enough functional hydrophilic groups to allow reversible aggregation and self-emulsification, but that is still soluble in hydrophobic organic solvents. The requirements are *a priori* contradictory but can be solved by inferring a hydrophobic to hydrophilic transition in the polymer shell during the emulsification procedure, *i.e.* by creating a polymer shell with masked amphiphilic properties. Hydrophilic or/and pH-responsive moieties can be masked by using trimethylsilyl protecting groups.<sup>204</sup> The protecting group was advantageously used to allow the copolymerization of hydrophobic



monomers with 2-trimethylsilyloxyethyl acrylate or trimethylsilyl methacrylate to yield hydroxyl<sup>205-206</sup> or carboxylic acid groups after desilylation.<sup>206-209</sup>

### 7.1 Formation of surfactant-free nanocapsules and nanoparticles

As mentioned in [chapter 6.2](#), statistical copolymers of styrene and methacrylic acid (MAA) containing more than 14% MAA are not suitable for the use in the emulsion-solvent evaporation process since these copolymers are not soluble in chloroform. In order to achieve a copolymer shell with a high amount of MAA, the amphiphilicity and pH-responsivity of the polymer shells was encoded in the chemical structure of the polymer by copolymerizing a hydrophobic monomer with monomers bearing masked carboxylic acid. Thus, trimethylsilyl methacrylate (TMSMA) was copolymerized with various amounts of styrene (S) in solution by free-radical polymerization. The reaction scheme is shown in [Figure 7.1](#).

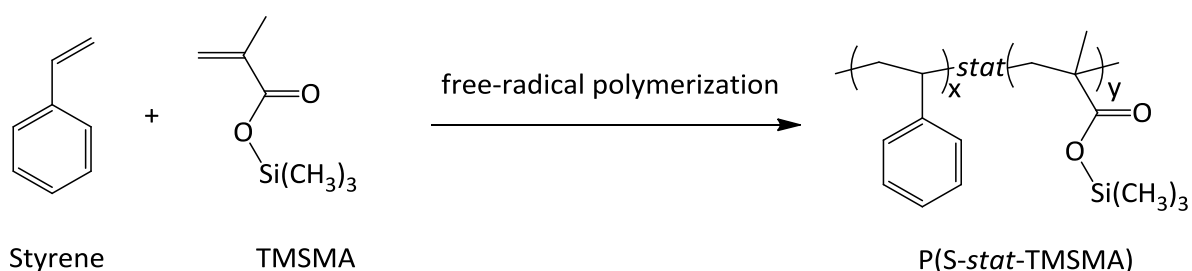


**Figure 7.1** Reaction scheme for the synthesis of poly(styrene-stat-trimethylsilyl methacrylate [P(S-stat-TMSMA)]).

The characteristics of the synthesized copolymers are shown in [Table 7.1](#). The compositions and the molecular weights of the synthesized copolymers were determined by <sup>1</sup>H NMR spectroscopy and GPC, respectively.

**Table 7.1** Composition and molecular weights of the synthesized copolymers.

Entry	polymer	$M_w$ [g·mol <sup>-1</sup> ]	$M_n$ [g·mol <sup>-1</sup> ]	PDI
SC42	P(S <sub>0.87</sub> -stat-TMSMA <sub>0.13</sub> )	54,250	29,350	1.85
SC43	P(S <sub>0.71</sub> -stat-TMSMA <sub>0.29</sub> )	57,400	31,000	1.85
SC45	P(S <sub>0.52</sub> -stat-TMSMA <sub>0.48</sub> )	76,650	45,950	1.67

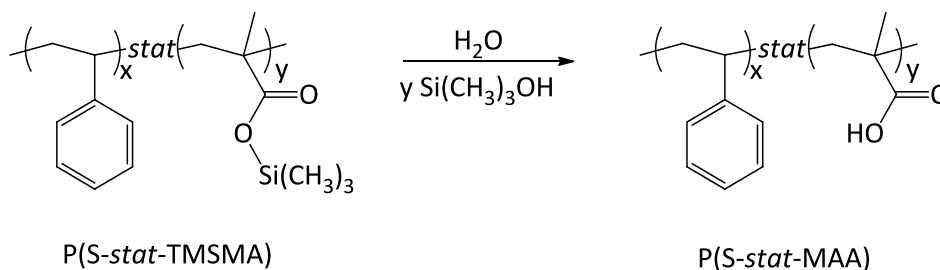
The obtained statistical copolymers of styrene and TMSMA (13, 29, 48 mol% TMSMA) were dissolved in a mixture of chloroform and hexadecane. The solution was then added to a certain amount of basic aqueous solution, stirred, and further homogenized by sonication. An overview of the synthesized capsules and particles is given in Table 7.2.

**Table 7.2** Colloids prepared by the surfactant-free emulsion-solvent evaporation technique.

Entry	polymer	HD [mg]	$D_h$ [nm]	morphology
JF186-1	P(S <sub>0.87</sub> -stat-TMSMA <sub>0.13</sub> )	300	160 ± 50	capsules
JF190-1	P(S <sub>0.71</sub> -stat-TMSMA <sub>0.29</sub> )	300	190 ± 70	capsules
JF184-4	P(S <sub>0.52</sub> -stat-TMSMA <sub>0.48</sub> )	300	130 ± 40	capsules
JF190-3 <sup>a</sup>	P(S <sub>0.71</sub> -stat-TMSMA <sub>0.29</sub> )	300	190 ± 40	capsules
JF186-3	P(S <sub>0.87</sub> -stat-TMSMA <sub>0.13</sub> )	12.5	110 ± 40	particles
JF184-5	P(S <sub>0.71</sub> -stat-TMSMA <sub>0.29</sub> )	12.5	130 ± 40	particles

<sup>a</sup>1 mg *N*-(2,6-diisopropylphenyl) perylene-3,4-dicarbonacidimide (PMI) added to the dispersed phase.

The desilylation of the P(S-*stat*-TMSMA) copolymer occurred during the emulsification and yielded P(S-*stat*-MAA) as shown in Figure 7.2.

**Figure 7.2** Scheme of the desilylation reaction of the copolymer P(S-*stat*-TMSMA).

The kinetics of desilylation during preparation was monitored by <sup>1</sup>H NMR spectroscopy (Figure 7.3) and revealed that almost complete desilylation (91%) occurred after 24 h.

After 1 h of emulsification and just before the sonication step, ~50% of the protected groups were desilylated.

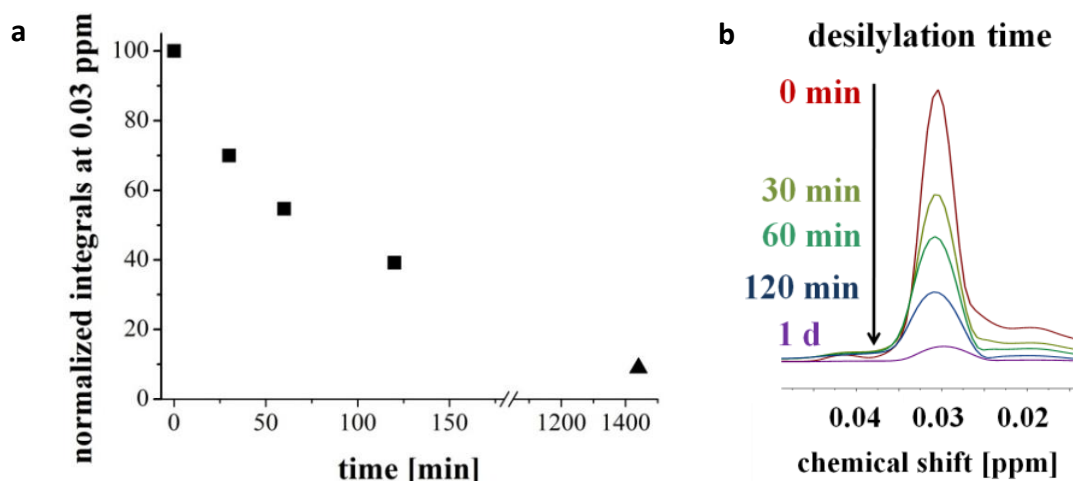


**Figure 7.3** Plot of the amount of remaining TMSMA versus time for the preparation of surfactant-free  $P(S_{0.71}\text{-stat-TMSMA}_{0.29})$  nanocapsules (a). Samples were taken from stirred surfactant-free emulsions (■) and from the resulting dispersion of nanocapsules after sonication and evaporation (▲). The section of the  $^1\text{H}$  NMR spectra in the range of the signal for the TMS group is shown in (b).

The *in-situ* desilylation provided amphiphilic properties to the copolymer and allowed the stabilization of the droplets and the nanocapsules after the evaporation of the chloroform. The colloids were found to be colloidally stable and displayed a hydrodynamic diameter of  $190 \pm 70$  nm as measured by DLS. The successful formation of core-shell nanoparticles was evidenced by transmission electron microscopy when using the copolymers  $P(S_{0.87}\text{-stat-TMSMA}_{0.13})$  and  $P(S_{0.71}\text{-stat-TMSMA}_{0.29})$  as precursors for the shell formation (Figure 7.4a,b).

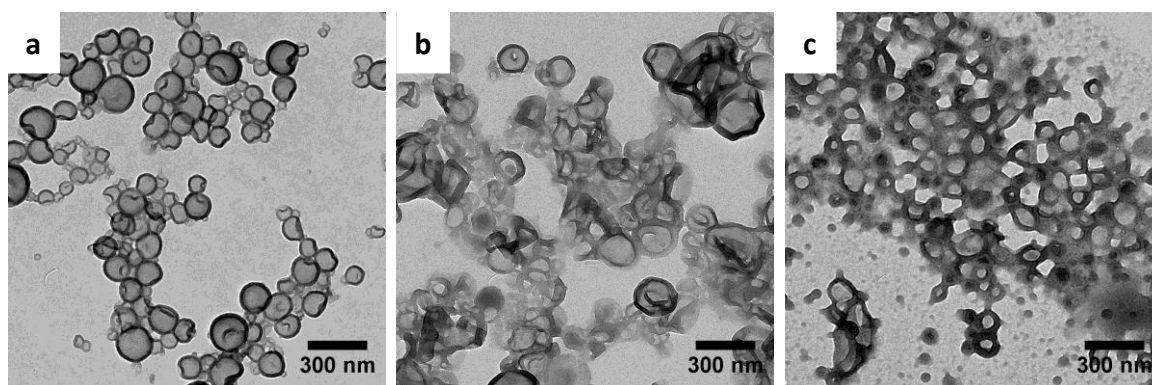


**Figure 7.4** TEM micrographs of desilylated nanocapsules prepared via surfactant-free emulsion-solvent evaporation technique with (a)  $P(S_{0.87}\text{-stat-TMSMA}_{0.13})$  (JF186-1), (b)  $P(S_{0.71}\text{-stat-TMSMA}_{0.29})$  (JF190-1), (c)  $P(S_{0.52}\text{-stat-TMSMA}_{0.48})$  (JF184-4).

However, more TMSMA units in the copolymer are detrimental to the nanocapsule structure. Less defined structures were hence formed with  $P(S_{0.52}\text{-stat-TMSMA}_{0.48})$  owing to the higher hydrophilicity and therefore higher solubility of the desilylated copolymer in water (Figure 7.4c). 29% of MAA units in the copolymer shell is already a remarkable high amount that cannot be reached by directly using a copolymer of styrene and methacrylic acid because of the non-solubility of the latter copolymer in suitable solvents in the solvent evaporation process, such as chloroform. Therefore, the strategy of the *in-situ* desilylation of the chloroform-soluble copolymers is necessary to fabricate a polymer shell enriched with a high amount of MAA.

This is the first reported emulsion solvent-evaporation process that yields nanocapsules without surfactant. The procedure is very versatile since monolithic nanoparticles (without liquid core) could be also synthesized by the same method. TEM micrographs are shown in Figure 7.5.

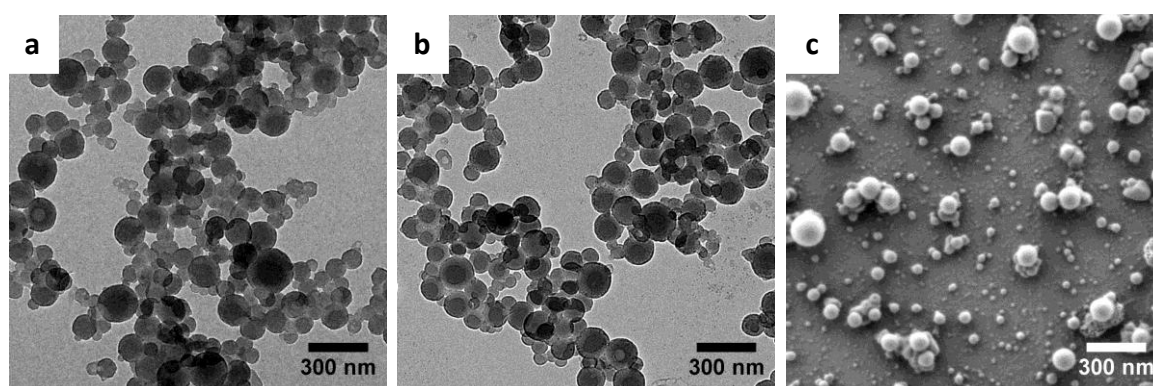


**Figure 7.5** TEM micrographs of surfactant-free prepared nanoparticles with (a) desilylated  $P(S_{0.87}\text{-stat-TMSMA}_{0.13})$  (JF186-3), (b)  $P(S_{0.71}\text{-stat-TMSMA}_{0.29})$  (JF184-5). (c) SEM micrograph of the latter particles.

### 7.2 pH-responsive stability

Since the masked units yielded carboxylic acid groups, the amount of charges on the shell and therefore the efficiency of the electrostatic stabilization depends on the pH of the dispersion. Macroscopic inspections of the dispersion with a desilylated  $P(S_{0.71}\text{-stat-TMSMA}_{0.29})$  shell at high and low pH evidenced the stabilization and destabilization of the dispersions of nanocapsules, respectively (Figure 7.6a). A schematic illustration of the aggregation and redispersion process of the nanocapsules is shown in Figure 7.6c.

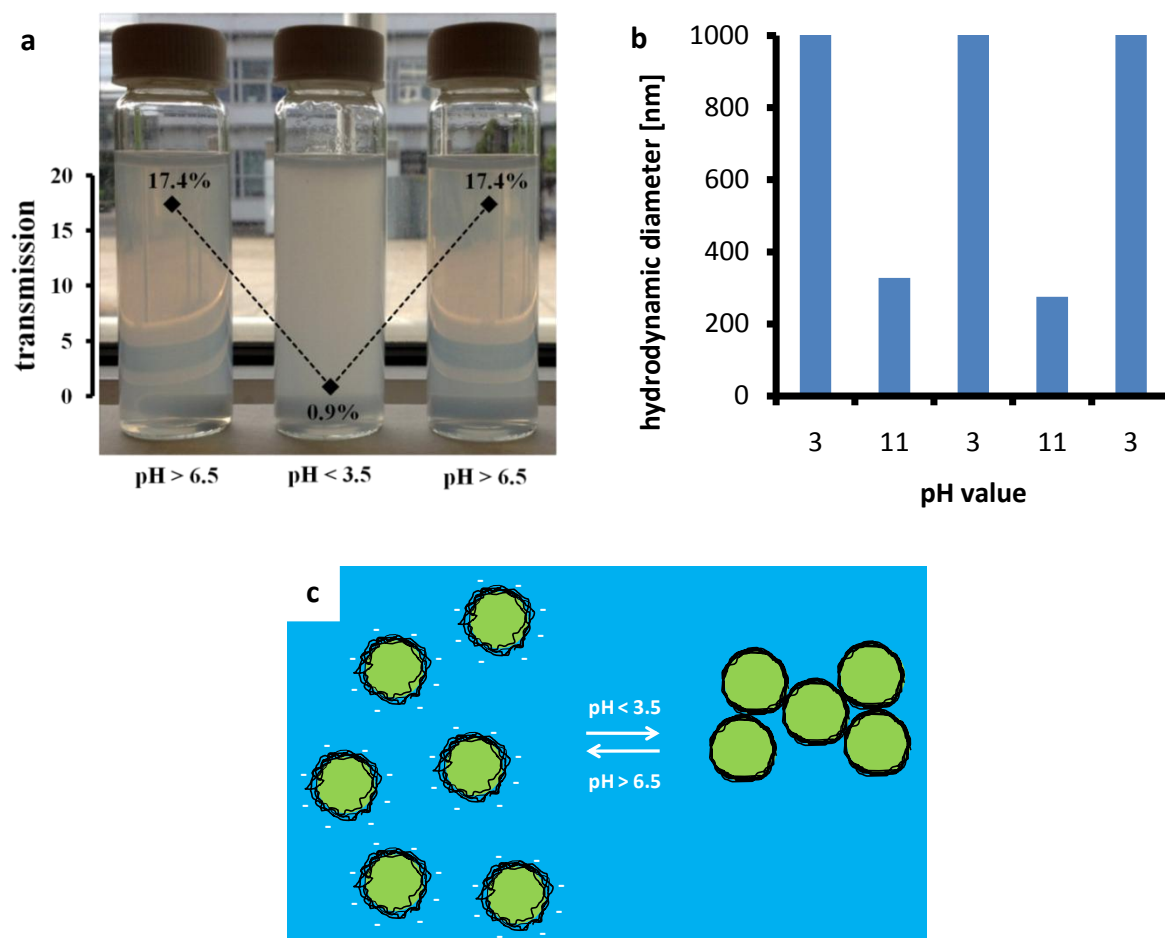


**Figure 7.6** The destabilization and redispersion of the  $P(S_{0.71}\text{-stat-TMSMA}_{0.29})$  nanocapsules can be monitored visually and by turbidimetry (a), and by DLS (b). Aggregates with sizes above  $1\ \mu\text{m}$  are counted as  $1\ \mu\text{m}$  in the diagram. (c) Schematics of the aggregation-redispersion of the nanocapsules dispersion upon switch of pH.

The flocculations and redispersion were found to be reversible. The pH-responsive behavior was further investigated by DLS measurements performed on the dispersion submitted to different pH values. The size of the polydisperse aggregates was found to be larger than  $1\ \mu\text{m}$  at  $\text{pH} = 3$  ( $D_{\text{aggregates}} \sim 10.9 \pm 8.0\ \mu\text{m}$  for  $P(S_{0.71}\text{-stat-TMSMA}_{0.29})$  nanocapsules, Figure 7.7) and could be switched back to  $\sim 300\ \text{nm}$  by increasing the pH again (Figure 7.6b).

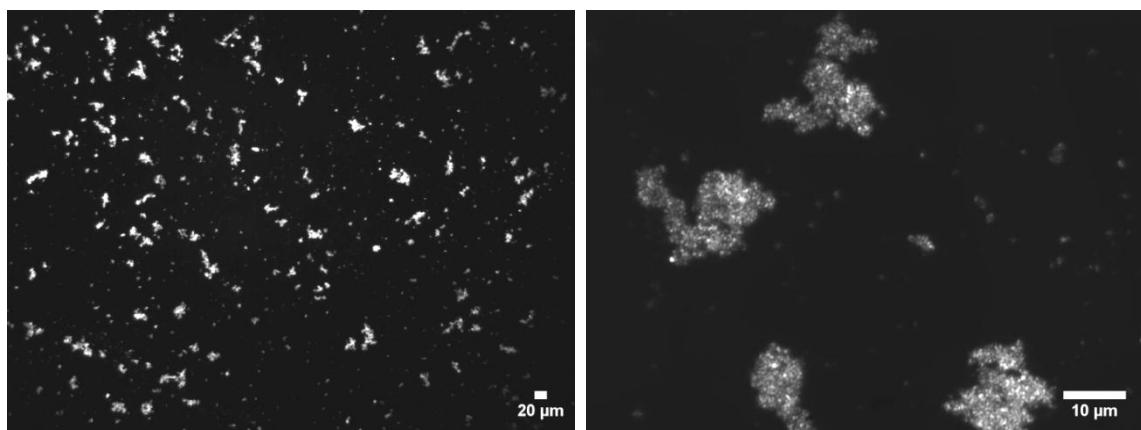


**Figure 7.7** Optical microscope images of aggregated nanocapsules with  $P(S_{0.71}\text{-stat-TMSMA}_{0.29})$  at  $\text{pH} = 3$  (sample JF190-1) in different magnifications.  $D_{\text{Aggregates}} \sim 10.9 \pm 8.0 \mu\text{m}$  (average of 200 measurements).

The transition was found to be fully reversible, *i.e.* 100% of the nanocapsules could be redispersed after aggregation, as proved by turbidity measurements. The transmission of the redispersed nanocapsules was independent on the number of cycles.

Lower amounts of methacrylic units in the copolymer shell do not allow the switching of the colloidal stability. Indeed, the hydrodynamic diameters of nanocapsules of desilylated  $P(S_{0.87}\text{-stat-TMSMA}_{0.13})$  (Figure 7.8) remained constant. This demonstrates further the unique character of the synthetic strategy. Indeed, copolymers with a higher amount of methacrylic acid are not soluble in chloroform and therefore the *in-situ* desilylation or any form of deprotection of a carboxylic acid is necessary to yield nanocapsules with a pH-responsive stability via this simple emulsion-solvent evaporation method.

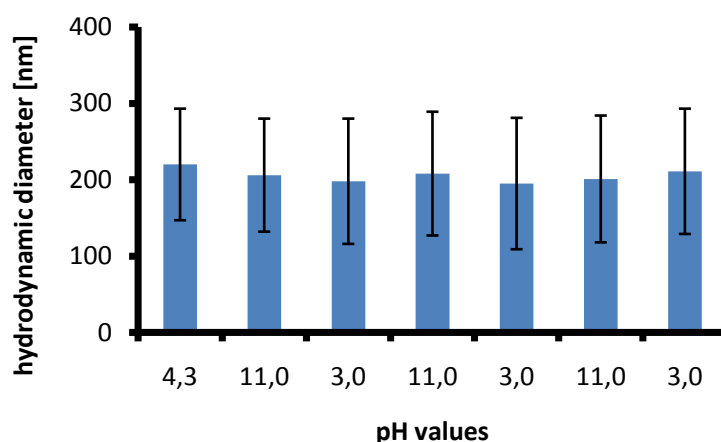


**Figure 7.8** On the contrary to the desilylated  $P(S_{0.71}\text{-stat-TMSMA}_{0.29})$  nanocapsules, nanocapsules from desilylated  $P(S_{0.87}\text{-stat-TMSMA}_{0.13})$ , do not show a pH-dependent stability as measured by DLS.

To prove that the switching was controlled by the electrostatic stabilization displayed by the negatively charged nanocapsules shells, further experiments were performed by adding a non-ionic block copolymer surfactant to the dispersions. Steric stabilization of the nanocapsules occurred efficiently at concentrations of the block copolymer surfactant above  $4 \text{ mg}\cdot\text{mL}^{-1}$  (Figure 7.9), for which the switching effect upon pH variation was no longer observed.

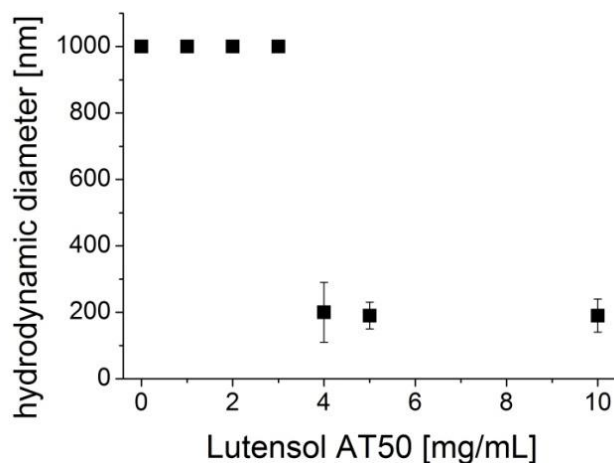


**Figure 7.9** Plot of the hydrodynamic diameters of the surfactant-free dispersion of nanocapsules from desilylated  $P(S_{0.71}\text{-stat-TMSMA}_{0.29})$  (JF190-1) versus concentration of Lutensol AT50 in the continuous phase. Aggregates with sizes above  $1 \mu\text{m}$  are counted as  $1 \mu\text{m}$  in the diagram.

### 7.3 Concentration

The last major drawback of the emulsion-solvent evaporation technique is that the colloids produced by this method display usually a very low amount of dispersed phase ( $\sim 6 \text{ wt}\%$  in Figure 7.10a, Table 7.3). It is shown that the switching of colloidal stability can be efficiently used to concentrate the nanocapsules dispersion. The nanocapsules were destabilized, filtered, and the separated solid could be redispersed to yield concentrated nanocapsules dispersions (Figure 7.10a, Table 7.3) with  $\sim 32 \text{ wt}\%$  dispersed phase. It should be noted, that an increase of the dispersed phase from 5.6 to 31.9 wt% is accompanied with a decrease of the total mass of the dispersion by 82% without loss of capsules.

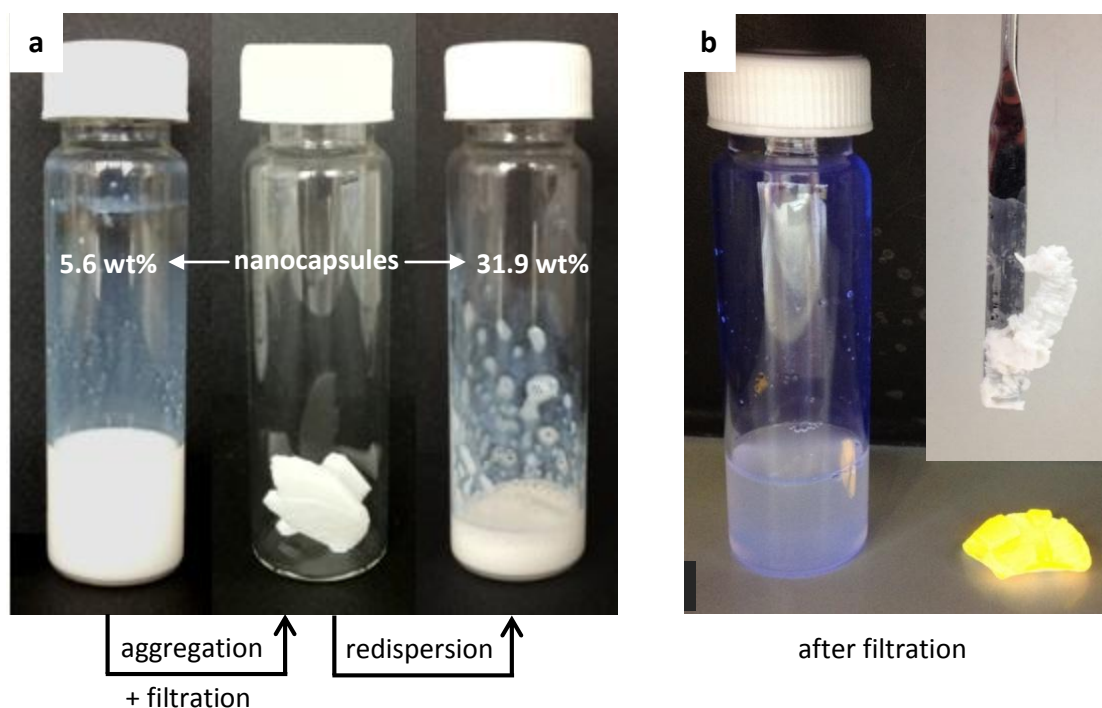


**Figure 7.10** The aggregation and subsequent redispersion allows increasing the concentration of the  $P(S_{0.71}\text{-stat-TMSMA}_{0.29})$  nanocapsules in water (**a**). The nanocapsules can be used to encapsulate a fluorescent dye (sample JF184-5, Table 7.2). After pH-triggered aggregation, the dye is present in the residue as identified by irradiation ( $\lambda = 366 \text{ nm}$ ) the filtrate and the residue (**b**).

**Table 7.3** Characteristics of sample JF190-1 after aggregation, separation, and redispersion.

Entry	$\varphi_d^a$ [wt%]	solid content <sup>b</sup> [wt%]	$D_n$ [nm]
after synthesis	5.6	3.0	$190 \pm 70$
after 2 <sup>nd</sup> filtration	-	17.7	-
after 2 <sup>nd</sup> redispersion	31.9	15.6	$190 \pm 80$

<sup>a</sup> fraction of the dispersed phase  $\varphi_d$  measured by gravimetry with HD still inside the nanocapsules;

<sup>b</sup> measured after freeze-drying followed by drying under vacuum (=only shell material).

Control experiments performed by a tentative preparation of nanocapsules with lower wt% of dispersed phase (18 and 23 wt%) directly by using more copolymer, hexadecane, and chloroform failed to yield stable miniemulsions. Indeed, such large amount of dispersed phase favors coalescence between the droplets and gelation occurs during the tentative emulsification procedure. The concept of separation and concentration was exemplary demonstrated for nanocapsules encapsulating a fluorescent dye (sample JF184-5, Figure 7.10b).



## 7.4 Encapsulation of ROMP monomer and catalyst

The switchable nanocapsules were also used to encapsulate monomers and catalysts analogous to chapter 6.2. This surfactant-free method was used to encapsulate the ROMP monomer DCPD and Hoveyda-Grubbs' catalyst 2<sup>nd</sup> generation. The composition of the synthesized nanocontainers is listed in Table 7.4. TEM and SEM micrographs are displayed in Figure 7.11.

**Table 7.4** Composition of the nanocontainers for the encapsulation of healing agents.

Entry	polymer	dispersion containing	$D_h$ [nm]
JF195-1	$P(S_{0.71}\text{-stat-TMSMA}_{0.29})$	DCPD	$160 \pm 40$
JF194-4	$P(S_{0.71}\text{-stat-TMSMA}_{0.29})$	Grubbs' catalyst	$210 \pm 80$

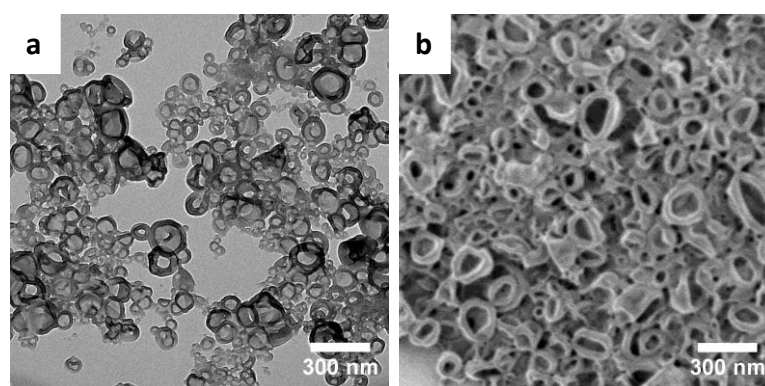


**Figure 7.11** (a) TEM micrograph of  $P(S_{0.71}\text{-stat-TMSMA}_{0.29})$  nanocontainers for the encapsulation of DCPD (JF195-1), and (b) SEM micrograph of  $P(S_{0.71}\text{-stat-TMSMA}_{0.29})$  nanocontainers for the encapsulation of Hoveyda-Grubbs' catalyst 2<sup>nd</sup> Generation (JF194-4).

The nanocapsule dispersion JF195-1 was then aggregated and redispersed and the amount of encapsulated DCPD was found to remain constant (~80% of the initial amount), meaning that no loss of encapsulated substances occurred during the switching of the pH (Table 7.5). The amount of encapsulated DCPD was determined by <sup>1</sup>H NMR spectroscopy in presence of maleic acid as internal standard (Figure 7.12).

**Table 7.5** Content of core and shell for  $P(S_{0.71}\text{-stat-TMSMA}_{0.29})$  nanocapsules (sample 195-1).

Entry	$\varphi_d^a$ [wt%]	solid content <sup>b</sup> [wt%]	encapsulated DCPD [wt%]
after synthesis	4.8	2.6	78
aggregated solid	19.4	10.6	76
after redispersion	17.2	9.3	78

<sup>a</sup> calculated with measured amount of encapsulated DCPD;

<sup>b</sup> measured after freeze-drying and further drying the dispersions under vacuum at 80 °C.

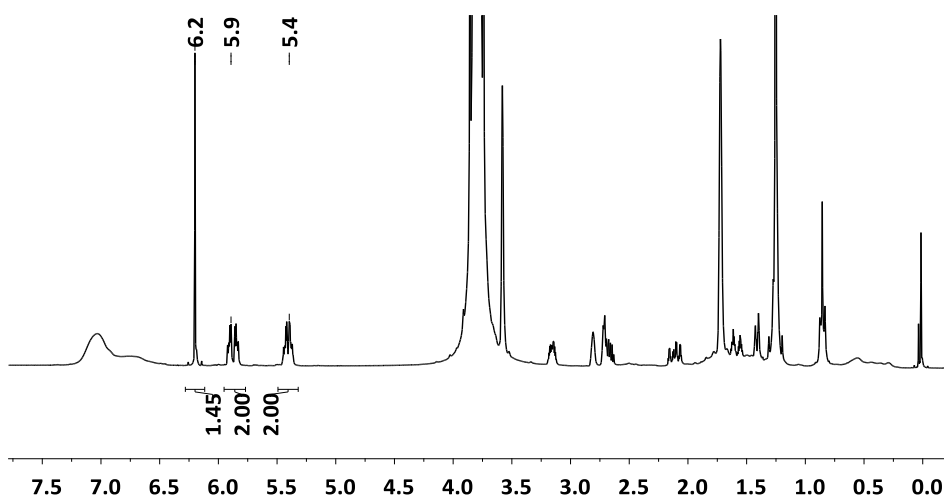


**Figure 7.12**  $^1\text{H}$  NMR spectrum of sample JF195-1 with encapsulated DCPD. The dispersion was dissolved in THF and maleic acid was added as internal standard. The peak at 6.2 ppm corresponds to maleic acid and the peaks at 5.9 and 5.4 ppm correspond to DCPD.

## 7.5 pH-responsive release

However, the switching did not allow the release of the core, a feature that can be interesting for some applications. Therefore nanocapsules displaying a pH-responsive shell and a pH-responsive core were synthesized. Oleic acid (Figure 7.13) was selected as core and could be encapsulated at pH = 3 in nanocontainers with  $D_h = 230 \pm 80$  nm (Entry JF209-2, Table 7.6).

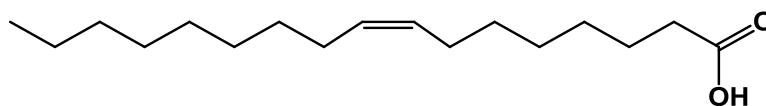


**Figure 7.13** Chemical structure of oleic acid.

For sufficient stabilization, the dispersion was synthesized with SDS as surfactant. The TEM micrograph is shown in Figure 7.14a. There is less contrast for the sample between the core and the shell compared to other samples. This is due to the fact that the oleic acid was not evaporated from the capsules in the vacuum of the TEM chamber.

**Table 7.6** Compositions for the preparation of the nanocapsules with encapsulated oleic acid for pH-responsive release.

Entry	polymer	treatment	$D_h$ [nm]	morphology
JF209-2	$P(S_{0.71}\text{-stat-TMSMA}_{0.29})$	after synthesis	$230 \pm 80$	colloidal
JF209-2_pH10	$P(S_{0.71}\text{-stat-TMSMA}_{0.29})$	after addition of NaOH	$450 \pm 320$	undefined
JF209-2_pH3	$P(S_{0.71}\text{-stat-TMSMA}_{0.29})$	after further addition of HCl	$180 \pm 80$	undefined

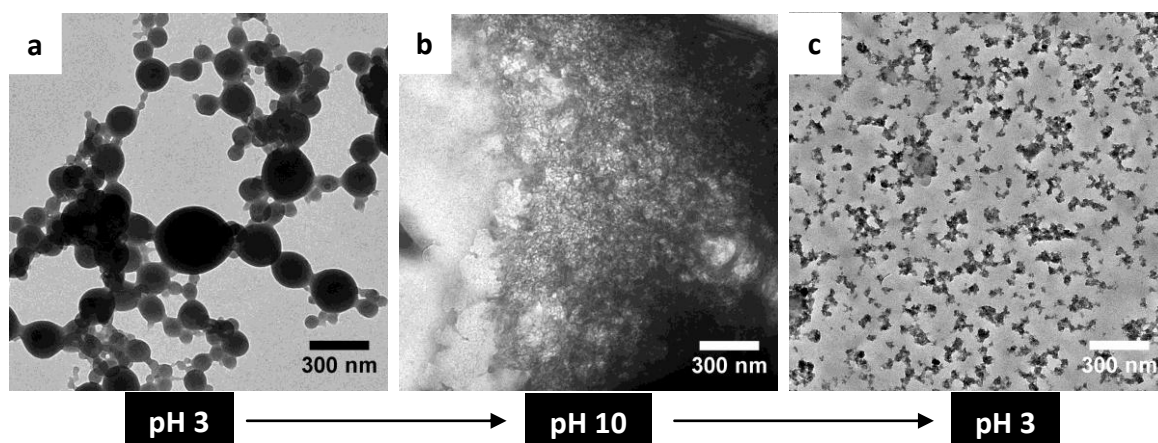


**Figure 7.14** TEM micrographs of desilylated  $P(S_{0.71}\text{-stat-TMSMA}_{0.29})$  nanocapsules with encapsulated oleic acid (a) after synthesis at pH 3, (b) after addition of NaOH at pH 10, (c): after further addition of HCl at pH 3.

Increasing of the pH yielded deprotonation of the acid, which diffused to the continuous phase. After switching the pH to 10 and also back to pH=3, no nanocapsules could be observed anymore. Undefined structures with much smaller sizes were indeed detected by TEM (Figure 7.14b,c). These structures were the result of aggregated collapsed chains of desilylated  $P(S_{0.71}\text{-stat-TMSMA}_{0.29})$ . So, it was also possible to induce a non-reversible response by changing the pH in order to release the liquid core of the nanocapsules.

### 7.6 Conclusions

A new concept for the synthesis of nanocapsules with pH-responsive behavior from surfactant-free emulsions using copolymers of styrene and trimethylsilyl methacrylate (TMSMA) was described in this chapter. The proposed synthetic approach combines two novelties in colloid science. Firstly, this is first synthesis of nanocapsules by the emulsion-solvent evaporation process in the absence of surfactant. Secondly, the pH-responsive stability is controlled by the chemistry of the polymer shell that is defined *in-situ* by desilylation during the self-emulsification process. The kinetic of the desilylation was monitored by  $^1\text{H}$  NMR spectroscopy which showed almost complete desilylation after 24h. Fully reversible aggregation allows for the separation of the nanocapsules without evaporation or centrifugation and therefore the structural integrity of the nanocontainers is preserved. Switching the colloidal stability could be also used to concentrate the nanocapsule dispersion up to 5 times. Self-healing agents were encapsulated successfully in stable state, which was proven by  $^1\text{H}$  NMR spectroscopy. Hence, the pH-responsive release of oleic acid from nanocapsules was demonstrated.

Finally, the possibility of preparing nanocapsules without surfactant and subsequently concentrating them in water by switching the pH is environmentally friendly. Nanocapsules could be concentrated without evaporation of water, which is energy demanding. Furthermore, energy and resources dissipated in transport are saved by the fact that the nanocapsules can be separated directly after their production and redispersed where they are used. The simple proposed synthetic strategy could also be used by desilylating other functions such as alcohols, amines or alkynes, or, to a larger extent, by deprotecting other groups.<sup>210</sup> The masked groups could be also introduced in other copolymer structures to prepare nanocapsules for biomedical applications.

## 8 Incorporation of the nanocapsules into a zinc matrix by electrodeposition

### 8.1 Introduction

Having successfully demonstrated the efficient encapsulation of self-healing agents in various polymeric and inorganic nanocontainers in the previous chapters, these nanocontainers should further find applications in the field of corrosion prevention. The nanocapsules could be incorporated into zinc composite coatings in order to provide autonomic healing of the protection layer damaged by environmental influences. The incorporation process was performed by electrochemical codeposition of zinc-nanocapsule composite coatings from zinc sulfate solutions at low pH values ( $\leq 4$ ).

The electrodeposition was carried out on a rotating disc (or cylinder) electrode (Figure 8.1). In this arrangement, the electrolyte solutions containing nanocapsules are brought to the surface by a disk rotating in the electrolyte. The rotation of the rotating electrode – in this case with a disk of stainless steel as substrate on top – drags the material to the surface where it can react and get deposited. For a successful incorporation, the nanocapsules are adsorbed on the surface and get incorporated during the electrochemical deposition of the zinc.

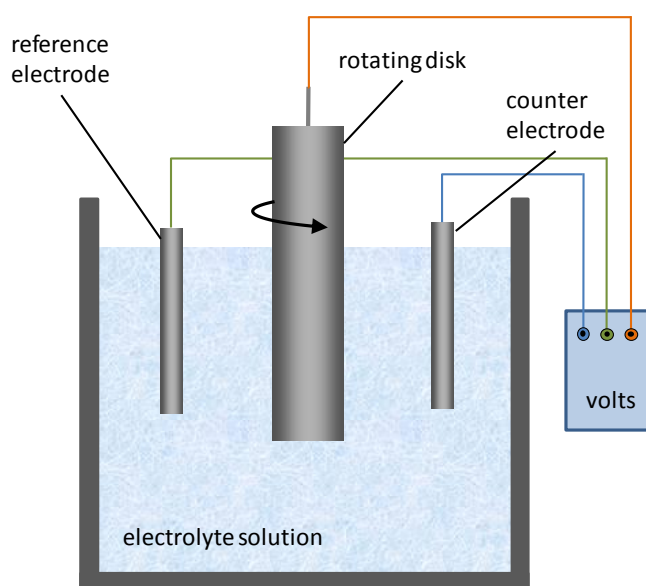


**Figure 8.1** Schematic of the cell of a rotating disk electrode (RDE). The electrolyte solution consists of the electrolyte and the dispersion of the nanocapsules to be deposited.

Three types of zinc composite coatings with incorporated nanoparticles are reported in literature (Figure 8.2).<sup>211</sup> In type (a), the particles are mainly adsorbed on top of the coating. The particles are not incorporated, thus no enhancement of the properties is expected. In type (b), the particles are entrapped in the coating leading to poorer mechanical properties compared to pure zinc layers, since the composite coating is more porous. The system with particles well dispersed inside of the coating is shown in type (c), where the mechanical stability and the healing efficiency is expected to be the best of all types, but also the most challenging.

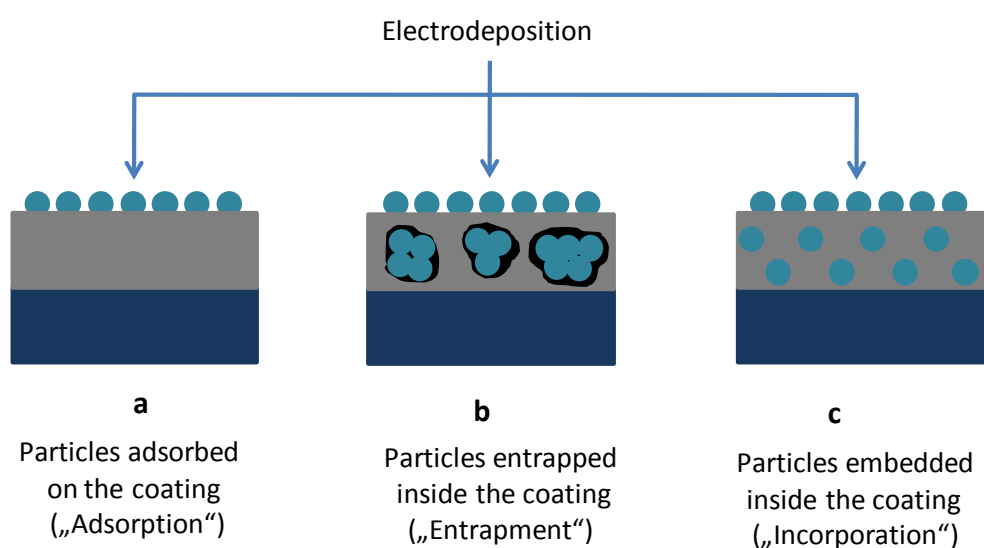


**Figure 8.2** Schemes of possible nanocomposite coatings formed by electrodeposition. Adapted from Khan et al.<sup>211</sup>

### 8.2 Electrodeposition

Various dispersions containing silica or polystyrene based nanocapsules were used for electrochemical codeposition into zinc composite coatings (Table 8.1). The electrodeposition process was carried out for non-functionalized and functionalized silica nanocapsules reported in chapter 5, and for functionalized polystyrene nanocontainers described in chapter 4. Some nanocapsules were additionally modified with cysteamine or polyvinylpyrrolidone (PVP) in order to provide a stronger attractive interaction with the substrate. The modifications led to a favorable incorporation, which was also shown in

previous investigations for the codeposition of silica nanoparticles.<sup>211</sup> The chemical structures of the additives are shown in Figure 8.3.

**Table 8.1** Overview of the dispersions used for electrochemical codeposition.

Entry	shell material		$D_h$ [nm]	incorporation [vol%]
	main	functionalization/ modification		
<b>silica nanocapsules reported in chapter 5</b>				
JF41-2	silica	-	140 ± 70	-
JF41-2_CYS	silica	cysteamine	140 ± 70	1.3
JF107-5	silica	5% NH <sub>2</sub>	120 ± 60	2.0
JF69-3	silica	20% SH	110 ± 60	2.6
JF92-2	silica	50% SH	130 ± 50	4.8
<b>polymer nanocapsules reported in chapter 4</b>				
JF166-2	PS	COOH	260 ± 80	-
JF64-1	PS	PEG	280 ± 80	-
JF136-1	PS	SO <sub>3</sub> H PVP	290 ± 120	3.6
JF166-4	PS	SO <sub>3</sub> H PEG	240 ± 30	4.1
JF96-1	PS	SO <sub>3</sub> H PEG PVP	390 ± 80	6.0
JF166-3	PS	NH <sub>2</sub>	440 ± 170	7.8
JF166-6	PS	NH <sub>2</sub> PEG	490 ± 170	11.7

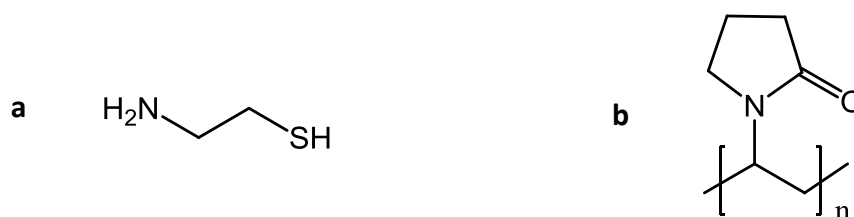


**Figure 8.3** Chemical structures of the additives (a) cysteamine and (b) polyvinylpyrrolidone (PVP).

The crucial requirement for the nanocapsules is that they should be incorporated into the matrix and therefore a good dispersibility of the capsules in the aqueous zinc solution. This is not trivial since the deposition is usually carried out at low pH of approximately 2 in aqueous solutions of highly concentrated electrolytes. This issue can be overcome by introducing

functional groups in the shell of the capsules.<sup>13</sup> Many functionalized nanocapsules presented in the previous chapters were found to be suitable for codeposition (Table 8.1). For experimental details of the used silica capsules and polymer capsules see chapter 9.4 and chapter 9.3, respectively. Experimental details of the samples modified by cysteamine and PVP are described in chapter 9.8. The volume fractions of incorporated capsules are presented graphically in Figure 8.4.

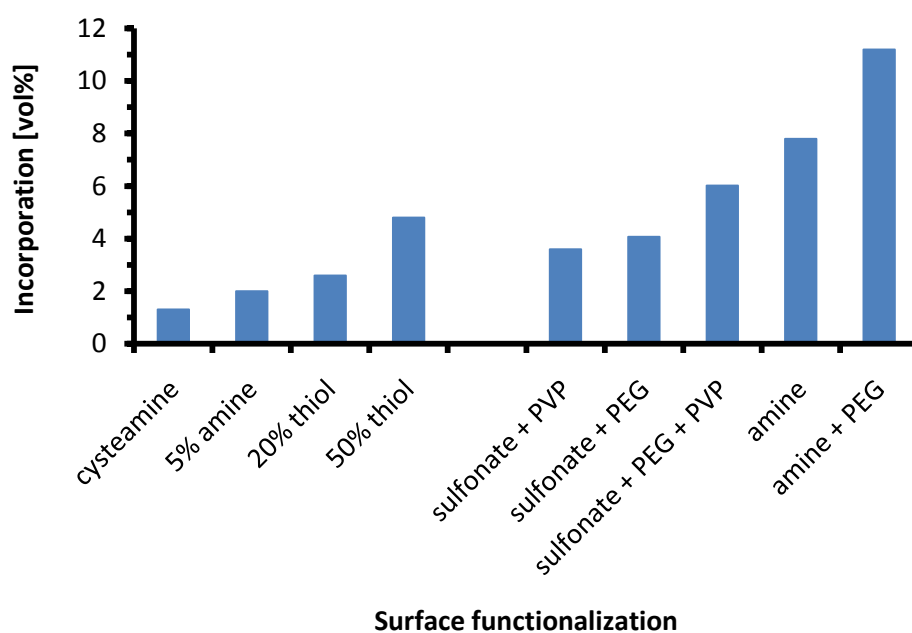


**Figure 8.4** Plot of surface functionalization vs. volume of incorporation into the zinc matrix of non-functionalized and functionalized silica nanocapsules (left row) in addition to functionalized polystyrene nanocapsules (right row).

Dispersions of non-functionalized and unmodified silica nanocapsules were found to be stable in the electrolyte solution but these capsules were not incorporated into the zinc matrix. This behavior is similar to reports in the literature for unmodified silica particles.<sup>212</sup> Capsules modified with cysteamine or functionalized with amine- and thiol-groups were successfully incorporated up to a volume fraction of 4.8 vol%. The incorporation was evidenced qualitatively by SEM micrographs of the zinc coatings after electrodeposition (Figure 8.5) and quantitatively by EDX analysis (Figure 8.4 left row). The deeper nanocapsules are incorporated into the zinc matrix the fewer secondary electrons can escape and so the darker they appear. Therefore, incorporated capsules appear dark whereas adsorbed capsules show bright colors, which can be observed in Figure 8.5c.



Capsules modified by cysteamine (JF41-2\_CYS) could be incorporated in low amounts although no capsules could be observed on the surface of the zinc layers (Figure 8.5a). It was found that a higher number of functional groups was beneficial for the incorporation. The measured volume fractions for the codeposition of the silica capsules are mostly higher compared to the values for functionalized or modified silica particles reported in literature.<sup>211</sup>

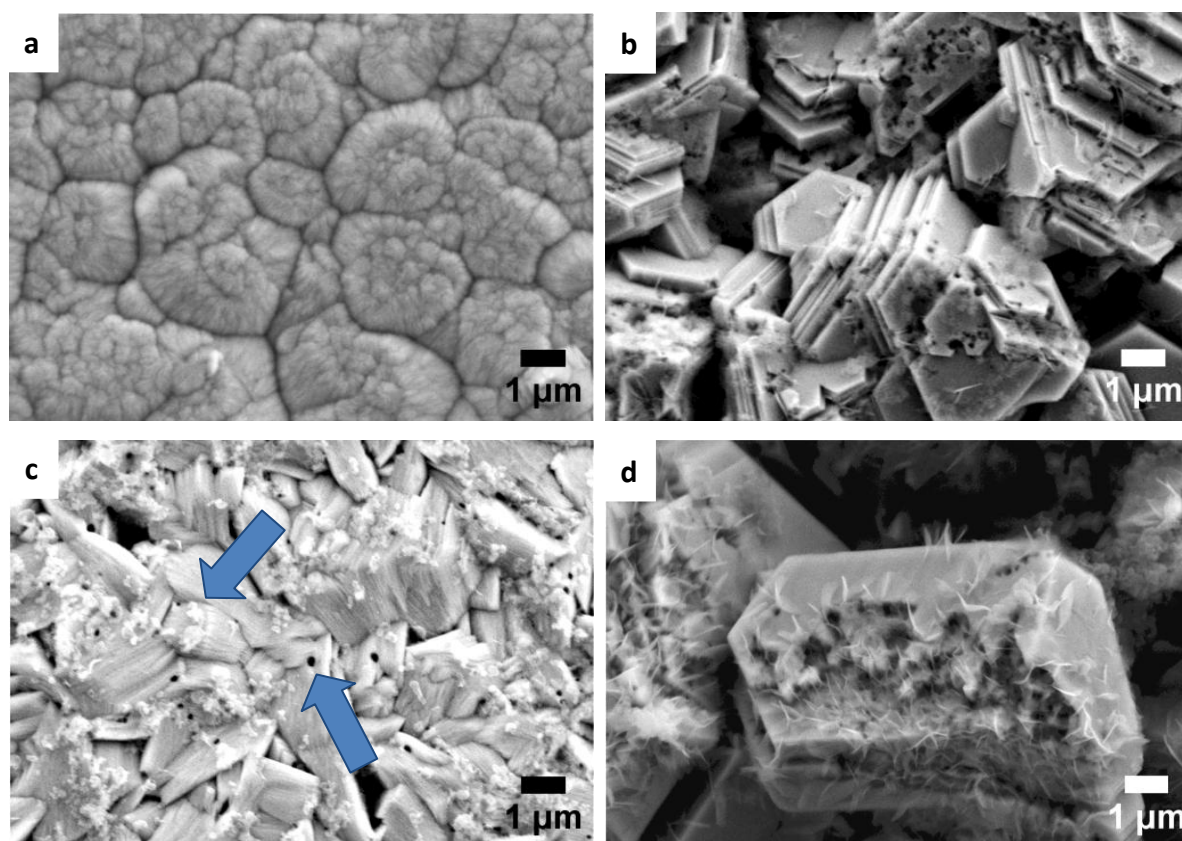


**Figure 8.5** SEM micrographs of zinc coatings containing silica nanocapsules bearing various functionalizations (a) JF41-2\_CYS (cysteamine modified), (b) JF107-5 (5% NH<sub>2</sub>), (c) JF69-3 (20% SH), (d) JF92-2 (50% SH). The arrows show bright adsorbed and dark incorporated nanocapsules.

Carboxyl- and PEG-functionalized polystyrene capsules were not dispersible in ZnSO<sub>4</sub> solution and therefore they were not used for the embedding process. Capsules bearing sulfonate or amine groups were incorporated with a volume fraction up to 11.7%, as summarized in Figure 8.4 right row. Incorporated nanocapsules could be observed in all SEM micrographs (Figure 8.6). Furthermore, amine functionalized colloids showed an up to 3 times higher incorporation compared to sulfonate ones. It was turned out that an

additional PEG functionalization as well as the addition of PVP had a beneficial effect on the codeposition. Apart from the effect of the functionalization, the size of the polymer colloids had an influence on their embedding in the matrix. Larger polymer capsules of the same functionalization were incorporated more favorably compared to smaller ones.

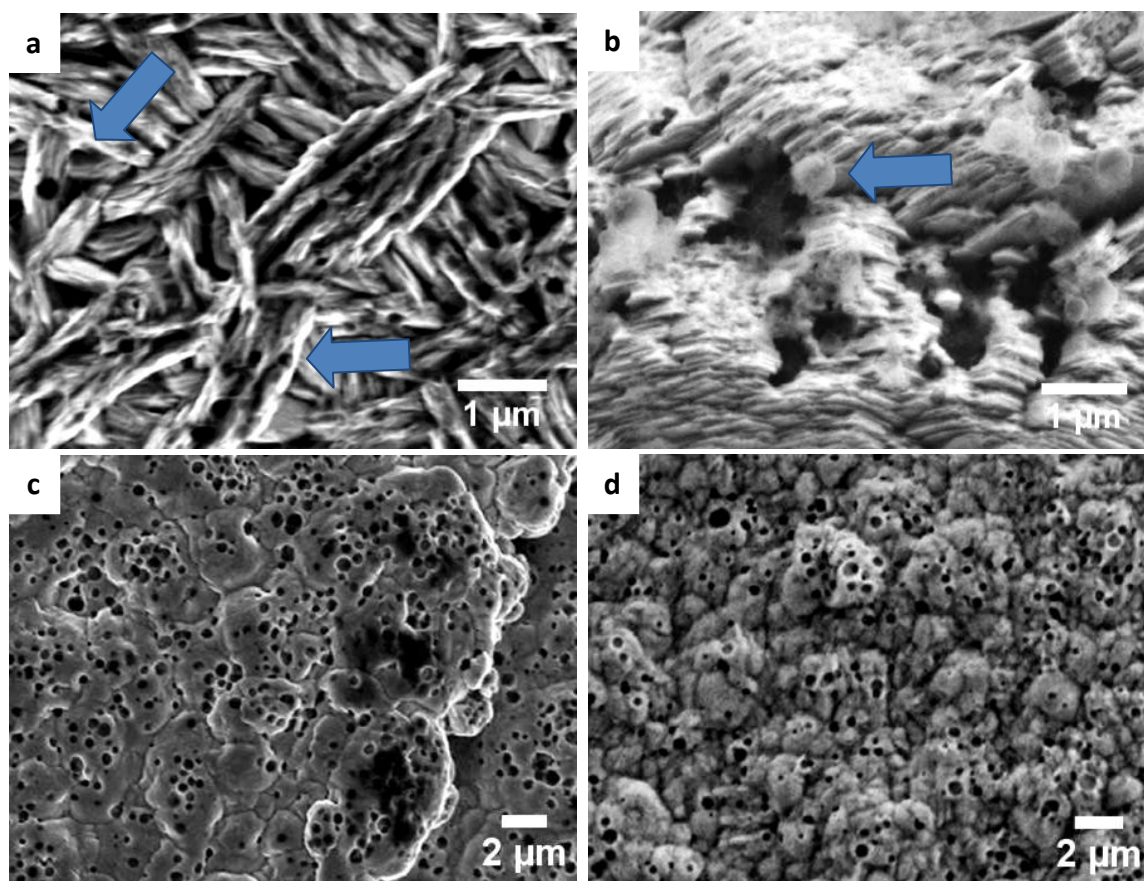


**Figure 8.6** SEM images of zinc coatings containing the polymer nanocapsules with different shell materials (a) JF166-4  $P(S\text{-}co\text{-}SMA\text{-}co\text{-}PEG)$ , (b) JF96-1  $P(S\text{-}co\text{-}SMA\text{-}co\text{-}PEG)\text{-PVP}$ , (c) JF166-3  $P(S\text{-}co\text{-}AEMA)$ , and (d) JF166-6  $P(S\text{-}co\text{-}AEMA\text{-}co\text{-}PEG)$ . The arrows show bright adsorbed and dark incorporated nanocapsules.

These explanations give a first overview of the electrochemical deposition of the nanocapsules. More detailed descriptions and discussions can be found in the PhD theses of *Ashokanand Vimalanandan* and *The Hai Tran* working at the Max Planck Institute for Iron Research in Düsseldorf.

## 9 Experimental details

### 9.1 Chemicals

Name	abbreviation	supplier	purity
0.5 M ammonia in dioxane		Sigma Aldrich	
1-bromododecane		Acros Organics	98%
1 M HCl in water		VWR	
1 M NaOH in water		VWR	
1-phenylheptadecane	PHD	Sigma Aldrich	97%
2,2'-azobis(2-methylbutyronitrile	V59	Wako	
2-aminoethyl-methacrylate hydrochloride	AEMA	Sigma Aldrich	90%
2 M trimethylsilyl-diazomethane in hexane	TMS-diazomethane	Sigma Aldrich	
3-aminopropyltriethoxysilane	APTES	Alfa Aesar	95%
3-mercaptopropyltrimethoxysilane	MPTMS	Sigma Aldrich	98%
4-(dimethylamino)pyridine	DMAP	Sigma Aldrich	99%
5,5'-dithiobis-(2-nitrobenzoic acid)	DTNB	Sigma Aldrich	99%
5-ethylidene-2-norbornene	EN	Sigma Aldrich	99%
5-norbornen-2-yl acetate	NA	Sigma Aldrich	98%
acrylamide	AAM	Sigma Aldrich	98%
cetyltrimethylammonium chloride	CTMA-Cl	Acros Organics	99%
chloroform		VWR	99.8%
cyclohexane		Sigma Aldrich	99%
deuterium oxide		Sigma Aldrich	99.9%
dichloromethane	DCM	VWR	99%
dicyclopentadiene	DCPD	Sigma Aldrich	97%
divinylbenzene, mixture of 1,2-divinylbenzene and 1,4-divinylbenzene purified by passing through a column filled with alumina	DVB	Merck	95%
ethanol	EtOH	Sigma Aldrich	99.5%
fluorescamine		Sigma Aldrich	98%
Grubbs' catalyst 1 <sup>st</sup> generation		Sigma Aldrich	97%
Hoveyda-Grubbs' catalyst 2 <sup>nd</sup> generation		Sigma Aldrich	
isopropanol	IP	Sigma Aldrich	99%
lauryl methacrylate		Sigma Aldrich	96%
methacrylic acid	MAA	Sigma Aldrich	99%
methyl methacrylate	MMA	Sigma Aldrich	99%

## 9 Experimental details

Name	Abbreviation	Supplier	Purity
methanol	MeOH	Fischer Scientific	99.9%
<i>n</i> -hexadecane	HD	Sigma Aldrich	99%
<i>n</i> -hexane		Fisher Scientific	98.9%
<i>N,N'</i> -dicyclohexylcarbodiimide	DCC	Sigma Aldrich	99%
octamethylcyclotetrasiloxane		Sigma Aldrich	99%,
perfluorodecaline		Merck	99%
poly(2,6-dimethyl-1,4-phenylene oxide, $M_w \sim 30,000 \text{ g}\cdot\text{mol}^{-1}$ )	PPO	Sigma Aldrich	
poly(dimethylsiloxane) diglycidyl ether terminated, $M_w \sim 800 \text{ g}\cdot\text{mol}^{-1}$	PDMS-DE	Sigma Aldrich	
poly(ethylene glycol) methyl ether methacrylate, $M_n \sim 300 \text{ g}\cdot\text{mol}^{-1}$	PEGMA	Sigma Aldrich	
poly(L-lactide, $M_w \sim 126,000 \text{ g}\cdot\text{mol}^{-1}$ )	PLLA	Biomer	
poly(methyl methacrylate), $M_w \sim 120,000 \text{ g}\cdot\text{mol}^{-1}$	PMMA	Sigma Aldrich	
poly(vinyl acetate), $M_w \sim 184,000 \text{ g}\cdot\text{mol}^{-1}$	PVAc	Acros Organics	
poly(vinylcinnamate), $M_w \sim 500,000 \text{ g}\cdot\text{mol}^{-1}$	PVCi	Sigma Aldrich	
poly(vinylformal), $M_w \sim 10,000 \text{ g}\cdot\text{mol}^{-1}$	PVF	Sigma Aldrich	
potassium salt of 3-sulfopropyl methacrylate	SMA	Sigma Aldrich	98%
sodium acetate		Sigma Aldrich	99%
sodium dodecylsulfate	SDS	Alfa Aesar	99%
sodium hydrogencarbonate		Sigma Aldrich	99.5%
styrene			
<i>purified by passing through a column filled with alumina</i>	S	Merck	99%
tetraethoxysilane	TEOS	Alfa Aesar	98%
tetrahydrofuran	THF	Sigma Aldrich	99.9%
dry tetrahydrofuran	THF	Acros Organics	99.8%
toluene	TOL	Sigma Aldrich	99.7%
trimethylsilyl methacrylate <i>purified distilling under vacuum and stored until use at -20 °C</i>	TMSMA	Sigma Aldrich	98%
tris(hydroxymethyl)-aminoethane	Tris	Acros Organics	99.8%
xylene	XYL	Acros Organics	99%

All chemicals were used as received unless otherwise stated. Demineralized water was used throughout the work.

## 9.2 General characterization of the samples

### 9.2.1 DLS

The sizes of the nanocapsules were evaluated by determining their hydrodynamic diameters by DLS using a Nicomp particle sizer (model 380, PSS, Santa Barbara, CA) at a fixed scattering angle of 90°.

### 9.2.2 TEM and SEM

Samples diluted with water were deposited on 400-mesh carbon-coated copper grids and left to dry prior to analysis with transmission electron microscopy (TEM) performed on a Zeiss EM 902 operating at 80 kV. Measurements with scanning electron microscopy (SEM) were carried out on a Zeiss Leo 1530 Gemini apparatus on samples deposited on silica substrates and subsequently dried.

## 9.3 Efficient encapsulation of self-healing agents in polymer nanocontainers functionalized by orthogonal reactions

### *Encapsulation of monomers by free-radical polymerization in miniemulsion*

1.82 g of hydrophobic vinyl monomers (S, DVB) were mixed with 100 mg V59 and different amounts of HD and DCPD. If not otherwise stated, 4 g of the mixture HD/DCPD as core material were used. For samples without hydrophilic monomers 2 g of hydrophobic monomers were used. Unless otherwise stated, 8 mg of surfactant in 24 g water were mixed with 180 mg hydrophilic vinyl monomers (SMA, MAA, AEMA) and/or 120 mg of PEGMA. SDS was used overall as surfactant except for samples with AEMA, in which CTMA-Cl was used. The two solutions were mixed, stirred for 1 h and sonicated under cooling with an ice bath for 120 s at 70% amplitude in a pulse regime (30 s sonication, 10 s pause; Branson 450 W sonifier with a 1/2" tip). The polymerization was performed at 72 °C for 16 h.

### *Self-healing reaction*

All self-healing experiments were performed under air conditions. Measured amounts of sample JF166-1 (containing DCPD) were mixed with either THF, a solution of Hoveyda-Grubbs' catalyst 2<sup>nd</sup> generation dissolved in THF, or 3 g of silica nanocapsules with encapsulated Hoveyda-Grubbs' catalyst 2<sup>nd</sup> generation analogous to the sample JF136-4 described in [chapter 9.4](#). The mixtures were stirred for 5 min, sonicated for 2 min at 70% amplitude in a pulse regime (30 s sonication, 10 s pause) using a Branson 450 W sonifier and a 1/2" tip, and then stirred for 72 h. The contents and conditions for the self-healing reactions are summarized in [Table 4.7](#). The dispersions were freeze-dried and then further dried by a treatment in a vacuum oven at 80 °C for 72 h.

### *Measurements of colloidal stability*

For measurements of the colloidal stability of the dispersions towards increasing ionic strength, the dispersions (JF64-1, JF166-1, JF166-2, JF166-3, JF166-4, JF166-5, and JF166-6) were diluted with aqueous solutions of KCl of different concentrations (0.01 M, 0.1 M, 1 M and 5 M KCl solution).

### *<sup>1</sup>H NMR measurements*

<sup>1</sup>H NMR measurements were performed on a Bruker Avance spectrometer of 300 MHz with dispersions prepared in D<sub>2</sub>O instead of H<sub>2</sub>O. The investigation of the reactivity of DCPD during the formation process and the determination of the conversion of the hydrophilic comonomer was carried out by dissolving the dispersions prepared in D<sub>2</sub>O in THF-*d*<sub>8</sub>.

### *Determination of functional groups*

The amount of functional groups on the surface of the capsules were determined by titration experiments performed on a particle charge detector (Mütek GmbH, Germany) in combination with a Titrino automatic titrator (Metrohm AG, Switzerland). The sulfonic and carboxylic groups were titrated with the positively charged polyelectrolyte poly(diallyldimethylammonium chloride) (PDADMAC). The amine groups were titrated with the negatively charged polyelectrolyte poly(ethylene sulfonate) (PES-Na). The titration was

carried out on 10 mL of the dispersion which was diluted to a solid content of 0.1 wt% before measurement. The number of functional groups/nm<sup>2</sup>  $N_g$  was then calculated from the following formula:

$$N_g = \frac{N_A \cdot C_{PEL} \cdot V_{PEL} \cdot D_n \cdot 10^{24}}{6 \cdot \left( \frac{m_{shell}}{\rho_{shell}} + \frac{m_{core}}{\rho_{core}} \right)} \quad \text{Equation 10}$$

where  $N_A$  is the Avogadro's constant ( $\sim 6.022 \cdot 10^{23} \text{ mol}^{-1}$ ),  $C_{PEL}$  [mol·l<sup>-1</sup>] and  $V_{PEL}$  [l] the concentration and volume of polyelectrolyte used to titrate the functional groups,  $D$  [nm] the diameter of the core-shell particles,  $m_{shell}$  [g] and  $\rho_{shell}$  [kg·m<sup>3</sup>] the mass and density of the polymer shell,  $m_{core}$  [g] and  $\rho_{core}$  [kg·m<sup>3</sup>] the mass and density of the liquid core.

For determination of charges per nm<sup>2</sup> using Equation 10, several assumptions had to be taken:

- The density of the polystyrene in the capsules is the same as the density of bulk polystyrene. The assumption was already shown to be correct for non-porous particles as measured by gradient ultracentrifugation;<sup>213-215</sup>
- The influence of the comonomer on the density is neglected. Indeed the amount of functional comonomer represents only 8.5 – 14.2 wt% of the total monomer amount;
- No DCPD, non-polymerized styrene, and HD diffused out of the capsules during the dialysis. This assumption is based on the comparison of the hydrodynamic diameters before and after the dialysis of the latexes (Table 9.1);
- 50% of non-polymerized styrene was present in the core of the nanocapsules, which is an approximation based on the measured conversion. The density of the mixture HD:DCPD:styrene 2:1:1 was then measured and found to be  $\sim 0.86 \text{ g}\cdot\text{mL}^{-1}$ .

**Table 9.1** Comparison of the hydrodynamic diameters of the dispersions before and after dialysis.

Entry	$D_h$ [nm]	
	before dialysis	after dialysis
JF166-1	310 ± 70	310 ± 90
JF166-2	250 ± 80	260 ± 80
JF166-3	440 ± 160	440 ± 170
JF166-4	260 ± 60	240 ± 30
JF166-5	280 ± 70	270 ± 80
JF166-6	340 ± 370	490 ± 170

### AFM measurements

The dynamic mode of the AFM in a liquid environment (Nanoscope III, Veeco Instruments, CA) was used to characterize topographic structure of the nanocapsules with Veeco NP type A cantilevers [tip radius = 20 nm (Nom = 20 nm, max 60 nm)] for imaging. The nanocapsules were diluted (1:1000 in mQ water) and injected with a micropipette into the liquid cell. It is estimated that 30-40  $\mu\text{l}$  of the material is needed to fill the liquid cell and its inner inlet/outlet pipes around. In order to perform the measurement with particles present on a surface, the silicon substrate was to be modified. After standard cleaning procedure of Si wafers (ethanol, acetone, mQ water sonic baths, and subsequent treatment in  $\text{H}_2\text{O}:\text{H}_2\text{O}_2:\text{NH}_3$  25:2:2 mL solution in 80 °C for  $\frac{1}{2}$  h), the silanization of the surfaces was performed using a solution of 4-aminopropyltrimetoxysilane in toluene (RT, 12h, 2 mM). The surface was further protonated with a 0.1 M HCl aqueous solution to vary the surface charge.

## 9.4 Design and characterization of functionalized silica nanocontainers for self-healing materials

### Encapsulation of DCPD in non-functionalized and functionalized nanocapsules

Unless otherwise stated, following amounts were used for the synthesis: 2 g of silica precursors (TEOS and MPTMS) were mixed with 0.33 g of HD and 0.33 g DCPD, and were stirred with 30 mL of a  $0.77 \text{ mg}\cdot\text{mL}^{-1}$  aqueous solution of CTMA-Cl for 5 min. The emulsions were sonicated under ice cooling for 180 s at 70% amplitude in a pulse regime (30 s sonication, 10 s pause) using a Branson 450 W sonifier and a 1/2" tip. When APTES was used, the APTES precursor dissolved in 0.5 mL of water was added after a given time while stirring



the miniemulsion. The resulting miniemulsions were stirred at room temperature overnight to obtain the silica nanocapsules.

#### *Encapsulation of the Grubbs' catalyst*

The whole procedure was carried out under argon atmosphere in a glovebox and degassed solvents/water to protect the Grubbs' catalyst from oxygen. A known amount of catalyst was dissolved in known amounts of precursor, hexadecane, and solvent (Table 5.7). The mixture was stirred with 15 mL of a  $0.77 \text{ mg} \cdot \text{mL}^{-1}$  solution of CTMA-Cl in water for 5 min. The emulsions were sonicated under argon atmosphere with ice cooling for 180 s at 70% amplitude in a pulse regime (30 s sonication, 10 s pause) using a Branson 450 W sonifier and a 1/4" tip. The resulting miniemulsions were stirred at room temperature overnight to obtain the silica nanocapsules. Some miniemulsions were performed with D<sub>2</sub>O instead of H<sub>2</sub>O to investigate the stability of the catalyst with <sup>1</sup>H NMR spectroscopy. EDX measurements were carried out on a JEOL JEM-1400.

#### *Self-healing reaction*

10 g of the dispersion with encapsulated DCPD was mixed with 2 g of the dispersion with encapsulated Grubbs' catalyst (see Table 5.8). The mixture was stirred for 5 min, sonicated with and without argon and ice cooling for 5 min at 70% amplitude in a pulse regime (30 s sonication, 10 s pause) using a Branson 450 W sonifier and a 1/4" tip, and the mixture was stirred for another 15 h. A white precipitate can be observed due to the polymerization. The dispersions were freeze-dried followed by a treatment in a vacuum oven at 80 °C before performing <sup>13</sup>C MAS-NMR spectroscopy and TGA measurements.

#### *<sup>29</sup>Si MAS-NMR spectroscopy*

Quantitative <sup>29</sup>Si MAS-NMR spectra have been recorded with a Bruker Avance II spectrometer operating at 300.23 MHz <sup>1</sup>H Larmor frequency using a commercial double resonance MAS probe supporting MAS rotors with 7 mm outer diameter. Direct excitation spectra were acquired with a small excitation angle of ~20 ° at 25 kHz rf-nutation frequency and 60 s relaxation delay between subsequent transients. In order to avoid line broadening

due to dipolar couplings, SPINAL64 hetero-nuclear decoupling at 50 kHz rf-nutation frequency has been applied.<sup>216</sup> Typically 1600 - 2000 transients with 4096 data points and 20  $\mu$ s dwell time have been recorded. The  $^{29}\text{Si}$  NMR signals are referenced to tetrakis(trimethylsilyl)silane,<sup>217</sup> and the assignment of  $T^{(n)}$  and  $Q^{(n)}$  groups is taken from literature.<sup>218</sup> The content of  $T^{(n)}$  and  $Q^{(n)}$  groups was quantified *via* deconvolution of the  $^{29}\text{Si}$  MAS-NMR spectra using the DMfit program by Massiot et al.,<sup>219</sup> because the overlapping NMR signals of different  $T^{(n)}$  and  $Q^{(n)}$  groups could not be quantified by integration.

### *$^{13}\text{C}$ CP-MAS-NMR spectroscopy*

$^{13}\text{C}$  CP-MAS-NMR spectra were recorded on a Bruker DSX console operating at 500.12 Mhz  $^1\text{H}$  Larmor frequency and 20 kHz MAS with a CP contact time of 2 ms.

### *Thermogravimetric analysis*

The TGA measurements were carried out with a Mettler-Toledo 851 thermogravimetric analyzer with temperatures from 50  $^{\circ}\text{C}$  to 700  $^{\circ}\text{C}$  at a heating rate of 10  $^{\circ}\text{C min}^{-1}$  under a nitrogen atmosphere with a flow rate of 30  $\text{mL}\cdot\text{min}^{-1}$ .

### *Determination of thiol and amine groups*

The thiol groups on the silica were titrated with the Ellman's reagent (DTNB).<sup>220</sup> A DTNB stock solution consisting of 50 mM sodium acetate and 2 mM DTNB in water was prepared. The buffer solution was a 1 M Tris solution adjusted to pH 8.2 with 1 M HCl. 10  $\mu\text{L}$  of the silica dispersions were added to a solution of 200  $\mu\text{L}$  DTNB stock solution, 400  $\mu\text{L}$  Tris buffer and 890  $\mu\text{L}$  water. After stirring for 10 min at RT, optical absorbance at 412 nm was measured with a Tecan Infinite M1000 plate reader and was averaged on 10 measurements. The procedures followed the method used by other authors for thiol,<sup>221</sup> except that in our case our functional groups are bounded on particles and not on molecules. The procedure was also used for the titration of thiol groups of polymer particles.<sup>222</sup>

The amine groups were titrated by a method used by a method reported by Ganachaud et al. for polymer particles.<sup>223</sup> Briefly, 10  $\mu\text{L}$  of the silica dispersions were added to a mixture of 500  $\mu\text{L}$  of a 5 mM fluorescamine solution in methanol and 490  $\mu\text{L}$  of a 0.6 M  $\text{NaHCO}_3$  solution in water. After stirring for 30 min at RT, the fluorescence intensity at 480 nm was

determined using an excitation wavelength of 420 nm on a Tecan Infinite M1000 plate reader and was averaged on 10 measurements. The reactions for the titrations are schematized in Figure 5.12. DTNB as well as fluorescamine were reacted with the corresponding functional groups. For the quantification of thiol groups (Figure 5.12a), the fluorescence of the released 5-mercapto-2-nitrobenzoic acid was determined. The primary amine groups (Figure 5.12b) were determined by measuring the fluorescence of the capsules having reacted with fluorescamine. The calibrations were performed by mixing 5, 10 or 20  $\mu\text{L}$  of a 0.3 wt% MPTMS solution in THF, 200  $\mu\text{L}$  DTNB, 400  $\mu\text{L}$  Tris buffer, 890  $\mu\text{L}$  water and 10  $\mu\text{L}$  TEOS capsules. The blank value (pure TEOS capsules in the same mixture) was always subtracted from determined absorptions before further calculation. The calibration for amine titration was analogous to the calibration for thiol groups but the corresponding chemicals and amounts as described above.

### *XPS measurements*

The XPS spectra (PHI 5600 spectrometer) were collected at photoemission angles of 45 degrees with respect to the surface normal. The energy resolution of the spectrometer was set to 0.4 eV/step at a pass energy of 187.85 eV for survey scans and to 0.125 eV/step at a 29.35 eV pass energy for region scans. Curve fitting was carried out with CasaXPS software version 2.3.14. The charging of the sample surfaces was corrected by setting the graphite and aliphatic (C-C, C-H) photoelectron signal contribution to be at 285.0 eV. The sample was directly used as powders without pressing them into pills to avoid breakage of the nanocapsules.

## **9.5 Encapsulation of self-healing agents in polymer nanocapsules**

### *Encapsulation of self-healing agents in polymer nanocapsules*

Unless otherwise stated, the following procedure was performed: polymer (250 mg), non-solvent/healing agent (250 mg) and 5 mL chloroform were mixed and stirred at 600 rpm for 20 min. Then 10 mL of a SDS aqueous solution (1.0 mg mL<sup>-1</sup>) was added, followed by stirring at 1100 rpm for 1 h. The solution was then sonicated with a sonifier (Branson W450D Digital, half inch tip) for 2 min (30 s pulse and 10 s pause) in the presence of an ice-bath. The

mini-emulsion was kept stirring in an oil bath at 40 °C overnight to evaporate chloroform. When dichloromethane instead of chloroform was used, the evaporation was carried out at room temperature. Overview of synthesized samples are presented in [Table 6.1](#).

### *<sup>1</sup>H NMR spectroscopy*

<sup>1</sup>H NMR spectra were measured at room temperature on Avance 300 using deuterated chloroform as solvent. Before measurement, samples were centrifuged and redispersed in water several times, and dried in a vacuum oven at 40 °C for 24 h.

## 9.6 Copolymer structures tailored for the preparation of nanocapsules

### *Synthesis of the copolymers*

The block copolymer from styrene and methyl methacrylate P(S<sub>0.48</sub>-*b*-MMA<sub>0.52</sub>) was synthesized by anionic polymerization.<sup>175</sup> The molecular weight and the composition of the blocks were measured by GPC ([Table 6.2](#)) and <sup>1</sup>H NMR. The random copolymers were synthesized by free-radical polymerization in solution. For this, known amounts of styrene and comonomer were dissolved in THF ([Table 9.2](#)), repeatedly degassed and bubbled with Argon. The solution was heated to 80 °C in a flask equipped with a reflux condenser and placed in an oil bath. A certain amount of AIBN dissolved in 4 mL of THF was added to the solution to reach a final concentration of 286 mg·L<sup>-1</sup> and the mixture was stirred for 6 h under argon. The reaction was then cooled at 0 °C in an ice-bath. The copolymer was precipitated in an appropriate solvent mixture ([Table 9.2](#)), filtrated, washed with the solvent mixture, and dried at 80 °C under vacuum. The chemical structures of the obtained copolymers are shown in [Figure 6.13](#).

**Table 9.2** Composition and characteristics of the polymerization reactions

Entry	polymer	styrene amount [g·L <sup>-1</sup> ]	comonomer amount [g·L <sup>-1</sup> ]	precipitation		yield [%] <sup>a</sup>
				solvent(s)	ratio	
<b>copolymers with MAA units</b>						
SC10	P(S <sub>0.91</sub> -stat-MAA <sub>0.09</sub> )	255.2	23.1	EtOH:H <sub>2</sub> O	75:25	8.1
SC5	P(S <sub>0.86</sub> -stat-MAA <sub>0.14</sub> )	257.3	23.6	EtOH:H <sub>2</sub> O	75:25	10.2
SC35	P(S <sub>0.72</sub> -stat-MAA <sub>0.28</sub> )	192.2	68	EtOH:H <sub>2</sub> O	75:25	7.6
SC38	P(S <sub>0.67</sub> -stat-MAA <sub>0.33</sub> )	200.3	70.9	EtOH:H <sub>2</sub> O	75:25	5.8
SC11	P(S <sub>0.47</sub> -stat-MAA <sub>0.53</sub> )	142.9	137.5	EtOH:H <sub>2</sub> O	75:25	7.8
<b>copolymers with MMA units</b>						
SC13	P(S <sub>0.88</sub> -stat-MMA <sub>0.12</sub> )	257.7	27.5	MeOH	100	9.4
SC39	P(S <sub>0.69</sub> -stat-MMA <sub>0.31</sub> )	200.1	82.4	MeOH	100	11.1
SC41	P(S <sub>0.67</sub> -stat-MMA <sub>0.33</sub> )	200.4	82.4	MeOH	100	11.4
SC6	P(S <sub>0.53</sub> -stat-MMA <sub>0.47</sub> )	143.0	137.6	MeOH	100	11.3
SC15 <sup>b</sup>	P(S <sub>0.50</sub> -stat-MMA <sub>0.50</sub> )	144.1	137.3	MeOH	100	8.0
SC14	P(S <sub>0.49</sub> -stat-MMA <sub>0.51</sub> )	143.3	137.6	MeOH	100	10.8
<b>copolymers with AAm units</b>						
SC31	P(S <sub>0.73</sub> -stat-AAm <sub>0.27</sub> )	308.6	23.4	IP:H <sub>2</sub> O	50:50	10.8
SC44	P(S <sub>0.67</sub> -stat-AAm <sub>0.33</sub> )	308.6	23.4	MeOH	100	10.5
SC32	P(S <sub>0.50</sub> -stat-AAm <sub>0.50</sub> )	240.0	70.2	MeOH	100	8.2

<sup>a</sup> after precipitation and drying of the copolymers<sup>b</sup> reaction time of 3h instead of 6 h

### Polymer analogues reactions

The polymer analogue reactions were amidification or esterification. The esterification was carried out with TMS-diazomethane using conditions similar to what was reported in the literature for different substrates (Figure 6.14, top).<sup>224</sup> 1 g of P(S<sub>0.47</sub>-stat-MAA<sub>0.53</sub>) was suspended in 100 mL of anhydrous toluene under argon. A 6 mL aliquot of TMS-diazomethane was added dropwise followed by the dropwise addition of 0.384 g methanol. The reaction was continued for 12 h and the resulting copolymer was completely soluble in the solvent. The copolymer was precipitated in methanol, filtrated, and dried at 80 °C in a vacuum-oven and was named P(S<sub>0.47</sub>-stat-MMA<sub>0.53</sub>). The amidifications of the methacrylic acid copolymers were carried out following a procedure that reported amidification of different substrates (Figure 2, bottom).<sup>225</sup> Then, 0.75 g of P(S<sub>0.72</sub>-stat-MAA<sub>0.28</sub>) was dissolved

in 10 mL of anhydrous THF. A 10 mg DMAP sample and 10 mL of a 0.5 M ammonia solution in dioxane were added to the solution. After cooling to 0 °C, a solution of 1.347 g of DCC in THF was added and stirred at 0 °C for 10 min. The reaction was warmed up to room temperature while stirring and let further stir for 24 h. The precipitated urea was filtrated, THF evaporated, and the solid was dissolved in DCM and precipitated in methanol. The copolymer was then dried at 80 °C in a vacuum-oven and was named P(S<sub>0.72</sub>-stat-MAA<sub>0.24</sub>-stat-MAA<sub>0.04</sub>). The molecular weights of the copolymers are given in [Table 6.2](#).

### *Preparation of the miniemulsions with subsequent solvent evaporation*

A 300 mg sample of the synthesized copolymers was dissolved in either 2.5 or 5.0 g of chloroform, and 300 mg of a nonsolvent was added to the solution. The transparent solutions were mixed with 10 mL of a 1.0 or 2.0 mg·mL<sup>-1</sup> aqueous solution of SDS and stirred for 1 h at room temperature. The obtained emulsions were sonicated under ice cooling for 120 s at 70% amplitude in a pulse regime (30 s sonification, 10 s pause) using a Branson 450 W sonifier and a 1/4" tip. The miniemulsions were then heated overnight at 40 °C under mechanical stirring (700 rpm) to evaporate the chloroform. The temperature and the rotational speed of the stirring were limited to promote the phase separation between the polymer and the nonsolvent. Indeed, if stirring is too fast or if the temperature too high, acorn particles can be also obtained. An overview of the synthesized samples is given in [Table 6.3](#).

### *Encapsulation of monomers and catalysts for ring-opening metathesis polymerization*

The encapsulation was carried out following the process described above with 10 mg of SDS except that a certain amount of monomers or Hoveyda-Grubbs' catalyst 2<sup>nd</sup> generation were dissolved in the dispersed phase (see [Table 6.5](#)). For the encapsulation of the catalyst, the preparation was performed under argon, and the evaporation of chloroform was carried out for 6 h at room temperature under a flux of argon. For NMR measurements, the nanocapsules with monomer for metathesis polymerization were prepared with 0.3:0.15:0.15:2.5:0.01:10 P(S-*b*-MMA):HD:norbornene derivative:CHCl<sub>3</sub>:SDS:D<sub>2</sub>O (wt:wt). A 2 mg sample of 4,4-dimethyl-4-silapentane-1-sulfonic acid (DSS) was mixed with 0.8 g of dispersion before the <sup>1</sup>H NMR measurements.

### *Self-healing reaction*

The self-healing reactions were carried out in air atmosphere. 4 g of the dispersion with encapsulated DCPD were mixed with 1 g of the dispersion with encapsulated Grubbs' catalyst (Table 6.6). After stirring for 5 min, the mixtures were sonicated under ice cooling for 1 min at 70% amplitude using a Branson 450W sonifier and a 1/8" tip and stirred for another 15 h. The dispersions were freeze-dried and then dried at 80 °C under vacuum. FT-IR measurements on pressed KBr pellets were used to verify that the self-healing reaction occurred and the conversion was determined gravimetrically.

### *Gel permeation chromatography (GPC)*

Gel permeation chromatography (GPC) was used to estimate the apparent molecular weights of the synthesized polymers and their polydispersity. The polymers were dissolved in THF to reach a concentration of 5 mg·mL<sup>-1</sup> and filtered through a 0.45 µm Teflon filter. The elution rate was 1.0 mL·min<sup>-1</sup> and both UV- (254 nm) and RI-detectors were used. The resulting apparent molecular weights were calculated using polystyrene standards.

### *<sup>1</sup>H NMR Measurements*

The <sup>1</sup>H NMR spectra have been recorded with a Bruker Avance 300 spectrometer operating at 300.23 MHz <sup>1</sup>H Larmor frequency. 10 mg of the synthesized polymers were dissolved in 0.7 mL THF-*d*<sub>8</sub>, CDCl<sub>3</sub> or DMSO-*d*<sub>6</sub>, depending on the solubility of the polymers. The assignment for the <sup>1</sup>H NMR peaks for the copolymers with acrylamide and methacrylamide were performed using values reported in the literature.<sup>226</sup>

### *Elemental Analysis*

The elemental analysis (C, H, N) was performed on an Elementar Vario EL III Elemental Analyzer.

### *Measurement of contact angle*

For the measurements of the contact angle, the films were spin-coated (3000 rpm, 60 s) on a pre-cleaned Si-wafer from polymer solutions in THF (10 mg polymer in 10 mL THF). The

thicknesses of the films (~45 nm) were determined with a step profiler (KLA Tencor P16+). The contact angle was measured with a sessile drop configuration on a contact angle meter Dataphysics OCA35 (Data Physics Instruments GmbH, Germany). A droplet of 3  $\mu\text{L}$  water was deposited on the surface of the polymer film and the shape of the droplet was recorded immediately for determination of the contact angle. The measurement was repeated 4 times at different positions of the films.

### *Measurement of interfacial tension*

The interfacial tension  $\gamma_{ow}$  between aqueous solutions of surfactant and hexadecane was measured with a SVT20 spinning drop tensiometer (Dataphysics, Germany) at 25 °C with a spinning rate of 10,000 rpm. The interfacial tension is determined from the radius  $R$  of the cylinder formed by the hexadecane (density  $\rho_o$ ) phase upon spinning, which is surrounded by the aqueous solutions (density  $\rho_w$ ) present in a capillary rotating with a speed  $\omega$ . The interfacial tension is then calculated using Equation 11.<sup>227</sup>

$$\gamma_{ow} = \frac{(\rho_w - \rho_o)\omega^2 R^3}{4} \quad \text{Equation 11}$$

## 9.7 Self-stabilized pH-responsive nanocapsules

### *Synthesis of the copolymers*

The copolymers were synthesized by free-radical polymerization in solution. Known amounts of styrene and TMSMA in dry THF were degassed and bubbled with argon three times. After heating the solution to 80 °C in a flask equipped with a reflux condenser, certain amounts of AIBN dissolved in 4 mL THF were added (Table 9.3). The mixture was stirred at 80 °C for 6 h under argon atmosphere. The polymerization was then stopped by cooling to 0 °C in an ice-bath. After precipitation in dry ice cold *n*-hexane, the polymer was filtrated, washed with the precipitant, and dried at 80 °C under vacuum. The molecular weight and the composition of the copolymer were measured by GPC and  $^1\text{H}$  NMR (Table 7.1).



**Table 9.3** Composition for the polymerization reactions.

Entry	polymer	styrene [g·L <sup>-1</sup> ]	TMSMA [g·L <sup>-1</sup> ]	AIBN [mg]	dry THF [ml]	yield <sup>a</sup> [%]
SC42	P(S <sub>0.87</sub> -stat-TMSMA <sub>0.13</sub> )	257.4	43.4	80.1	280	10.7
SC43	P(S <sub>0.71</sub> -stat-TMSMA <sub>0.29</sub> )	200.2	130.3	80.7	280	7.9
SC45	P(S <sub>0.52</sub> -stat-TMSMA <sub>0.48</sub> )	145.5	217.5	37.0	130	7.4

<sup>a</sup> after precipitation and drying of the copolymers

#### Preparation of surfactant-free nanocapsules and nanoparticles

300 mg of synthesized copolymers were dissolved in 5 g chloroform and 300 mg of HD (12.5 mg HD in the case of nanoparticles). The solutions were mixed with 10 mL of a 0.02 mmol·mL<sup>-1</sup> aqueous solution of NaOH (200 μL 1 M NaOH + 9.8 mL H<sub>2</sub>O). After stirring of 1h at 1000 rpm sonication was carried out under ice cooling for 120 s at 70% amplitude in a pulse regime (30 s sonication, 10 s pause) using a Branson 450 W sonifier and a 1/2" tip. To evaporate the chloroform the miniemulsions were then stirred overnight at RT at 700 rpm. The compositions of the synthesized colloids are summarized in Table 7.2.

#### Kinetics of desilylation

300 mg of P(S<sub>0.71</sub>-stat-TMSMA<sub>0.29</sub>) were dissolved in 5 g CHCl<sub>3</sub> and 300 mg HD. The solution was mixed with a 0.02 mmol·mL<sup>-1</sup> aqueous solution of NaOH and stirred at RT at 1000 rpm without evaporation of CHCl<sub>3</sub>. Samples were taken at fixed time intervals and directly freeze-dried. Further, a sample of surfactant-free dispersion of nanocapsules with desilylated P(S<sub>0.71</sub>-stat-TMSMA<sub>0.29</sub>) (JF190-1) was also frozen. After freeze-drying and treatment at 80 °C under vacuum, each sample was dissolved in d<sub>8</sub>-THF and investigated by <sup>1</sup>H NMR spectroscopy. For quantitative analysis the integrals of the aromatic signals (6-8 ppm) were compared with the integrals of the TMS-group (0.03 ppm).

#### Turbidity measurements

Turbidity measurements were carried out in transmission with a red light He-Ne laser (JDSU, model 1145P, 633 nm, 25mW) through the diluted samples under constant magnetic stirring (300 rpm) and detection of the light by a photodiode detector. 200 μL of the dispersion of nanocapsules with desilylated P(S<sub>0.71</sub>-stat-TMSMA<sub>0.29</sub>) (JF190-1) were mixed with 30.1 mL

H<sub>2</sub>O and 100  $\mu$ L of 1 M HCl (for aggregation). 100  $\mu$ L of 1 M NaOH were added for redispersion.

### *Aggregation of the nanocapsules in the presence of a non-ionic block copolymer surfactant*

Surfactant-free dispersion of nanocapsules from desilylated P(S<sub>0.71</sub>-stat-TMSMA<sub>0.29</sub>) (JF190-1, [Table 7.2](#)) containing various concentrations of Lutensol AT50 were prepared and the pH was adjusted to 3 by adding 1 M HCl. DLS measurements were performed on the dispersions at the different stages.

### *Increase of the amount of dispersed phase (concentration)*

200  $\mu$ L of a 1M HCl was added to 8.5 g of the nanocapsule dispersion with desilylated P(S<sub>0.71</sub>-stat-TMSMA<sub>0.29</sub>) shell (JF190-1). The dispersion was filtered and the residue was then redispersed by addition of 200  $\mu$ L 1 M NaOH under stirring and sonication in an ultrasound-bath. The procedure was repeated in the same way, only the amount of added 1 M NaOH was changed to 150  $\mu$ L. The amount of dispersed phase (core-shell) and the solid content (only the shell) of the dispersions were investigated gravimetrically ([Table 7.3](#)).

### *Preparation of nanocapsules for the encapsulation of DCPD and Grubbs' catalyst*

300 mg of synthesized copolymers were dissolved in a mixture of 5 g chloroform, 200 mg DCPD and 100 mg HD. For the encapsulation of the catalyst a mixture of 5 g chloroform, 300 mg HD and 15 mg Hoveyda-Grubbs' catalyst 2<sup>nd</sup> generation was used. The solutions were mixed with 10 mL of a 0.02 mmol·mL<sup>-1</sup> aqueous solution of NaOH. After stirring of 1h at 1000 rpm sonication was carried out under ice cooling for 120 s at 70% amplitude in a pulse regime (30 s sonication, 10 s pause) using a Branson 450 W sonifier and a 1/2" tip. To evaporate the chloroform the miniemulsions were then stirred overnight at RT at 700 rpm. For the encapsulation of the catalyst, the preparation was performed under argon, and the evaporation of chloroform was carried out for 6 h at room temperature under a flux of argon. An overview of the synthesized capsules is given in [Table 7.4](#).

### *Aggregation of the nanocapsules with encapsulated DCPD*

150  $\mu\text{L}$  of 1M HCl were added to 6 g of the dispersion containing DCPD (JF195-1) to aggregate the nanocapsules and the dispersion was filtrated. For redispersion, 0.479 g of the wet solid was mixed with 50  $\mu\text{L}$  1M NaOH and 150  $\mu\text{L}$  water, stirred and treated in an ultrasonic bath until complete redispersion. For determination of the DCPD amount, 50-200 mg of each samples were dissolved in  $d_8$ -THF in the presence of 2 mg maleic acid as internal standard for  $^1\text{H}$  NMR spectroscopy.

### *Preparation of the nanocapsules with encapsulated oleic acid at pH3*

300 mg of synthesized copolymers were dissolved in 5 g chloroform, 50 mg of HD and 250 mg of oleic acid. The solution was mixed with 10 mg SDS dissolved in 10 mL of a 0.002  $\text{mmol}\cdot\text{mL}^{-1}$  aqueous solution of HCl (20  $\mu\text{L}$  1 M HCl + 9.98 mL  $\text{H}_2\text{O}$ ) resulting to pH 3. After stirring 1h at 1000 rpm, sonication was carried out under ice cooling for 120 s at 70% amplitude in a pulse regime (30 s sonification, 10 s pause) using a Branson 450 W sonifier and a 1/2" tip. To evaporate the chloroform, the miniemulsions were then stirred overnight at RT at 700 rpm. The adjustment to pH 10 and further to pH 3 was done by adding 1.5 mL of 1 M NaOH or 1.5 mL HCl, respectively. An overview is given in [Table 7.6](#).

## **9.8 Incorporation of nanocapsules into a zinc matrix by electrodeposition**

### *Synthesis of PVP modified polymer nanocapsules JF96-1 and JF136-1*

1.82 g of styrene were mixed with 100 mg V59, 2 g HD, and 2 g DCPD. 16 mg of SDS in 24 g water were mixed with 180 mg hydrophilic vinyl monomer SMA and in case of JF96-1 with additional 120 mg of PEGMA. The two solutions were mixed, stirred for 1 h and sonicated under cooling with an ice bath for 120 s at 70% amplitude in a pulse regime (30 s sonication, 10 s pause, Branson 450 W sonifier with a 1/2" tip). The polymerization was performed at 72  $^\circ\text{C}$  for 16 h.

### *Electrodeposition*

Known amounts of the dispersions containing nanocapsules were filled up to a volume of 20 mL using degassed demineralized water in order to obtain capsule concentrations of 16 mg/mL. 3.2 g ZnSO<sub>4</sub> and 1 g Na<sub>2</sub>SO<sub>4</sub> were then added to the diluted dispersions. In case of cysteamine modified capsules, 77 mg cysteamine was added in addition. After adjusting the pH with 1N H<sub>2</sub>SO<sub>4</sub>, the electrochemical deposition was performed on a Rotating Disc Electrode (RDE) with a rotational speed of 2500 – 4000 rpm at -400 mA for 2 min.

### *Amount of nanocapsules incorporated into the zinc coating*

The amount of nanocapsules incorporated into the zinc matrix was determined by energy dispersive x-ray analysis (EDX) carried out on a cross-sectional cut at three different locations of 100 μm<sup>2</sup> area. The atomic percentages were deduced with Inca software and converted to volume fractions using the bulk densities of silica or polystyrene and zinc as well as the density of the mixture HD/DCPD, which was measured and found to be 0.88 g·mL<sup>-1</sup>.

## 10 Conclusions

Within this thesis, new approaches for capsule-based self-healing materials have been investigated. The encapsulation of self-healing agents in functional nanocapsules was carried out by three different preparation methods in miniemulsion.

Firstly, the synthesis of core-shell particles encapsulating monomers for ring-opening metathesis polymerization by free-radical polymerization in miniemulsion droplets is described. Various chemical functionalizations of the shell were introduced by orthogonal reactions. Detailed investigations on the distribution of the charged functional groups on the nanocapsule surface were performed. The orthogonal reaction, the role of the surfactant, the ratio of core material to monomer, and the variation of solvent quality were found to have an influence on the structure of the colloids. Furthermore, the colloidal and mechanical stability of the functionalized nanocontainers was investigated by salting out and atomic force microscopy, respectively. Self-healing experiments were carried out successfully verifying that the encapsulated reagents remained active after encapsulation.

In the second part of the results and discussion, the synthesis of silica nanocontainers for self-healing materials by hydrolysis and polycondensation of alkoxy silanes at the interface of miniemulsion droplets is reported. This approach allows the efficient encapsulation of monomer and solutions of catalysts suitable for metathesis polymerization in a one-step process. The size of the nanocapsules, thickness of their shell, and solid content of the dispersions could be varied in a wide range. X-ray photoelectron spectroscopy and  $^{29}\text{Si}$  NMR spectroscopy showed that the outer part of the shell was enriched with amine functionalization compared to the composition of the bulk whereas the contrary was found for thiol-functionalized shells. The self-healing agents remained active after encapsulation as proved by successful self-healing reactions monitored by thermogravimetric analysis and  $^{13}\text{C}$  NMR spectroscopy.

The third concept deals with the preparation of polymer nanocapsules by the emulsion-solvent evaporation process as a mild method for the encapsulation of self-healing agents.

In the first part, a general and facile method to load self-healing agents into polymer nanocapsules using various commercial available polymers as shell materials is described. Nanocontainers filled with healing agents used for solvent- or plasticizer-assisted self-healing could be obtained. In addition, the encapsulation of various monomers for ionic, condensation, and radical self-healing polymerization reactions could be demonstrated.

In the second part of this section, copolymers of styrene and various hydrophilic monomers were synthesized by free-radical polymerization and polymer-analogue reactions. These statistical copolymers were as suitable as block copolymers for the preparation of well-defined core-shell nanoparticles with an emulsion-solvent evaporation process. Acrylamide, acrylic acid, and methyl methacrylate units are playing the role of the structure-directing agent during the phase separation between the liquid core and the polymer inside the droplets. Monomers and catalysts for ring-opening metathesis polymerization could be successfully encapsulated and were found to remain active after encapsulation, which was confirmed by successful self-healing experiments.

Furthermore, a new concept for the synthesis of nanocapsules with pH-responsive behavior from surfactant-free emulsions using copolymers of styrene and trimethylsilyl methacrylate is described. The proposed synthetic approach allows the first synthesis of nanocapsules by the emulsion-solvent evaporation process in absence of surfactant. In addition, the pH-responsive stability of the capsules is controlled by the chemistry of the polymer shell that is defined *in-situ* by desilylation during the self-emulsification process. Fully reversible aggregation allows for the separation of the nanocapsules from the continuous phase without evaporation or centrifugation. Switching the colloidal stability could be also used to concentrate the nanocapsule dispersions up to 5 times. In addition, self-healing agents could be encapsulated successfully in stable state.

The last part of this work was focused on the electrochemical codeposition of monomer filled nanocapsules for application in corrosion prevention. Silica nanocapsules as well as polymer nanocontainers could be successfully incorporated into the zinc matrix up to 11.7 vol%. In the case of inorganic core-shell particles, modification with cysteamine and the functionalization with thiol or amine groups had a beneficial effect on the incorporation behavior. Polymer nanocapsules functionalized with amine or sulfonate groups were found

to be most favorably incorporated. An additional functionalization with poly(ethylene glycol) and the modification with polyvinylpyrrolidone had further an advantageous effect on the incorporation.

The main aspects of the three preparation routes for the encapsulation of self-healing agents described in this thesis are summarized in [Table 10.1](#).

**Table 10.1** Properties of the functional nanocontainers.

Method	material		$D_h$ [nm]	$\varphi_d$ [wt%]	encapsulation of	
	main	functional groups			monomer	catalyst
<b>(a)</b> radical polymerization	PS	-SO <sub>3</sub> H -COOH -NH <sub>2</sub>	$240 \leq \Phi \leq 490$	$\leq 20.3$	Y	N
<b>(b)</b> hydrolysis and polycondensation	silica	-NH <sub>2</sub> -SH	$120 \leq \Phi \leq 410$	$\leq 25.5$	Y	Y
<b>(c)</b> solvent evaporation	PS	-COOH	$170 \leq \Phi \leq 360$	$\leq 5.6$	Y	Y

Depending on the procedure, different functional groups could be introduced, *e.g.* for better compatibility between the capsules and an embedding matrix. In the case of silica nanocontainers **(b)**, the diameter could be varied and adjusted in wide ranges, whereas the amount of dispersed phase  $\varphi_d$  for the method **(c)** is limited to relatively small values. The three methods were suitable for encapsulating of both catalyst and monomer for ring-opening metathesis polymerization except method **(a)**, for which only the latter could be encapsulated.

The different approaches for the synthesis of functionalized inorganic or polymeric nanocapsules with encapsulated self-healing agents are a promising basis for further research in the field of capsule-based self-healing materials.





## 11 Zusammenfassung

Im Rahmen dieser Arbeit wurden neue Ansätze für das Konzept der kapselbasierten Selbstheilungsmaterialien untersucht. Die Verkapselung von Selbstheilungsreagenzien in funktionellen Nanokapseln wurde mittels drei verschiedener Herstellungsmethoden in Miniemulsion durchgeführt.

Zuerst wurde die Synthese von Kern-Schale-Partikeln mit verkapselten Monomeren für die Ringöffnungs-Metathese-Polymerisation über freie radikalische Polymerisation in Miniemulsionstropfen beschrieben. Durch orthogonale Reaktionen wurden verschiedene chemische Funktionalisierungen in die Schale eingebracht. Hierzu wurden detaillierte Untersuchungen zur Verteilung der geladenen funktionellen Gruppen auf der Kapseloberfläche durchgeführt. Die orthogonale Reaktion, die Rolle des Tensides, das Verhältnis von Kernmaterial zu Monomer sowie die Variation der Lösungsmittelqualität hatte dabei einen Einfluss auf die Struktur der Kolloide. Daneben wurde die kolloidale und mechanische Stabilität der funktionalisierten Nanocontainer mittels Aussalzen beziehungsweise Rasterkraftmikroskopie untersucht. Die Heilungsreagenzien blieben auch nach der Verkapselung aktiv, was durch erfolgreich durchgeführte Selbstheilungsexperimente gezeigt werden konnte.

Im zweiten Abschnitt des Ergebnisteils wurde die Synthese von Silica-Nanocontainern für Selbstheilungsmaterialien über Hydrolyse und Polykondensation von Alkoxysilanen an der Grenzfläche der Miniemulsionstropfen beschrieben. Dieser Ansatz ermöglichte die effiziente Verkapselung sowohl von Monomeren als auch von Lösungen der Katalysatoren für die Metathese-Polymerisation in einem Einstufenprozess. Die Größe der Kapseln, die Dicke der Schale und der Feststoffgehalt der Dispersionen konnte dabei in einem weiten Bereich variiert werden. Durch  $^{29}\text{Si}$ -NMR-Spektroskopie und Röntgen-Photoelektronen-Spektroskopie konnte gezeigt werden, dass der äußere Teil der Schale im Vergleich zur Ausgangszusammensetzung mit Amin-Funktionalität angereichert war. Im Fall der Thiol-funktionalisierten Schale wurde hingegen ein gegenteiler Gradient beobachtet. Anhand von erfolgreich durchgeführten Selbstheilungsreaktionen, die über Thermogravimetrie und

$^{13}\text{C}$ -NMR-Spektroskopie verfolgt wurden, konnte gezeigt werden, dass die Selbstheilungsreagenzien nach der Verkapselung aktiv blieben.

Das dritte Konzept behandelte die Herstellung von polymeren Nanokapseln mittels Emulsions-Lösungsmittelverdampfungstechnik, welche eine milde Methode zur Verkapselung darstellt. Im ersten Teil wurde eine allgemeine und einfache Vorgehensweise beschrieben, in der Selbstheilungsreagenzien in polymeren Nanokapseln unter Verwendung von kommerziell erhältlichen Polymeren als Schalenmaterial verkapselt wurden. Dabei konnten Nanokapseln - gefüllt mit Reagenzien zur Verwendung von lösungsmittel- und weichmacherunterstützter Selbstheilung - erhalten und zudem Monomere für Selbstheilungsreaktionen basierend auf ionischer und radikalischer Polymerisation sowie auf Polykondensation verkapselt werden.

Im zweiten Teil dieses Abschnittes wurden Copolymere aus Styrol und verschiedenen hydrophilen Monomeren über freie radikalische Polymerisation sowie über polymeranaloge Reaktionen hergestellt. Diese statistischen Copolymere waren ebenso wie Blockcopolymere zur Herstellung von wohldefinierten Kern-Schale-Nanopartikeln mittels Emulsions-Lösungsmittelverdampfungsprozess geeignet. Die Acrylamid-, Acrylsäure- und Methylmethacrylat-Einheiten spielten dabei während der Phasenseparation zwischen dem flüssigen Kern und dem Polymer in den Tropfen die strukturbestimmende Rolle. Zudem konnten Monomere und Katalysatoren für die Ringöffnungs-Metathese-Polymerisation erfolgreich verkapselt werden. Die verkapselten Reagenzien waren nach dem Herstellungsprozess weiterhin aktiv, was durch erfolgreiche Selbstheilungsreaktion nachgewiesen wurde.

Desweiteren wurde ein neues Konzept für die Synthese von pH-responsiven Nanokapseln aus tensidfreien Emulsionen unter Verwendung von Copolymeren aus Styrol und Trimethylsilylmethacrylat beschrieben. Der vorgeschlagene synthetische Ansatz ermöglichte dabei die erste Synthese von Nanokapseln über den Emulsions-Lösungsmittelverdampfungsprozess in Abwesenheit eines Tensides. Zudem wurde die pH-responsive Stabilität der Kapseln durch die chemische Zusammensetzung der Polymerhülle bestimmt, welche *in-situ* durch Desilylierung während des Emulgierungsprozesses gebildet wurde. Eine vollständig reversible Aggregation ermöglichte

die Trennung der Nanokapseln von der kontinuierlichen Phase ohne Verdampfen oder Zentrifugieren. Durch Verändern der kolloidalen Stabilität konnte die Konzentration der Nanokapseldispersionen auf das bis zu fünffache erhöht werden. Darüber hinaus war es möglich, Selbstheilungsreagenzien in stabilem Zustand zu verkapseln.

Der letzte Teil dieser Arbeit behandelte die elektrochemische Abscheidung von mit Monomer gefüllten Nanokapseln zur Anwendung im Korrosionsschutz. Silica-Kapseln sowie polymerbasierte Nanocontainer konnten erfolgreich mit bis zu 11,7 Vol.-% in eine Zink-Matrix eingebettet werden. Im Fall der anorganischen Kern-Schale Partikel hatte eine Modifizierung mit Cysteamin sowie eine Funktionalisierung mit Thiol- bzw. Aminogruppen eine vorteilhafte Wirkung auf das Einbauverhalten der Kapseln. Polymere Nanokapseln, die mit Amin- oder Sulfonatgruppen funktionalisiert waren, wurden dabei bevorzugt eingebaut, wobei auch eine zusätzliche Funktionalisierung mit Polyethylenglykol sowie die Modifizierung mit Polyvinylpyrrolidon eine begünstigende Wirkung auf den Einbau hatte.

Die wichtigsten Aspekte der in dieser Dissertation beschriebenen Synthesewege zur Verkapselung von Selbstheilungsreagenzien sind in [Tabelle 11.1](#) zusammengefasst.

**Tabelle 11.1** Eigenschaften der funktionalisierten Nanokapseln.

Methode	Material		$D_h$ [nm]	$\varphi_d$ [Gew%]	Verkapselung vom	
	Hauptmaterial	funktionelle Gruppe			Monomer	Katalysator
(a) radikalische Polymerisation	PS	-SO <sub>3</sub> H -COOH -NH <sub>2</sub>	$240 \leq \Phi \leq 490$	$\leq 20,3$	Ja	Nein
(b) Hydrolyse und Polykondensation	Silica	-NH <sub>2</sub> -SH	$120 \leq \Phi \leq 410$	$\leq 25,5$	Ja	Ja
(c) Lösungsmittel- verdampfung	PS	-COOH	$170 \leq \Phi \leq 360$	$\leq 5,6$	Ja	Ja

Je nach Verfahren konnten verschiedene funktionelle Gruppen eingeführt werden, um z.B. eine bessere Verträglichkeit zwischen den Kapseln und der umgebenden Matrix zu ermöglichen. Im Falle der Silica-Kapseln (**b**) konnte der Durchmesser in einem weiten Bereich variiert und eingestellt werden, wohingegen die Menge an disperser Phase  $\varphi_d$  in Methode (**c**) auf relativ kleine Werte begrenzt ist. Alle drei Methoden sind geeignet um sowohl Katalysator als auch Monomer für die Ringöffnungs-Metathese-Polymerisation zu verkapseln – mit Ausnahme von Verfahren (**a**), bei dem nur Letzteres verkapseln werden konnte.

Basierend auf den vorgestellten Ergebnissen sind die verschiedenen Ansätze für die Synthese von funktionalisierten anorganischen und polymeren Nanocontainern mit verkapselten Selbstheilungsreagenzien eine vielversprechende Grundlage für die weitere Forschung auf dem Gebiet der kapselbasierten Selbstheilungsmaterialien.

## Abbreviations and characters

### Abbreviations

1D, 2D, 3D	one-, two-, three-dimensional
AAM	acrylamide
AEMA	2-aminoethyl methacrylate
AFM	atomic force microscopy
AIBN	azobisisobutyronitrile
APTES	(3-aminopropyl)triethoxysilane
APTMS	(3-aminopropyl)trimethoxysilane
ATRP	atom transfer radical polymerization
BAP	2,2-bis(azidomethyl)-1,3-propanediol
BCA	<i>n</i> -butyl cyanoacrylate
cmc	critical micelle concentration
CTMA-Cl	cetyltrimethylammonium chloride
DA	Diels-Alder
DAB	1,4-diaminobutane
DBTL	di- <i>n</i> -butyltin dilaurate
DCC	<i>N,N'</i> -dicyclohexylcarbodiimide
DCPD	dicyclopentadiene
DET	diethylenetriamine
DLS	dynamic light scattering
DMDNT	dimethyldineodecanoate
DSS	4,4-dimethyl-4-silapentane-1-sulfonic acid
DVB	divinylbenzene
<i>e.g.</i>	<i>exempli gratia</i> ; for example
ENB	5-ethyliden-2-norbornene
EDX	energy dispersive x-ray spectroscopy
FT-IR	fourier transform infrared spectroscopy
GDP	gross domestic product
GMA	glycidyl methacrylate
GPC	gel permeation chromatography
HD	hexadecane

HDI	1,6-hexamethylene diisocyanate
HEMA	2-hydroxyethyl methacrylate
HMDA	1,6-hexanediamine
HOPDMS	hydroxyl end-functionalized polydimethylsiloxane
<i>i.e.</i>	<i>id est</i> ; that is
IPDI	isophorone diisocyanate
LbL	layer-by-layer
MAA	methacrylic acid
MAS	magic angle spinning
MMA	methyl methacrylate
monomer-[m]	monomer for metathesis polymerization
monomer-[r]	monomer for free-radical polymerization
MPS	3-(trimethoxysilyl)propyl methacrylate
MPTMS	3-mercaptopropyltrimethoxysilane
NA	5-norbornen-2-yl acetate
NIPAM	<i>n</i> -isopropyl acrylamide
NMR	nuclear magnetic resonance
PDADMAC	poly(diallyldimethylammonium chloride)
PDCPD	poly(dicyclopentadiene)
PDES	polydiethoxysiloxane
PDI	polydispersity
PDMS	poly(dimethylsiloxane)
PDMS-DE	poly(dimethylsiloxane) diglycidyl ether terminated
PDVB	poly(divinylbenzene)
PEGMA	poly(ethylene glycol) methacrylate
PEI	poly(ethylene imine)
PHD	1-phenylheptadecane
PLLA	poly(L-lactide)
PMAA	poly(methacrylic acid)
PMI	<i>N</i> -(2,6-diisopropylphenyl) perylene-3,4-dicarbonacidimide
PMMA	poly(methyl methacrylate)
PPO	poly(2,6-dimethyl-1,4-phenylene oxide)
PS	polystyrene
PSS	poly(sodium 4-styrenesulfonate)

---

PVAc	poly(vinyl acetate)
PVCi	poly(vinyl cinnamate)
PVF	poly(vinyl formal)
PVP	polyvinylpyrrolidon
RAFT	reversible addition-fragmentation chain transfer polymerization
rDA	retro-Diels-Alder
RDE	rotating disk electrode
ROMP	ring-opening metathesis polymerization
S	styrene
SDS	sodium dodecyl sulfonate
SEM	scanning electron microscopy
SMA	sulfopropyl methacrylate
SS	sodium <i>p</i> -styrene sulfonate
TDI	tolylene 2,4-diisocyanate
TEGDMA	triethylene glycol dimethacrylate
TEM	transmission electron microscopy
TEOS	tetraethoxysilane
TGA	thermo gravimetric analysis
THF	tetrahydrofurane
TMAEMA	<i>tert</i> -butylaminoethyl methacrylate
TMS	trimethylsilyl
TMSMA	trimethylsilyl methacrylate
TOL	toluene
UF	urea-formaldehyde
V59	2,2'-azobis(2-methylbutyronitrile)
wt%	weight percent
XPS	X-ray photoelectron spectroscopy
XYL	xylene

## Characters and symbols

### Greek

$\alpha$	aperture angle
$\delta$	Hildebrandt solubility parameter
$\gamma$	interfacial tension
$\zeta$	zeta
$\eta$	dynamic viscosity
$\theta$	contact angle
$\lambda$	wavelength
$\rho$	density
$\varphi_c$	fraction of the core of dispersed phase
$\varphi_d$	fraction of dispersed phase

### Latin

$A$	interfacial area
$D_h$	hydrodynamic diameter
$D_T$	translational diffusion coefficient
$G$	free surface energy
$k_B$	Boltzmann constant
$M_n$	number averaged molecular weight
$M_w$	weight averaged molecular weight
$n$	refractive index
$P$	molar parachor
$P_L$	Laplace pressure
$r$	resolution
$R$	radius
$R_H$	hydrodynamic diameter
$S$	spreading coefficient
$T$	temperature
$T_g$	glass transition temperature
$V$	volume



---

## References

- (1) Gosh, S. K. *Self-healing Materials: Fundamentals, Design, Strategies, and Applications*; WILEY-VCH Verlag GmbH & Co. KGaA: Weinheim, **2009**.
- (2) Riccardi, M. P.; Duminuco, P.; Tomasi, C.; Ferloni, P. *Thermochimica Acta* **1998**, *321*, 207.
- (3) Sánchez-Moral, S.; García-Guinea, J.; Luque, L. L.; González-Martín, R.; López-Arce, P. *Materiales de Construcción* **2004**, *54*, 23.
- (4) Craven, J. M. US Patent 3435003, **1969**.
- (5) Dry, C. *Smart Materials and Structures* **1994**, *3*, 118.
- (6) Dry, C. *Composite Structures* **1996**, *35*, 263.
- (7) White, S. R.; Sottos, N. R.; Geubelle, P. H.; Moore, J. S.; Kessler, M. R.; Sriram, S. R.; Brown, E. N.; Viswanathan, S. *Nature* **2001**, *409*, 794.
- (8) Lieser, M. J.; Xu, J.; Owens Corning: **2010**.
- (9) Aramaki, K. *Corrosion Science* **2002**, *44*, 1375.
- (10) Directive 2000/53/EC on end-of-life vehicles. 2000/53/EC; **2000**. p. 9.
- (11) Directive 2002/95/EC on the restriction of the use of certain hazardous substances in electrical and electronic equipment (RoHS). 2002/95/EC; **2002**. p. 19.
- (12) Coutts, R. S. P.; Campbell, M. D. *Composites* **1979**, *10*, 228.
- (13) Hughes, J. D. H. *Composites Science and Technology* **1991**, *41*, 13.
- (14) Ma, P.-C.; Siddiqui, N. A.; Marom, G.; Kim, J.-K. *Composites Part a-Applied Science and Manufacturing* **2010**, *41*, 1345.
- (15) Lagaly, G.; Schulz, O.; Zimehl, R. *Dispersionen und Emulsionen*; Steinkopff Verlag: Darmstadt, **1997**.
- (16) Dörfler, H. D. *Grenzflächen und Kolloidchemie*; VCH: Weinheim, **1994**.
- (17) Dörfler, H. D. *Grenzflächen und Kolloid-Disperse Systeme*; Springer Verlag: Heidelberg, **2002**.
- (18) Ugelstad, J.; Lervik, H.; Gardinovacki, B.; Sund, E. *Pure and Applied Chemistry* **1971**, *26*, 121.
- (19) Ugelstad, J.; El-Aasser, M. S.; Vanderhoff, J. W. *Journal of Polymer Science: Polymer Letters Edition* **1973**, *11*, 503.
- (20) Landfester, K.; Bechthold, N.; Forster, S.; Antonietti, M. *Macromolecular Rapid Communications* **1999**, *20*, 81.
- (21) Landfester, K. *Macromolecular Rapid Communications* **2001**, *22*, 896.
- (22) Schramm, L. L. *Emulsions, Foams, and Suspensions*; Wiley, **2005**.
- (23) Musyanovych, A.; Landfester, K. In *Macromolecular Engineering. Precise Synthesis, Materials Properties, Applications*; Matyjaszewski, K., Gnanou, Y., Leibler, L., Eds.; WILEY-VCH: Weinheim, **2007**.
- (24) Torza, S.; Mason, S. G. *Journal of Colloid and Interface Science* **1970**, *33*, 67.
- (25) Berg, J.; Sundberg, D.; Kronberg, B. *Polymer Materials: Science and Engineering* **1986**, *64*, 367.
- (26) Berg, J.; Sundberg, D.; Kronberg, B. *Journal of Microencapsulation* **1989**, *6*, 327.
- (27) Sundberg, D. C.; Casassa, A. P.; Pantazopoulos, J.; Muscato, M. R.; Kronberg, B.; Berg, J. *Journal of Applied Polymer Science* **1990**, *41*, 1425.

- (28) Muroi, S.; Hashimoto, H.; Hosoi, K. *Journal of Polymer Science: Polymer Chemistry Edition* **1984**, *22*, 1365.
- (29) Okubo, M.; Yamada, A.; Matsumoto, T. *Journal of Polymer Science Part a-Polymer Chemistry* **1980**, *18*, 3219.
- (30) Okubo, M.; Katsuta, Y.; Matsumoto, T. *Journal of Polymer Science Part C-Polymer Letters* **1982**, *20*, 45.
- (31) Joensson, J.-E.; Hassander, H.; Toernell, B. *Macromolecules* **1994**, *27*, 1932.
- (32) Chen, Y. C.; Dimonie, V.; El-Aasser, M. S. *Journal of Applied Polymer Science* **1992**, *45*, 487.
- (33) Karlsson, L. E.; Karlsson, O. J.; Sundberg, D. C. *Journal of Applied Polymer Science* **2003**, *90*, 905.
- (34) Lee, S.; Rudin, A. *Journal of Polymer Science Part A: Polymer Chemistry* **1992**, *30*, 2211.
- (35) Landfester, K. *Angewandte Chemie-International Edition* **2009**, *48*, 4488.
- (36) Decher, G.; Hong, J. D.; Schmitt, J. *Thin Solid Films* **1992**, *210*, 831.
- (37) Johnston, A. P. R.; Cortez, C.; Angelatos, A. S.; Caruso, F. *Current Opinion in Colloid & Interface Science* **2006**, *11*, 203.
- (38) Decher, G. *Science* **1997**, *277*, 1232.
- (39) Donath, E.; Sukhorukov, G. B.; Caruso, F.; Davis, S. A.; Möhwald, H. *Angewandte Chemie International Edition* **1998**, *37*, 2201.
- (40) Caruso, F. *Chemistry – A European Journal* **2000**, *6*, 413.
- (41) Caruso, F.; Caruso, R. A.; Mohwald, H. *Science* **1998**, *282*, 1111.
- (42) Kato, N.; Schuetz, P.; Fery, A.; Caruso, F. *Macromolecules* **2002**, *35*, 9780.
- (43) Shenoy, D. B.; Antipov, A. A.; Sukhorukov, G. B.; Mohwald, H. *Biomacromolecules* **2003**, *4*, 265.
- (44) Berth, G.; Voigt, A.; Dautzenberg, H.; Donath, E.; Mohwald, H. *Biomacromolecules* **2002**, *3*, 579.
- (45) Landfester, K. *Angewandte Chemie International Edition* **2009**, *48*, 4488.
- (46) Tiarks, F.; Landfester, K.; Antonietti, M. *Langmuir* **2001**, *17*, 908.
- (47) Scott, C.; Wu, D.; Ho, C.-C.; Co, C. C. *Journal of the American Chemical Society* **2005**, *127*, 4160.
- (48) Wu, D.; Scott, C.; Ho, C.-C.; Co, C. C. *Macromolecules* **2006**, *39*, 5848.
- (49) Musyanovych, A.; Landfester, K. In *Surface and Interfacial Forces - from Fundamentals to Applications*; Auernhammer, G. K., Butt, H. J., Vollmer, D., Eds. **2008**; Vol. 134, p 120.
- (50) Crespy, D.; Stark, M.; Hoffmann-Richter, C.; Ziener, U.; Landfester, K. *Macromolecules* **2007**, *40*, 3122.
- (51) Torini, L.; Argillier, J. F.; Zydowicz, N. *Macromolecules* **2005**, *38*, 3225.
- (52) Johnsen, H.; Schmid, R. B. *Journal of Microencapsulation* **2007**, *24*, 731.
- (53) Galleone, S. F.; Labrosse, A.; Marteaux, L.; Schirosi, H.; Zimmermann, H. **2009**.
- (54) Peng, B.; Chen, M.; Zhou, S. X.; Wu, L. M.; Ma, X. H. *Journal of Colloid and Interface Science* **2008**, *321*, 67.
- (55) Cao, Z.; Dong, L.; Li, L.; Shang, Y.; Qi, D.; Lv, Q.; Shan, G.; Ziener, U.; Landfester, K. *Langmuir* **2012**, *28*, 7023.
- (56) de Faria, T. J.; de Campos, A. M.; Senna, E. L. *Macromolecular Symposia* **2005**, *229*, 228.

- 
- (57) Paiphansiri, U.; Tangboriboonrat, P.; Landfester, K. *Macromolecular Bioscience* **2006**, *6*, 33.
- (58) Dowding, P. J.; Atkin, R.; Vincent, B.; Bouillot, P. *Langmuir* **2004**, *20*, 11374.
- (59) Loxley, A.; Vincent, B. *Journal of Colloid and Interface Science* **1998**, *208*, 49.
- (60) Atkin, R.; Davies, P.; Hardy, J.; Vincent, B. *Macromolecules* **2004**, *37*, 7979.
- (61) Crespy, D.; Landfester, K. *Beilstein Journal of Organic Chemistry* **2010**, *6*, 1132.
- (62) Luo, Y. W.; Zhou, X. D. *Journal of Polymer Science Part a-Polymer Chemistry* **2004**, *42*, 2145.
- (63) Herrmann, C.; Bannwarth, M. B.; Landfester, K.; Crespy, D. *Macromolecular Chemistry and Physics* **2012**, *213*, 829.
- (64) Yang, H.; Mendon, S. K.; Rawlins, J. W. *Express Polymer Letters* **2008**, *2*, 349.
- (65) Crespy, D.; Musyanovych, A.; Landfester, K. *Colloid & Polymer Science* **2006**, *284*, 780.
- (66) Cao, Z. H.; Shan, G. R.; Sheibat-Othman, N.; Putaux, J. L.; Bourgeat-Lami, E. *Journal of Polymer Science Part A: Polymer Chemistry* **2010**, *48*, 593.
- (67) Baier, G.; Musyanovych, A.; Dass, M.; Theisinger, S.; Landfester, K. *Biomacromolecules* **2010**, *11*, 960.
- (68) Paiphansiri, U.; Dausend, J.; Musyanovych, A.; Mailaender, V.; Landfester, K. *Macromolecular Bioscience* **2009**, *9*, 575.
- (69) Baier, G.; Siebert, J. M.; Landfester, K.; Musyanovych, A. *Macromolecules* **2012**, *45*, 3419.
- (70) Li, W.; Yoon, J. A.; Matyjaszewski, K. *Journal of the American Chemical Society* **2010**, *132*, 7823.
- (71) Yang, J.; Lee, J.; Kang, J.; Lee, K.; Suh, J.-S.; Yoon, H.-G.; Huh, Y.-M.; Haam, S. *Langmuir* **2008**, *24*, 3417.
- (72) Oh, W.-K.; Kim, S.; Choi, M.; Kim, C.; Jeong, Y. S.; Cho, B.-R.; Hahn, J.-S.; Jang, J. *ACS Nano* **2010**, *4*, 5301.
- (73) Liu, W.; Chen, G.; He, G.; He, Z.; Qian, Z. *Journal of Materials Science* **2011**, *46*, 6758.
- (74) Schneider, G.; Decher, G. *Nano Letters* **2004**, *4*, 1833.
- (75) Shchukin, D. G.; Möhwald, H. *Small* **2007**, *3*, 926.
- (76) Shchukin, D. G.; Möhwald, H. *Advanced Functional Materials* **2007**, *17*, 1451.
- (77) Grigoriev, D. O.; Bukreeva, T.; Moehwald, H.; Shchukin, D. G. *Langmuir* **2008**, *24*, 999.
- (78) Rahman, M. M.; Elaissari, A. *Journal of Materials Chemistry* **2012**, *22*, 1173.
- (79) Bird, R.; Freemont, T. J.; Saunders, B. R. *Chemical Communications* **2011**, *47*, 1443.
- (80) Bird, R.; Freemont, T.; Saunders, B. R. *Soft Matter* **2012**, *8*, 1047.
- (81) Bird, R.; Tungchaiwattana, S.; Freemont, T.; Saunders, B. R. *Soft Matter* **2012**, *8*, 3062.
- (82) Blaiszik, B. J.; Kramer, S. L. B.; Olugebefola, S. C.; Moore, J. S.; Sottos, N. R.; White, S. R. In *Annual Review of Materials Research, Vol 40*; Clarke, D. R., Ruhle, M., Zok, F., Eds. **2010**; Vol. 40, p 179.
- (83) Murphy, E. B.; Bolanos, E.; Schaffner-Hamann, C.; Wudl, F.; Nutt, S. R.; Auad, M. L. *Macromolecules* **2008**, *41*, 5203.
- (84) Luo, X.; Ou, R.; Eberly, D. E.; Singhal, A.; Viratyaporn, W.; Mather, P. T. *ACS Applied Materials & Interfaces* **2009**, *1*, 612.
- (85) Varley, R. J.; van der Zwaag, S. *Acta Materialia* **2008**, *56*, 5737.
- (86) Chen, X. X.; Dam, M. A.; Ono, K.; Mal, A.; Shen, H. B.; Nutt, S. R.; Sheran, K.; Wudl, F. *Science* **2002**, *295*, 1698.
- (87) Chen, X. X.; Wudl, F.; Mal, A. K.; Shen, H. B.; Nutt, S. R. *Macromolecules* **2003**, *36*, 1802.

- (88) Park, J. S.; Takahashi, K.; Guo, Z.; Wang, Y.; Bolanos, E.; Hamann-Schaffner, C.; Murphy, E.; Wudl, F.; Hahn, H. T. *Journal of Composite Materials* **2008**, *42*, 2869.
- (89) Park, J. S.; Kim, H. S.; Hahn, H. T. *Composites Science and Technology* **2009**, *69*, 1082.
- (90) Hayes, S. A.; Jones, F. R.; Marshiya, K.; Zhang, W. *Composites Part a-Applied Science and Manufacturing* **2007**, *38*, 1116.
- (91) Hayes, S. A.; Zhang, W.; Branthwaite, M.; Jones, F. R. *Journal of the Royal Society Interface* **2007**, *4*, 381.
- (92) Kalista, S. J., Jr.; Ward, T. C. *Journal of the Royal Society Interface* **2007**, *4*, 405.
- (93) Kalista, S. J., Jr. *Mechanics of Advanced Materials and Structures* **2007**, *14*, 391.
- (94) Varley, R. J.; van der Zwaag, S. *Polymer Testing* **2008**, *27*, 11.
- (95) Cordier, P.; Tournilhac, F.; Soulie-Ziakovic, C.; Leibler, L. *Nature* **2008**, *451*, 977.
- (96) Burnworth, M.; Tang, L.; Kumpfer, J. R.; Duncan, A. J.; Beyer, F. L.; Fiore, G. L.; Rowan, S. J.; Weder, C. *Nature* **2011**, *472*, 334.
- (97) Oconnor, K. M.; Wool, R. P. *Journal of Applied Physics* **1980**, *51*, 5075.
- (98) Wool, R. P.; Oconnor, K. M. *Journal of Applied Physics* **1981**, *52*, 5953.
- (99) McGarel, O. J.; Wool, R. P. *Journal of Polymer Science Part B-Polymer Physics* **1987**, *25*, 2541.
- (100) Yamaguchi, M.; Ono, S.; Terano, M. *Materials Letters* **2007**, *61*, 1396.
- (101) Yamaguchi, M.; Ono, S.; Okamoto, K. *Materials Science and Engineering B-Advanced Functional Solid-State Materials* **2009**, *162*, 189.
- (102) Dry, C.; Sottos, N. R. In *Smart Structure and Materials*; Varadan, V. K., Ed.; SPIE Proc.: 1993, p 438.
- (103) Bleay, S. M.; Loader, C. B.; Hawyes, V. J.; Humberstone, L.; Curtis, P. T. *Composites Part a-Applied Science and Manufacturing* **2001**, *32*, 1767.
- (104) Pang, J. W. C.; Bond, I. P. *Composites Part a-Applied Science and Manufacturing* **2005**, *36*, 183.
- (105) Pang, J. W. C.; Bond, I. P. *Composites Science and Technology* **2005**, *65*, 1791.
- (106) Williams, H. R.; Trask, R. S.; Bond, I. P. *Smart Materials & Structures* **2007**, *16*, 1198.
- (107) Williams, H. R.; Trask, R. S.; Bond, I. P. *Composites Science and Technology* **2008**, *68*, 3171.
- (108) Toohey, K. S.; Sottos, N. R.; Lewis, J. A.; Moore, J. S.; White, S. R. *Nature Materials* **2007**, *6*, 581.
- (109) Toohey, K. S.; Sottos, N. R.; White, S. R. *Experimental Mechanics* **2009**, *49*, 707.
- (110) Toohey, K. S.; Hansen, C. J.; Lewis, J. A.; White, S. R.; Sottos, N. R. *Advanced Functional Materials* **2009**, *19*, 1399.
- (111) Brown, E. N.; Sottos, N. R.; White, S. R. *Experimental Mechanics* **2002**, *42*, 372.
- (112) Brown, E. N.; White, S. R.; Sottos, N. R. *Composites Science and Technology* **2005**, *65*, 2466.
- (113) Brown, E. N.; White, S. R.; Sottos, N. R. *Composites Science and Technology* **2005**, *65*, 2474.
- (114) Brown, E. N.; White, S. R.; Sottos, N. R. *Journal of Materials Science* **2004**, *39*, 1703.
- (115) Brown, E. N.; Kessler, M. R.; Sottos, N. R.; White, S. R. *Journal of Microencapsulation* **2003**, *20*, 719.
- (116) Rule, J. D.; Sottos, N. R.; White, S. R. *Polymer* **2007**, *48*, 3520.
- (117) Kirkby, E. L.; Rule, J. D.; Michaud, V. J.; Sottos, N. R.; White, S. R.; Manson, J.-A. E. *Advanced Functional Materials* **2008**, *18*, 2253.

- 
- (118) Jones, A. S.; Rule, J. D.; Moore, J. S.; Sottos, N. R.; White, S. R. *Journal of the Royal Society Interface* **2007**, *4*, 395.
- (119) Kirkby, E. L.; Michaud, V. J.; Manson, J. A. E.; Sottos, N. R.; White, S. R. *Polymer* **2009**, *50*, 5533.
- (120) Moll, J. L.; White, S. R.; Sottos, N. R. *Journal of Composite Materials* **2010**, *44*, 2573.
- (121) Kessler, M. R.; Sottos, N. R.; White, S. R. *Composites Part a-Applied Science and Manufacturing* **2003**, *34*, 743.
- (122) Patel, A. J.; Sottos, N. R.; Wetzel, E. D.; White, S. R. *Composites Part a-Applied Science and Manufacturing* **2010**, *41*, 360.
- (123) Kessler, M. R.; White, S. R. *Composites Part a-Applied Science and Manufacturing* **2001**, *32*, 683.
- (124) Sanada, K.; Yasuda, I.; Shindo, Y. *Plastics Rubber and Composites* **2006**, *35*, 67.
- (125) Wilson, G. O.; Moore, J. S.; White, S. R.; Sottos, N. R.; Andersson, H. M. *Advanced Functional Materials* **2008**, *18*, 44.
- (126) Chipara, M. D.; Chipara, M.; Shansky, E.; Zaleski, J. M. *Polymers for Advanced Technologies* **2009**, *20*, 427.
- (127) Wilson, G. O.; Caruso, M. M.; Reimer, N. T.; White, S. R.; Sottos, N. R.; Moore, J. S. *Chemistry of Materials* **2008**, *20*, 3288.
- (128) Wilson, G. O.; Porter, K. A.; Weissman, H.; White, S. R.; Sottos, N. R.; Moore, J. S. *Advanced Synthesis & Catalysis* **2009**, *351*, 1817.
- (129) Kamphaus, J. M.; Rule, J. D.; Moore, J. S.; Sottos, N. R.; White, S. R. *Journal of the Royal Society Interface* **2008**, *5*, 95.
- (130) Li, H. Y.; Wang, R. G.; Liu, W. B. *J. Reinf. Plast. Compos.* **2012**, *31*, 924.
- (131) Rule, J. D.; Brown, E. N.; Sottos, N. R.; White, S. R.; Moore, J. S. *Advanced Materials* **2005**, *17*, 205.
- (132) Liu, X.; Lee, J. K.; Yoon, S. H.; Kessler, M. R. *Journal of Applied Polymer Science* **2006**, *101*, 1266.
- (133) Lee, J. K.; Hong, S. J.; Liu, X.; Yoon, S. H. *Macromolecular Research* **2004**, *12*, 478.
- (134) Yin, T.; Zhou, L.; Rong, M. Z.; Zhang, M. Q. *Smart Materials & Structures* **2008**, *17*.
- (135) Yin, T.; Rong, M. Z.; Zhang, M. Q.; Zhao, J. Q. *Smart Materials & Structures* **2009**, *18*.
- (136) Yin, T.; Rong, M. Z.; Wu, J.; Chen, H.; Zhang, M. Q. *Composites Part a-Applied Science and Manufacturing* **2008**, *39*, 1479.
- (137) Rong, M. Z.; Zhang, M. Q.; Zhang, W. *Advanced Composites Letters* **2007**, *16*, 167.
- (138) Keller, M. W.; White, S. R.; Sottos, N. R. *Advanced Functional Materials* **2007**, *17*, 2399.
- (139) Keller, M. W.; White, S. R.; Sottos, N. R. *Polymer* **2008**, *49*, 3136.
- (140) Cho, S. H.; White, S. R.; Braun, P. V. *Advanced Materials* **2009**, *21*, 645.
- (141) Beiermann, B. A.; Keller, M. W.; Sottos, N. R. *Smart Materials & Structures* **2009**, *18*.
- (142) Yuan, Y. C.; Rong, M. Z.; Zhang, M. Q.; Chen, J.; Yang, G. C.; Li, X. M. *Macromolecules* **2008**, *41*, 5197.
- (143) Jin, H.; Mangun, C. L.; Stradley, D. S.; Moore, J. S.; Sottos, N. R.; White, S. R. *Polymer* **2012**, *53*, 581.
- (144) Billiet, S.; Van Camp, W.; Hillewaere, X. K. D.; Rahier, H.; Du Prez, F. E. *Polymer* **2012**, *53*, 2320.
- (145) Xiao, D. S.; Yuan, Y. C.; Rong, M. Z.; Zhang, M. Q. *Polymer* **2009**, *50*, 2967.
- (146) Xiao, D. S.; Yuan, Y. C.; Rong, M. Z.; Zhang, M. Q. *Polymer* **2009**, *50*, 560.

- (147) Gragert, M.; Schunack, M.; Binder, W. H. *Macromolecular Rapid Communications* **2011**, *32*, 419.
- (148) Caruso, M. M.; Delafuente, D. A.; Ho, V.; Sottos, N. R.; Moore, J. S.; White, S. R. *Macromolecules* **2007**, *40*, 8830.
- (149) Caruso, M. M.; Blaiszik, B. J.; White, S. R.; Sottos, N. R.; Moore, J. S. *Advanced Functional Materials* **2008**, *18*, 1898.
- (150) Zako, M.; Takano, N. *Journal of Intelligent Material Systems and Structures* **1999**, *10*, 836.
- (151) Suryanarayana, C.; Rao, K. C.; Kumar, D. *Progress in Organic Coatings* **2008**, *63*, 72.
- (152) Kumar, A.; Stephenson, L. D.; Murray, J. N. *Progress in Organic Coatings* **2006**, *55*, 244.
- (153) Sauvant-Moynot, V.; Gonzalez, S.; Kittel, J. *Progress in Organic Coatings* **2008**, *63*, 307.
- (154) Grigoriev, D. O.; Koehler, K.; Skorb, E.; Shchukin, D. G.; Moehwald, H. *Soft Matter* **2009**, *5*, 1426.
- (155) Yang, J.; Keller, M. W.; Moore, J. S.; White, S. R.; Sottos, N. R. *Macromolecules* **2008**, *41*, 9650.
- (156) Huang, M.; Yang, J. *Journal of Materials Chemistry* **2011**, *21*, 11123.
- (157) Meng, L. M.; Yuan, Y. C.; Rong, M. Z.; Zhang, M. Q. *Journal of Materials Chemistry* **2010**, *20*, 6030.
- (158) Wang, H. P.; Yuan, Y. C.; Rong, M. Z.; Zhang, M. Q. *Macromolecules* **2010**, *43*, 595.
- (159) Yao, L.; Yuan, Y. C.; Rong, M. Z.; Zhang, M. Q. *Polymer* **2011**, *52*, 3137.
- (160) Cho, S. H.; Andersson, H. M.; White, S. R.; Sottos, N. R.; Braun, P. V. *Advanced Materials* **2006**, *18*, 997.
- (161) Blaiszik, B. J.; Sottos, N. R.; White, S. R. *Composites Science and Technology* **2008**, *68*, 978.
- (162) Jackson, A. C.; Bartelt, J. A.; Marczewski, K.; Sottos, N. R.; Braun, P. V. *Macromolecular Rapid Communications* **2011**, *32*, 82.
- (163) van den Dungen, E. T. A.; Klumperman, B. *Journal of Polymer Science Part A: Polymer Chemistry* **2010**, *48*, 5215.
- (164) Ouyang, X.; Huang, X.; Pan, Q.; Zuo, C.; Huang, C.; Yang, X.; Zhao, Y. *Journal of Dentistry* **2011**, *39*, 825.
- (165) Maia, F.; Tedim, J.; Lisenkov, A. D.; Salak, A. N.; Zheludkevich, M. L.; Ferreira, M. G. S. *Nanoscale* **2012**, *4*, 1287.
- (166) Brown, E. N.; Kessler, M. R.; Sottos, N. R.; White, S. R. *Journal of Microencapsulation* **2003**, *20*, 719.
- (167) Kessler, M. R.; White, S. R. *Journal of Polymer Science Part a-Polymer Chemistry* **2002**, *40*, 2373.
- (168) Yuan, L.; Liang, G.; Xie, J.; Li, L.; Guo, J. *Polymer* **2006**, *47*, 5338.
- (169) Cosco, S.; Ambrogio, V.; Musto, P.; Carfagna, C. *Journal of Applied Polymer Science* **2007**, *105*, 1400.
- (170) Hughes, A. E.; Cole, I. S.; Muster, T. H.; Varley, R. J. *NPG Asia Mater* **2010**, *2*, 143.
- (171) *Nicomp 380 User Manual* Santa Barbara, 2003.
- (172) Elias, H. G. *Makromoleküle, Band 1, Grundlagen*; 5. Auflage ed.; Hüthig & Wepf Verlag, **1990**.
- (173) Flegler, S. L.; Heckman, J. W.; Klomparens, K. L. *Elektronenmikroskopie*; Spektrum Akademischer Verlag: Heidelberg, **1995**.

- 
- (174) Mulisch, M.; Welsch, U. In *Romeis - Mikroskopische Technik*; 18. Auflage ed.; Spektrum Akademischer Verlag: Heidelberg, **2010**.
- (175) Staff, R. H.; Rupper, P.; Lieberwirth, I.; Landfester, K.; Crespy, D. *Soft Matter* **2011**, *7*, 10219.
- (176) Dschagarova, E.; Sarbov, I.; Mateva, R. *Die Angewandte Makromolekulare Chemie* **1979**, *81*, 193.
- (177) Florez, L.; Herrmann, C.; Cramer, J. M.; Hauser, C. P.; Koynov, K.; Landfester, K.; Crespy, D.; Mailänder, V. *Small* **2012**, *8*, 2222.
- (178) Landfester, K. In *Annual Review of Materials Research*; Annual Reviews: Palo Alto, **2006**; Vol. 36, p 231.
- (179) B. Arkles, J. S., J. Zazyczny, P. Mehta *Silanes and Other Coupling Agents*, 1992.
- (180) Rossow, T. *Preparation of Inorganic Nanoparticles from Confined Precursors in Miniemulsion*, Practical work at the Max Planck Institute for Polymer Research, **2010**.
- (181) Taber, D. F.; Frankowski, K. J. *The Journal of Organic Chemistry* **2003**, *68*, 6047.
- (182) Guadagno, L.; Longo, P.; Raimondo, M.; Naddeo, C.; Mariconda, A.; Vittoria, V.; Iannuzzo, G.; Russo, S. *Composites Part B: Engineering* **2011**, *42*, 296.
- (183) Jackson, A. C.; Bartelt, J. A.; Braun, P. V. *Advanced Functional Materials* **2011**, *21*, 4705.
- (184) Paramonov, S. E.; Bachelder, E. M.; Beaudette, T. T.; Standley, S. M.; Lee, C. C.; Dashe, J.; Frechet, J. M. J. *Bioconjugate Chemistry* **2008**, *19*, 911.
- (185) Skirtach, A. G.; Dejugnat, C.; Braun, D.; Susha, A. S.; Rogach, A. L.; Parak, W. J.; Mohwald, H.; Sukhorukov, G. B. *Nano Letters* **2005**, *5*, 1371.
- (186) Sankaranarayanan, J.; Mahmoud, E. A.; Kim, G.; Morachis, J. M.; Almutairi, A. *Acs Nano* **2010**, *4*, 5930.
- (187) Caruso, M. M.; Schelkopf, S. R.; Jackson, A. C.; Landry, A. M.; Braun, P. V.; Moore, J. S. *Journal of Materials Chemistry* **2009**, *19*, 6093.
- (188) Johnston, A. P. R.; Such, G. K.; Caruso, F. *Angewandte Chemie-International Edition* **2010**, *49*, 2664.
- (189) Tokiwa, Y.; Calabia, B. P. *Applied Microbiology and Biotechnology* **2006**, *72*, 244.
- (190) Razumovskii, L. P.; Moiseev, Y. V.; Kuznetsova, A. G.; Zaikov, G. E. *Bulletin of the Academy of Sciences of the Ussr Division of Chemical Science* **1975**, *24*, 1391.
- (191) Chen, B.; Zhan, X.; Yi, L.; Chen, F. *Chinese Journal of Chemical Engineering* **2007**, *15*, 661.
- (192) McMurry, J. E. *Organic Chemistry*; 8th ed.; Brooks/Cole Cengage Learning: Belmont, CA, USA, **2012**.
- (193) Saini, G.; Leoni, A.; Franco, S. *Die Makromolekulare Chemie* **1971**, *144*, 235.
- (194) Boudevska, H.; Todorova, O. *Die Makromolekulare Chemie* **1985**, *186*, 1711.
- (195) Fujihara, H.; Yamazaki, K.; Matsubara, Y.; Yoshihara, M.; Maeshima, T. *Journal of Macromolecular Science: Part A - Chemistry* **1979**, *13*, 1081.
- (196) Dong, Y.; Sundberg, D. C. *Journal of Colloid and Interface Science* **2003**, *258*, 97.
- (197) Van Krevelen, D. W. *Properties of Polymers*; 3rd ed.; Elsevier B. V., 2003.
- (198) Quayle, O. R. *Chemical Reviews* **1953**, *53*, 439.
- (199) Tanaka, T.; Okayama, M.; Okubo, M. *Macromolecular Symposia* **2010**, *288*, 55.
- (200) Amalvy, J. I.; Wanless, E. J.; Li, Y.; Michailidou, V.; Armes, S. P.; Duccini, Y. *Langmuir* **2004**, *20*, 8992.
- (201) Amalvy, J. I.; Armes, S. P.; Binks, B. P.; Rodrigues, J. A.; Unali, G. F. *Chemical Communications* **2003**, 1826.

- (202) Hui, D.; Nawaz, M.; Morris, D. P.; Edwards, M. R.; Saunders, B. R. *Journal of Colloid and Interface Science* **2008**, *324*, 110.
- (203) Motornov, M.; Sheparovych, R.; Lupitskyy, R.; MacWilliams, E.; Hoy, O.; Luzinov, I.; Minko, S. *Advanced Functional Materials* **2007**, *17*, 2307.
- (204) Mori, H.; Müller, A. H. E. *Progress in Polymer Science* **2003**, *28*, 1403.
- (205) Mühlebach, A.; Gaynor, S. G.; Matyjaszewski, K. *Macromolecules* **1998**, *31*, 6046.
- (206) Makrikosta, G.; Georgas, D.; Siakali-Kioulafa, E.; Pitsikalis, M. *European Polymer Journal* **2005**, *41*, 47.
- (207) D. N. Andreev, D. N. A., N. A. Solovskaya *Russian Chemical Bulletin* **1972**, *21*, 1361.
- (208) Mormann, W.; Ferbitz, J. *Macromolecular Chemistry and Physics* **2002**, *203*, 2616.
- (209) Iván, B.; Haraszti, M.; Erdődi, G.; Scherble, J.; Thomann, R.; Mülhaupt, R. *Macromolecular Symposia* **2005**, *227*, 265.
- (210) Jarowicki, K.; Kocienski, P. *Journal of the Chemical Society-Perkin Transactions 1* **2001**, 2109.
- (211) Khan, T. R.; Erbe, A.; Auinger, M.; Marlow, F.; Rohwerder, M. *Science and Technology of Advanced Materials* **2011**, *12*.
- (212) Azizi, M.; Schneider, W.; Plieth, W. *Journal of Solid State Electrochemistry* **2005**, *9*, 429.
- (213) Vauthier, C.; Schmidt, C.; Couvreur, P. *Journal of Nanoparticle Research* **1999**, *1*, 411.
- (214) Desgouilles, S.; Vauthier, C.; Bazile, D.; Vacus, J.; Grossiord, J.-L.; Veillard, M.; Couvreur, P. *Langmuir* **2003**, *19*, 9504.
- (215) Urban, M.; Musyanovych, A.; Landfester, K. *Macromolecular Chemistry and Physics* **2009**, *210*, 961.
- (216) Fung, B. M.; Khitrin, A. K.; Ermolaev, K. *Journal of Magnetic Resonance* **2000**, *142*, 97.
- (217) Marsmann, H. C.; Raml, W.; Hengge, E. *Z.Naturforsch.(B)* **1980**, *35*, 1541.
- (218) Engelhardt, G.; Michel, D. *High-Resolution Solid-State NMR of Silicates and Zeolites*; Wiley: Chichester, **1987**.
- (219) Massiot, D.; Fayon, F.; Capron, M.; King, I.; Le Calvé, S.; Alonso, B.; Durand, J.-O.; Bujoli, B.; Gan, Z.; Hoatson, G. *Magnetic Resonance in Chemistry* **2002**, *40*, 70.
- (220) Ellman, G. L. *Archives of biochemistry and biophysics* **1959**, *82*, 70.
- (221) Bulaj, G.; Kortemme, T.; Goldenberg, D. P. *Biochemistry* **1998**, *37*, 8965.
- (222) Delair, T.; Marguet, V.; Pichot, C.; Mandrand, B. *Colloid & Polymer Science* **1994**, *272*, 962.
- (223) Ganachaud, F.; Mouterde, G.; Delair, T.; Elaïssari, A.; Pichot, C. *Polymers for Advanced Technologies* **1995**, *6*, 480.
- (224) Hashimoto, N.; Aoyama, T.; Shioiri, T. *Chemical & pharmaceutical bulletin* **1981**, *29*, 1475.
- (225) Sheehan, J. C.; Hess, G. P. *Journal of the American Chemical Society* **1955**, *77*, 1067.
- (226) Berg-Feld, M. C.; Klesper, E. *Polymer Bulletin* **1981**, *6*, 201.
- (227) Vonnegut, B. *Review of Scientific Instruments* **1942**, *13*, 6.



## **Acknowledgements**



## **Appendix**

### ***Curriculum vitae***

Name:

Date of Birth:

Place of Birth:

**List of publications**

- (1) **J. Fickert**, P. Rupper , R. Graf , K. Landfester, D. Crespy  
Design and Characterization of Functionalized Silica Nanocontainers for Self-Healing Materials  
*Journal of Materials Chemistry* **2012**, *22*, 2286.
- (2) Y. Zhao, **J. Fickert**, K. Landfester, D. Crespy  
Encapsulation of Self-Healing Agents in Polymer Nanocapsules  
*Small* **2012**, *8*, 2954.
- (3) **J. Fickert**, M. Makowski, M. Kappl, K. Landfester, D. Crespy  
Efficient Encapsulation of Self-Healing Agents in Polymer Nanocontainers functionalized by orthogonal reactions  
*Macromolecules* **2012**, *45*, 6324.
- (4) **J. Fickert**, C. Wohnhaas, A. Turshatov, K. Landfester, D. Crespy  
Copolymer Structures Tailored for the Preparation of Nanocapsules  
*Macromolecules* **2013**, *46*, 573.
- (5) **J. Fickert**, K. Landfester, D. Crespy  
Self-Stabilized pH-Responsive Nanocapsules  
*submitted*
- (6) T. H. Tran, A. Vimalanandan, **J. Fickert**, K. Landfester, D. Crespy, M. Rohwerder  
Electrolytic Codeposition of Silica and Polymer Nanocapsules with Zinc  
*in preparation*
- (7) **J. Fickert**, K. Landfester, D. Crespy  
Redox-Responsive Silica Nanocapsules  
*in preparation*

---

**Oral and poster contributions**

- 06/2011      **Third International Conference on Self-Healing Materials**, Bath, UK  
Poster presentation  
*Synthesis of Nanocontainers for Self-Healing Reactions based on ROMP*
- 05/2012      **BASF SE**, Ludwigshafen, Germany  
Oral presentation  
*Functionalized Nanocapsules for Self-Healing Materials*
- 06/2012      **World Polymer Congress**, Blacksburg, USA  
Oral presentation  
*Functionalized Nanocapsules for Self-Healing Materials*
- 10/2012      **Smart Polymers**, Mainz, Germany  
Poster presentation  
*Responsive Nanocapsules for Self-Healing Materials*
- 11/2012      **Federal University of Ceará**, Fortaleza, Brasil  
Oral presentation  
*Nanocapsules for Self-Healing Materials*

## Erklärung

Hiermit versichere ich gemäß § 10 Abs. 3d der Promotionsordnung vom 24.07.2007, dass ich die als Dissertation vorgelegte Arbeit selbst angefertigt und alle benutzten Hilfsmittel (Literatur, Apparaturen, Material) in der Arbeit angegeben habe.

Mainz, den

---

Johannes Fickert